

COUPLING BETWEEN DIFFUSION OF BIODIESEL AND LARGE
DEFORMATION IN ELASTOMERS: FROM EXPERIMENTAL
INVESTIGATION TO CONSTITUTIVE MODELING

CH'NG SHIAU YING

FACULTY OF ENGINEERING
UNIVERSITY OF MALAYA
KUALA LUMPUR

2014

COUPLING BETWEEN DIFFUSION OF BIODIESEL AND
LARGE DEFORMATION IN ELASTOMERS: FROM
EXPERIMENTAL INVESTIGATION TO CONSTITUTIVE
MODELING

CH'NG SHIAU YING

THESIS SUBMITTED IN FULFILMENT
OF THE REQUIREMENTS
FOR THE DEGREE OF DOCTOR OF PHILOSOPHY

FACULTY OF ENGINEERING
UNIVERSITY OF MALAYA
KUALA LUMPUR

2014

UNIVERSITI MALAYA

ORIGINAL LITERARY WORK DECLARATION

Name of Candidate: Ch'ng Shiau Ying

Registration/Matrix No.: KHA100097

Name of Degree: The Degree of Doctor of Philosophy

Title of Project Paper/Research Report/Dissertation/Thesis ("this Work"): Coupling

be-tween diffusion of biodiesel and large deformation in elastomers: from experimental
in-vestigation to constitutive modeling

Field of Study: Mechanical Aspect of Polymer

I do solemnly and sincerely declare that:

- (1) I am the sole author/writer of this Work;
- (2) This work is original;
- (3) Any use of any work in which copyright exists was done by way of fair dealing and for permitted purposes and any excerpt or extract from, or reference to or reproduction of any copyright work has been disclosed expressly and sufficiently and the title of the Work and its authorship have been acknowledged in this Work;
- (4) I do not have any actual knowledge nor do I ought reasonably to know that the making of this work constitutes an infringement of any copyright work;
- (5) I hereby assign all and every rights in the copyright to this Work to the University of Malaya ("UM"), who henceforth shall be owner of the copyright in this Work and that any reproduction or use in any form or by any means whatsoever is prohibited without the written consent of UM having been first had and obtained;
- (6) I am fully aware that if in the course of making this Work I have infringed any copyright whether intentionally or otherwise, I may be subject to legal action or any other action as may be determined by UM.

Candidate's Signature

Date

Subscribed and solemnly declared before,

Witness's Signature

Date

Name:

Designation:

ABSTRACT

Due to the concern of limited fossil fuel reserve and stringent emission regulations, there is a tremendous increase in the demand for renewable energy in Malaysia. The introduction of biodiesel is by far considered as the most promising solution. Nevertheless, particular composition of biodiesel leads to material compatibility issue especially in industrial applications involving elastomeric materials. Indeed, it is established that the exposure of elastomers to biodiesel yields to a material degradation which reduces their performance. When elastomeric components are subjected to fluctuating mechanical loading and simultaneously are exposed to aggressive solvent such as biodiesel, two important aspects may contribute to the material degradations: diffusion of solvents resulting to swelling and fluctuating mechanical loading leading to fatigue failure. Since the interactions between the above aspects are not fully understood, it is crucial to investigate and to model the corresponding coupled diffusion-mechanical deformation phenomenon for durability analysis of the components. The first part of this thesis focuses on the experimental investigation on the swelling of elastomers in biodiesel in the absence and in the presence of static mechanical deformations. The former and the latter are referred to as free swelling and constrained swelling respectively. To this end, original devices and specimens are developed so that swelling tests can be conducted on the elastomers while they are simultaneously subjected to various deformation modes: simple extension, simple torsion and simultaneous extension/torsion. It is observed that the presence of static mechanical loading affects significantly the swelling characteristics of elastomers in biodiesel. Moreover, it is found that when a swollen elastomer is subjected to cyclic loading conditions, inelastic responses such stress-softening due to Mullins effect, hysteresis and permanent set decrease as the degree of swelling increases. The second part of this thesis deals with the continuum mechanical modeling of swelling. First, the the-

oretical framework of the model consistent with the second law of thermodynamics is established. More precisely, the proposed model is based on the multiplicative decomposition of the deformation gradient tensor along with the concept of strain amplification factor to account for the effect of carbon black filler. Using this theoretical framework, two particular cases are considered: (1) modeling the Mullins effect in swollen elastomers and (2) prediction of the equilibrium swelling of elastomers in biodiesel in the absence and in the presence of static mechanical deformation. It is observed that the model gives a qualitatively good agreement with experimental observations. Finally, the model for predicting the equilibrium swelling is implemented as a user-supplied subroutine in the finite element package ABAQUS to analyze the complex phenomena which occur during coupled biodiesel diffusion-mechanical deformations in elastomers.

ABSTRAK

Kebimbangan terhadap persimpangan bahan api fosil yang terhad dan peraturan pelepasan yang ketat, terdapat peningkatan tinggi dalam permintaan untuk tenaga boleh diperbaharui di Malaysia. Pengenalan biodiesel dianggap sebagai penyelesaian yang paling menjanjikan setakat ini. Walau bagaimanapun, komposisi tertentu dalam biodiesel menimbulkan isu keserasian untuk bahan tertentu terutamanya dalam aplikasi industri yang melibatkan bahan-bahan elastomer. Malah, pendedahan elastomer kepada biodiesel membawa kepada degradasi bahan yang mengurangkan prestasi elastomer. Apabila komponen elastomer mengalami bebanan mekanik berulang dan didedahkan kepada cecair yang agresif seperti biodiesel, dua aspek penting boleh menyumbang kepada degradasi bahan: peresapan pelarut yang menyebabkan bengkak and beban mekanik berulang yang menyebabkan kegagalan lesuan. Oleh disebabkan interaksi antara aspek-aspek yang dibincang di atas adalah tidak difahami sepenuhnya, maka amatlah penting untuk menyiasat and membina model untuk mengkaji resapan pelarut dalam kehadiran beban mekanik untuk analisis ketahanan komponen. Bahagian pertama penyelidikan ini memberi tumpuan kepada siasatan eksperimen pada bengkak elastomer dalam biodiesel dalam keadaan ketiadaan and kehadiran bebanan mekanik statik. Untuk tujuan ini, alat-alat asal and spesimen yang tertentu dicipta supaya ujian rendaman boleh dilakukan ke atas elastomer semasa mereka tertakluk kepada pelbagai mod beban mekanik: lanjutan mudah, putaran mudah and lanjutan/putaran serentak. Permerhatian menunjukkan kehadiran beban mekanik statik memberi kesan ketara ke atas pembengkakan spesimen. Selain itu, didapati bahawa apabila elastomer yang bengkak tertakluk kepada beban mekanik berulang, tindak balas tidak kenyal seperti kesan Mullins, histerisis dan pengenduran tegasan mengurang apabila tahap bengkak meningkat. Bahagian kedua penyelidikan ini berkaitan dengan model mekanikal kontinum bengkak. Pertama, rangka kerja teori model yang

selaras dengan undang-undang kedua termodinamik ditubuhkan. Model yang dicadangkan adalah berdasarkan kepada penguraian pendaraban daripada tensor kecerunan ubah bentuk bersama-sama dengan konsep ketegangan faktor amplifikasi untuk mengambil kira kesan pengisian karbon hitam. Dengan menggunakan rangka kerja teori ini, dua kes diambil-kira: (1) model kesan Mullins dalam elastomer bengkak dan (2) ramalan bengkak keseimbangan elastomer dalam biodiesel dalam ketiadaan and kehadiran beban mekanik statik. Pemerhatian menunjukkan bahawa model memberi persetujuan yang baik secara kualitatif dengan keputusan eksperimen. Akhir sekali, model untuk meramalkan bengkak keseimbangan dilaksanakan sebagai subrutin pengguna yang dibekalkan dalam pakej unsur terhingga ABAQUS untuk menganalisis fenomena kompleks yang berlaku di bawah peresapan-ubah bentuk serentak dalam elastomer.

ACKNOWLEDGEMENTS

It was year 2011 when I decided to pursue my study and I could not describe my feeling when it finally comes to an end now. I could not have done this without the support from my family and friends.

First and foremost, I would like to express my sincere gratitude to my supervisor, Dr. Andri Andriyana for his patient in continuing guiding me whenever I am lost. He is not only just being a mentor in my academic, but I appreciate his advice to me in life and my future undertaking. Also, I would like to thank my co-supervisor, Dr. Roslina Ahmad for providing me guidance throughout the years.

Next, my thesis will never be completed without the help from *Team France*. I would like to thank Professor Erwan Verron and Dr. Violette Brulliard for their guidance especially in ABAQUS. I will never forget the time I spent in France and how it widen my eyesight in terms of education and cultural difference. A big thank you to all my friends in France for the wonderful time I spent there.

Besides, I would like to thank all my friends in University of Malaya for all the up and down in these years. All those talk, lunch and laughter will forever remain as one of my greatest moment here.

Last and but least, I would like to dedicate this to my beloved parent and family for their endless support on my decision. A personal big thank to Mr. Aw for always believe in me and encourage me when I am frustrated. My life will never be complete without each of them and I am grateful to be the lucky one.

TABLE OF CONTENTS

ORIGINAL LITERARY WORK DECLARATION	ii
ABSTRACT	iii
ABSTRAK	v
ACKNOWLEDGEMENTS	vii
TABLE OF CONTENTS	viii
LIST OF FIGURES	xi
LIST OF TABLES	xvi
LIST OF SYMBOLS AND ACRONYMS	xvii
LIST OF APPENDICES	xix
CHAPTER 1: INTRODUCTION	1
1.1 General research background	1
1.2 Research objectives	3
1.3 Dissertation organization	4
CHAPTER 2: LITERATURE REVIEW	6
2.1 Generality on elastomer	6
2.1.1 Structure of elastomer	8
2.1.2 Basic ingredients of elastomer	9
2.1.3 Some industrial elastomers	12
2.1.3 (a) Natural Rubber (NR)	12
2.1.3 (b) Nitrile Butadiene Rubber (NBR)	13
2.1.3 (c) Polychloroprene (CR)	14
2.1.3 (d) Styrene Butadiene Rubber (SBR)	15
2.2 Mechanical responses of elastomer	15
2.2.1 Mechanical responses under monotonic loading	16
2.2.2 Mechanical responses under cyclic loading	17
2.2.2 (a) Stress-softening (Mullins effect)	17
2.2.2 (b) Hysteresis	19
2.2.2 (c) Permanent set	20
2.3 Constitutive equations for hyperelastic materials	22
2.4 Factors affecting durability of elastomer	26
2.4.1 Mechanical loading history	27
2.4.2 Environment	28
2.4.3 Elastomer compounding	28
2.5 Fillers in elastomer and strain amplification factor	29
2.6 Swelling of elastomer	31

2.6.1	Physical descriptions	32
2.6.2	Thermodynamics of swelling	32
2.6.3	The elastic properties of a swollen elastomer	35
2.6.4	Effect of deformation on swelling	37
2.7	Models for Mullins effect	39
2.7.1	Existing models in dry elastomer	39
2.7.2	Existing extension models for swollen elastomer	41
2.8	Models for coupled diffusion-deformation	41
2.9	Biofuels	45
2.9.1	Palm biodiesel	46
2.9.2	Advantages and disadvantages of biodiesel	47
2.9.3	Compatibility of elastomer with biodiesel	48
CHAPTER 3: METHODOLOGY		51
3.1	Experimental program	53
3.1.1	Design of specimen and device	53
3.1.1 (a)	Constrained swelling 1: static uniaxial strain	53
3.1.1 (b)	Constrained swelling 2: static multiaxial strain (Design 1)	58
3.1.1 (c)	Constrained swelling 3: static multiaxial strain (Design 2)	61
3.1.2	Experimental setup	66
3.1.2 (a)	Immersion test and swelling measurement	66
3.1.2 (b)	Mechanical testing	67
3.2	Continuum mechanical modeling	70
3.2.1	Kinematics	70
3.2.2	Stress response	72
3.2.2 (a)	Case 1: Stress-strain response of swollen elastomers	74
3.2.2 (b)	Case 2: Prediction of equilibrium swelling	77
3.2.3	Mullins effect	79
3.2.3 (a)	Constitutive equations	80
3.2.3 (b)	Two-phase model for Mullins effect in swollen elastomer	82
3.3	Finite element analysis	83
3.3.1	Finite Element Analysis using ABAQUS	84
3.3.2	User subroutine and notes on its implementation	86
CHAPTER 4: EXPERIMENTAL RESULTS AND DISCUSSION		89
4.1	Swelling results	89
4.1.1	Stress-free swelling	89
4.1.1 (a)	Stress-free swelling without device	89
4.1.1 (b)	Stress-free swelling with device	91
4.1.2	Constrained swelling 1: static uniaxial strain	93
4.1.3	Constrained swelling 2: static multiaxial strain (Design 1)	98
4.1.4	Constrained swelling 3: static multiaxial strain (Design 2)	100
4.2	Mechanical responses	102
4.2.1	Mechanical responses under monotonic tensile loading	102
4.2.2	Mechanical responses under cyclic loading	103
4.3	Mechanical quantity affecting swelling	111
4.4	Discussion on the experimental specimen and device	123

4.4.1	Constrained swelling 1: static uniaxial strain	123
4.4.2	Constrained swelling 2: static multiaxial strain (Design 1)	124
4.4.3	Constrained swelling 3: static multiaxial strain (Design 2)	126
CHAPTER 5: MODELING RESULTS AND DISCUSSION		127
5.1	Stress-strain relationship at a given degree of swelling	127
5.1.1	Data treatment	127
5.1.2	Form of material functions	130
5.1.3	Identification of material parameters	132
5.1.4	Comparison between model and experiment	135
5.1.5	Simulation for other degrees of swelling	138
5.1.6	Simulation for other deformation modes	141
5.2	Prediction of equilibrium swelling	149
5.2.1	Constitutive equations	150
5.2.2	Analytical solution for simple problems	152
	5.2.2 (a) Free swelling	152
	5.2.2 (b) Constrained swelling	155
5.2.3	Identification of material parameters	159
5.2.4	Comparison between model and experiment	160
5.3	Finite element simulation	161
5.3.1	Free swelling	161
5.3.2	Constrained swelling	164
5.3.3	Remark for the case of torsion	172
CHAPTER 6: CONCLUSION AND FUTURE WORKS		173
6.1	Conclusion	173
6.2	Suggestions for future works	174
APPENDICES		176
Bibliography		180
LIST OF PUBLICATIONS		188

LIST OF FIGURES

Figure 2.1	Evolution of polymer elastic modulus as a function of temperature (Harper, 1996).	7
Figure 2.2	Schematic representation of molecular structure in an (a) unstressed state and in a (b) stressed state.	8
Figure 2.3	Structure of elastomer (a) before vulcanization and (b) after vulcanization (Jha, 2008).	9
Figure 2.4	Molecular structure of NR.	12
Figure 2.5	Molecular structure of NBR.	13
Figure 2.6	Molecular structure of CR.	14
Figure 2.7	Molecular structure of SBR.	15
Figure 2.8	Stress-strain response of an elastomer.	16
Figure 2.9	Stress-strain responses of a 50 phr carbon black filled SBR under simple uniaxial tension and cyclic uniaxial tension with increasing maximum stretch every 5 cycles (Diani et al., 2009).	17
Figure 2.10	Softening of elastomers due to the Mullins effect (Bauman, 2008).	18
Figure 2.11	Cyclic loading of tensile specimen exhibiting hysteresis (Bauman, 2008).	20
Figure 2.12	Permanent set in elastomer observed after loading and unloading (Bauman, 2008).	21
Figure 3.1	Flow chart describing the methodology of the present work.	52
Figure 3.2	Dimension of dumbbell specimen following ASTM standard D412-C.	53
Figure 3.3	Metallic plate for uniaxial tensile loading.	54
Figure 3.4	Complete device and specimen for constrained swelling 1.	55
Figure 3.5	Exploded view of the experimental device and specimen used for constrained swelling 1.	55
Figure 3.6	Experimental device for constrained swelling 1: (a) with no tensile strain (initially stress-free) and (b) under tensile strain.	57
Figure 3.7	Specimen geometry of the diabolo-shape specimen.	59
Figure 3.8	Exploded view of the experimental device and specimen of Design 1.	60
Figure 3.9	Experimental device for constrained swelling 2: (a) with no mechanical loading (initially stress-free) and (b) under twist angle θ and axial extension ΔL . For practical purposes during the experiment, the initial distance between two metallic plates is chosen as the initial length L_o .	61
Figure 3.10	Ring-shape specimen for Design 2.	62
Figure 3.11	Detailed dimension of the ring-shape specimen.	63
Figure 3.12	Exploded view of the experimental device and specimen of Design 2.	64
Figure 3.13	Experimental device for constrained swelling 3: (a) with no mechanical loading (initially stress-free) and (b) under twist angle θ and axial extension ΔL .	65
Figure 3.14	Instron uniaxial test machine.	68

Figure 3.15	Cyclic test at constant maximum strain.	69
Figure 3.16	Cyclic test with increasing maximum strain.	69
Figure 3.17	Illustration of the deformation.	71
Figure 3.18	Flow of a complete ABAQUS analysis.	84
Figure 3.19	Global flow in ABAQUS/Standard.	86
Figure 4.1	Volume change of stress-free elastomer specimens (without device) with different carbon black content.	90
Figure 4.2	Rates of swelling of stress-free specimens (without device).	91
Figure 4.3	Volume change of stress-free specimens (with device) with different carbon black content.	92
Figure 4.4	Rates of swelling of stress-free specimens (with device).	92
Figure 4.5	Volume change of elastomer specimens with different carbon black content at $\lambda = 1$.	93
Figure 4.6	Volume change of elastomer specimens with different carbon black content at $\lambda = 1.25$.	94
Figure 4.7	Volume change of elastomer specimens with different carbon black content at $\lambda = 1.5$.	94
Figure 4.8	Volume change of specimens at different tensile strains for unfilled elastomer.	96
Figure 4.9	Volume change of specimens at different tensile strains for filled elastomer (25 wt% carbon black).	96
Figure 4.10	Volume change of specimens at different tensile strains for filled elastomer (40 wt% carbon black).	97
Figure 4.11	(a) Mass change and (b) volume change of NBR after 1 week immersion in palm biodiesel	99
Figure 4.12	(a) Mass change and (b) volume change for different twisting angle.	101
Figure 4.13	Monotonic stress-strain response of dry specimens with different carbon black content.	102
Figure 4.14	Stress-strain curves under monotonic tensile loading.	103
Figure 4.15	Stress-strain curve under 5 cycles of loading for dry specimen ($J_s = 1$).	104
Figure 4.16	Stress-strain curve under 5 cycles of loading for swollen specimen ($J_s = 1.05$).	105
Figure 4.17	Stress-strain curve under 5 cycles of loading for swollen specimen ($J_s = 1.07$).	105
Figure 4.18	Stress-softening in dry and swollen elastomers calculated at second uploading.	107
Figure 4.19	Stress-strain curve under cyclic loading with increasing maximum strain for dry specimen ($J_s = 1$).	108
Figure 4.20	Stress-strain curve under cyclic loading with increasing maximum strain for swollen specimen ($J_s = 1.05$).	108
Figure 4.21	Stress-strain curve under cyclic loading with increasing maximum strain for swollen specimen ($J_s = 1.07$).	109
Figure 4.22	Material responses under cyclic loading with increasing maximum stretch for dry specimen ($J_s = 1$).	110

Figure 4.23	Material responses under cyclic loading with increasing maximum stretch for swollen specimen ($J_s = 1.05$).	110
Figure 4.24	Material responses under cyclic loading with increasing maximum stretch for swollen specimen ($J_s = 1.07$).	111
Figure 4.25	Initial hydrostatic part of Cauchy stress at different radial position for Design 1.	115
Figure 4.26	Stress state under torsion in the specimen for Design 1.	116
Figure 4.27	Average initial hydrostatic part of Cauchy stress at different twisting angle for (a) NBR and (b) NBR without tensile strain.	118
Figure 4.28	Volume change as a function of average hydrostatic component of stress.	120
Figure 4.29	Initial hydrostatic part of Cauchy stress at different radial positions for Design 2.	121
Figure 4.30	Average initial hydrostatic part of Cauchy stress for different twist angles.	122
Figure 4.31	Volume change as a function of average hydrostatic stress for different immersion durations.	123
Figure 5.1	Treated experimental data for dry elastomer ($J_s = 1$)	128
Figure 5.2	Treated experimental data for swollen elastomer ($J_s = 1.05$)	129
Figure 5.3	Treated experimental data for swollen elastomer ($J_s = 1.07$)	129
Figure 5.4	Evolution of the initial volume fraction of the soft domain as a function of degree of swelling.	134
Figure 5.5	Comparison between the proposed model and treated experimental data for dry elastomer ($J_s = 1$).	136
Figure 5.6	Comparison between the proposed model and treated experimental data for swollen elastomer ($J_s = 1.05$).	137
Figure 5.7	Comparison between the proposed model and treated experimental data for swollen elastomer ($J_s = 1.07$).	137
Figure 5.8	Evolution of effective volume fraction of soft phase as a function of maximum tensile strain.	138
Figure 5.9	Model response under uniaxial extension for swollen elastomer ($J_s = 1.1$).	139
Figure 5.10	Model response under uniaxial extension for swollen elastomer ($J_s = 1.15$).	139
Figure 5.11	Model response under uniaxial extension for swollen elastomer ($J_s = 1.2$).	140
Figure 5.12	Evolution of effective volume fraction of soft phase as a function of maximum tensile strain.	140
Figure 5.13	Model response under planar extension for dry elastomer ($J_s = 1$).	142
Figure 5.14	Model response under planar extension for swollen elastomer ($J_s = 1.05$).	143
Figure 5.15	Model response under planar extension for swollen elastomer ($J_s = 1.07$).	143
Figure 5.16	Model response under planar extension for swollen elastomer ($J_s = 1.1$).	144

Figure 5.17 Model response under planar extension for swollen elastomer ($J_s = 1.15$).	144
Figure 5.18 Model response under planar extension for swollen elastomer ($J_s = 1.2$).	145
Figure 5.19 Evolution of effective volume fraction of soft phase under planar extension.	145
Figure 5.20 Model response under equibiaxial extension for dry elastomer ($J_s = 1$).	146
Figure 5.21 Model response under equibiaxial extension for swollen elastomer ($J_s = 1.05$).	146
Figure 5.22 Model response under equibiaxial extension for swollen elastomer ($J_s = 1.07$).	147
Figure 5.23 Model response under equibiaxial extension for swollen elastomer ($J_s = 1.1$).	147
Figure 5.24 Model response under equibiaxial extension for swollen elastomer ($J_s = 1.15$).	148
Figure 5.25 Model response under equibiaxial extension for swollen elastomer ($J_s = 1.2$).	148
Figure 5.26 Evolution of effective volume fraction of soft phase under equibiaxial extension.	149
Figure 5.27 Equilibrium swelling degree vs. filler content.	153
Figure 5.28 Equilibrium swelling degree for different filler content vs. shear modulus of the dry elastomer.	155
Figure 5.29 Illustration of experimental setup for uniaxial constrained swelling.	156
Figure 5.30 Comparison between model and experimental data for stress-free immersion.	161
Figure 5.31 Finite element analysis of the degree of swelling in the equilibrium state for stress-free immersion (unfilled elastomer).	162
Figure 5.32 Finite element analysis of the degree of swelling in the equilibrium state for stress-free immersion (25 % filled elastomer).	162
Figure 5.33 Finite element analysis of the degree of swelling in the equilibrium state for stress-free immersion (40 % filled elastomer).	163
Figure 5.34 Comparison between experimental data, analytical solution and FEA results for stress-free immersion.	164
Figure 5.35 Finite element analysis of the degree of swelling in the equilibrium state for constrained immersion ($\lambda = 1$, unfilled elastomer).	165
Figure 5.36 Finite element analysis of the degree of swelling in the equilibrium state for constrained immersion ($\lambda = 1$, 25 % filled elastomer).	165
Figure 5.37 Finite element analysis of the degree of swelling in the equilibrium state for constrained immersion ($\lambda = 1$, 40 % filled elastomer).	166
Figure 5.38 Finite element analysis of the degree of swelling in the equilibrium state for constrained immersion ($\lambda = 1.25$, unfilled elastomer).	167
Figure 5.39 Finite element analysis of the degree of swelling in the equilibrium state for constrained immersion ($\lambda = 1.25$, 25 % filled elastomer).	168
Figure 5.40 Finite element analysis of the degree of swelling in the equilibrium state for constrained immersion ($\lambda = 1.25$, 40 % filled elastomer).	168
Figure 5.41 Finite element analysis of the degree of swelling in the equilibrium state for constrained immersion ($\lambda = 1.50$, unfilled elastomer).	169

Figure 5.42	Finite element analysis of the degree of swelling in the equilibrium state for constrained immersion ($\lambda = 1.50$, 25 % filled elastomer).	169
Figure 5.43	Finite element analysis of the degree of swelling in the equilibrium state for constrained immersion ($\lambda = 1.50$, 40 % filled elastomer).	170
Figure 5.44	λ_{s1} as a function of position x_{1m} .	171
Figure 5.45	Comparison between FEA results and experimental results.	172

LIST OF TABLES

Table 2.1	Strain energy density functions for hyperelasticity.	25
Table 2.2	Basic properties of diesel and palm biodiesel (Benjumea et al., 2008).	47
Table 3.1	Mechanical loading conditions for Design 1	62
Table 3.2	Mechanical loading conditions for Design 2	65
Table 5.1	Summary of material parameters required in the proposed model.	132
Table 5.2	Values of material parameters used in the proposed model.	135
Table 5.3	Material parameters used in model.	152
Table 5.4	Determination of volume of biodiesel molecule.	159
Table 5.5	Determination of Flory-Huggins interaction parameter.	160

LIST OF SYMBOLS AND ACRONYMS

T_g	Glass transition temperature
phr	parts per hundred
ACN	Acrylonitrile
NR	Natural rubber
NBR	Nitrile butadiene rubber
CR	Polychloroprene
SBR	Styrene butadiene rubber
W	Strain energy density function
\mathbf{F}	Deformation gradient tensor
\mathbf{X}	Material point in the reference configuration
\mathbf{x}	Material point in the current configuration
\mathbf{C}	Right Cauchy-Green tensor
\mathbf{B}	Left Cauchy-Green tensor
$\boldsymbol{\sigma}$	Cauchy stress tensor
q	Lagrange multiplier
U	Internal energy
Q	Heat energy
S	Entropy
A	Helmholtz free energy
λ	Extension ratio
N	Chain density per unit volume
k	Boltzmann constant
G	Shear modulus
T	Absolute temperature
IR	Isoprene rubber
IIR	Butyl rubber
EPDM	Ethylene propylene elastomer
$\hat{\lambda}$	Amplified axial stretch
X	Strain amplification factor
E_o	Elastic modulus of unfilled elastomer
\hat{E}	Elastic modulus of filled elastomer
v_f	Filler volume fraction
ε	Observed elongation
$\hat{\varepsilon}$	Actual elongation
ΔG_1	Gibbs free energy of dilution
ΔS_m	Entropy associated with mixing process
v_1	volume fraction of solvent in mixture
v_2	Volume fraction of elastomer in mixture
n	Number of solvent molecules
x	number of segment of a polymeric chain
R	Gas constant
χ	Flory Huggins interaction parameter
ρ	density
CDM	Continuum damage mechanics
PE	Pseudo-elastic
ASTM	American Society of Testing and Materials
SEM	Scanning electron microscopy
FTIR	Fourier transform infrared

C_o	unswollen-unstressed dry state
C	swollen-stressed state
C_s	swollen-unstressed configuration
\mathbf{F}_s	Swelling part of deformation
\mathbf{F}_m	Mechanical part of deformation
J_s	Degree of swelling
v	Volume occupied by a solvent molecule
c	Number of solvent molecule absorbed per unit dry volume
\mathbf{I}	Identity tensor
μ_o	Chemical potential of unmixed pure solvent
W_s	Free energy due to mixing
W_m	Strain energy function per unit volume of swollen-unstressed state
\mathcal{D}_{int}	Internal dissipation
\mathbf{P}	1st Piola-Kirchhoff stress tensor
μ	Chemical potential
\mathbf{j}	Fluid flux
$\hat{\mathbf{P}}$	Engineering stress with respect to swollen-unstressed configuration
κ	Scalar internal variable
\mathcal{A}_κ	Thermodynamic force associated with κ
v_s	Effective volume fraction of soft phase
FEA	Finite element analysis
γ	Angle of torsion (in rad) per unit length
C	Material parameter
R_i	Inner radius
R_o	Outer radius
R_c	Critical radius
t	Thickness
R_m	Mean radius
\mathcal{L}	Langevin function
$\lambda_{ch,sp}$	Amplified mechanical chain stretch
λ_{ch}	Macroscopic mechanical chain stretch
v_{ss}	Theoretical maximum value of v_s
v_{so}	Initial soft phase volume fraction
M_w	Molecular weight of the solvent
A_v	Avogadro number

LIST OF APPENDICES

Appendix A	User subroutine for UHYPER, UVARM	177
------------	-----------------------------------	-----

CHAPTER 1

INTRODUCTION

1.1 General research background

The worldwide rapid evolution of technology has improved the quality of life and has motivated the development of various industries. However, this intense growth of industries leads to pollution issue and to depletion of natural resources. For instance, fossil fuels which are the main source of energy become scarce. Recently, public awareness on fossil fuels depletion and concern on environmental pollution issue have highlighted the need for alternative renewable energy sources (Abdul Kader & Bhowmick, 2003). Among the available alternatives, biodiesel is gaining popularity owing to its attractive features pertaining to economical, environment and energy considerations. Biodiesel consists of long chain fatty acid methyl esters derived from renewable biological sources such as vegetable oil or animal fat by transesterification process (Leung et al., 2010). The production of biodiesel has increased tremendously since it exhibits comparable fuel properties and offers advantages over conventional diesel (Agarwal, 2007).

Palm oil biodiesel is one of the potential types of biodiesel that being foreseen as a promising alternative for conventional diesel. This is highly beneficial for Malaysia as the world's second largest palm oil producers (Jayed et al., 2011). Overall, the future development on palm biodiesel looks promising, keeping in view that the increasing demand of biodiesel as alternative fuel. However, the main obstacle that limits the usage of biodiesel is its low oxidation stability issue. Oxidation of biodiesel leads to formation of corrosive acids and deposits which results to additional requirement on the material compatibility in the diesel engine (Díaz-Ballote et al., 2009). Indeed, in the case of elastomeric compo-

nents such as seals, pipes, gaskets and o-rings, change in fuel composition often creates a number of problems. Compatibility studies of several types of elastomers in diesel and palm biodiesel have been conducted (Trakarnpruk & Porntangjitlikit, 2008; Haseeb et al., 2010, 2011). However, it is to note that these works only focused on physical degradations related to swelling, hardness and tensile strength of materials. The corresponding degradation may reduce the compatibility and capability of elastomers to perform over required service conditions.

In addition to the environmental factor which causes swelling, many factors are known to influence the durability of elastomeric materials during the service including mechanical loading history, elastomer formulation and constitutive response (Mars, 2001). Studies on the above factors are crucial in order to develop durable elastomeric compounds and to provide a reliable durability analysis of elastomers. For engineering applications involving exposure to aggressive solvent and fluctuating mechanical loading, there are two major degradations to consider: swelling due to diffusion of solvents into elastomer and fatigue damage due to long term cyclic loading. However, majority of existing studies involving fatigue of elastomers only consider the fatigue behaviour in ambient (non-aggressive) environment (Mars and Fatemi (2002) and the works of Verron and Andriyana (2008); Le Cam et al. (2008); Andriyana, Saintier, and Verron (2010); Brieu et al. (2010); Le Cam and Toussaint (2010); Le Cam et al. (2013) among others). Considerably fewer studies which explicitly deal with the fatigue failure analysis of elastomers in aggressive environments are available (Zuyev et al., 1964; Magryta et al., 2006; Hanley, 2008; Abu-Abdeen & Elamer, 2010; Chai, Andriyana, et al., 2013).

Swelling of elastomers under static immersion in solvents have been extensively studied (see Treloar (1975) and references herein). However, investigations on coupled diffusion-deformation problems, i.e. swelling in the presence of multiaxial stress state, are less common. The earliest work dealing with the problem can be found in the work of

Flory and Rehner (1943). Recent works on coupled diffusion-deformation are reported in Rajagopal et al. (1986); Fukumori et al. (1990); Durning and Morman (1993); Baek and Srinivasa (2004); Hong et al. (2008); Soares (2009); Chester and Anand (2010); Duda et al. (2010); Chai et al. (2011). Based on their observations, it is generally reported that swelling is affected by the presence of mechanical loading. The amount of swelling increases under tensile loading while the opposite phenomenon is observed for compressive loading. Nevertheless, the effect of a multiaxial stress state on swelling remains ambiguous as there are not many references found in the literature. Thus, there is a need to investigate and to model the swelling of elastomers due to exposure to biodiesel in the presence of mechanical loading.

The present work investigates the swelling behaviour of elastomers exposed to biodiesel in the absence and in the presence of static mechanical deformations. For this purpose, original specimens and devices are developed so that immersion tests of elastomers in biodiesel can be conducted while the specimens are simultaneously subjected to static mechanical loading. Based on experimental findings, a simple phenomenological model is proposed to capture the degradation of elastomers upon exposure to biodiesel. Being a first attempt, the proposed model is restricted to the prediction of degradation in the equilibrium state without considering the time transient effects. In addition, the proposed model is able to capture the stress-strain response of dry and swollen elastomers particularly Mullins effect under cyclic loading. Other inelastic responses such as hysteresis and permanent set are not considered. Finally, the proposed model is implemented into the commercial finite element code ABAQUS in order to simulate the degradation of elastomers under coupled diffusion-deformation conditions.

1.2 Research objectives

The objectives of this research work can be summarized as follow:

1. To develop original devices for investigating swelling of elastomers in biodiesel in the presence of static mechanical deformations.
2. To investigate the interaction between diffusion of biodiesel and large deformation in elastomers.
3. To develop a simple continuum mechanical model to describe the above interaction.
4. To implement the proposed model in the commercial finite element code ABAQUS in order to simulate the coupling between diffusion of biodiesel and large deformation in elastomeric materials.

1.3 Dissertation organization

This thesis is organized as follows. Chapter 1 provides general background and objectives of the research. Four main objectives are highlighted. Chapter 2 gives a brief literature review relevant to this research. The review provides an introduction on the elastomers and the corresponding mechanical responses under monotonic and cyclic mechanical loading. In addition, factors affecting the durability of elastomers are reviewed. Subsequently, the swelling phenomena of elastomers with emphasis to biodiesel are reviewed. Existing models on coupled diffusion-deformation are also included in the review. Chapter 3 describes the experimental procedures for this research. Experimental works which include the design of specimens and devices, immersion test and mechanical test are provided. In the modeling part, the development of a model consistent with the second law of thermodynamics to capture the coupled diffusion-large deformation is derived. Chapter 4 presents the experimental findings and discussion of the experimental data. Swelling characteristics of elastomers in the absence and in the presence of static mechanical deformation are discussed and the mechanical responses of dry and swollen elastomers are presented. In Chapter 5, the efficiency of the proposed model is assessed

by comparing the theoretical predictions with experimental observations. Finally, Chapter 6 summarizes the current research work and provides suggestions for improvements and directions for future works.

CHAPTER 2

LITERATURE REVIEW

In this chapter, a brief literature review on works relevant to this thesis is presented. The subjects discussed include the general characteristics of elastomer, mechanical responses of elastomers under monotonic and cyclic loading, factors affecting durability of elastomer, swelling phenomena of elastomers in a solvent with emphasis on biodiesel, filler effect in elastomers and discussion on the existing models for coupling of diffusion with large deformations.

2.1 Generality on elastomer

Elastomer, derived from elastic polymer, is a class of polymeric materials having the ability to be deformed to a large deformation when a force is applied to it and it can essentially return to its original shape when the force is released. Being a polymer, it is composed of repeating structural units called monomers. The monomers, which are usually made of carbon, hydrogen, oxygen and silicon, are connected by covalent bonds created during the polymerization process.

Similarly to all polymers, elastomer is highly sensitive to temperature. They exist in two states with respect to the temperature level as shown in Figure 2.1: the glassy state at which the thermal energy level is too low to allow significant molecular mobility, which results in high stiffness and consequently less elasticity, and the rubbery state where the material is much more flexible due to the larger molecular mobility. The temperature at which the transition occurs is referred to as the glass transition temperature, T_g .

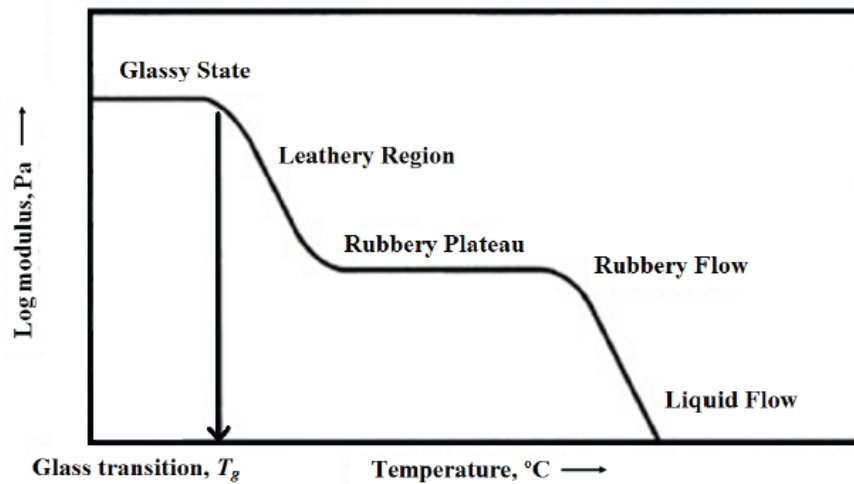


Figure 2.1: Evolution of polymer elastic modulus as a function of temperature (Harper, 1996).

In an unstressed state, elastomers are amorphous polymers existing above their glass transition temperature. Considerable segmental motion is possible and thus they are relatively soft, extremely ductile and having low density at room temperature. Crystallization of elastomers can occur due to deformation as a result from the application of mechanical loading. Figure 2.2 illustrates the molecular chain of an elastomer in a unstressed (amorphous) state (a) and in a stressed state (b).

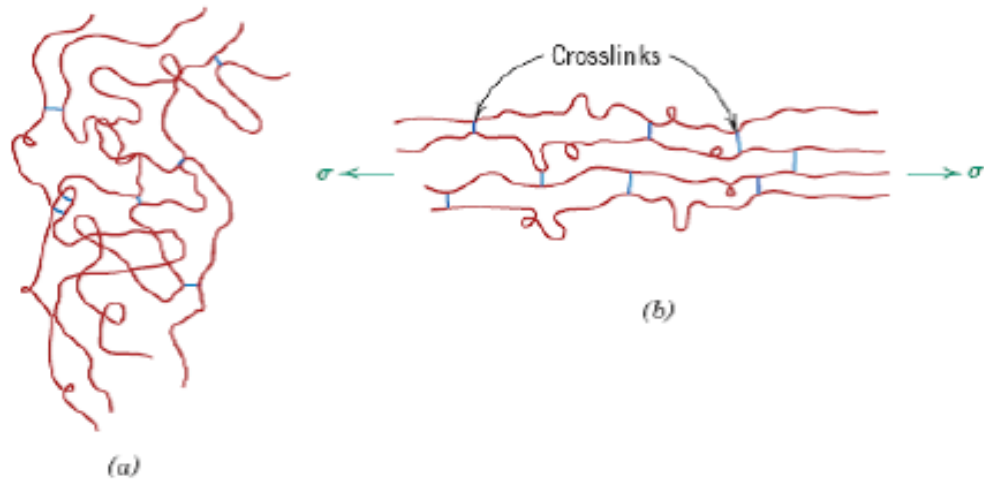


Figure 2.2: Schematic representation of molecular structure in an (a) unstressed state and in a (b) stressed state.

In nature, elastomer can be obtained by harvesting the sap from certain trees in the form of latex. The collected latex is a sticky and milky colloid and is not practically usable unless it is processed with vulcanization and compounded with additives. Major additives used in elastomer compounds include fillers, antioxidants, antiozonants, curing agents and processing aids (Franta, 2012). There are basically two major types of elastomer: natural rubber and synthetic rubber. A brief introduction on natural rubber and some types of synthetic rubber is provided in the following subsection.

2.1.1 Structure of elastomer

The structure of an elastomer can be viewed as a three-dimensional network consisting of randomly coiled chains. Each primary chain is linked to other chains at intersection point known as cross-links. The chains can be linked by either physical or chemical cross-links. Elastomers formed through chemical cross-links are referred as thermosets where the chains are linked through co-polymerization or cross-linking methods (vulcanization) by using suitable vulcanizing agents (sulphur or peroxide) as shown in Figure 2.3. Hence, generally a thermoset may swell when it is in contact with the solvent, but does not dis-

solve (Koleske, 1995).

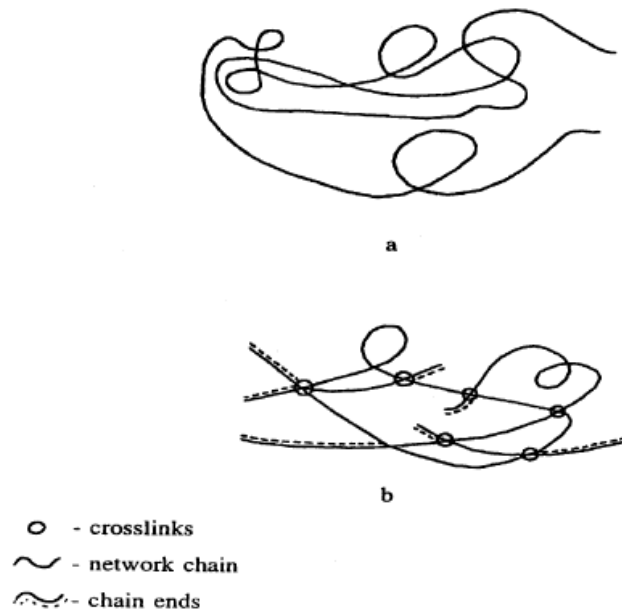


Figure 2.3: Structure of elastomer (a) before vulcanization and (b) after vulcanization (Jha, 2008).

On the other hand, elastomers formed through physical cross-links are referred as thermoplastics where the chains are joined by physical entanglements. The linkage can be obtained through chain adsorption onto the surface of the filler, formation of small crystallites, coalescence of ionic groups or glassy sequences in block copolymers. These linkages are temporary and can be easily breakdown by the presence of a solvent or an increase of temperature. Thus, thermoplastics may dissolve in some suitable solvents especially in the presence of heat (Connell, 2005).

2.1.2 Basic ingredients of elastomer

As mentioned earlier, a number of ingredients are added and compounded to both natural and synthetic rubber in order to obtain the desirable properties. Different combinations can be used based on the application purpose. Typically, the amount of each ingredient is measured based on parts per hundred (phr).

Polymer resin

Being the main ingredient in an elastomer compound, the polymer resin gives the bases for chemical, physical and molding properties. Typical polymers are distinguished by their chemical performance and viscosity rating. An example for a Nitrile (Buna-N) compound is the amount of Acrylonitrile (ACN). The higher the ACN, the better is the oil resistance. The amount of additives added depend on the weight of the polymer resin used. The ratio of additives is normally expressed by weight added per 100 parts by weight of the polymer resin (phr) (Rodgers et al., 2004).

Curing agent (5-10 phr)

The most important ingredient in an elastomer compound is the curing agent which causes the linking of polymeric chains as discussed in the previous subsection. In order to avoid premature cure, they are usually added at the end of the mixing process. Sulphur is the most common curing agent used in elastomer compounds to form carbon-sulphur-carbon bonds and is normally used with accelerators (thiazoles) to facilitate the reaction (Franta, 2012).

Another less common curing agent, e.g. peroxide, forms carbon-carbon bonds. Peroxides decompose on heating to form radicals, which in turns create carbon radicals on the polymer molecules. The carbon radicals then combine to form carbon-carbon bonds. These bonds are more resistant to heat and oxidative attack, thus possess higher service temperatures.

Filler (30-60 phr)

Fillers are originally introduced into the compounding to reduce the cost and to increase stiffness and hardness. Common fillers include carbon blacks, silica and silicates. They are often used as reinforcement in the elastomer to improve the service life of an elastomeric component (Voet, 1980). The simple action of adding fillers enhances the

mechanical properties of cross-linked elastomers such as increased stiffness, modulus, rupture energy, tear strength, tensile strength, cracking resistance, fatigue resistance, and abrasion resistance (Dannenberg, 1975) in many cases. The colour of the elastomeric products is affected by the type of filler used in the compounding where carbon black will produce black color while white clays and some mineral fillers are used to produce the desired colour.

Antioxidant (1-3 phr)

Antioxidants help to protect the compound from thermo-oxidative ageing at high temperature while in use and while the compound is being mixed. They are normally added in small amounts to disrupt the free-radical oxidation reactions that can break the polymers bonds and reduce service life of the compound (Flora, 2009). Examples of antioxidants include amines and phenols.

Antiozonants (1-3 phr)

Antiozonants are used in small amounts to bloom out on the surface and react there, after molding to protect the rubber from ozone attack. Atmospheric ozone often reacts with elastomers containing carbon-carbon double bonds, resulting in breakage of molecules at the surface (Rodgers et al., 2004). An example of an antiozonant is diamine. An alternative protection method is to include paraffin wax in the formulation. The wax forms a protective skin on the surface and a common example can be seen on new tires. The surface of a new tire will have a wax feel or show a slight haze.

Processing aids (5-30 phr)

Various oils are used as processing aids to incorporate all the dry ingredients used in the compounding. They are added to make mixing and extrusion easier. Adding more oil can also lower the hardness of the rubber. Thus, depending on the properties required, the

amount of oils added into the compounding varies from 5-30 phr (Franta, 2012).

2.1.3 Some industrial elastomers

Depending on the composition of the rubber compound, different elastomers with different properties can be produced. Although natural rubber holds an important place in the market, different commercial elastomers known as synthetic rubbers were produced widely especially after World War II. Synthetic rubbers are produced to overcome the limits of natural rubber and are modified by reinforcement with other materials (Franta, 2012). Among the most important synthetic rubbers include Nitrile Butadiene Rubber, Polychloroprene and Styrene Butadiene Rubber. In the following, brief information on the properties of natural rubber and some synthetic rubbers are discussed.

2.1.3 (a) Natural Rubber (NR)

Natural Rubber (NR) can be obtained directly from harvesting the latex of certain trees, predominantly *Hevea brasiliensis* tree. NR is a coagulated form of the latex by adding appropriate additives. The molecular structure of NR consists of polymer chains all having an almost perfect *cis*-1,4-structure as shown in Figure 2.4 and hence it is also known as *cis*-1,4-polyisoprene.

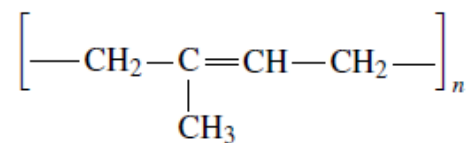


Figure 2.4: Molecular structure of NR.

NR crystallizes upon stretching, resulting in a higher tensile strength and thus exhibits high resistance to crack growth at severe deformation. It serves as an ideal choice for many applications that require good resistance to abrasion. However, it has poor resistance towards heat, ozone, oil and hydrocarbon solvents. Thus, in order to overcome the

limits of NR, various synthetic rubbers were produced to apply at different applications that require certain properties (Rodgers et al., 2004).

2.1.3 (b) Nitrile Butadiene Rubber (NBR)

Nitrile Butadiene Rubber (NBR) is a synthetic rubber copolymer of acrylonitrile (ACN) and butadiene. It is composed of unsaturated copolymers of 2-propenenitrile and various butadiene monomers (1,2-butadiene and 1,3-butadiene). The molecular structure of NBR is shown in Figure 2.5. NBR is prepared by emulsion polymerization using free-radical polymerization. The most important property and advantage of NBR is the high resistance to oil, fuel and other chemicals. The degree of resistance varies considerably with the ratio of acrylonitrile to butadiene. In general, the resistance to oil increases with the increasing acrylonitrile content within the elastomer. However, it is unlikely to have a high composition of acrylonitrile in the elastomer as this will lower the flexibility of the material (Franta, 2012).

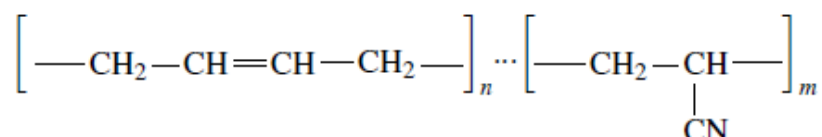


Figure 2.5: Molecular structure of NBR.

In addition to its resistance to oils, it also has good elongation properties as well as adequate resilience, tensile and compression set. As compared to natural rubber, NBR is more resistant to oils and acids, but with poorer strength and flexibility properties. NBR is a general purpose elastomer used as seal energizer or for low pressure applications such as hydraulics and pneumatics. Generally, NBR is used to make hoses, O-rings, pneumatic seals, low pressure hydraulic seals, gaskets, washer, and grommets to handle fuel and oil in automotive and aeronautical industry. Due to its cost of production, NBR is usually

not in consideration for material selections when oil resistance is not a major problem. NBR is generally attacked by ozone, ketones, esters, aldehydes, chlorinated and nitro hydrocarbons. Thus, it does not perform well in applications involving consideration such as weather, ozone, sunlight and flame (Patil & Coolbaugh, 2005).

2.1.3 (c) Polychloroprene (CR)

Similarly to NBR, Polychloroprene (CR) is a synthetic rubber produced by emulsion polymerization of chloroprene using free-radical polymerization. Unlike other elastomers that are vulcanized with sulphur or peroxides, CR is prepared by reacting the chlorine atoms on the chain with active metal oxides. The molecular structure of CR is given in Figure 2.6. Common metal oxides which are used in producing CR include zinc oxide and magnesium oxide.

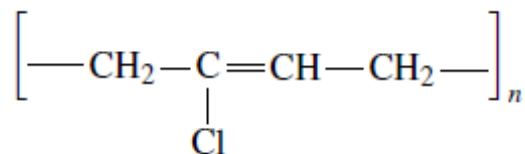


Figure 2.6: Molecular structure of CR.

In general, CR provides good chemical stability and maintains flexibility over a wide temperature range. It is moderately resistant to oil and ozone. CR has a variety of properties that make it popular, including being abrasion-resistant, chemical-resistant, waterproof, stretchable, and buoyant. As compared to other elastomers, CR offers outstanding physical toughness, a wider operating temperature range and excellent resistance to ozone, sun and weather (Dick & Annicelli, 2001).

CR is one of the best all-purpose elastomers and thus making it as the most popular used industrial rubber. It is generally used for bumpers, pads, seating and gaskets in industry applications. CR is generally attacked by strong oxidizing acids, esters, ketones,

chlorinated, aromatic and nitro hydrocarbons (Patil & Coolbaugh, 2005).

2.1.3 (d) Styrene Butadiene Rubber (SBR)

Styrene Butadiene Rubber (SBR) is the most widely used synthetic rubber since it is similar to NR in most of its properties and is the lowest cost and highest volume elastomer available. SBR is synthesized mainly via free radical emulsion polymerization in water with a fatty acid, or anionically in solution with butyl lithium. It consists of a copolymer of butadiene and styrene and the molecular structure is shown in Figure 2.7.

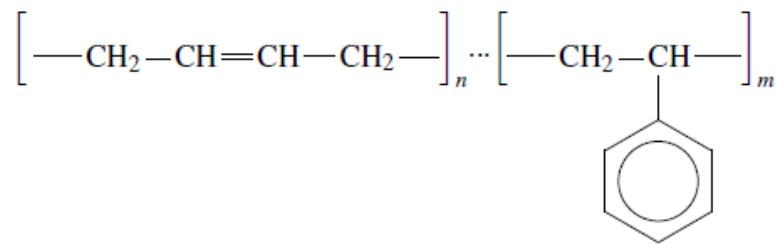


Figure 2.7: Molecular structure of SBR.

Although the physical properties are slightly poorer than those of NR, it is extensively used because it is tougher and has better resistance to heat and flex cracking with significant cost saving. Some applications of SBR include tires, shoes, mechanical goods, sponge and foamed products, hose, and adhesive.

2.2 Mechanical responses of elastomer

In this section, the general mechanical responses of dry elastomer under static monotonic and cyclic loading are discussed. Under cyclic loading, inelastic responses such as hysteresis, stress-softening and permanent set are observed. In addition, a brief discussion on each phenomenon is given.

2.2.1 Mechanical responses under monotonic loading

A typical stress-strain curve for an elastomer under monotonic tensile loading is shown in Figure 2.8. It is observed that the stress-strain response is highly non-linear where there is no constant value of the elastic modulus which can be attributed to the material. Indeed, the elastic modulus varies with increasing extension. In the region of relative small strain, the stress needed to overcome secondary bonding and to stretch the elastomer is low. The high increment in the stress needed at higher strain is due to the primary covalent bonds along the molecular backbone (Gent, 1992).

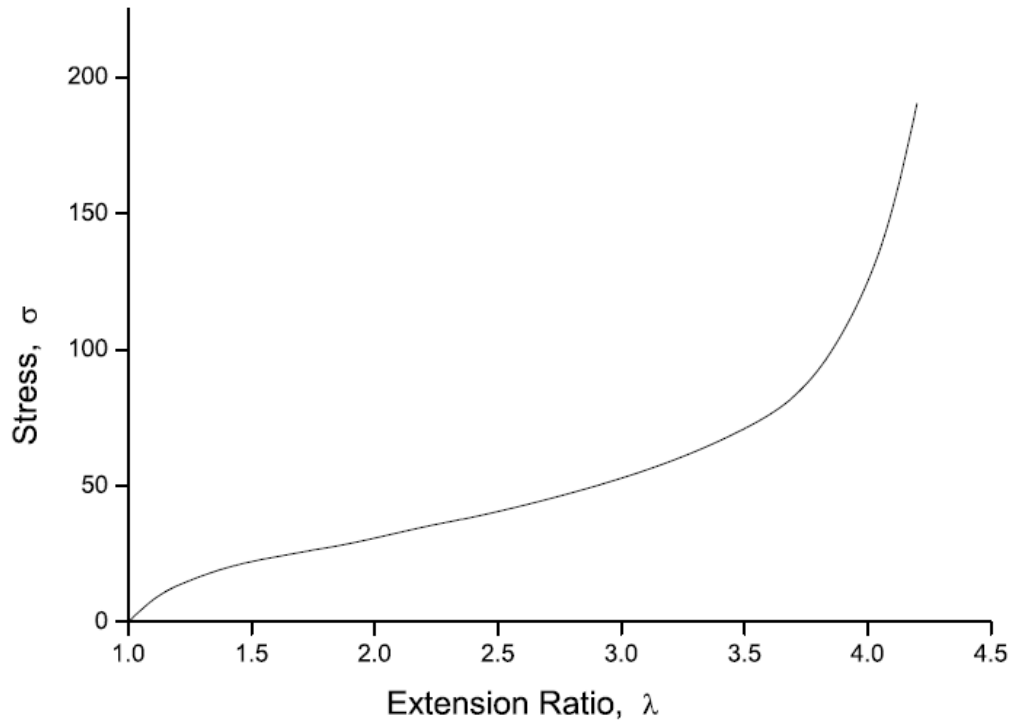


Figure 2.8: Stress-strain response of an elastomer.

The non-linear elastic stress-strain behaviour of elastomer is described using hyperelastic constitutive models. Various models have been proposed with the aim to reproduce the stress-strain responses under different loading conditions (uniaxial, equibiaxial, biaxial, simple or pure shear). Further discussion on hyperelastic constitutive models is given in Section 2.3

2.2.2 Mechanical responses under cyclic loading

Under cyclic loading, an elastomer exhibits strong inelastic responses such as hysteresis, stress-softening (Mullins effect) and permanent set as shown in Figure 2.9. In this figure, the stress-strain responses under simple uniaxial tension and cyclic uniaxial tension with increasing maximum stretch every five cycles are presented. The hysteresis, stress-softening and permanent set are briefly discussed in the following sections.

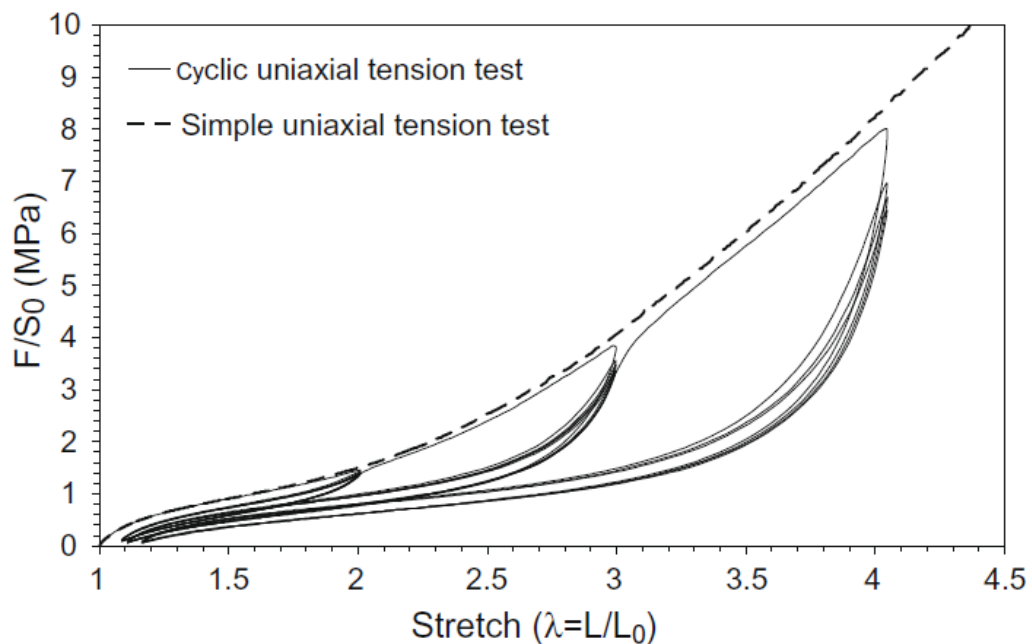


Figure 2.9: Stress-strain responses of a 50 phr carbon black filled SBR under simple uniaxial tension and cyclic uniaxial tension with increasing maximum stretch every 5 cycles (Diani et al., 2009).

2.2.2 (a) *Stress-softening (Mullins effect)*

Stress softening or more commonly known as Mullins effect is the most noticeable loading history-dependent effect observed in the cyclic stress-strain response of an elastomer. This phenomenon was firstly observed by Bouasse and Carrière (1903) and was intensively studied by Mullins (1948) resulting in a phenomenon bearing the name. The stress-strain response resulting from a cyclic, quasi-static deformation conducted by

Mullins is shown in Figure 2.10.

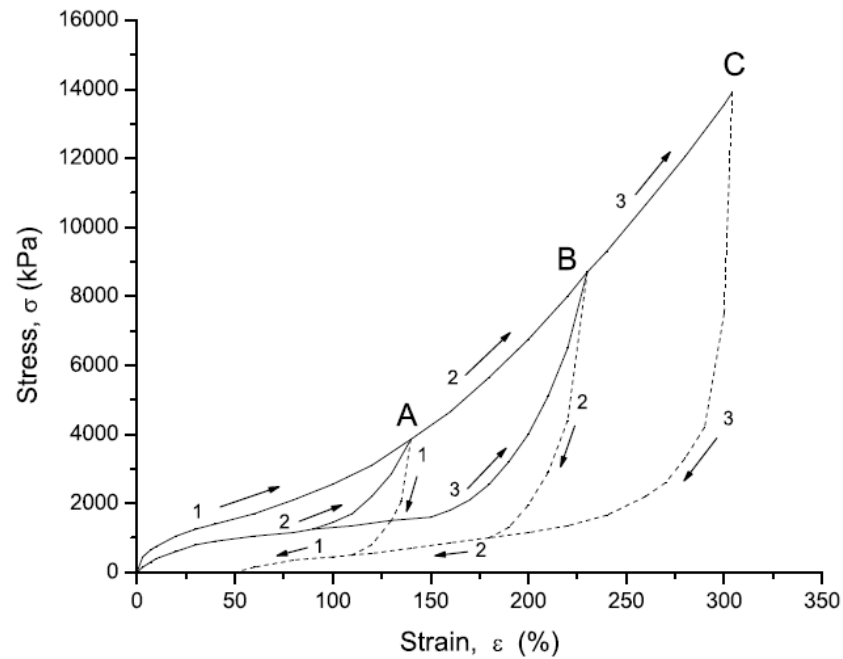


Figure 2.10: Softening of elastomers due to the Mullins effect (Bauman, 2008).

Based on the figure, it is observed that the elastomer exhibits a relatively stiff response during the first loading. On the subsequent unloading and reloading, the material shows significant decrease in the stress level which leads to a softer path as shown by the dashed lines in Figure 2.10. The Mullins effect is characterized by the decrease of the stress level in both the unloading and reloading during the first couples of loading cycles. After several loading cycles, the stress-strain response stabilizes and the following loading cycles merely retrace the path of the stabilized stress-strain curve. Thus, in any design involving elastomeric components under cyclic loading, it is important to consider the Mullins effect in order to prevent undesirable failure. While stress-softening is commonly observed in filled and unfilled crystallized elastomers, no study has reported its occurrence in an unfilled uncrystallized elastomer (Diani et al., 2009).

Several observations were concluded by Diani et al. (2009) from the materials exhibiting softening effect:

1. Most of the softening, which is characterized by a lower resulting stress for the same applied strain, appears after the first load.
2. After a few cycles (values up to 10 are reported in the literature depending on the material nature), the material responses coincide during the following cycles, aside from a fatigue effect.
3. The softening appears for stretches lower or equal to the maximum stretch ever applied.
4. When the extension exceeds the maximum extension previously applied, the materials' stress-strain response returns on the same path than the monotonous uniaxial tension test stress-strain response after a transition, which increases with the amount of strain.
5. The softening increases progressively with the increasing maximum stretch.

2.2.2 (b) *Hysteresis*

Hysteresis is a phenomenon characterized by the difference in stress between the uploading and unloading stress-strain curve experienced by the elastomer in the same loading cycle. This phenomenon is depicted in Figure 2.11. The difference in stress determines the amount of energy dissipated during cyclic deformation. It can be related to either viscoelasticity (Bergström & Boyce, 1998), viscoplasticity (Lion, 1996, 1997) and strain-induced crystallization (Trabelsi et al., 2003) depending on the material. For a filled elastomer, hysteresis loss may be attributed to:

1. Molecular friction accompanying deformation of the elastomer phase (Dannenberg, 1966).
2. Polymer-filler detachment.

3. Breakdown of filler structure and weak polymeric chains (Kar & Bhowmick, 1997).

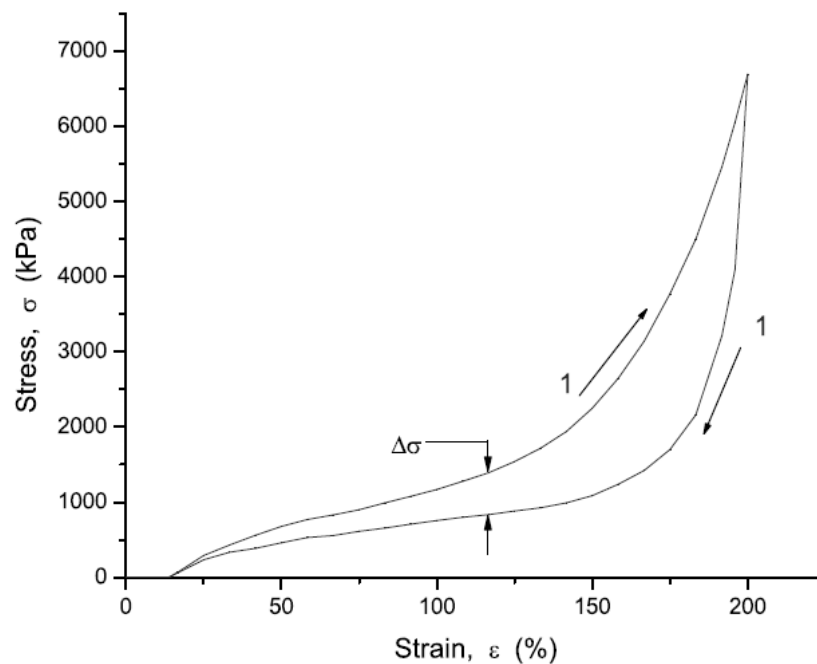


Figure 2.11: Cyclic loading of tensile specimen exhibiting hysteresis (Bauman, 2008).

Hysteresis loss increases with strain rate, strain level and the amount of filler content. Conversely, it decreases with increasing temperature and increasing mean strain (Mills & Walker, 1980). In addition, larger hysteresis loss is reported in the crack tip region and it is likely the main contributor to tearing energy at high crack growth rates (Tsunoda et al., 2000). Under cyclic mechanical loadings, the hysteresis is significantly larger for the first loading cycle and subsequently the amount of hysteresis reduces and stabilizes (Yamaguchi et al., 2003). Recently, a number of works focusing on the relation between hysteresis and fatigue life of elastomers have been conducted (See works of Ayoub et al. (2010); Zaïri et al. (2008, 2005)).

2.2.2 (c) *Permanent set*

Permanent set is a phenomenon which refers to the residual strain after the elastomer is being loaded and unloaded. The graphical representation is shown in Figure 2.12. Permanent set occurs during unloading and it is a phenomena caused by the resistance

by the new bonds formed by the rupture chain segments from the deformation when the material deforms back to the original shape (Marin, 1962). However, the effect of permanent set decreases slowly with time and essentially disappears after a sufficiently large period of annealing (Dorfmann & Ogden, 2004). The amount of permanent set depends on the time in the deformed state, the amount of carbon black in the material and also on the maximum elongation attained by the elastomer prior to unloading.

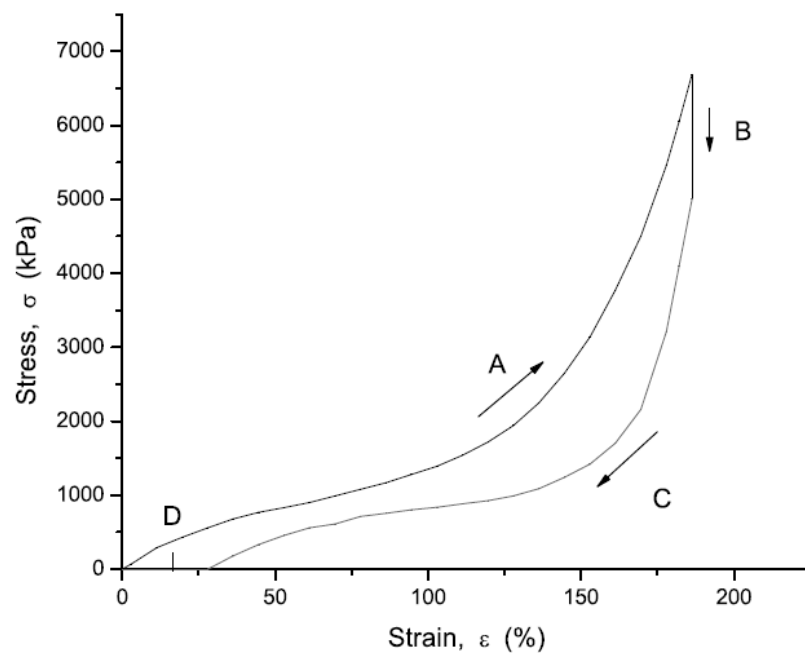


Figure 2.12: Permanent set in elastomer observed after loading and unloading (Bauman, 2008).

Under cyclic loadings, the major part of permanent set is generated during the first unloading cycle. The magnitude of permanent set continues to increase through the subsequent unloading cycles but eventually it reaches a constant value (Dorfmann & Ogden, 2004). The magnitude of permanent set for unfilled elastomers is relatively small and often negligible. However, for filled elastomers the effect is significant and increases with the amount of filler in the elastomer (Lion, 1996).

2.3 Constitutive equations for hyperelastic materials

While the stress-strain behaviour can be observed through experimental work, mathematical models can be developed through constitutive theories to represent the real behaviour of the material. There is a large number of constitutive theories available in the literature. For instance, the readers can consult contributions from Truesdell and Noll (1992) and Barenblatt and Rivlin (1997). Obviously, interests are laid on the development of a model that (Mars, 2001):

1. reproduces a good fit to the observed stress-strain responses under different strain states.
2. minimizes the number of material parameters determined through experimental data.
3. is physically meaningful.

Depending on the approach used to develop the strain energy density function, hyperelastic constitutive models can be classified into three major types (Marckmann & Verron, 2006):

1. Phenomenological models. The models are developed based on mathematical developments of the strain energy function W without the considerations of the microstructure and the molecular nature of the material. Generally, the material parameters used in the models do not have any physical meaning. Moreover, there is a limitation with such models when they are used out of the deformation range in which the parameters were identified. Examples of models developed based on this approach are Fung, Mooney-Rivlin, Odgen, Generalized-polynomial and Yeoh.
2. Physically-based models. The models are developed from physical motivation based on both physics of polymer chain network and statistical thermodynamics

considerations. Different strain energy functions depending on the assumptions made are developed to describe the mechanical responses. The mathematical formulation is relatively complex in most of the models. However, the parameters used in the models generally contain physical meaning. Typical models based on this approach are Neo-Hookean, 3-chain and 8-chain(Arruda-Boyce) models.

3. Hybrids of phenomenological and physically-based models. Examples of models under this category include Gent and Van der Waals models.

Phenomenological models

Using the phenomenological approach, the mechanical responses of the elastomer are usually described by postulating the existence of a strain energy density function (W) which depends on the deformation gradient tensor \mathbf{F} :

$$W = W(\mathbf{F}) \quad (2.1)$$

The deformation gradient tensor is defined by:

$$\mathbf{F} = \text{Grad}\mathbf{x} = \frac{\partial \mathbf{x}}{\partial \mathbf{X}} \quad (2.2)$$

In the above expression, \mathbf{X} is the material point in the reference configuration and \mathbf{x} represents the position of the same material point in the current configuration. Considering the objectivity principle, W can be written as a function of the right or left Cauchy-Green tensors, given by $\mathbf{C} = \mathbf{F}^T\mathbf{F}$ and $\mathbf{B} = \mathbf{F}\mathbf{F}^T$ respectively, i.e.:

$$W = W(\mathbf{B}) \quad \text{or} \quad W = \hat{W}(\mathbf{C}) \quad (2.3)$$

By assuming the isotropy of the material, the invariants of \mathbf{B} and \mathbf{C} are equal and W can be further expressed as a function of them:

$$W = W(I_1, I_2, I_3) \quad (2.4)$$

where,

$$I_1 = \text{tr}\mathbf{B} \quad I_2 = \frac{1}{2}(I_1^2 - \text{tr}(\mathbf{B}^2)) \quad I_3 = \det(\mathbf{B}) \quad (2.5)$$

Elastomers are often considered as incompressible and thus there is no significant volume change during the deformations, i.e. $I_3 = 1$. Therefore, the strain energy depends only on the first and second invariants: $W = W(I_1, I_2)$. Finally, by considering the second law of thermodynamics, it can be shown that the Cauchy stress tensor σ is given by (Holzapfel, 2000),

$$\sigma = q\mathbf{I} + 2 \left[\frac{\partial W(I_1, I_2)}{\partial I_1} + I_1 \frac{\partial W(I_1, I_2)}{\partial I_2} \right] \mathbf{B} - 2 \frac{\partial W(I_1, I_2)}{\partial I_2} \mathbf{B}^2 \quad (2.6)$$

where q is an arbitrary scalar (Lagrange multiplier) due to the incompressibility assumption. It can be determined from the equilibrium equations taking into account appropriate boundary conditions. As shown in Equation (2.6), the stress response can be entirely determined once the form of hyperelastic strain energy density W is postulated. Table 2.1 summarizes some of the well-known strain energy density function for hyperelastic models.

Physically-based models

Physically-based models are founded on the microscopic response of polymer chains in the network. The expression for each model differs from each other depending on the assumptions made to reproduce the response (Marckmann & Verron, 2006). The fundamental relations can be obtained from the laws of thermodynamics. The first law of

Table 2.1: Strain energy density functions for hyperelasticity.

Model	Year	Equation
Mooney-Rivlin	1940	$W = C_{10}(I_1 - 3) + C_{01}(I_2 - 3)$
Neo-Hookean	1943	$W = \frac{G}{2}(I_1 - 3), \quad G = nkT$
3-chain	1943	$W = nkT \left[\frac{\lambda}{\sqrt{N}}\beta + \ln \frac{\beta}{\sinh \beta} \right], \quad \beta = \mathcal{L}^{-1} \left(\frac{\lambda}{\sqrt{N}} \right)$
Gent and Thomas	1958	$W = C(I_1 - 3) + C_2 \ln \left(\frac{I_2}{3} \right)$
Ogden	1972	$W = \sum_{n=1}^N \frac{\mu_n}{\alpha_n} (\lambda_1^{\alpha_n} + \lambda_2^{\alpha_n} + \lambda_3^{\alpha_n} - 3)$
Van der Waals	1986	$W = G \left[-(\lambda_m^2 - 3)[\ln(1 - \Theta) + \Theta] - \frac{2}{3} \left(\frac{\bar{I} - 3}{2} \right)^{3/2} \right]$
Yeoh	1993	$W = C_{10}(I_1 - 3) + C_{20}(I_1 - 3)^2 + C_{30}(I_1 - 3)^3$
Arruda-Boyce	1993	$W = G \left(\frac{1}{2}(I_1 - 3) + \frac{1}{20\lambda_m^2}(I_1^2 - 9) + \frac{11}{1050\lambda_m^4}(I_1^3 - 27) + \frac{19}{7000\lambda_m^6}(I_1^4 - 81) + \frac{519}{673750\lambda_m^8}(I_1^5 - 243) + \dots \right)$
Gent	1996	$W = -\frac{E}{6}(\lambda_m - 3) \ln \left[1 - \frac{I_1 - 3}{\lambda_m - 3} \right]$

thermodynamics provides the definition of internal energy:

$$dU = \delta Q + \delta W \quad (2.7)$$

where δQ is the heat absorbed by the system and δW is the work done by external forces.

For any reversible process, the second law defines the entropy change dS as:

$$TdS = \delta Q \quad (2.8)$$

Hence, the combination of these two equations leads to:

$$dU = TdS + \delta W \quad (2.9)$$

In discussing the equilibrium of reversible system, it is convenient to introduce the Helmholtz free energy A , which is defined by the relation:

$$A = U - TS \quad (2.10)$$

For a change taking place at constant temperature:

$$dA = dU - TdS \quad (2.11)$$

By replacing Equation (2.11) into (2.9), we obtain:

$$dA = dW \quad (\text{constant temperature}) \quad (2.12)$$

which implies that in a reversible isothermal process the change in Helmholtz free energy is equal to the work done on the system by external forces.

Next, in order to obtain the constitutive model, the simplest case is considered where a unit cube is subjected to homogeneous deformation with three principal extension ratios λ_1, λ_2 and λ_3 . For Gaussian network, the change in entropy ΔS due to deformation is given by:

$$\Delta S = -\frac{1}{2}Nk(\lambda_1^2 + \lambda_2^2 + \lambda_3^2 - 3) \quad (2.13)$$

where N is the chain density per unit volume and k is the Boltzmann constant. The Helmholtz free energy can be obtained by assuming that there is no change of internal energy during deformation, i.e. $A = -T\Delta S$ and hence:

$$A = \frac{1}{2}NkT(\lambda_1^2 + \lambda_2^2 + \lambda_3^2 - 3) = \frac{1}{2}G(\lambda_1^2 + \lambda_2^2 + \lambda_3^2 - 3) \quad (2.14)$$

where $G = NkT$ and is commonly known as the shear modulus of the material. The above expression of A is known as neo-Hookean model.

2.4 Factors affecting durability of elastomer

There are many factors which influence the durability of elastomeric components including the mechanical loading history, the environment and the elastomer compound-

ing (Mars, 2001). An in depth understanding of these factors is necessary to predict the fatigue life of the elastomer accurately and to design an efficient and reliable elastomeric component. In this section, the influence of these factors on the durability of elastomeric components is briefly discussed.

2.4.1 Mechanical loading history

The mechanical loading history is usually characterized by several parameters such as maximum, minimum, alternating and mean loading. The stress-strain response of an elastomeric component is highly dependent on the mechanical loading history. One of the most significant characteristics of an elastomer which depends on the maximum load attained previously is the Mullins effect (see Section 3.2.3). On the other hand, the effect of minimum or mean loading depends on the type of elastomer and filler used. For elastomers which exhibit strain crystallization such as natural rubber, the increase in the minimum strain at constant maximum strain improves the durability of the elastomer (Fielding, 1943). However, this phenomenon is not observed for non-crystallizing elastomers. In addition, the frequency of loading is also an important factor which affects the lifetime of an elastomeric components. High loading frequency shortens the lifetime by creating additional thermal energy in the material which causes severe degradation (Becker et al., 1998). It is to note that while there are many attempts to obtain understanding on the effects of mechanical loading history on the durability of elastomer, there is still lack of understanding on the effects of multiaxial loading mostly due to the difficulties in conducting experimental works (Mars, 2001). In real life application, elastomeric components rarely operate under simple mechanical loading and thus there is a great need for the ability to determine the effects of multiaxial loading on the failure of elastomers.

2.4.2 Environment

The environment during service plays an important role in determining the durability of elastomers. Indeed, in reality elastomeric components are often in contact with various chemical reactants and operate under high temperature conditions. High temperature possess a deleterious effect on elastomers, in particularly to non strain-crystallizing elastomers (Lake & Lindley, 1964). Elevated temperature stimulates chemical reactions such as oxidation that can cause additional degradation in elastomers. Oxidation causes aging which leads to embrittlement and reduced the resistance to failure and thus, shorter fatigue life (Blackman & McCall, 1970). Another major consideration from the service environment is the chemical reactants such as acidic gaseous or aggressive solvents.

2.4.3 Elastomer compounding

The compounding of a synthetic elastomer includes the polymer resin and additives such as filler, antioxidants, antiozonants, vulcanizing agent, curing agent and processing oil. The mechanical properties of elastomers can be varied by modifying the compounding formulation and the manufacturing process. Primary consideration on the selection of elastomeric component is the type of elastomer. The service life of an elastomeric component is highly affected by the strain crystallization as mentioned in Sections 2.4.1 and 2.4.2. Elastomers that exhibit strain crystallization include natural rubber (NR), polychloroprene (CR) and isoprene rubber (IR) while nitrile butadiene rubber (NBR), styrene butadiene rubber (SBR), butyl rubber (IIR) and ethylene propylene elastomer (EPDM) show little or no strain crystallization (Gent, 1992). In addition, the incorporation of filler in the elastomer compounding has a pronounced effect to the elastomer properties depending on two factors: the type of the filler used and the volume fraction of filler in the elastomer. The effect of filler will be discussed in detail in the following section.

2.5 Fillers in elastomer and strain amplification factor

Generally, filler is initially introduced into the elastomer to reduce the production cost and to increase the stiffness and other properties such as tensile strength and resistance to abrasion, tear, fatigue and cracking (Voet, 1980). The addition of a small amount of filler into the elastomer can have a strong influence on its mechanical response particularly the inelastic responses such as the Mullins effect, hysteresis and stress relaxation. However, the mechanism by which the macroscopic stress-strain behaviour is affected by the filler is often a subject of debate. Two main discussions are available in the literature about the effect of filler on the overall mechanical response: molecular level explanation and continuum level explanation. From the molecular level standpoint, filler increases the crosslink density since additional crosslinking takes place at the filler-matrix interface (Bueche, 1960) and the segmental mobility is reduced around the filler particles (Kraus, 1978). Other considerations from the molecular level include the size, shape and structure of the filler (Mullins, 1950). Meanwhile for the continuum level, the presence of filler is postulated as strain amplifier for the elastomeric matrix around the filler.

Mullins and Tobin (1957) considered filled elastomer as if it is a composite system with the concept of amplified strain. Based on this concept, fillers are considered as rigid particles which do not participate in the deformation when a macroscopic strain/stretch is applied to the elastomer. As a result, the average strain in the elastomer matrix is amplified over the macroscopic applied strain since the rigid fillers contribute little or none to the deformation.

For uniaxial tensile stress-strain behavior, the amplified axial stretch is given by:

$$\hat{\lambda} = 1 + X(\lambda - 1) \quad (2.15)$$

where X is the strain amplification factor which depends on the filler volume fraction,

shape and distribution while λ is the macroscopic axial stretch. The amplification factor is based on the original work of Einstein (1906) who investigates the enhancement of the viscosity of a particle-filled liquid. Following these works, Smallwood (1944) estimated that the amplification factor of fillers in the elastic modulus of the elastomer is similar to the enhancement of the viscosity of liquids. Thus, the effective elastic modulus is given by:

$$\hat{E} = E_o(1 + 2.5v_f) \quad (2.16)$$

where \hat{E} and E_o are the elastic moduli of the filled and unfilled elastomer respectively and v_f is the filler volume fraction.

While Equation (2.16) is shown to be fitted well with the observed elastic behaviour of elastomers containing a low volume fraction of filler ($v_f < 0.1$), serious departures are observed for higher volume fraction of filler. Guth (1945) suggested that this deviation can be improved by considering the interactions between the neighbouring filler particles and proposed the well-known Guth-Gold model for an elastomer incorporated with spherical rigid filler particles (Guth & Simha, 1936; Guth & Gold, 1938):

$$\hat{E} = E_o(1 + 2.5v_f + 14.1v_f^2) \quad (2.17)$$

Various attempts are available in the literature for the modification of the strain amplification factor. Other than the amplification factor proposed by Einstein (1906) and Guth and Gold (1938), Nielsen (1966) derived an equation to describe the relation between the actual microscopic elongation of the elastomer relative to the observed elongation of a filled elastomer based on a calculation similar to that used by Bueche (1960) to explain the Mullins effect, given by,

$$\hat{\epsilon} = \epsilon \left(\frac{1}{1 - v_f^{1/3}} \right) \quad (2.18)$$

where $\hat{\varepsilon}$ is the actual microscopic elongation and ε is the observed elongation. Note that Equation (2.18) is equal to Equation (2.15) with $X = \frac{1}{1-v_f^{1/3}}$. Although in Mullins and Tobin (1957), the amplification factor is only applied to the uniaxial stretch, this theory was further extended and generalized to three dimensional deformation states by Bergström and Boyce (1999) by applying the amplification factor to the first invariant of the right Cauchy-Green strain tensor, $I_1 = \text{tr}(\mathbf{C})$:

$$\hat{I}_1 = 3 + X(I_1 - 3) \quad (2.19)$$

where \hat{I}_1 is the amplified first invariant and the amplification factor X chosen from any of the available models as discussed above.

2.6 Swelling of elastomer

Both natural and synthetic elastomers possess the ability to swell in suitable solvents. During swelling, the diffusion of small molecules from the solvent into the elastomer leads to the expansion of the three dimensional polymer network and this phenomenon is known as swelling (Treloar, 1975). The swelling phenomenon is viewed as one form of degradation experienced by elastomers since the increase in the distance between two chains leads to the reduction of secondary bonding (Callister, 1997), which in turns reduces the strength of the elastomers. Swelling in elastomers can be measured in terms of mass or volume change (Flory, 1942; Treloar, 1975). Based on their nature of interaction, elastomers can be broadly divided into two classes, namely water-swelling and organic-liquid-swelling classes. The first group includes cellulose, proteins, etc while the second group includes elastomers and organic high polymers (Treloar, 1975). In this section, the physical description of swelling is given. The thermodynamics of swelling and the elastic properties of swollen elastomers are recalled and discussion on the effect of deformation

on swelling is provided with the examples of some existing works from the literature.

2.6.1 Physical descriptions

From the physical point of view, swelling in elastomers takes place through diffusion which involves two processes (George & Thomas, 2001):

1. The solvent molecules first occupy the polymer surface until reaching a concentration through adsorption.
2. The solvent molecules penetrate further into the depth of the polymer network until reaching equilibrium swelling by adsorption.

Since swelling is a diffusion-controlled process, increasing the thickness of the elastomer and viscosity of the solvent will increase the resistance to swelling of an elastomeric component (Gent, 1992).

2.6.2 Thermodynamics of swelling

The main concern about swelling of elastomers in solvent is the equilibrium swelling at constant temperature and pressure. For this purpose, the equilibrium between two phases has to be considered where the solvent is the pure phase while the mixed phase is the elastomer. The free energy resulting from swelling can be described by the Gibbs free energy of dilution, ΔG_1 which can be expressed in a separable form consisting of the heat of dilution, ΔH_1 and the entropy of dilution, ΔS_1 .

$$\Delta G_1 = \Delta H_1 - T\Delta S_1 \quad (2.20)$$

Equation (2.20) is expressed in terms of the energy per unit mole of solvent transferred.

In this expression, the heat of dilution is defined as,

$$\Delta H = \Delta U + p\Delta V \quad (2.21)$$

where U is the internal energy, p is the pressure and V is the volume. When p is the atmospheric pressure, the value of $p\Delta V$ becomes rather small and thus negligible. In this case, ΔH and ΔU are practically equivalent based on Equation (2.21). Equilibrium is achieved when the free energy with respect to the changes in the composition of the phases is minimum. In other words, the free energy due to the transfer of a small quantity of solvent molecules from the pure phase to the mixed phase shall be zero (Treloar, 1975).

Thus,

$$\Delta G_1 = 0 \quad \Leftrightarrow \quad \Delta U = T\Delta S_1 \quad (2.22)$$

The significance of thermodynamics quantities on swelling was verified through experimental data of Gee and Treloar (1942) for unvulcanized natural elastomer in benzene where the entropy of dilution, the free energy and the heat of dilution are plotted as a function of the solvent volume fraction. It was shown from the experimental data that the term $T\Delta S_1$ is always positive and relatively large while the heat term ΔH_1 is rather small (Treloar, 1975). Thus, the conclusion was drawn that the driving force for a swelling process is the associated entropy while the heat of dilution being relatively unimportant. The entropy is related directly to the configurational arrangements of the molecules and is greatly affected by the length of the molecules. The increase in entropy may be calculated by the number of configurations available to the system at any given composition. A simple calculation was proposed by Flory (1942) and Huggins (1942b) where the solvent and elastomer molecules are considered to be arranged on a three-dimensional lattice of sites.

The vacant site may be occupied either by a solvent molecule or by a single segment of the elastomer chain. Under this theory, the entropy associated with the mixing process is given as

$$\Delta S_m = -k(n \ln v_1 + N \ln v_2) \quad (2.23)$$

where k is the Boltzmann's constant, v_1 and v_2 are the respective volume fractions of solvent and elastomer in the mixture while n and N are the number of solvent molecules and elastomer molecules respectively. Following this, the entropy per mole of dilution with respect to the solvent component can be written as

$$\Delta S_1 = -R[\ln(1 - v_2) + (1 - 1/x)v_2] \quad (2.24)$$

where x is the number of segments of a polymeric chain and R is the gas constant. To obtain the free energy of dilution ΔG_1 , Flory (1942) introduced an expression for the heat of dilution ΔH_1 ,

$$\Delta H_1 = \alpha v_2^2 \quad (2.25)$$

and the total free energy of dilution in Equation (2.20) becomes

$$\Delta G_1 = RT[\ln(1 - v_2) + (1 - 1/x)v_2 + (\alpha/RT)v_2^2] \quad (2.26)$$

On the other hand, an alternative theory proposed by Huggins (1942b) suggests a more precise analysis of the number of sites available to segments of the elastomer molecule subsequent to the third segment. The expression of the entropy of dilution contains an additional term in v_2^2 and therefore the resultant free energy of dilution becomes

$$\Delta G_1 = RT[\ln(1 - v_2) + (1 - 1/x)v_2 + \chi v_2^2] \quad (2.27)$$

where χ may be written as:

$$\chi = \chi_o + \alpha/RT \quad (2.28)$$

in which χ_o and α are constants. In the case where the number of segments in the elastomeric chain is sufficiently large, $1/x$ becomes very small and Equations (2.26) and (2.27) reduce to:

$$\Delta G_1 = RT[\ln(1 - v_2) + v_2 + \chi v_2^2] \quad (2.29)$$

This expression is generally known as the Flory-Huggins mixing equation (Treloar, 1975). This equation contains only one single parameter χ which is dependent on the particular solvent-solid combination. This suggests that there is no restriction introduced by the lattice model, and the resulting equation has a degree of generality exceeding that which would be strictly justified on the basis of the model (Treloar, 1975).

2.6.3 The elastic properties of a swollen elastomer

To define the effect of swelling on the mechanical properties of a cross-linked elastomer, Treloar (1975) proposed that the dry elastomer is in the form of a cube of unit edge length which contains N chains per unit volume. The degree of swelling is defined in terms of the volume fraction of the elastomer, v_2 in the mixture phase of elastomer and solvent where the volume swelling ratio is $1/v_2$ with respect to the dry state. Using this definition, the corresponding linear stretch of the swollen elastomer can be written as:

$$\lambda_o = 1/v_2^{1/3} \quad (2.30)$$

by assuming the material undergoes isotropic swelling. Note that the parameter v_2 is introduced to define the state of swelling, regardless of whether or not this state is the equilibrium state. In addition, the nature of the solvent is not considered in the development of the theory.

Swelling is an isotropic expansion of the polymeric network which is accompanied by a reduction in the network entropy. Any additional stress to the swollen elastomer will result in a further reduction of entropy due to the deformation of the swollen network. Thus, the total reduction of entropy for the transformation from the initial unswollen-unstressed state to the final swollen-stressed state is the sum of two contributions: purely swelling and the subsequent mechanical loading.

Consider that the original unit cube swells in the ratio $1/v_2$ and is subsequently deformed to dimensions l_1, l_2 and l_3 . For the Gaussian network, the total entropy, $\Delta S'_o$ with respect to the unswollen-unstressed state can be written in the form:

$$\Delta S'_o = -\frac{1}{2}Nk(l_1^2 + l_2^2 + l_3^2 - 3) \quad (2.31)$$

The change in the entropy, ΔS_o associated with the isotropic swelling in the ratio λ_o in the absence of stress is:

$$\Delta S_o = -\frac{1}{2}Nk(3\lambda_o^2 - 3) = -\frac{1}{2}Nk(3v_2^{-2/3} - 3) \quad (2.32)$$

The difference between these two quantities gives the entropy of deformation, $\Delta S'$ of the swollen network:

$$\Delta S' = \Delta S'_o - \Delta S_o = -\frac{1}{2}Nk(l_1^2 + l_2^2 + l_3^2 - 3v_2^{-2/3}) \quad (2.33)$$

This expression is often more convenient to be expressed in terms of the extension ratios λ_1, λ_2 and λ_3 referred to the swollen-unstressed state. By writing $l_1 = \lambda_1\lambda_o = \lambda_1v_2^{-1/3}$, the expression defined per unit volume of the unswollen-unstressed state becomes:

$$\Delta S' = -\frac{1}{2}Nkv_2^{-2/3}(\lambda_1^2 + \lambda_2^2 + \lambda_3^2 - 3) \quad (2.34)$$

Therefore, the entropy of deformation, ΔS defined per unit volume of the swollen-unstressed state is given by:

$$\Delta S = v_2 \Delta S' = -\frac{1}{2} N k v_2^{1/3} (\lambda_1^2 + \lambda_2^2 + \lambda_3^2 - 3) \quad (2.35)$$

The corresponding free energy function thus becomes:

$$A = -T \Delta S = \frac{1}{2} N k T v_2^{1/3} (\lambda_1^2 + \lambda_2^2 + \lambda_3^2 - 3) \quad (2.36)$$

Comparison with strain energy function for dry elastomers in Equation (2.14) shows that both equations have the same form, except for the factor $v_2^{1/3}$ in the modulus. Thus, if G and G' are denoted as the shear modulus for the dry and the swollen elastomer respectively, we can write:

$$G' = G v_2^{1/3} = \frac{\rho R T}{M_c} v_2^{1/3} \quad (2.37)$$

where ρ is the density in the unswollen state. This result implies that the effect of swelling leads to a reduction of the modulus in inverse proportion to the cube root of the swelling ratio, without changing the form of the stress-strain relation. Recent works by Chai et al. (2011) showed a deviation from the above relation for elastomers swollen in biodiesel.

2.6.4 Effect of deformation on swelling

Swelling of elastomers under more complex conditions where there is a presence of stress or mechanical restraint was first discussed by Flory and Rehner (1944) and also by Gee (1946) for the case of simple tensile stress. It was found that the elastomer absorbs more solvent in the presence of tensile stress, compared with that for the stress-free elastomer. Following this, Treloar (1950, 1975) discussed the theory for the general case of homogeneous strain. Equations for uniaxial extension, bi-axial extension and uniaxial

compression were developed. In the development of the theory, the total free energy is considered to be the sum of two terms: one corresponds to the mixing of the polymer network and the solvent molecules and the other corresponds to the free energy of deformation. A number of works have been conducted to study the effect of deformation on swelling since then and few examples will be discussed here.

Fukumori et al. (1990) studied the effects of tensile strain on the swelling behaviour of acrylonitrile-butadiene copolymer rubber vulcanizates by real-time pulsed nuclear magnetic resonance (n.m.r.) measurements and volume swelling measurements at equilibrium. From the n.m.r. measurements, the initial swelling rate and the swelling ratio at equilibrium were shown to increase with tensile strain. The presence of reinforcing fillers in the rubber matrix was observed to restrict the increase of the swelling rate through some oriented structure induced by stretching. On the other hand, the reinforcing fillers were proposed to cause a strain amplification effect. This causes the increase of the average local strain in the rubber matrix, thereby enhances the swelling ratio more remarkably proportional to the filler concentration as compared with that of the unfilled system.

Busfield et al. (2000) measured the dynamic storage and loss moduli of carbon black filled natural rubber by conducting testing with small oscillations that were superimposed on a range of tensile pre-strains. In their observations, they dynamic storage and loss moduli were independent of the pre-strain at small pre-strains but there was a remarkably increase in both the storage and the loss moduli at higher pre-strains. The authors suggested that the dynamic behaviour of swollen filled rubber was the combined effects of a reduction in the modulus of the rubber matrix which was caused by the swelling action and a reduction in the effective volume fraction of filler.

Recently, Chai et al. (2011) investigated the diffusion of biodiesel into rubber specimens in the presence of large strain. Original device comprised of four rectangular stainless steel plates with spacer bars in between was developed to introduced pre-compression

on the rubber specimens while they were immersed into biodiesel. Different pre-compressive strains and biodiesel blends were considered. They found that the swelling in rubbers increases with the increase of the palm biodiesel content and decreases with the increase of pre-compressive strain. It was also observed that the presence of biodiesel and the increase in its content reduce significantly the mechanical strength of the rubber and the evolution of shear modulus ratio of swollen and dry rubbers as a function of applied compressive stress was investigated.

In sum, swelling in elastomer is greatly affected by the presence of mechanical deformation in the elastomer. Thus, there is a necessity to consider the effect of mechanical deformation during the development of a model to capture the diffusion of a solvent into the elastomer. A detailed discussion on modeling the coupled diffusion-deformation will be presented in Section 2.8.

2.7 Models for Mullins effect

2.7.1 Existing models in dry elastomer

As reviewed by Diani et al. (2009), there are many efforts in proposing different theories to explain the Mullins effect in dry elastomer. Nevertheless, no unanimous microscopic explanation for this softening is available up to this date (Marckmann et al., 2002; Diani et al., 2009). The first attempt to describe the Mullins effect is through a phenomenological approach. Mullins and Tobin (1957) proposed that the elastomer initially contains both hard and soft phases. During the deformation process, the hard phase transforms into the soft one. Their theory was successfully adopted into a number of works (Wineman & Huntley, 1994; Huntley et al., 1997; Beatty & Krishnaswamy, 2000; Qi & Boyce, 2004). Simo (1987) adopted the concept of Continuum Damage Mechanics (CDM) where Mullins effect was considered as a damage phenomenon and was described by a scalar damage parameter. Thus the material response is characterized by multiplying

the classical hyperelastic strain energy with a reducing parameter representing the damage level. Different forms of damage parameter were proposed in the literature (Miehe, 1995; Ogden & Roxburgh, 1999; Chagnon et al., 2004). In contrast to Miehe (1995) and Chagnon et al. (2004) who assumed that damage evolves when the applied level of deformation is undergone by the material for the first time, Ogden and Roxburgh (1999) proposed that damage stays zero when the material is subjected to a level of deformation never applied, and evolves in the range of submaximal deformation. The latter is known as the Pseudo-Elastic (PE) model.

The second approach is based on a physical interpretation (Govindjee & Simo, 1991; Kilian et al., 1994; Klüppel & Schramm, 2000; Marckmann et al., 2002; Freund et al., 2011). Marckmann et al. (2002) reported the development of a new network alteration theory to describe the Mullins effect where they considered the Mullins effect as consequence of breakage of links inside the material, involving both filler-matrix and chain interaction links. This new alteration theory was implemented by modifying the eight-chain constitutive equation of Arruda and Boyce (1993). The accuracy of the resulting constitutive equation was demonstrated on cyclic uniaxial experiments for both natural rubbers and synthetic elastomers. Chagnon et al. (2006) later modified this network alteration theory to include the dangling chains effect in the network and proposed that the number of monomers involved in the elastic response of the material is a decreasing function of the maximum deformation. Further refinements to account for deformation-induced anisotropy in Mullins effect were proposed in the literature. Indeed, as pointed out early by Mullins (1948) and more recently in Laraba-Abbes et al. (2003); Diani et al. (2006); Itskov et al. (2006); Machado et al. (2012), the material undergoes significant anisotropy softening due to the application of mechanical loading.

2.7.2 Existing extension models for swollen elastomer

In contrast to dry elastomers, only few studies on the observation and modeling of the Mullins effect in swollen elastomers are available in the literature (Webber et al., 2007; Lin et al., 2010; Andriyana et al., 2012; Chai, Andriyana, et al., 2013; Chai, Verron, et al., 2013; Ch'ng et al., 2014). Indeed, it was reported that the Mullins effect is also observed for swollen elastomers (Andriyana et al., 2012) and it is necessary to model the Mullins effect taking into consideration the swelling effect. The Mullins effect is observed to decrease as the degree of swelling increases. To model the observation, the existing models for dry elastomer can be modified in order to account for the degree of swelling. For example, Chai, Verron, et al. (2013) proposed an extension of pseudo elastic model of Ogden and Roxburgh (1999).

2.8 Models for coupled diffusion-deformation

Modeling the mechanical response of swollen elastomers has become a necessity since in a number of applications, it is inevitable that elastomers will be in contact with solvent during the service. Number of studies were devoted to the diffusion of liquids or gases in elastomers. However, most of the studies do not consider the influence of deformation on the diffusion process (Rajagopal, 2003). As clearly mentioned in the previous discussion, the effect of deformation on swelling cannot be omitted and must be taken into account in developing efficient constitutive models.

From a thermodynamic point of view, swollen elastomer is a complex system in which diffusion of solvents into a large strain elastic solid leads to swelling. Two main approaches have been adopted to propose constitutive models (Rajagopal, 2003):

1. The first approach is based on the seminal work of Biot (1941) and on the studies of Truesdell and Toupin (1960), and Bowen (1976) who proposed a mathematical framework to describe the thermodynamics of mixtures. In this theory, the kine-

matics of each component of the mixture is considered and the total stress is the sum of the stress in each component. It leads to several difficulties: the application of the second law of thermodynamics is arguable and the determination of relevant boundary conditions is not an easy task (Rajagopal, 1995). Nevertheless, this approach has been successfully adopted to develop a number of constitutive equations (Rajagopal, 2003). A recent example of this theory can be found in Ehlers et al. (2010) and the references herein.

2. In recent literature, a more tractable theory, that considers the swollen elastomers as a single continuum body has been considered. This theory was suggested by Rajagopal et al. (1986) and firstly introduced by Durning and Morman (1993). Several authors have recently improved it in different ways (Baek & Srinivasa, 2004; Hong et al., 2008; Chester & Anand, 2010; Duda et al., 2010). In fact, all these models are inspired by the simple models proposed by Flory (1953) and Treloar (1975) for elastomer swelling. They are based on the definition of a free energy function that includes three contributions: the one of the "unmixed" pure solvent, the one of solvent-polymer mixing (classically given by the Flory (1942)-Huggins (1942a) expression), and the elastic free energy due to the deformation of the polymer network. In most of the papers, the elastic free energy is based on the Gaussian statistical mechanical models for the change in the configurational entropy with respect to the dry configuration. This approach being limited to moderate strain, both Boyce et al. (2001) for equilibrium problems and Chester and Anand (2010) for transient problems have proposed to use the eight-chain model of Arruda and Boyce (1993), which accounts for limited chain extensibility.

Baek and Srinivasa (2004) proposed a model of slow diffusion of a fluid into a swelling solid undergoing large deformation. The model predicts the stress in the solid

as well as the diffusion rates. Their approach is based on the balance laws of a single continuum with mass diffusion, which overcomes the difficulties inherent in the theory of mixtures in specifying boundary conditions. Based upon the continuity of the chemical potential, a "natural" boundary condition is derived by the use of a variational approach, based on maximizing the rate of dissipation. They showed the differential equations resulting from the use of mixture theory in the absence of inertial effects can be recast into an identical equation obtained using their approach. Finally, it is shown that their results show excellent agreement with the experimental data of Paul and Ebra-Lima (1970) for a variety of solvents.

Following the work of Baek and Srinivasa (2004), Soares (2009) modeled the diffusion of a fluid through a spherical elastic solid undergoing large deformation. The model is based on a variational method and on the assumption of continuity of the chemical potential across the solid-fluid interface. The balance laws for a single continuum with mass diffusion are cast in spherical coordinates, and suitable boundary conditions are posed to describe the radial diffusion of fluid through an elastic spherical shell with finite thickness. The inner surface is adjacent to a rigid wall, either impermeable or permeable, while the outside surface is in contact with the fluid that swells the solid, diffuses through it, and exerts a hydrostatic pressure on its surface.

Hong et al. (2008) formulated a theory of the coupled mass transport and large deformation. The free energy of the polymer was considered as a result from two molecular processes: stretching the network and mixing the network with the small molecules. Both solvents and solids were taken to be incompressible, a constraint enforced by using a Lagrange multiplier, which coincides with the osmosis pressure or the swelling stress. The polymer can undergo large deformation of two modes: fast processes of local rearrangement of molecules, allowing the polymer to change shape but not volume and slow process of long-range migration of the small molecules, allowing the polymer to change

both shape and volume. The authors assumed that the local rearrangement is instantaneous, and model the long-range migration by assuming that the small molecules diffuse inside the polymer. The theory was illustrated with a layer of gel constrained in its plane and subject to a weight in the normal direction. The scaling behaviour of a gel under a conical indenter was also predicted.

Duda et al. (2010) presented the theory for the behaviour of a solid undergoing two independent processes: a macroscopic or mechanical process due to the deformation of the solid and a microscopic or chemical process due to the migration of a chemical species through the solid. Their theory was based on the theory of balances, namely the mechanical force balance and the transport balance for the chemical species. The basic equations of the theory were obtained from the combination with thermodynamically consistent constitutive relations. They showed that the possibility of a mechanically induced phase transition was governed by two parameters: the Flory interaction parameter and a parameter given by the product between the number of cross-linked units per unit reference volume and the molecular volume of the liquid molecule. As for diffusion, their theory was able to describe the pressure-induced diffusion in swollen membranes.

Chester and Anand (2010) formulated a continuum-mechanical theory to describe the various coupled aspects of fluid permeation and large deformations of elastomeric gels. The constitutive theory developed was consistent with modern treatments of continuum thermodynamics, and material frame-indifference. The expression for the free energy was considered based on a Flory-Huggins model for the free energy due to mixing of the fluid with the polymer network, coupled with a non-Gaussian statistical-mechanical model for the change in configurational entropy. As representative examples of application of the theory, they studied (a) three-dimensional swelling-equilibrium of an elastomeric gel in an unconstrained, stress-free state and (b) the following one-dimensional transient problems: (i) free-swelling of a gel, (ii) consolidation of an already swollen

gel and (iii) pressure-difference-driven diffusion of organic solvents across elastomeric membranes.

2.9 Biofuels

There is a tremendous increase in the demand for renewable energy, natural gas and nuclear energy due to the concern of stringent emission regulations and limited fossil fuel reservations. The total renewable energy demand will increase significantly, whereby fuel from biomass, also known as biofuel, will be the major resources followed by solar and hydro energy (Kalam & Masjuki, 2008). The introduction of biofuel as an alternative fuel is also considered by far as the most promising solution to the issue of fossil fuels depletion and environmental pollution (Herzog et al., 2001).

Biodiesel is the most common type of biofuel. Chemically, biodiesel is referred as mono-alkyl-esters of long-chain fatty acids derived from transesterification of vegetable oils or animal fats (Trakarnpruk & Porntangjitlikit, 2008). These chemicals are better known as fatty acid methyl esters (FAME). Since its properties are very much akin to diesel, biodiesel can be used in compression ignition engines with little or no modifications (Ramadhas et al., 2004). Biodiesel can be used in its pure form (referred to as B100) in modern diesel engines or to be blended with different composition of petroleum diesel to create a biodiesel blend. Pure biodiesel serves as the lowest emission diesel fuel but the utilization of pure biodiesel in diesel engines is not mature yet as there are still many problems need to be solved (Haseeb et al., 2010). Indeed, while biodiesel is a mixture of esters, conventional petroleum diesel consists of a mixture of hydrocarbon. This difference in the compositions leads to material compatibility issues especially in industrial applications involving elastomeric materials (Chai et al., 2011).

There are many available feedstocks in the market for use in biodiesel production including various types of vegetable oils as well as animal fats. Common sources of

biodiesel under research include palm oil, soy, sunflower, jatropha, rapeseed, corn, olive, castor, milkweed, linseed, mahua, mustard, algae etc (Haseeb et al., 2011). Since there are many palm tree plantations available in Malaysia, a significant number of research studies on palm biodiesel are conducted in Malaysia (Jayed et al., 2011). Further discussion on palm biodiesel is provided in the following subsections.

2.9.1 Palm biodiesel

Palm oil serves as the world's third most produced edible oil, following closely behind soya and rapeseed oil. Other than the usage for food industry, palm oil is also utilized in a wide array of cosmetics and pharmaceuticals and lately the increased demand for biodiesel production. The instability of the market fuel price increases the demand for alternative fuel sources for over the next decades. Thus, future development of palm oil is promising with the world market for palm oil growing steadily at about 8% per annum (Phosri et al., 2010).

Recently, many researches are on-going to explore the potential of palm oil as the alternative substitute for diesel. Malaysia is emerging as one of the leading biofuel producers with 91 plants approved and a handful now in operation. All are based on palm oil (Kalam & Masjuki, 2008). Since 1980s, Malaysia Palm oil Board (MPOB) collaborates with the local oil company, Petronas, to carry on the methanol transesterification of crude palm oil into palm biodiesel. The intensified production and increased potential usage of palm biodiesel makes Malaysia find itself as a potent country among the developing countries.

The differences in the chemical compositions result in differences between the properties of palm biodiesel and conventional petroleum diesel. Generally, palm biodiesel has higher density, heating value kinematic viscosity, boiling points and cetane index as compared to conventional petroleum diesel (Abdullah et al., 2009). However, palm biodiesel

has a gross heating value lower than diesel due to the presence of oxygen in the methyl ester molecules. It is to note that the flash point of palm biodiesel is higher than that of conventional diesel which can increase its storage ability as the temperature at which it can form an ignitable mixture in air is higher. The comparison between the basic properties of conventional petroleum diesel and palm biodiesel is tabulated in Table 2.2.

Table 2.2: Basic properties of diesel and palm biodiesel (Benjumea et al., 2008).

Properties	Units	ASTM standard	Diesel	Palm Biodiesel
Density at 25°C	kg/m ³	D1298	853.97	864.42
Mass high heating value	MJ/kg	D240	45.273	39.837
Volume high heating value (25°C)	MJ/m ³	D240	38662	34436
Cloud point	°C	D2500	-5.0	16.0
Cold filter plugging point	°C	D6371	-6.0	12.0
Kinematic viscosity at 40°C	mm ² /s	D445	4.33	4.71
Initial boiling point	°C	D86	181.5	302.2
Temperature at 50% recovered	°C	D86	284.9	326.5
Final boiling point	°C	D86	384.3	348.9
Calculated cetane index	-	D4737 D976	46.3 47.5	57.3 50.0

2.9.2 Advantages and disadvantages of biodiesel

There are a few advantages of biodiesel over conventional petrol diesel. Firstly, biodiesel is known as an environmentally friendly biofuel since the emission contains less pollutant than diesel. The emission of conventional diesel serves as one of the major contributor to global warming. Generally, biodiesel is biodegradable, non-toxic, and has relatively high flash point. Apart from that, biodiesel produces more lubricity and this prolongs the engine life and reduces the frequency of engine part replacement (Kaul et al., 2007).

However, there are also few disadvantages of biodiesel which need to be overcome in order to use it as an alternative source for fuel. Due to its difference in chemical structure, it is relatively more sensitive to oxidative and thermal degradation. Oxidation of biodiesel leads to the formation of corrosive acids and deposits which cause corrosion to the parts used in biodiesel. Thus, the oxidative stability becomes the major concern in biodiesel. In

addition, the high viscosity of vegetable oils and animal fats caused operational problems such as poor atomization upon injection into the combustion chamber. Lastly, the production of biodiesel can be varied based on the feedstock used and it is often produced out-of-specification, leading to contamination with corrosive agents such as water and sulphur. Although the addition of inhibitors extends the time before corrosion occurs in the engine parts (Maru et al., 2009), there are still many improvements needed before biodiesel can be used as a complete substitution to the conventional petroleum diesel.

2.9.3 Compatibility of elastomer with biodiesel

Although the compatibility of commonly used elastomeric components such as seals, gaskets and hose with conventional diesel has long been established, there is less information available on the compatibility of elastomers with biodiesel. Indeed, the degradation of elastomers is the major concern related to the compatibility issue in biodiesel. The impact of biodiesel on the degradation behaviour of elastomers was being investigated by a few studies. However, note that most of the studies only focus on physical degradations such as the measurement of swelling, hardness and tensile strength of the elastomers after immersion.

Bessee and Fey (1997) studied the effect of exposure to methyl soyester and diesel blends to elastomers based on several physical properties measurements which include swelling, tensile strength, elongation and hardness. They observed that nitrile rubber (NBR), nylon 6/6 and high-density polypropylene show significant changes in physical properties whereas Teflon, viton 401-C and viton GFLT were unaffected. Based on this observation, they concluded that fluorinated elastomers have higher resistance towards biodiesel. In addition, the compatibility appears to depend highly on the feedstock of biodiesel. Frame and McCormick (2005) evaluated the degradation of elastomers in diesel, diesel blend with 15% ethanol and 20% soy-derived biodiesel (B20). Various

elastomers such as peroxide-cured nitrile rubber (N1059), nitrile rubber (N674), high aceto-nitrile content rubber (N0497), unfilled fluorocarbon (V884) and filled fluorocarbon (V747) were investigated. The observation suggested that all these elastomers were fully compatible with B20 and diesel while severe degradation was observed in diesel blend with 15% ethanol.

On the other hand, Trakarnpruk and Porntangjitlikit (2008) were more interested in the production of biodiesel. They investigated the preparation of biodiesel by transesterification and the biodiesel was subsequently characterized. In addition, they also evaluated the impact of biodiesel on elastomer properties by investigating the compatibility of a diesel blend with 10% biodiesel (B10) with six types of commonly used elastomers which include NBR, HNBR, NBR/PVC, acrylic rubber, co-polymer FKM and terpolymer FKM. Immersion of elastomers for different durations (22, 670 and 1008h) at 100°C were conducted and the properties of elastomers were measured according to American Society of Testing and Materials (ASTM) standard. Swelling of elastomers was measured in terms of mass and volume change. Based on the results, the impact of biodiesel is more vigorous to the properties of NBR, NBR/PVC and acrylic rubber while co-polymer FKM and terpolymer FKM being less affected by the biodiesel.

Haseeb et al. (2010) conducted static immersion of various elastomers such as nitrile rubber (NBR), polychloroprene (CR) and fluoro-viton A in diesel (B0), blend of 10% biodiesel in diesel (B10) and biodiesel (B100). Immersion tests were carried out at 2 temperatures: 25°C and 50°C for a duration of 500h. The degradation of the elastomers was expressed in terms of mass and volume change after the immersion. In addition, the hardness, tensile strength and elongation of elastomers were also studied. The surface morphology was studied using scanning electron microscopy (SEM) while the structural changes was studied using Fourier Transform Infrared (FTIR). In this study, it was found that contrary to the degradation experienced by NBR and CR, fluoro-viton show good

resistance to degradation. Moreover, they concluded that biodiesel contains more carboxylic groups and elastomers degraded more in biodiesel than in conventional diesel.

More variation of immersion were conducted by Haseeb et al. (2011) where elastomers such as ethylene propylene diene monomer (EPDM), silicone rubber (SR), polychloroprene (CR), polytetrafluoroethylene (PTFE) and nitrile rubber (NBR) were immersed in diesel (B0), various diesel blends (B10, B20, B50) and pure biodiesel (B100). Immersion tests were conducted at room temperature for a total immersion duration of 1000 h. The degradation was characterized by measuring the change in weight and volume, hardness and tensile strength in a time interval of 250 h. They observed that CR and NBR swelled to a greater extent upon exposure to biodiesel while EPDM and SR experienced greater swelling in diesel. Meanwhile, PTFE showed relatively insignificant physical changes with the immersion. As a conclusion, the compatibility of elastomers was reported to be $PTFE > SR > NBR > EPDM > CR$.

In summary, all these observations suggest that fluorinated elastomers are more compatible for usage in biodiesel. Meanwhile, some common types of elastomers such as NBR, SBR, CR, NR etc show significant degradation upon exposure to biodiesel and thus are not suitable to use in biodiesel. However, the mechanisms of degradation of elastomers in biodiesel are not fully understood. The chemical structure of biodiesel which contains highly unstable fatty acids as well as unreacted mono-, di-, and triglycerides, glycerol and methanol may exhibit an unknown impact on the elastomers which require more in depth investigation (Haseeb et al., 2011). These unknown aspects remain an interesting research topic and more efforts are needed to establish the compatibility of elastomers with biodiesel.

CHAPTER 3

METHODOLOGY

Generally, the present work is divided into two parts. In the first part of work, the emphasis will be laid on the establishment of an experimental database. More precisely, the coupling between diffusion of biodiesel and multiaxial large deformations in elastomers containing different carbon black content will be investigated. For this purpose, original devices and specimens are developed so that swelling tests can be conducted on elastomers in the absence (free swelling) and in the presence of mechanical deformations (constrained swelling). Due to its wide use in sealing systems, nitrile butadiene rubber (NBR) is considered in the present work.

The second part of the work focuses on the development of a continuum mechanical model to capture the experimental observations. The development of the model is restricted to mechanical problems where only isothermal processes are considered. The corresponding constitutive equations will be derived under the framework of thermodynamics of irreversible processes. Finally, the proposed model will be implemented into the finite element code ABAQUS in order to simulate the responses of industrial elastomeric components. The overall works is described by a flow chart shown in Figure 3.1.

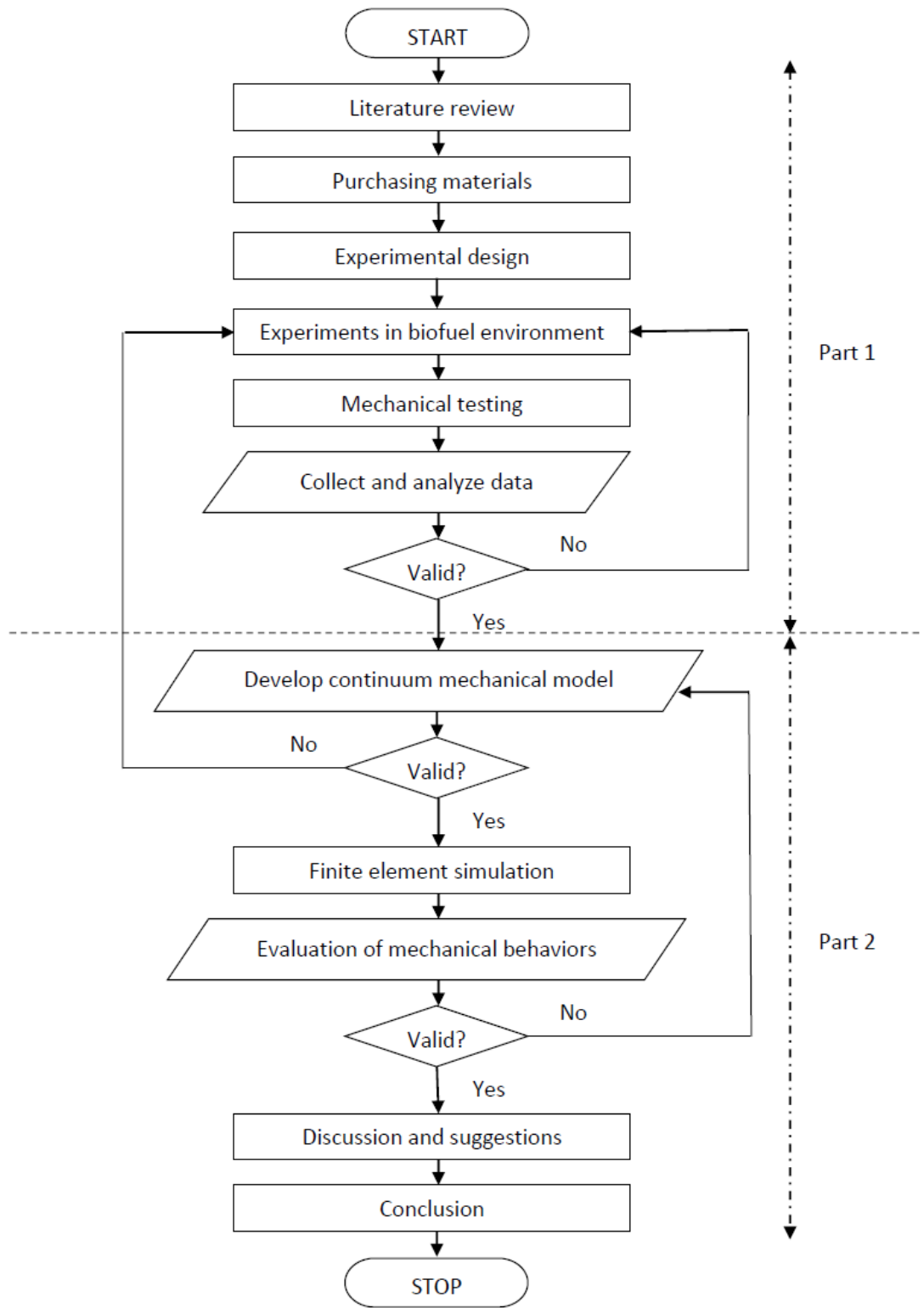


Figure 3.1: Flow chart describing the methodology of the present work.

3.1 Experimental program

To collect the experimental database for the purpose of the model validation, three different specimens and devices were designed throughout the whole work. Details of each specimen and device design will be given in the following sections.

3.1.1 Design of specimen and device

3.1.1 (a) Constrained swelling 1: static uniaxial strain

Dumbbell specimens following ASTM standard D412-C with a thickness of 2 mm are purchased from Malaysia Rubber Board. The materials include unfilled NBR and filled NBR with 25 and 40 wt% of carbon black, respectively. The detailed dimension of the dumbbell specimen used is provided in Figure 3.2.

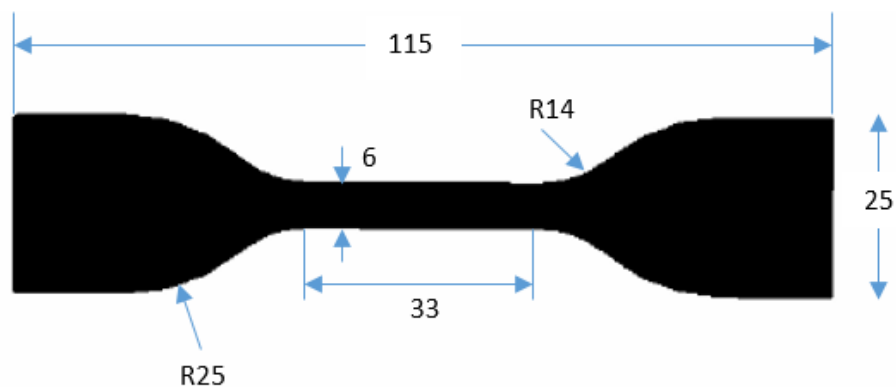


Figure 3.2: Dimension of dumbbell specimen following ASTM standard D412-C.

In order to apply static uniaxial strains to the specimens during the immersion tests, a special device is developed and the description of the device can be summarized as follow:

1. The device consists of four identical metallic plates (handles) and two long bolts. Each plate has four holes as shown in Figure 3.3. The device can accommodate three dumbbell specimens.

2. Two plates are attached on the upper and on the lower parts of the specimens. Bolts are inserted into the three holes located on the plates. The plates are then tightened using nuts. While doing this procedure, the long bolts are fitted into each side of the plates.
3. Uniaxial tensile strain can be applied by adjusting the nuts located at the long bolts between metallic plates until the desired strain level is achieved.

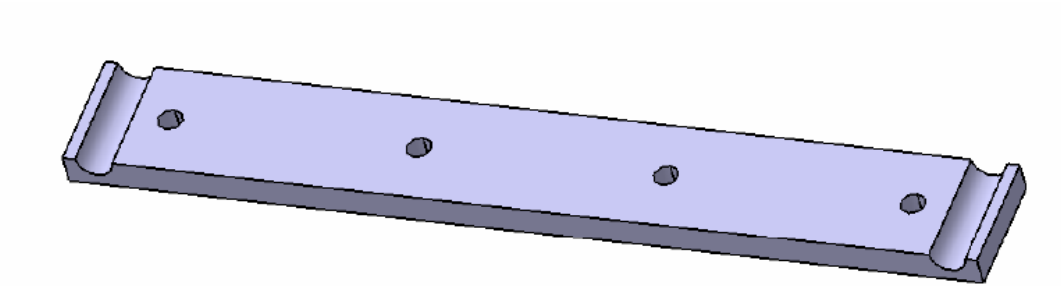


Figure 3.3: Metallic plate for uniaxial tensile loading.

The complete assembly of the device is shown in Figure 3.4 and the exploded view of all components in the device is given in Figure 3.5.

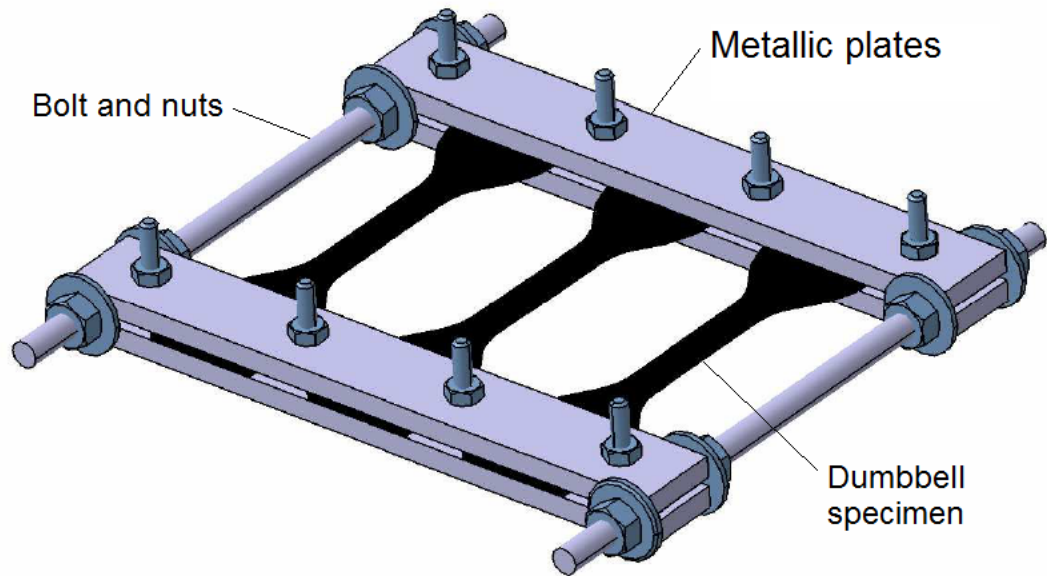


Figure 3.4: Complete device and specimen for constrained swelling 1.

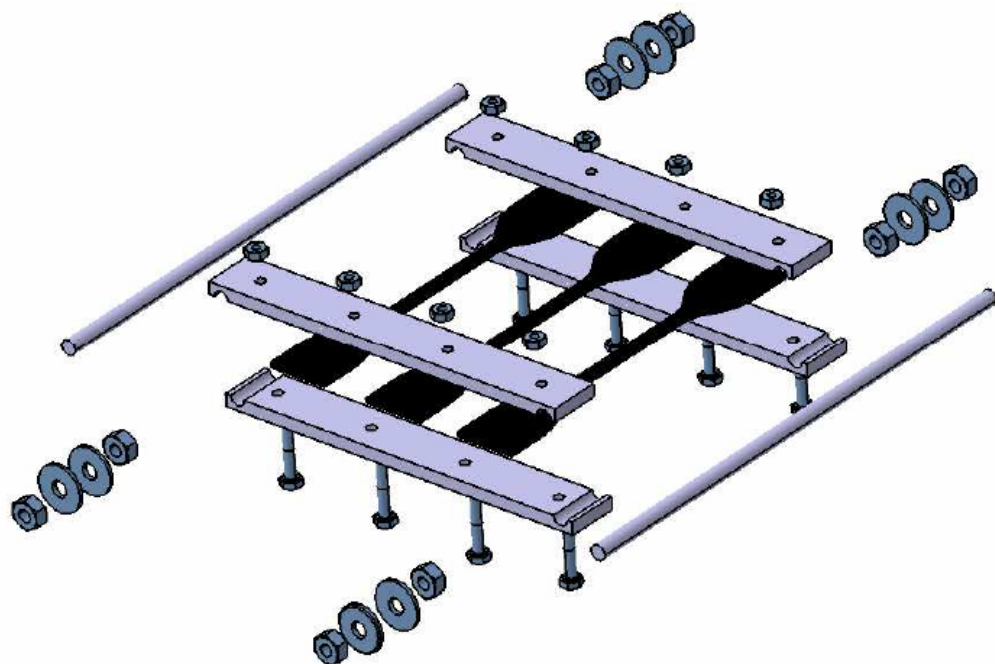


Figure 3.5: Exploded view of the experimental device and specimen used for constrained swelling 1.

As mentioned in the description, uniaxial tensile strain can be applied by adjusting

the nuts located at the long bolts between the metallic plates. A graphical illustration of the application of tensile strain is given in Figure 3.6. In this study, the distance between the metallic plates is fixed at three different constant stretches: $\lambda = 1.00, 1.25$ and 1.50 respectively. The stretch is defined as the ratio between the current length to the original length of the specimen between the two metallic plates. Note that the corresponding engineering strain is simply given by $\varepsilon = \lambda - 1$. For all imposed strain levels, immersion tests are conducted until equilibrium swelling is reached.

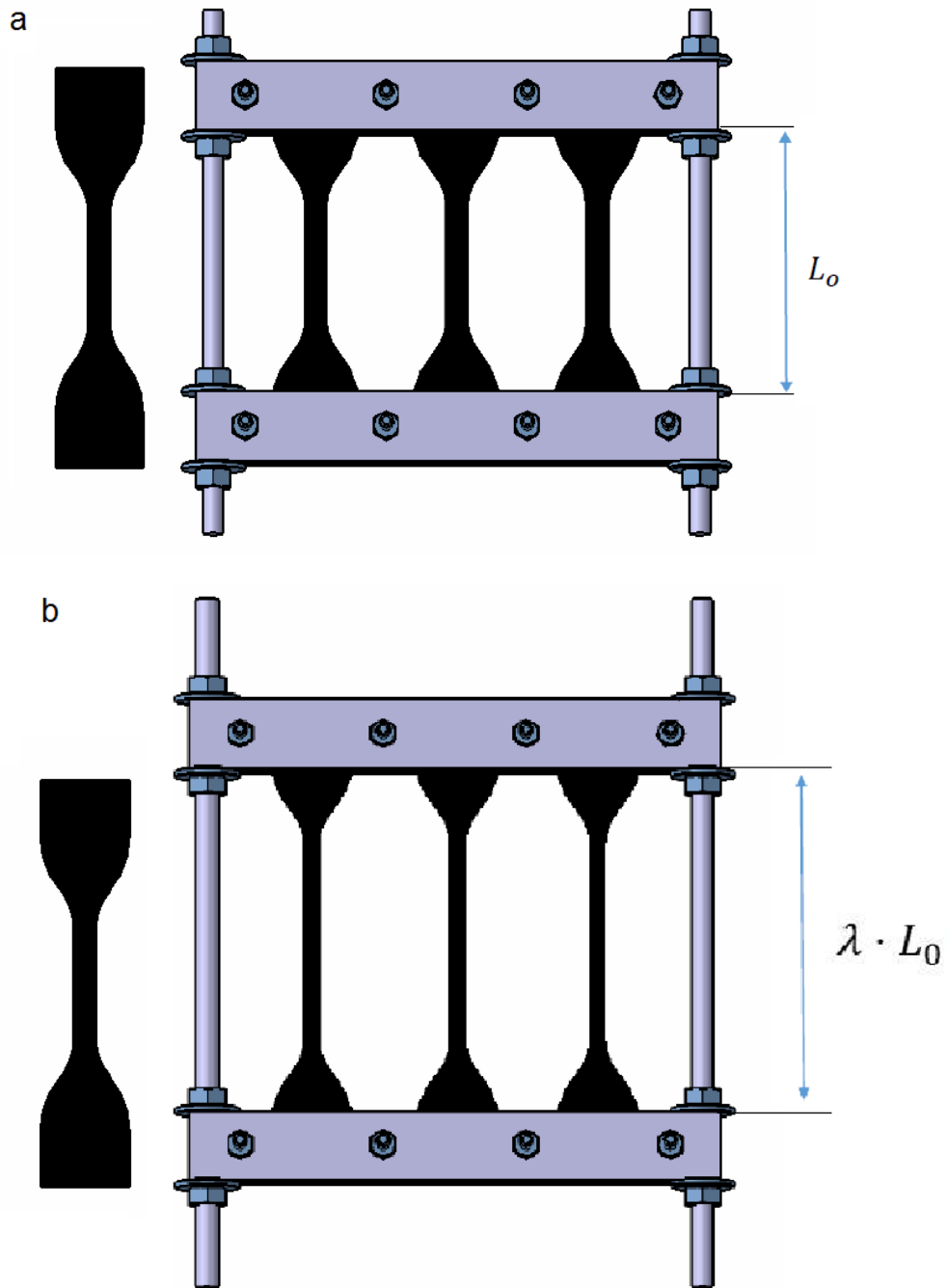


Figure 3.6: Experimental device for constrained swelling 1: (a) with no tensile strain (initially stress-free) and (b) under tensile strain.

Using this specimen and device, five different immersion tests are investigated where two of them are stress-free immersions while the rest are uniaxially-constrained immersions. For stress-free immersion, the experimental works are conducted with and without device. To ensure that the specimen undergoes stress-free immersion, the distance be-

tween the metallic plates is adjusted from time to time for immersion with device. As for stress-free immersion without device, the specimen is simply fully immersed in the solvent until equilibrium swelling is achieved.

3.1.1 (b) Constrained swelling 2: static multiaxial strain (Design 1)

To investigate the diffusion of palm biodiesel into elastomers undergoing multiaxial deformation, a hollow specimen is designed as shown in Figure 3.7. Since the focus of the present section is on the effect of the presence of static multiaxial strains, only NBR filled with 25 wt% of carbon black is considered.

The specimen used is a diabolo-like shape elastomer with a hollow cylinder inside to allow the diffusion of biodiesel from the inner and outer wall surfaces. Note that no standard is followed during the design of the specimen. The height of the specimen is 55 cm and it was designed to have a sufficiently thin wall in the middle part so that the equilibrium swelling can be achieved within a reasonably short period of time (Ch'ng et al., 2013). Both ends of the specimen have a hexagonal shape which permits the application of a static multiaxial mechanical loading during immersion. The detailed geometry of the specimen is shown in Figure 3.7.

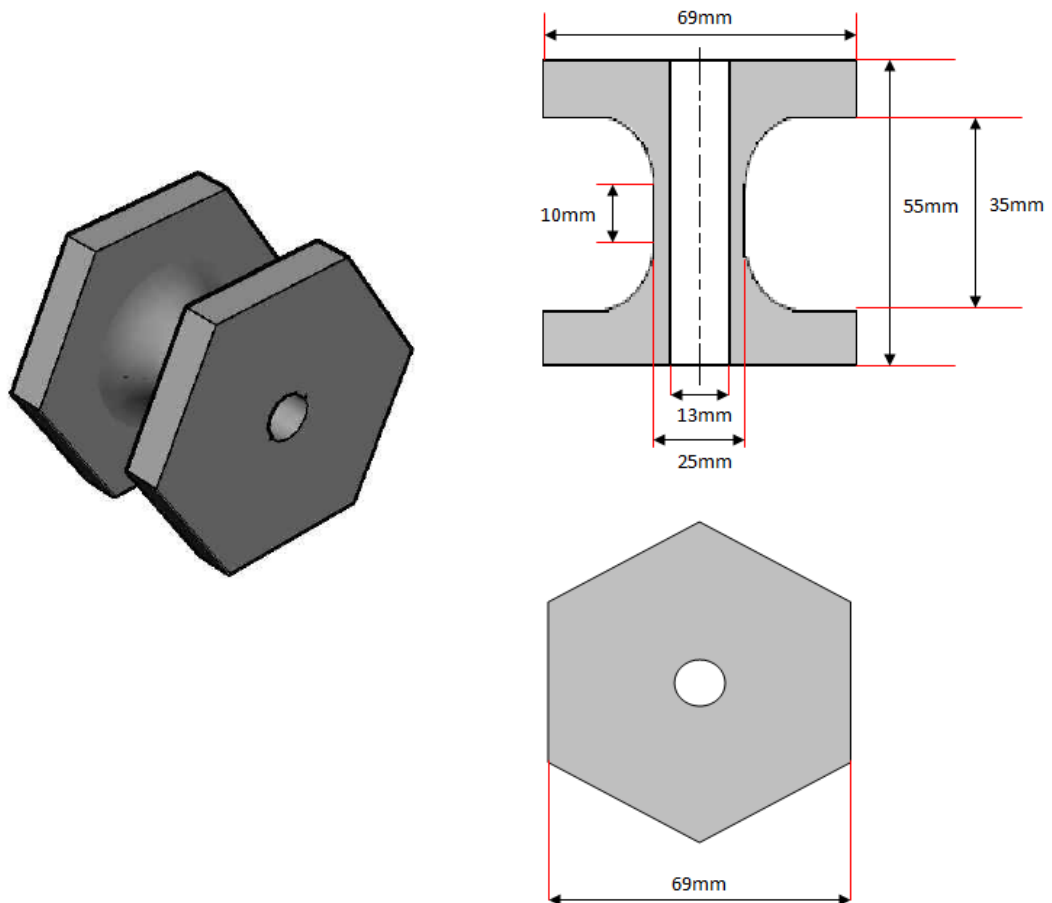


Figure 3.7: Specimen geometry of the diabolo-shape specimen.

A specially-designed device, referred to as Design 1 in the following, is developed for the diabolo-shape specimen. It consists of four circular metallic grips and two plates as shown in Figure 3.8. The main features of Design 1 are summarized as follow:

1. The device consists of four identical metallic grips which are screwed together at both ends of the elastomeric specimen. The inner part of the metallic grips is designed to fit in the hexagonal shape of the specimen. In this way, twist and axial extension/contraction can be imposed simultaneously to the specimen while the immersion test is carried out.
2. Each metallic grip consists of six identical holes which are symmetrically arranged

along circumferential direction. Different twists can be applied to the specimen by twisting the upper part of the metallic grip while fixing the lower part of the grip. Once the desired angle is obtained, bolts are inserted through the holes located at the lower and upper parts of the grip in order to maintain constant twist. Axial extension or contraction can be imposed by adjusting vertically the position of the nuts in the bolts as illustrated in Figure 3.9.

3. The rubber specimen has a diabolo-like shape with a hollow inside to allow the biodiesel to diffuse into the specimen from its inner and outer wall surfaces. Thus, it is expected that equilibrium swelling can be achieved within a reasonable period of time.
4. After the metallic grips are tightly screwed to the specimen, thin metallic plates are attached at both ends in order to prevent the diffusion of liquids from both specimen ends. Two o-rings with different diameters are inserted between plates and grips to provide a tight seal.

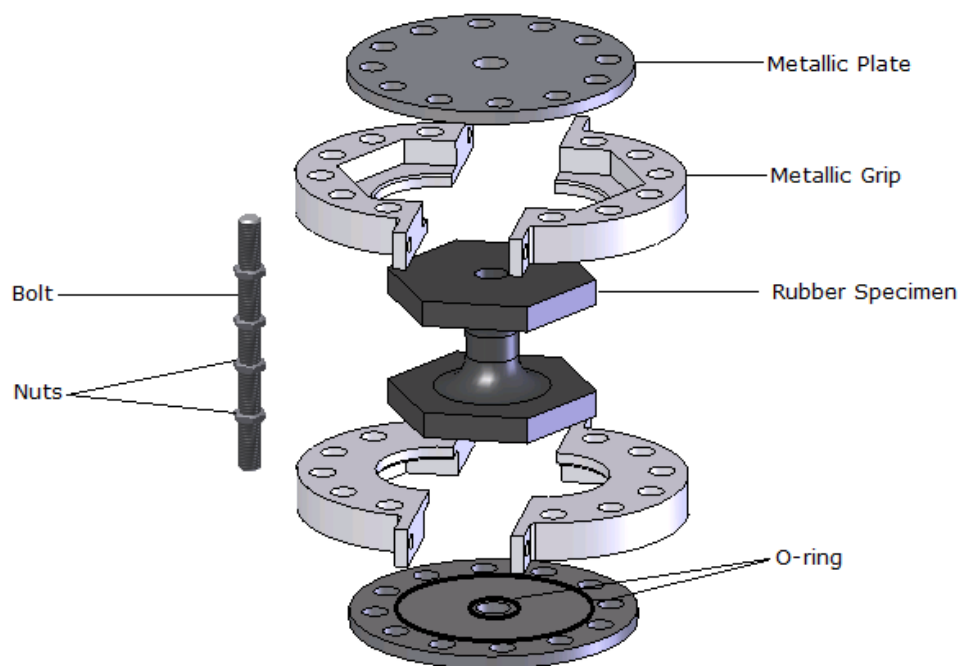


Figure 3.8: Exploded view of the experimental device and specimen of Design 1.

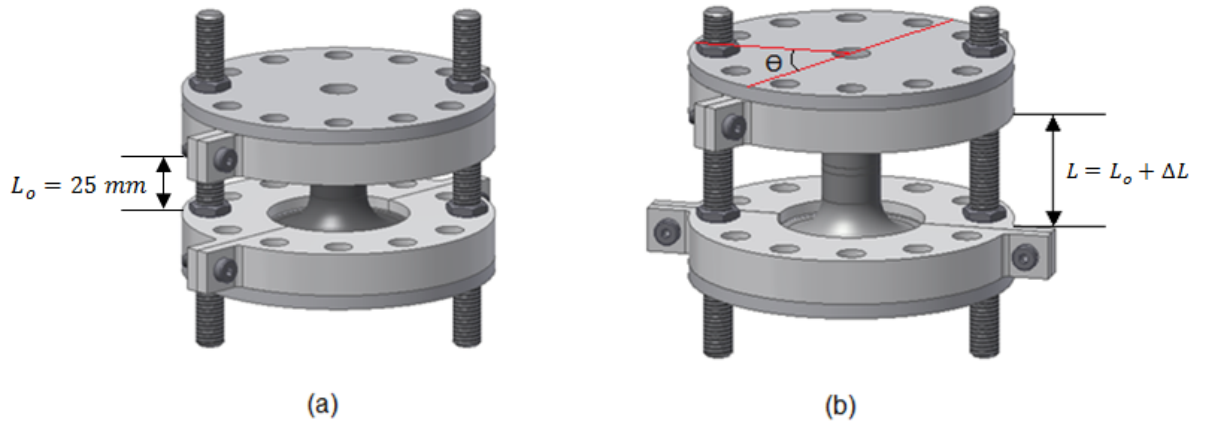


Figure 3.9: Experimental device for constrained swelling 2: (a) with no mechanical loading (initially stress-free) and (b) under twist angle θ and axial extension ΔL . For practical purposes during the experiment, the initial distance between two metallic plates is chosen as the initial length L_o

Using this design, sixteen different mechanical loading conditions are investigated. The details of these condition are given in Table 3.1.

Although Design 1 enables multiaxial mechanical loading to be imposed without any difficulty, some limitations are observed from this design (See Section 4.3 for further discussion). In order to overcome these limitations, an alternative specimen and device are proposed in the next Section and referred to as Design 2.

3.1.1 (c) Constrained swelling 3: static multiaxial strain (Design 2)

Following the problems encountered in Design 1, further improvements have been made to the existing design and improved specimen and device are developed. Similarly to Design 1, the improved Design 2 enables the investigation of diffusion of solvents into elastomers undergoing simultaneously multiaxial large deformations. A hollow, ring shaped specimen with 60 shore hardness and 25 wt% of carbon black is used and is shown in Figure 3.10. The height of the specimen is 30 cm with outer and inner radii of 43 and

Table 3.1: Mechanical loading conditions for Design 1

Specimen	Applied Load			
	Tensile Load		Torsional Load	
	Axial extension	Resulting stretch ratio	Twist angle	Resulting twist per unit length
	ΔL (mm)	$\lambda = L/L_o$	($^\circ$)	γ (rad/mm)
S0T0	0	1	0	0
S0T30	0	1	30	0.02094
S0T60	0	1	60	0.04189
S0T90	0	1	90	0.06283
S20T0	5	1.2	0	0
S20T30	5	1.2	30	0.01745
S20T60	5	1.2	60	0.03491
S20T90	5	1.2	90	0.05236
S40T0	10	1.4	0	0
S40T30	10	1.4	30	0.01496
S40T60	10	1.4	60	0.02992
S40T90	10	1.4	90	0.04489
S60T0	15	1.6	0	0
S60T30	15	1.6	30	0.01309
S60T60	15	1.6	60	0.02618
S60T90	15	1.6	90	0.03928

38 cm, respectively at the middle part. The detailed dimension of the cylindrical hollow specimen is given as Figure 3.11. As compared with Design 1 which has outer and inner radii of 12.5 and 6.5 cm, Design 2 has a larger diameter in order to facilitate the diffusion of solvents and to create a more uniform stress field under torsional loading.



Figure 3.10: Ring-shape specimen for Design 2.

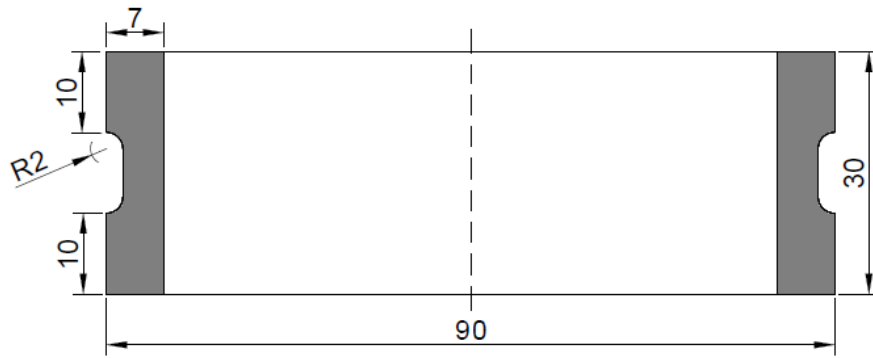


Figure 3.11: Detailed dimension of the ring-shape specimen.

Similarly to the previous specimen, a specially-designed device is developed for the ring-shaped specimen. The complete breakdown of Design 2 is shown in Figure 3.12. The main features of Design 2 can be summarized as follow:

1. The device consists of two identical circular metallic plates and four identical semi-circular metallic grips. Each plate and grip has sixteen and eight holes, respectively located at the angle of 10° apart from each other. Moreover, each side of the grip contains one additional hole. The device can accommodate one cylindrical hollow specimen.
2. The plates and grips are attached to the specimen. Bolts and nuts are used in each side of the grips in order to tighten the device.
3. The specimen in the device is twisted. The twist angle is held constant by inserting bolts into holes located on the grips and plates. A tensile strain can be applied by adjusting the nuts. Thus, the specimen is subjected to simultaneous tensile and torsion loadings as illustrated in Figure 3.13.

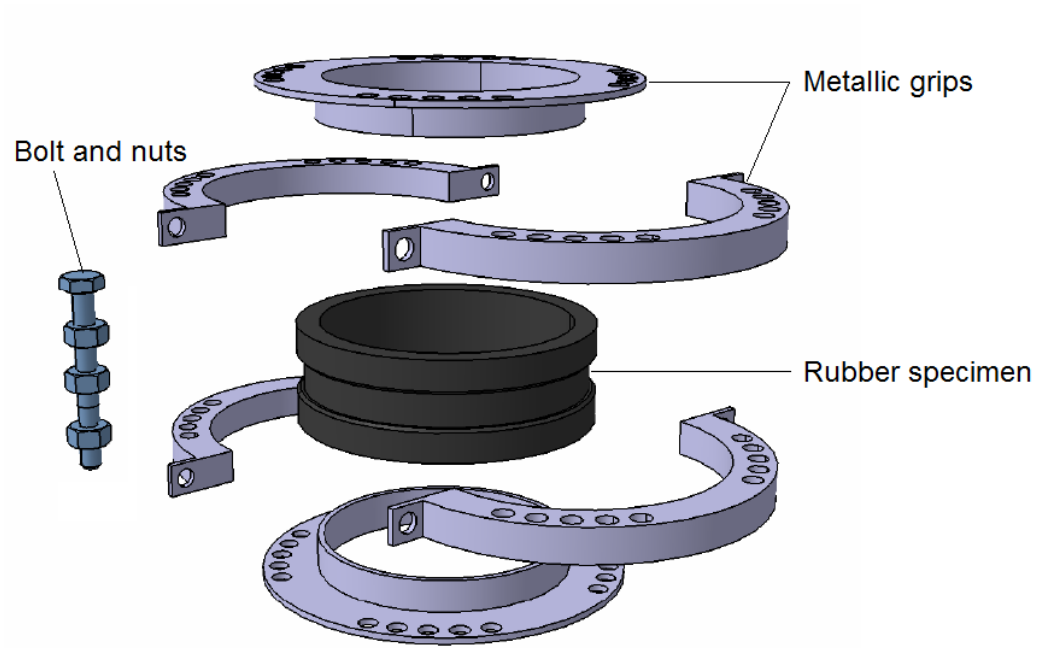


Figure 3.12: Exploded view of the experimental device and specimen of Design 2.

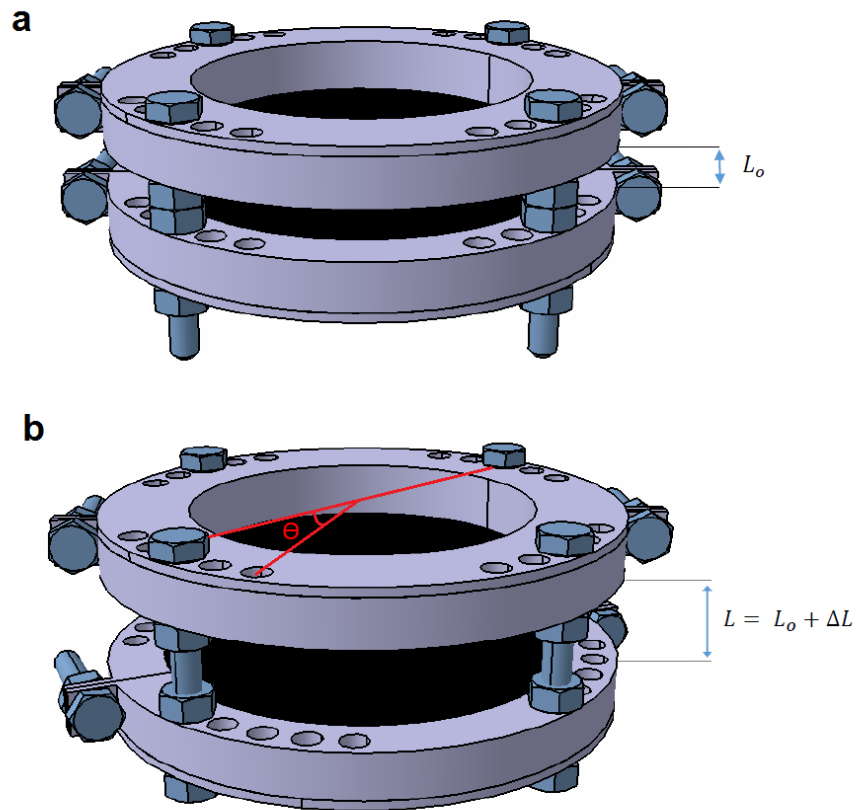


Figure 3.13: Experimental device for constrained swelling 3: (a) with no mechanical loading (initially stress-free) and (b) under twist angle θ and axial extension ΔL .

Since the diameter for Design 2 has been enlarged and the specimen length has been reduced, higher shear strain is expected for the lower twist angle as compared to Design 1. For this reason, three different mechanical loading conditions were carried out using Design 2. The load data are given in Table 3.2.

Table 3.2: Mechanical loading conditions for Design 2

Specimen	Torsional Load	
	Twist angle ($^{\circ}$)	Resulting twist per unit length, γ (rad/mm)
S0T0	0	0
S0T10	10	0.01746
S0T20	20	0.03491

As shown in Table 3.2, the resulting twist per unit length for twist angle of 20° is higher than 30° for Design 1. Thus, it is obvious that a higher shear/stress field can be

generated using Design 2. The advantages and limitations of Design 2 will be discussed in detail in Section 4.4.3.

3.1.2 Experimental setup

3.1.2 (a) Immersion test and swelling measurement

As mentioned previously, specially-designed specimen and devices were developed to investigate the effect of mechanical loadings on the diffusion of solvents. After the desired mechanical loading has been applied, the specimen and device are completely immersed in the solvent for the desired immersion period. In order to determine the swelling level, the mass of the specimen before and after the immersion test is measured. The detailed procedures of the immersion test can be summarized as follow:

1. Before the immersion test, the mass of the dry specimen is measured in air and in distilled water using digital weighting machine.
2. The specimen is subsequently attached into the experimental device to impose the mechanical loading.
3. The experimental devices are then immersed into the solvent at room temperature.
4. After the desire immersion period is achieved, the devices are removed from the biodiesel and the specimens are dismantled from the device. The specimens are then quickly dipped into acetone and cleaned with filter paper to remove excessive oil.
5. The mass of the specimens after immersion is measured as in Step 1. The percentage of mass change and volume change are calculated using the following simple relation (Trakarnpruk & Porntangjitlikit, 2008):

$$\% \text{ Mass Change} = \frac{M_2 - M_1}{M_1} \times 100 \quad (3.1)$$

$$\% \text{ Volume Change} = \frac{(M_2 - M_4) - (M_1 - M_3)}{(M_1 - M_3)} \times 100 \quad (3.2)$$

where M_1 and M_2 are the masses in air (gram) before and after immersion while M_3 and M_4 are the masses in water (gram) before and after immersion. To ensure repeatability of the results, three specimens were used to perform each test and the result presented in this study is the average value of three specimens.

3.1.2 (b) *Mechanical testing*

In order to investigate the effect of swelling, due to solvent diffusion, on the mechanical response of elastomer, mechanical tests were conducted on dry and swollen elastomers at room temperature using an Instron uniaxial test machine equipped with a 10 kN load cell as shown in Figure 3.14. The experimental setup is connected to a computer to record the experimental data. Since thermal effects are not considered in this study, all tests are conducted at a constant strain rate of 0.02 s^{-1} to avoid any excessive increase of temperature in the specimens.

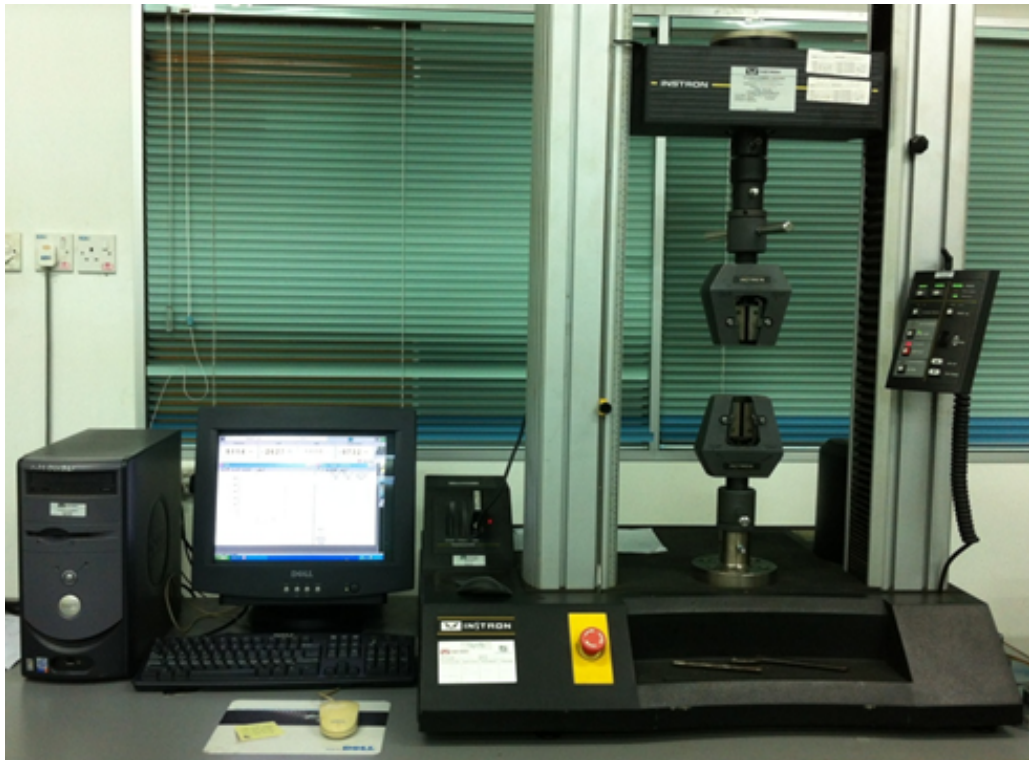


Figure 3.14: Instron uniaxial test machine.

Two types of mechanical tests are conducted and the descriptions of the testing are elaborated as follow:

1. Monotonic uniaxial tensile test. The specimens are subjected to an increasing monotonic tensile load until fracture.
2. Cyclic tensile test at constant maximum strain. The specimens are subjected to five cycles of tensile loading at constant maximum strain. The test is conducted using the displacement-controlled mode and the test profile is illustrated by Figure 3.15.
3. Cyclic tensile test with increasing maximum strain. The specimens are subjected to cyclic loadings with increasing maximum strain at an increment of 50 % per cycle. Note that the stretch is defined by the ratio between the current length to the initial length of the elastomer. In the case of swollen elastomer, the initial length

corresponds to the swollen-unstrained length. The test profile of the cyclic test is illustrated in Figure 3.16.

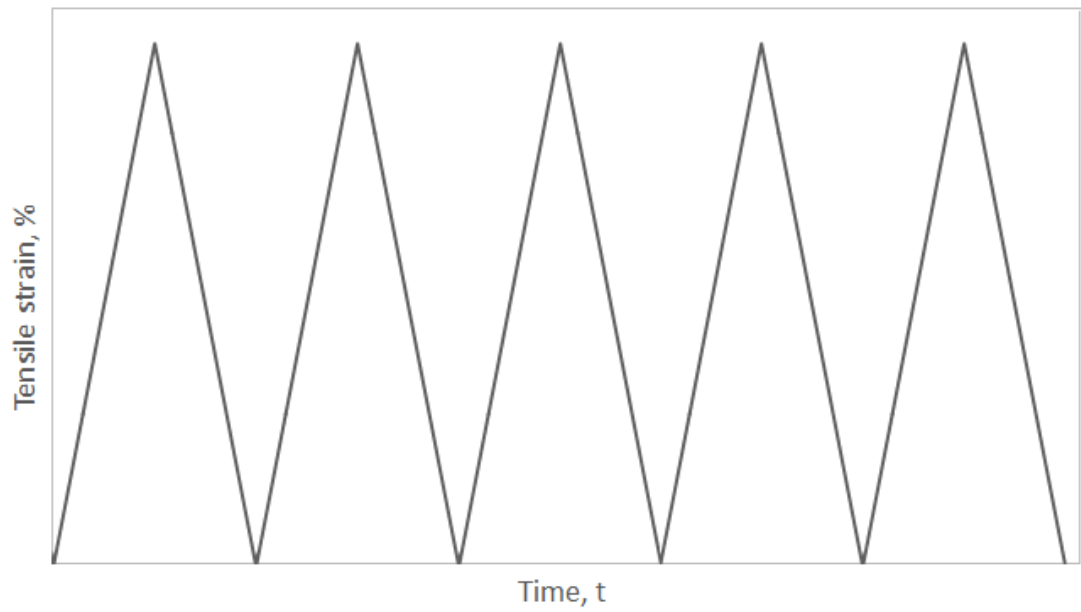


Figure 3.15: Cyclic test at constant maximum strain.

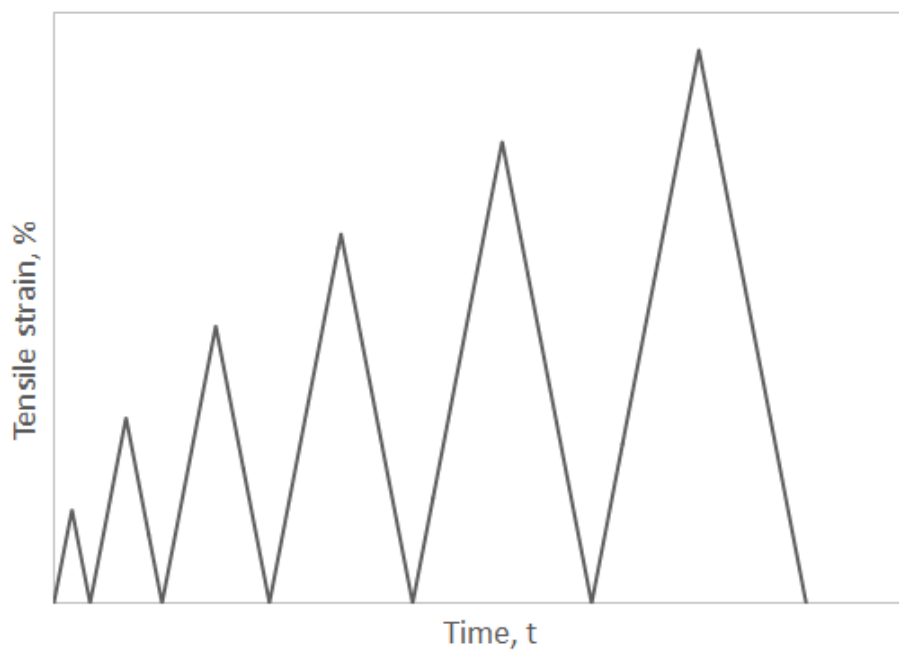


Figure 3.16: Cyclic test with increasing maximum strain.

3.2 Continuum mechanical modeling

In this discussion, a model based on an original definition of the elastic strain energy is proposed. The model adopts the multiplicative split of the deformation gradient into a swelling and a purely mechanical part. In the following, the split of deformation gradient is introduced to derive the constitutive equations for the coupled diffusion-deformation problem. The model for the stress response is then derived by considering the second law of thermodynamics. Finally, two particular cases are considered using the proposed model: prediction of the stress-strain response of swollen elastomers at a given degree of swelling and prediction of the equilibrium swelling of elastomers in the absence and in the presence of a static mechanical deformation.

3.2.1 Kinematics

We consider the diffusion of a solvent into an elastomer undergoing simultaneously a mechanical deformation. The general framework of large strain hyperelasticity is adopted and the material is considered to be homogeneous and isotropic at the Continuum Mechanics scale. Moreover, initially the material is in the dry state and the polymer network of the dry material is assumed as incompressible.

Similarly to the classical approaches adopted in plasticity (Lee, 1969), viscoelasticity (Sidoroff, 1974), compressibility (Ogden, 1984), and later extended to most of the large strain problems (Lubarda, 2004), we consider that the deformation gradient can be split into: a stress-free reversible change in volume due to swelling and an isochoric elastic deformation. The corresponding procedures and the splitting of the deformation gradient are illustrated in Figure 3.17.

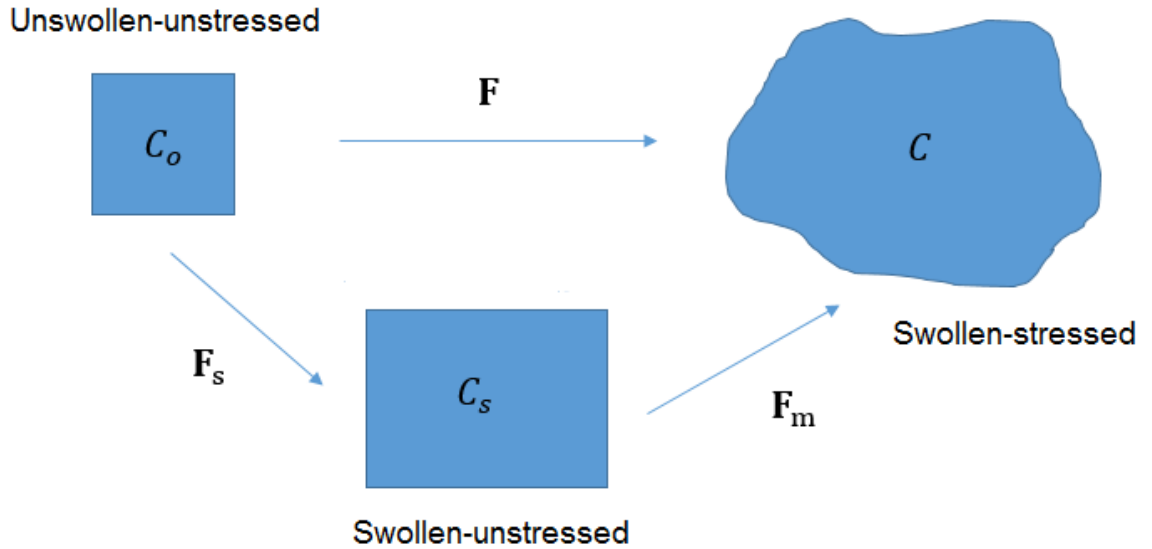


Figure 3.17: Illustration of the deformation.

When an elastomer deforms from its original unswollen-unstressed dry state (C_o) to the final swollen-stressed state (C), the total deformation gradient can be split into two parts as illustrated in Figure 3.17. Initially, the dry specimen is at the unswollen-unstressed configuration, C_o , with a volume of V_o . Then, the specimen undergoes a stress-free reversible volume change due to solvent diffusion which can be characterized by the swelling part of the total deformation gradient \mathbf{F} , denoted by \mathbf{F}_s . The resulting volume change at C_s (swollen-unstressed configuration) is described by the degree of swelling J_s which is given by:

$$J_s = \frac{V_s}{V_o} \tag{3.3}$$

where V_s is the volume of the swollen elastomer. Since the elastomer is assumed to be incompressible under mechanical loads, any changes in volume are assumed to be contributed by the addition of solvent molecules. If the volume occupied by a solvent molecule is denoted by v and the number of solvent molecules absorbed by the elastomer

per unit dry volume is given by c , the degree of swelling can be recast into:

$$J_s = 1 + vc \quad (3.4)$$

Since vc represents the volume fraction of solvent molecules with respect to the dry rubber, the value for J_s will always be greater than 1.

For isotropic swelling, the swelling part of the total deformation gradient, \mathbf{F}_s can be written as a function of J_s as follows:

$$\mathbf{F}_s = J_s^{1/3} \mathbf{I} \quad (3.5)$$

where \mathbf{I} is the identity tensor. For the next stage of deformation where the mechanical loading is imposed to the swollen elastomer, the corresponding deformation is characterized by the mechanical part of the deformation gradient tensor, \mathbf{F}_m . The volume of the swollen rubber is assumed to be constant during the transformation from C_s to the final swollen-stressed configuration C . Thus, the kinematic constraint during this deformation is $\det \mathbf{F}_m = 1$. In summary, the total deformation gradient for the transformation from the unswollen-unstressed configuration (C_o) to swollen-stressed configuration (C) can be described by:

$$\mathbf{F} = \mathbf{F}_s \mathbf{F}_m = J_s^{1/3} \mathbf{F}_m \quad (3.6)$$

3.2.2 Stress response

In order to describe the stress response, we postulate the existence of a strain energy function W , defined per unit of volume of the material in the unswollen-unstressed state. For the deformation between C_o and C_s due to the diffusion of the solvent into the material, the specific free energy which includes the chemical potential of the unmixed pure solvent $\mu_o c$ and the change due to mixing of the solvent with the polymer network

W_s is introduced. Since the deformation between C_s and C is considered as hyperelastic, a strain energy function $W_m(\mathbf{F}_m)$ per unit volume with respect to the swollen-unstressed state is introduced. Thus, the total free energy of the deformation is the sum of these two contributions:

$$W = \tilde{W}(\mathbf{F}) = \hat{W}(J_s, \mathbf{F}_m) = \mu_0 c + W_s(J_s) + J_s W_m(J_s, \mathbf{F}_m) \quad (3.7)$$

Note that W_s only depends on the fluid content c and consequently on J_s through Equation (3.4).

For isothermal mechanical processes in combination with diffusion, the second law of thermodynamics takes the form (Chester & Anand, 2010):

$$\mathcal{D}_{\text{int}} = \mathbf{P} : \dot{\mathbf{F}} + \mu \dot{c} - \dot{W} - \mathbf{j} \cdot \mathbf{Grad} \mu \geq 0 \quad (3.8)$$

where \mathcal{D}_{int} is the internal dissipation, \mathbf{P} is the 1st Piola-Kirchhoff stress tensor with respect to the unswollen-unstressed configuration, μ is the chemical potential in the elastomer and \mathbf{j} is the fluid flux. By recalling Equation (3.7), the strain energy W can be written as a function of both \mathbf{F}_m and J_s . Thus, the rate of change in the strain energy \dot{W} is given by:

$$\dot{W} = \left. \frac{\partial \hat{W}}{\partial J_s} \right|_{\mathbf{F}_m} \dot{J}_s + \left. \frac{\partial \hat{W}}{\partial \mathbf{F}_m} \right|_{J_s} : \dot{\mathbf{F}}_m \quad (3.9)$$

Similarly with reference to Equation (3.6), the rate of change in the deformation gradient is written as:

$$\dot{\mathbf{F}} = \frac{1}{3} J_s^{-2/3} \dot{J}_s \mathbf{F}_m + J_s^{1/3} \dot{\mathbf{F}}_m \quad (3.10)$$

By substituting Equations (3.4), (3.9) and (3.10) into Equation (3.8), the second law of

thermodynamics becomes:

$$\mathcal{D}_{\text{int}} = \left(J_s^{1/3} \mathbf{P} - \frac{\partial \hat{W}}{\partial \mathbf{F}_m} \Big|_{J_s} \right) : \dot{\mathbf{F}}_m + \left(\frac{1}{3} J_s^{-2/3} \mathbf{P} : \mathbf{F}_m + \frac{\mu}{v} - \frac{\partial \hat{W}}{\partial J_s} \Big|_{\mathbf{F}_m} \right) J_s - \mathbf{j} \cdot \mathbf{Grad} \mu \geq 0 \quad (3.11)$$

In the following, two particular cases are considered:

1. Case 1: Prediction of the stress-strain response of swollen elastomers at a given (constant) degree of swelling. More precisely, attention is given on the modeling of the Mullins effect in swollen elastomers.
2. Case 2: Prediction of the equilibrium swelling of elastomers in the absence and in the presence of static mechanical deformation.

3.2.2 (a) Case 1: Stress-strain response of swollen elastomers

In this case, the proposed model does not consider the general coupling between the diffusion of the solvent and the mechanical deformation. Indeed, it focuses on the mechanical responses of the swollen elastomer at a given (constant) degree of swelling, i.e. $\dot{J}_s = 0$. The parameter J_s is introduced merely as a means of defining the state of swelling of the network regardless of whether or not this state is the equilibrium state with respect to the absorption of solvent (Treloar, 1975). Being a first attempt to account for the effect of swelling on stress-softening, it is assumed that the solvent distribution across the cross sections is homogeneous and the swelling is uniform, thus $\mathbf{Grad} \mu = 0$. Consequently, the second law of thermodynamics in Equation (3.11) reduces to:

$$\mathcal{D}_{\text{int}} = \left(J_s^{1/3} \mathbf{P} - \frac{\partial \hat{W}}{\partial \mathbf{F}_m} \Big|_{J_s} \right) : \dot{\mathbf{F}}_m = 0 \quad (3.12)$$

which must be satisfied for all possible values of $\dot{\mathbf{F}}_m$. Considering that the mechanical deformation is isochoric, the incompressibility constraint can be written as (Holzapfel,

2000):

$$\det \mathbf{F}_m = 1 \quad \Leftrightarrow \quad \overline{\det \mathbf{F}_m} = 0 \quad \Leftrightarrow \quad \mathbf{F}_m^{-T} : \dot{\mathbf{F}}_m = 0 \quad (3.13)$$

The combination of Equations (3.12) and (3.13) leads to:

$$\left(J_s^{1/3} \mathbf{P} - \frac{\partial \hat{W}}{\partial \mathbf{F}_m} \Big|_{J_s} \right) = -q \mathbf{F}_m^{-T} \quad (3.14)$$

where q is an arbitrary scalar (Lagrange multiplier) which is classically referred as "hydrostatic pressure". The expression for q can be determined by applying appropriate boundaries conditions and solving the equilibrium equations. Hence, the stress-strain relationship can be obtained by rearranging Equation (3.14):

$$\mathbf{P} = -q J_s^{-1/3} \mathbf{F}_m^{-T} + J_s^{-1/3} \frac{\partial \hat{W}}{\partial \mathbf{F}_m} \Big|_{J_s} \quad (3.15)$$

Recalling Equation (3.7), the first Piola-Kirchhoff tensor given in Equation (3.15) can be recast to:

$$\mathbf{P} = -q J_s^{-1/3} \mathbf{F}_m^{-T} + J_s^{2/3} \frac{\partial W_m}{\partial \mathbf{F}_m} \quad (3.16)$$

The Cauchy stress tensor $\boldsymbol{\sigma}$ is related to the first Piola-Kirchhoff stress tensor through the transformation:

$$\boldsymbol{\sigma} = (\det \mathbf{F})^{-1} \mathbf{P} \mathbf{F}^T = -q J_s^{-1} \mathbf{I} + \frac{\partial W_m}{\partial \mathbf{F}_m} \mathbf{F}_m^T \quad (3.17)$$

Noting that (Holzapfel, 2000):

$$\frac{\partial W_m}{\partial \mathbf{F}_m} \mathbf{F}_m^T = \mathbf{F}_m \left(\frac{\partial W_m}{\partial \mathbf{F}_m} \right)^T = 2 \mathbf{F}_m \frac{\partial W_m}{\partial \mathbf{C}_m} \mathbf{F}_m^T \quad (3.18)$$

where $\mathbf{C}_m = \mathbf{F}_m^T \mathbf{F}_m$, the Cauchy stress tensor becomes:

$$\boldsymbol{\sigma} = -qJ_s^{-1} \mathbf{I} + 2\mathbf{F}_m \frac{\partial W_m}{\partial \mathbf{C}_m} \mathbf{F}_m^T \quad (3.19)$$

Assuming that the swollen elastomer is isotropic, $W_m(J_s, \mathbf{C}_m)$ may be expressed in terms of $\hat{W}_m(J_s, I_{1m}, I_{2m})$, where:

$$I_{1m} = \text{tr} \mathbf{C}_m \quad I_{2m} = \frac{1}{2}(I_{1m}^2 - \text{tr}(\mathbf{C}_m^2)) \quad (3.20)$$

Using chain rules, the Cauchy stress can be recast to:

$$\boldsymbol{\sigma} = -qJ_s^{-1} \mathbf{I} + 2 \left[\left(\frac{\partial \hat{W}_m}{\partial I_{1m}} + I_{1m} \frac{\partial \hat{W}_m}{\partial I_{2m}} \right) \mathbf{B}_m - \frac{\partial \hat{W}_m}{\partial I_{2m}} \mathbf{B}_m^2 \right] \quad (3.21)$$

where $\mathbf{B}_m = \mathbf{F}_m \mathbf{F}_m^T$ is the mechanical left Cauchy Green tensor. When dealing with swollen elastomers, it is often more convenient to express the engineering stress with respect to the swollen-unstressed state of the material, denoted as $\hat{\mathbf{P}}$. It's expression can be obtained from $\hat{\mathbf{P}} = (\det \mathbf{F}_m) \boldsymbol{\sigma} \mathbf{F}_m^{-T}$, which yields to:

$$\hat{\mathbf{P}} = -qJ_s^{-1} \mathbf{F}_m^{-T} + 2 \left[\left(\frac{\partial \hat{W}_m}{\partial I_{1m}} + I_{1m} \frac{\partial \hat{W}_m}{\partial I_{2m}} \right) \mathbf{F}_m - \frac{\partial \hat{W}_m}{\partial I_{2m}} \mathbf{F}_m \mathbf{C}_m \right] \quad (3.22)$$

Finally, the tensors $\hat{\mathbf{P}}$ and \mathbf{P} are simply related through:

$$\mathbf{P} = J_s^{2/3} \hat{\mathbf{P}} \quad (3.23)$$

In the case when \hat{W}_m is chosen to depend on the principal mechanical stretches λ_{im} , the principal Cauchy stresses σ_i can be related to the principal mechanical stretches as fol-

lows:

$$\sigma_i = -qJ_s^{-1} + \lambda_{im} \frac{\partial \hat{W}_m}{\partial \lambda_{im}} \quad \text{no sum on } i \quad (3.24)$$

and the corresponding engineering stress with respect to the swollen-unstressed configuration is given by:

$$\hat{P}_i = \frac{\sigma_i}{\lambda_{im}} \quad \text{no sum on } i \quad (3.25)$$

Remark 1 *In order to use Equations (3.24) and (3.25) for the modeling of the Mullins effect in swollen elastomers, a modification of the form of W_m in Equation (3.7) is needed and is given in detail in Section 3.2.3.*

3.2.2 (b) Case 2: Prediction of equilibrium swelling

Consider a process of diffusion of biodiesel into an elastomer undergoing simultaneously a static mechanical loading. After a certain period of time, equilibrium swelling is achieved. In this case, we have:

$$\mu = \mu_o = \text{constant} \quad \Longleftrightarrow \quad \mathbf{Grad} \mu = 0 \quad (3.26)$$

Thus, the second law of thermodynamics in Equation (3.11) reduces to:

$$\left(J_s^{1/3} \mathbf{P} - \frac{\partial \hat{W}}{\partial \mathbf{F}_m} \Big|_{J_s} \right) : \dot{\mathbf{F}}_m + \left(\frac{1}{3} J_s^{-2/3} \mathbf{P} : \mathbf{F}_m + \frac{\mu}{v} - \frac{\partial \hat{W}}{\partial J_s} \Big|_{\mathbf{F}_m} \right) \dot{J}_s \geq 0 \quad (3.27)$$

Using the argumentation of Coleman and Gurtin (1967), we obtain the following constitutive relation:

$$\mathbf{P} = -qJ_s^{-1/3} \mathbf{F}_m^{-T} + J_s^{-1/3} \frac{\partial \hat{W}}{\partial \mathbf{F}_m} \Big|_{J_s} = -qJ_s^{-1/3} \mathbf{F}_m^{-T} + J_s^{2/3} \frac{\partial W_m}{\partial \mathbf{F}_m} \quad (3.28)$$

which is similar to Equations (3.15) and (3.16) respectively.

The second constitutive relation obtained from Equation (3.27) is:

$$\left(\frac{1}{3} J_s^{-2/3} \mathbf{P} : \mathbf{F}_m + \frac{\mu}{\nu} - \frac{\partial \hat{W}}{\partial J_s} \Big|_{\mathbf{F}_m} \right) J_s = 0 \quad (3.29)$$

where \hat{W} can be represented on the basis of Equation (3.7):

$$\frac{\partial \hat{W}}{\partial J_s} \Big|_{\mathbf{F}_m} = \frac{\mu_o}{\nu} + \frac{1}{\nu} \frac{dW_s(c)}{dc} + W_m + J_s \frac{\partial W_m}{\partial J_s} \Big|_{\mathbf{F}_m} \quad (3.30)$$

By replacing Equation (3.30) into (3.29) and rearranging the equation we have:

$$\frac{\mu}{\nu} = \frac{\mu_o}{\nu} + \frac{1}{\nu} \frac{dW_s(c)}{dc} + W_m + J_s \frac{\partial W_m}{\partial J_s} \Big|_{\mathbf{F}_m} - \frac{1}{3} J_s^{-2/3} \mathbf{P} : \mathbf{F}_m \quad (3.31)$$

By recalling the expression of \mathbf{P} from Equation (3.28), the following equation can be established:

$$\begin{aligned} \mathbf{P} : \mathbf{F}_m &= \left(-q J_s^{-1/3} \mathbf{F}_m^{-T} + J_s^{2/3} \frac{dW_m}{d\mathbf{F}_m} \right) : \mathbf{F}_m \\ &= -3q J_s^{-1/3} + J_s^{2/3} \text{tr} \left(\frac{dW_m}{d\mathbf{F}_m} \mathbf{F}_m^T \right) \end{aligned} \quad (3.32)$$

The combination of Equation (3.17) and Equation (3.32) leads to:

$$\frac{1}{3} J_s^{-2/3} \mathbf{P} : \mathbf{F}_m = -q J_s^{-1} + \frac{1}{3} \text{tr}(\boldsymbol{\sigma} + q J_s^{-1} \mathbf{I}) = \frac{1}{3} \text{tr} \boldsymbol{\sigma} \quad (3.33)$$

where $\frac{1}{3} \text{tr} \boldsymbol{\sigma}$ is also known as the hydrostatic part of the Cauchy stress tensor. Finally, we obtain the equation for the chemical potential as:

$$\frac{\mu}{\nu} = \frac{\mu_o}{\nu} + \frac{1}{\nu} \frac{dW_s(c)}{dc} + W_m + J_s \frac{\partial W_m}{\partial J_s} \Big|_{\mathbf{F}_m} - \frac{1}{3} \text{tr} \boldsymbol{\sigma} \quad (3.34)$$

As mentioned earlier, $\mu = \mu_o$ holds under equilibrium conditions. Then, we obtain the

final form of the chemical potential as:

$$\frac{1}{v} \frac{dW_s(c)}{dc} + W_m + J_s \left. \frac{\partial W_m}{\partial J_s} \right|_{\mathbf{F}_m} - \frac{1}{3} \text{tr} \boldsymbol{\sigma} = 0 \quad (3.35)$$

By introducing proper strain energy function and free energy due to mixing, the degree of swelling in the equilibrium state can be obtained by solving Equation (3.35) for given static mechanical loading conditions.

3.2.3 Mullins effect

As a first step to model the mechanical response of elastomers under cyclic loadings for a given degree of swelling (Case 1 of Section 3.2.2), only the softening phenomenon (Mullins effect) is addressed. Here, softening in elastomers is considered as irreversible isotropic damage which can be represented by a scalar internal variable κ . Under such circumstances, the general multiplicative decomposition of the deformation gradient tensor illustrated in Figure 3.17 remains applicable. Nevertheless, the following points are worth noting:

1. During the transformation of the body from C_o to C , the elastomer undergoes two different kinds of softening:
 - a) Softening due to isotropic expansion (swelling) of polymeric network corresponding to the transformation from C_o to C_s . The network expansion increases the chain separation which results in a reduction of the secondary intermolecular bonding forces (Callister, 1997). Consequently, the material becomes softer.
 - b) Softening associated with the Mullins effect observed under cyclic mechanical loading. This softening which occurs during the transition from C_s to C is

often regarded as essentially being caused by the fillers in the elastomer matrix (Holzapfel, 2000).

2. Experiments showed that increasing the degree of swelling (i.e. increasing softening due to swelling) reduces the Mullins softening (Andriyana et al., 2012). While the precise link between the above two kinds of softening remains unclear, it appears that swelling softening affects the material capacity to accommodate further softening under mechanical loading.

3.2.3 (a) Constitutive equations

To describe the Mullins softening in an elastomer with a given degree of swelling, the strain energy in Equation (3.7) is extended as below:

$$W = \tilde{W}(\mathbf{F}, \kappa) = \hat{W}(J_s, \kappa, \mathbf{F}_m) = \mu_o c + W_s(J_s) + J_s W_m(J_s, \kappa, \mathbf{F}_m) \quad (3.36)$$

As a consequence, the internal dissipation for a given degree of swelling from Equation (3.12) then becomes:

$$\mathcal{D}_{\text{int}} = \left(J_s^{1/3} \mathbf{P} - \frac{\partial \hat{W}}{\partial \mathbf{F}_m} \Big|_{J_s, \kappa} \right) : \dot{\mathbf{F}}_m - \frac{\partial \hat{W}}{\partial \kappa} \Big|_{J_s, \mathbf{F}_m} \dot{\kappa} \geq 0 \quad (3.37)$$

The above inequality must be satisfied for all values of $\dot{\mathbf{F}}_m$ and $\dot{\kappa}$ with a kinematic constraint of $\det \mathbf{F}_m = 1$ (swollen elastomer is assumed to be incompressible). Following the arguments of Coleman and Gurtin (1967), the following constitutive equation is obtained for the first Piola-Kirchhoff stress:

$$\mathbf{P} = -q J_s^{-1/3} \mathbf{F}_m^{-T} + J_s^{-1/3} \frac{\partial \hat{W}}{\partial \mathbf{F}_m} \Big|_{J_s, \kappa} \quad (3.38)$$

Using Equation (3.36), the respective expressions for the Cauchy stress tensor and the second Piola-Kirchhoff tensors are:

$$\begin{aligned}\boldsymbol{\sigma} &= -qJ_s^{-1}\mathbf{I} + 2\left[\left(\frac{\partial\hat{W}_m}{\partial I_{1m}} + I_{1m}\frac{\partial\hat{W}_m}{\partial I_{2m}}\right)\mathbf{B}_m - \frac{\partial\hat{W}_m}{\partial I_{2m}}\mathbf{B}_m^2\right] \\ \hat{\mathbf{P}} &= -qJ_s^{-1}\mathbf{F}_m^{-T} + 2\left[\left(\frac{\partial\hat{W}_m}{\partial I_{1m}} + I_{1m}\frac{\partial\hat{W}_m}{\partial I_{2m}}\right)\mathbf{F}_m - \frac{\partial\hat{W}_m}{\partial I_{2m}}\mathbf{F}_m\mathbf{C}_m\right]\end{aligned}\quad (3.39)$$

These expressions are identical with Equations (3.21) and (3.22) obtained earlier. However, the final expressions are different since \hat{W} has an additional dependence on the damage variable κ . The constitutive equations in Equation (3.39) must be complemented by a kinetic relation which describes the evolution of the involved internal variable κ . The corresponding evolution equation has to be consistent with the non-negativity of the internal dissipation. To this end, we consider the remaining term in inequality (3.37) as follows:

$$\mathcal{D}_{\text{int}} = \mathcal{A}_\kappa \dot{\kappa} \geq 0 \quad \text{where} \quad \mathcal{A}_\kappa = -\left.\frac{\partial\hat{W}}{\partial\kappa}\right|_{J_s, \mathbf{F}_m} = -J_s \left.\frac{\partial\hat{W}_m}{\partial\kappa}\right|_{J_s, \mathbf{F}_m} \quad (3.40)$$

In the above expression, \mathcal{A}_κ is the thermodynamic force associated with the damage variable κ . Depending on the nature of the variable κ , different evolution equations $\dot{\kappa}$ can be adopted provided that they satisfy inequality (3.40). For instance, the simplest sufficient condition to fulfil the above inequality is:

$$\dot{\kappa} = \frac{1}{\tau(J_s)} \mathcal{A}_\kappa \quad (3.41)$$

where $\tau = \tau(J_s) > 0$ is a material function. This inequality must be fulfilled for thermodynamical reasons. In the following section, the form of the strain energy function \hat{W}_m and the evolution rule $\dot{\kappa}$ describing the Mullins effect in swollen elastomers are discussed based on the theory of the two-phase model of Mullins and Tobin (1957) and Qi and

Boyce (2004).

3.2.3 (b) *Two-phase model for Mullins effect in swollen elastomer*

The two-phase model used to describe the Mullins effect in dry elastomers was developed by Qi and Boyce (2004) and is based on a strain amplification factor as originally proposed by Mullins and Tobin (1957) (see Section 2.5). Mullins and Tobin (1957) described filled-elastomers as a two-phase system containing a hard phase and a soft phase. The strain is sustained only by the soft phase whose percentage increases with the maximum strain applied to the material. As strain is applied to the elastomer, a conversion from the hard phase to the soft phase takes place which is an irreversible process. The authors suggested that the irreversible conversion is the origin of the softening observed in the elastomer under cyclic loading. Since the strain is sustained solely by the soft phase, the local strain in the soft phase is necessarily amplified over that of the macroscopic applied strain. The combination of the hard-to-soft phase conversion along with the amplified strain serve as the basis of the two-phase model proposed by Qi and Boyce (2004) and will be reproduced in this research to describe the Mullins effect in swollen elastomers under cyclic loading.

Let v_s be the effective volume fraction of the soft phase and J_s be the degree of swelling. For an incompressible isotropic swollen elastomer undergoing stress-softening due to the Mullins effect, the strain energy function (per unit of material volume in unswollen-unstressed state) corresponding to the soft phase has a form:

$$\begin{aligned}
 \hat{W} &\equiv \hat{W}_{\text{sp}}(\mathbf{F}_m, X(v_s), v_s, J_s) \\
 &= \bar{W}_{\text{sp}}(\lambda_{1m}, \lambda_{2m}, X(v_s), v_s, J_s) \\
 &= W_{\text{sp}}(\lambda_{1m}, \lambda_{2m}, v_s, J_s)
 \end{aligned} \tag{3.42}$$

where X is the amplification factor which depends on the volume fraction v_s of the soft

phase. Following Qi and Boyce (2004), the dependence of X on v_s is given in a general polynomial form of:

$$X = 1 + 3.5(1 - v_s) + 18(1 - v_s)^2 \quad (3.43)$$

Consequently, the internal dissipation for a given degree of swelling from Equation (3.37) becomes:

$$\mathcal{D}_{\text{int}} = \left(J_s^{1/3} \mathbf{P} - \frac{\partial W_{\text{sp}}}{\partial \mathbf{F}_m} \Big|_{J_s, v_s} \right) : \dot{\mathbf{F}}_m - \frac{\partial W_{\text{sp}}}{\partial v_s} \Big|_{J_s, \mathbf{F}_m} \dot{v}_s \geq 0 \quad (3.44)$$

Using the argumentation of Coleman and Gurtin (1967), we obtain the following constitutive relations having similar forms to those given in Equations (3.24) and (3.25):

$$\begin{aligned} \sigma_i &= -qJ_s^{-1} + J_s^{-1} \lambda_{\text{im}} \frac{\partial W_{\text{sp}}}{\partial \lambda_{\text{im}}} \quad \text{no sum on } i \\ \hat{P}_i &= \frac{\sigma_i}{\lambda_{\text{im}}} \end{aligned} \quad (3.45)$$

The residual inequality then reduces to:

$$- \frac{\partial W_{\text{sp}}}{\partial v_s} \Big|_{J_s, \mathbf{F}_m} \dot{v}_s \geq 0. \quad (3.46)$$

The above inequality must be satisfied during arbitrary deformation histories. The form of W_{sp} and the flow rule \dot{v}_s describing the increase of the soft phase with deformation are specified in Section 5.1.2.

3.3 Finite element analysis

Finite element analysis (FEA) is the numerical simulation of the behaviour of a finite number of small subdomains, known as elements, to approximate the behaviour of a larger domain. FEA uses the numerical technique to find approximate solutions to boundary value problems for differential equations. FEA is extremely useful in the context of designing, prototyping, failure identification and to estimate the fatigue life of a compo-

ment. While applications in real life normally involve big and complicated design parts, problems solving by FEA results in a reduction of time and cost with a promising solution (Jha, 2008). In order to solve FEA problems, we need a FEA solver. In this study, ABAQUS is used. In this section, the analysis using ABAQUS is provided as well as some notes on implementing the developed constitutive model into the FEA code using the user-subroutine for a hyperelastic material (UHYPER).

3.3.1 Finite Element Analysis using ABAQUS

A complete ABAQUS analysis usually consists of three distinct stages: preprocessing, simulation and postprocessing. The analysis flow is shown in Figure 3.18.

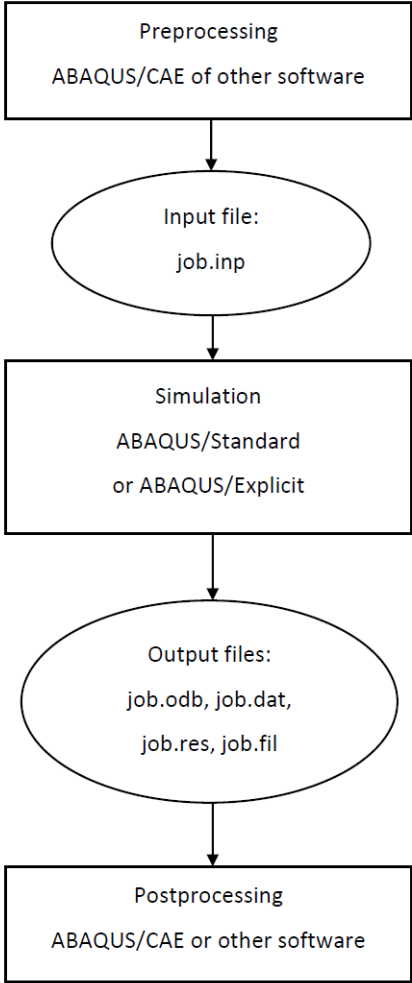


Figure 3.18: Flow of a complete ABAQUS analysis.

In the preprocessing stage, the model representing the physical problem must be defined in order to create an ABAQUS input file. The model can be created either by using the software ABAQUS/CAE or import from another CAE software. However, the input file for ABAQUS for simple analyses can be created directly using a text editor.

After the input file has been created, the simulation can be run by submitting a job in ABAQUS once the material parameters describing the mechanical behaviour of the material are provided. The material parameters can be entered as coefficients or determined by inserting experimental data. The FEA solver then determines the stiffness matrix, K^{el} based upon the spatial distribution, the material behaviour and the corresponding nodal loads at each element.

The results from the simulation can be evaluated in the postprocessing stage once the simulation is completed. Depending on the requirement of the analysis, various results such as displacements, stresses and other fundamental variables can be extracted from the simulation. The results can be evaluated using visualization module of ABAQUS/CAE or other postprocessor. A complete flow of data and actions from the start of an ABAQUS/Standard analysis to the end of a step is given in Figure 3.19.

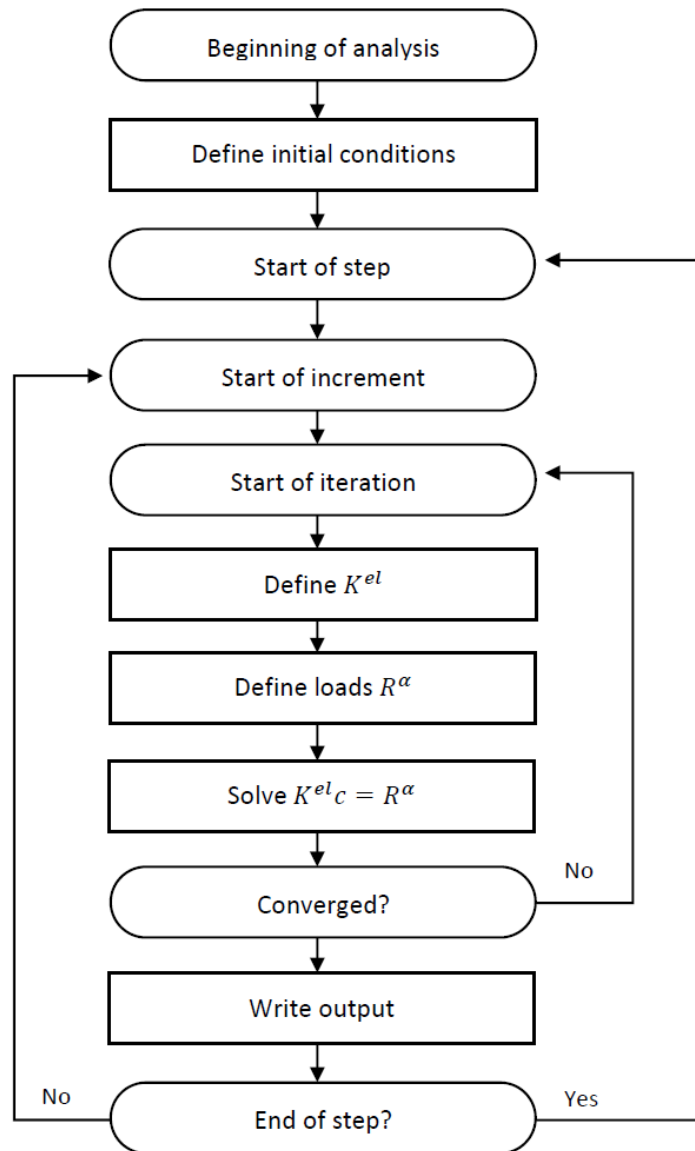


Figure 3.19: Global flow in ABAQUS/Standard.

3.3.2 User subroutine and notes on its implementation

There is a wide range of ABAQUS built-in models which are available for various analyses. However, if a particular analysis cannot be modeled with the available ABAQUS material models, a special code known as user subroutine is needed. In our case, a new constitutive model for a hyperelastic material has been developed. Thus, a user subroutine is needed to define the strain energy potential for the hyperelastic material. The user subroutine UHYPER:

1. is called at all material calculation points of elements for which the material definition contains user-defined hyperelastic behaviour.
2. can consider material behaviour dependent on field variables or state variables.
3. requires that the values of the derivatives of the strain energy density function of the hyperelastic material be defined with respect to the strain invariants.

In order to simulate using FEA, the mechanical behaviour of the elastomer has to be modeled using a strain energy function, W , which can be expressed as function of the strain invariants. However, the strain energy function is written with regard to the dry state as the reference. This can cause problems due to singularities in a numerical calculation. To avoid this problem, the reference state has to be modified such that the network, under vanishing mechanical load is in equilibrium with a solvent of chemical potential, μ_o (Hong et al., 2009). The modified network experiences isotropic swelling with principal stretches $\lambda_1 = \lambda_2 = \lambda_3$. If the free swelling stretch is denoted by λ_o , the modified deformation gradient with relative to the dry state can be written as:

$$\mathbf{F}_o = \begin{bmatrix} \lambda_o & 0 & 0 \\ 0 & \lambda_o & 0 \\ 0 & 0 & \lambda_o \end{bmatrix} \quad (3.47)$$

In numerical calculations, the modified free swelling state is used as the reference state, thus

$$\mathbf{F} = \mathbf{F}'\mathbf{F}_o \quad (3.48)$$

where \mathbf{F} is the deformation gradient of the current state relative to the dry state and \mathbf{F}' is the deformation gradient of the current state relative to the modified free swelling state.

Thus, the strain energy function from Equation (3.7) can be rewritten as:

$$\hat{W}'(\mathbf{F}', J_s) = \lambda_o^{-3} \hat{W}(\mathbf{F}, J_s) \quad (3.49)$$

The theory is implemented in ABAQUS by using the user-defined subroutine for hyperelastic material, UHYPER. The diffusion of the solvent is mimicked by a temperature-like variable.

CHAPTER 4

EXPERIMENTAL RESULTS AND DISCUSSION

This chapter presents the results obtained from experimental works described in the previous chapter. First, the general characteristics of swelling in biodiesel are explored. Two cases are considered: stress-free swelling and swelling in the presence of a static mechanical deformation (constrained swelling). The roles of mechanical deformation and carbon black content will be discussed.

In the second part, the mechanical responses of swollen elastomers are investigated. The effect of swelling on the inelastic responses of the elastomer under cyclic loading are discussed.

4.1 Swelling results

4.1.1 Stress-free swelling

As mentioned in Section 3.1.1 (a), stress-free swelling is conducted under two different conditions: with and without device. For stress-free swelling without device, the dumbbell specimens are immersed completely in the solvent without the device until equilibrium swelling is achieved. As for stress-free swelling with device, the distance between the metallic plates is adjusted from time to time to ensure that the swollen specimen is under stress-free condition. In this subsection, the swelling results and rates of swelling for both conditions are presented.

4.1.1 (a) Stress-free swelling without device

The variation of the volume change of unfilled and filled dumbbell specimen as a function of the immersion duration is shown in Figure 4.1. It can be seen that, regardless the amount of carbon black content, equilibrium swelling is achieved after around 600

hours of immersion. The percentage of volume change at equilibrium swelling is about 24 %, 17 % and 14 % for unfilled elastomer, and two filled elastomers with 25 and 40 % of carbon black content, respectively. The presence of carbon black appears to restrict the diffusion of the solvent into the elastomers since the elastomeric network becomes stiffer with the addition of filler (Ramesan, 2005). Thus, it provides more resistance and a barrier for solvent penetration (Abdul Kader & Bhowmick, 2003). Physically, the filled elastomer with 40 % of carbon black is the stiffest. For the unfilled specimen, the diffusion of solvent molecules into the elastomeric matrix is favorable as there is no filler preventing the diffusion of solvent into the free volume between the molecules (Kraus, 1963).

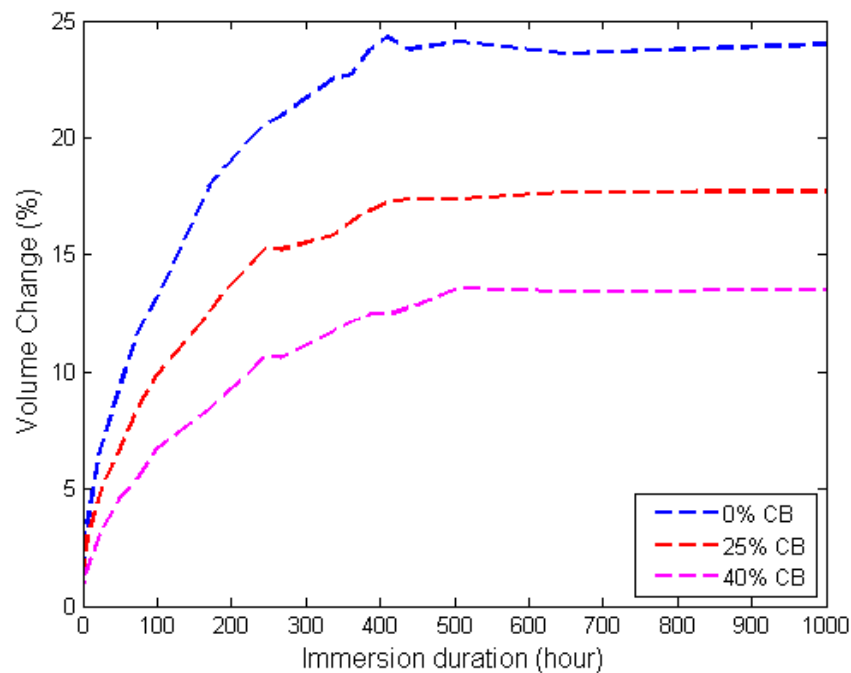


Figure 4.1: Volume change of stress-free elastomer specimens (without device) with different carbon black content.

The rates of swelling are depicted in Figure 4.2. In this figure, the swelling rate is obtained by calculating the slope of the swelling curve in Figure 4.1. From this figure, it is observed that the rate of swelling decreases with the immersion duration. The rate of

volume change is high at the initial stage and slowly descends until equilibrium swelling is achieved. Initially there is a high concentration gradient between the dry elastomer and the biodiesel, which leads to a high rate of solvent absorption. Subsequently, the rate of swelling decreases with the increase in immersion duration and approaches zero as the material reaches equilibrium swelling. As indicated in Figure 4.2, the introduction of filler appears to restrict the rate of swelling (Egwaikhide et al., 2007).

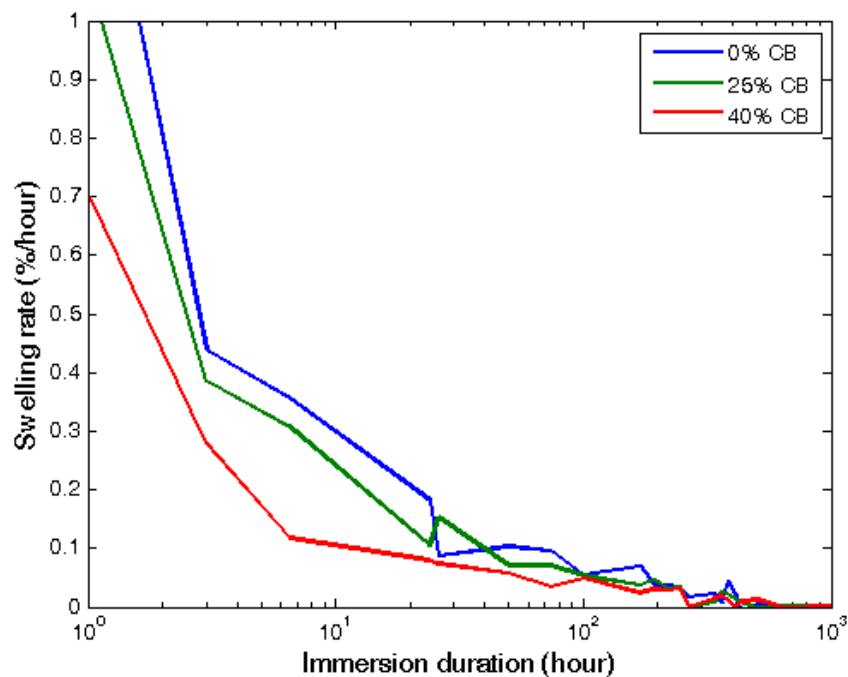


Figure 4.2: Rates of swelling of stress-free specimens (without device).

4.1.1 (b) Stress-free swelling with device

Figure 4.3 shows the resulting volume change from dry until equilibrium swelling. The resulting rates of swelling are depicted in Figure 4.4. It can be seen that the results for free swelling with and without device show exactly the same trend except for slightly higher volume change for the one without device. The reason for this observation could be caused by the boundary conditions at both ends of the specimen which are clamped with the device. At equilibrium swelling, the volume change recorded for unfilled and filled elastomers with 25 % and 40 % of carbon black content are 23 %, 17 % and 13.5 %

respectively.

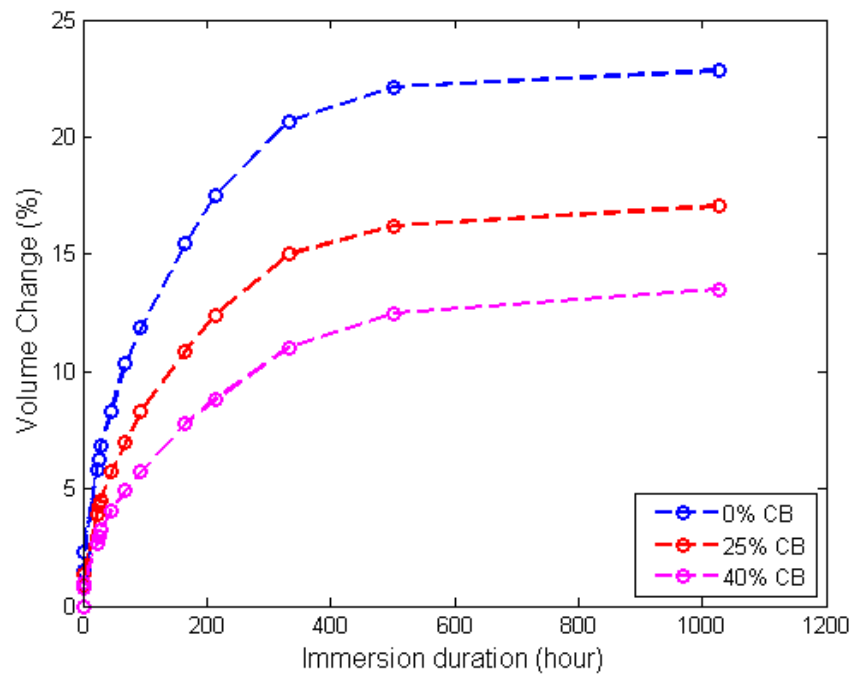


Figure 4.3: Volume change of stress-free specimens (with device) with different carbon black content.

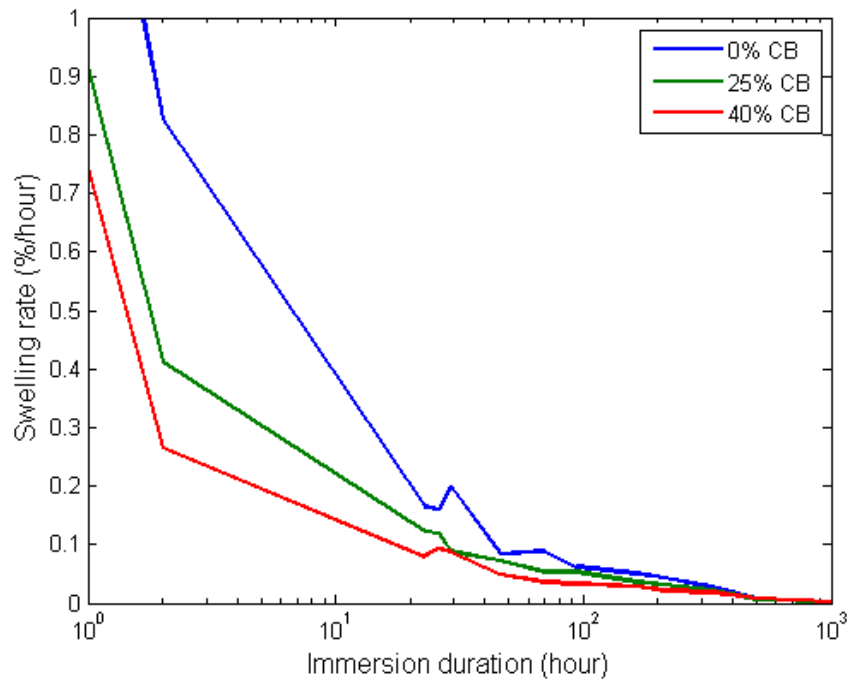


Figure 4.4: Rates of swelling of stress-free specimens (with device).

Remark 2 Note that in order to be able to compare the results between free swelling and constrained swelling, in the following parts, the results for free swelling with device are referred to whenever the case for free swelling is mentioned.

4.1.2 Constrained swelling 1: static uniaxial strain

In this section, the effect of the presence of a constant uniaxial mechanical strain on swelling is addressed. For this purpose, the distance between the metallic handles are fixed at 3 different constant stretches: $\lambda = 1.00$, 1.25 and 1.50, respectively. The stretch is defined as the ratio between the current length to the original length of the specimen between the two metallic handles. Note that the corresponding engineering strain is simply given by $\varepsilon = \lambda - 1$. The resulting volume change ratios are given in Figures 4.5, 4.6 and 4.7.

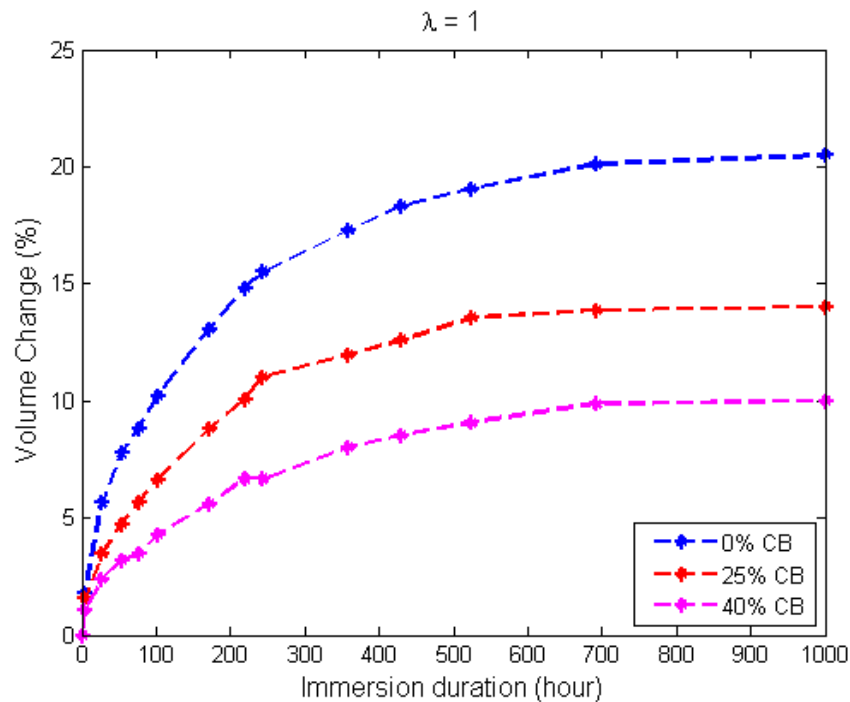


Figure 4.5: Volume change of elastomer specimens with different carbon black content at $\lambda = 1$.

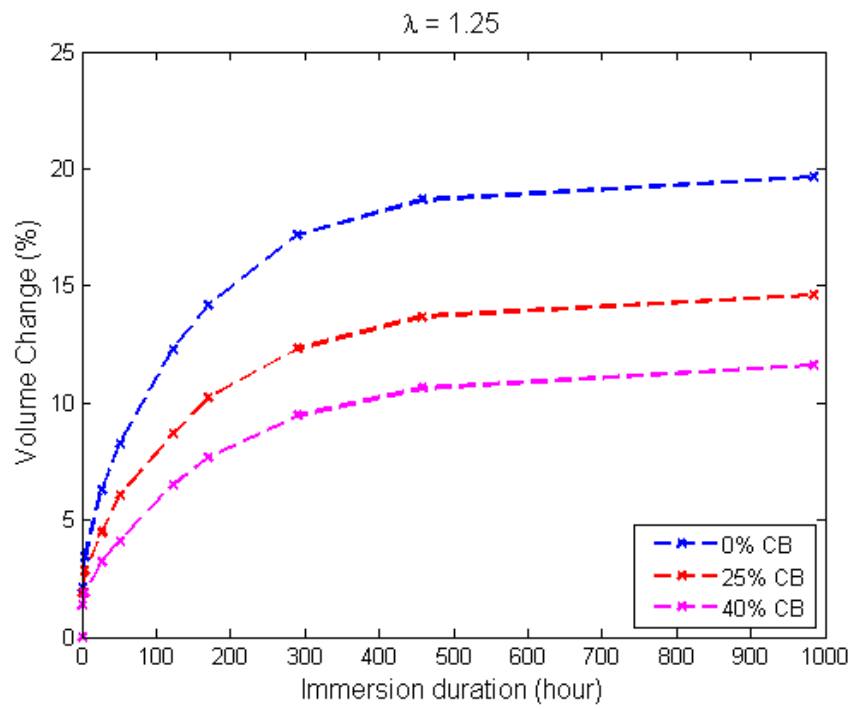


Figure 4.6: Volume change of elastomer specimens with different carbon black content at $\lambda = 1.25$.

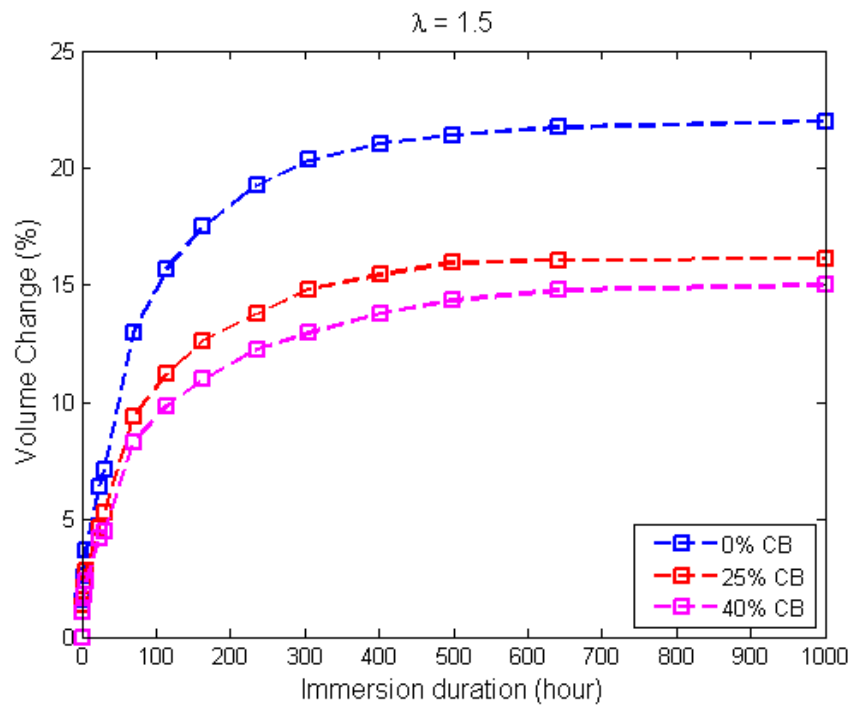


Figure 4.7: Volume change of elastomer specimens with different carbon black content at $\lambda = 1.5$.

Generally, for all imposed strain levels, the trend of swelling is similar to that for free swelling. The unfilled rubber specimens exhibit the highest swelling levels followed by the elastomer specimens with 25 and 40 wt% of carbon black. Moreover, as shown in Figures 4.8 to 4.10, the introduction of the static uniaxial strain appears to alter the swelling characteristics of elastomers (Bhattacharya & Bhowmick, 2008). For a given immersion duration, the uniaxial tensile strain acts as accelerator for the penetration of solvent molecules, i.e. the rate of swelling and thus the total swelling increase with increasing λ . While the additional tensile strain appears to increase the solvent uptake for filled elastomers, it is to note that for unfilled elastomer the equilibrium swelling for $\lambda = 1$ is greater than $\lambda = 1.25$. Although initially the volume change for $\lambda = 1.25$ is greater than $\lambda = 1$, the volume change of $\lambda = 1.25$ overtakes that for $\lambda = 1$ as indicated by point P in Figure 4.8. While the precise reason for this phenomenon is not known, it could be attributed to the buckling of the specimen for $\lambda = 1$. Indeed, after 300 hours of immersion, this specimen undergoes buckling. This buckling appears to modify the stress state in the specimen resulting in more solvent uptake.

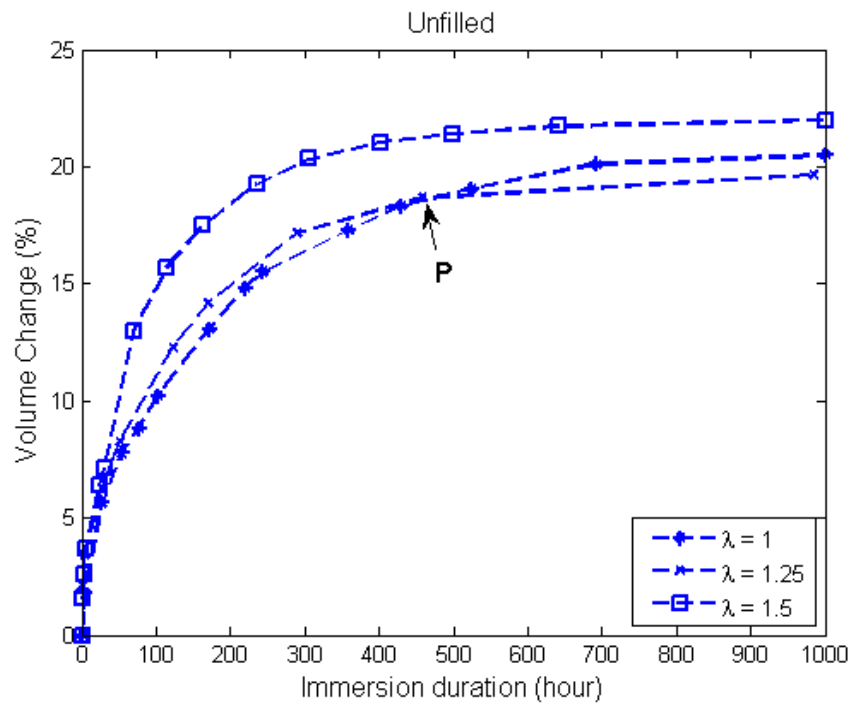


Figure 4.8: Volume change of specimens at different tensile strains for unfilled elastomer.

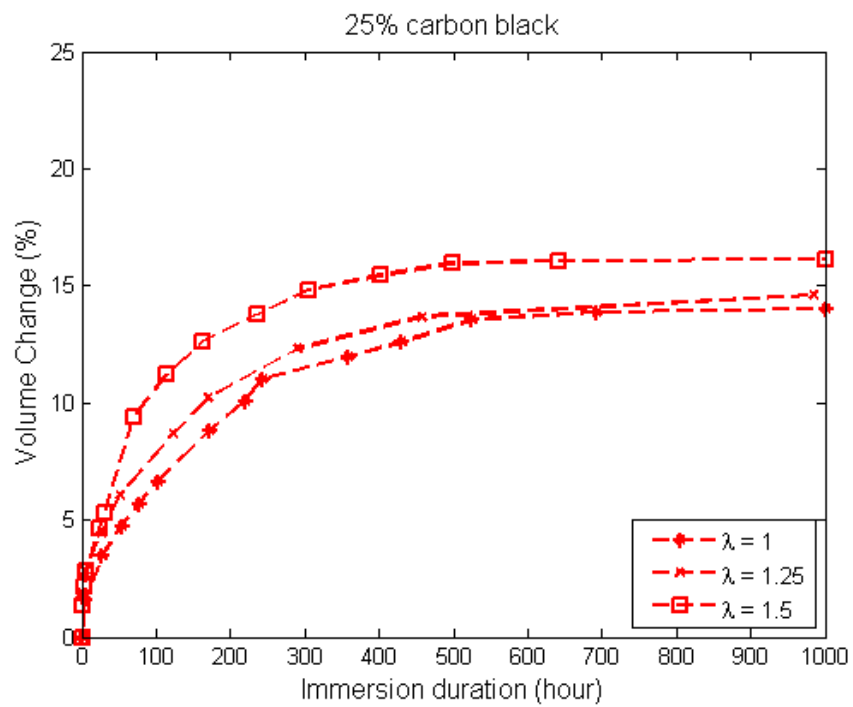


Figure 4.9: Volume change of specimens at different tensile strains for filled elastomer (25 wt% carbon black).

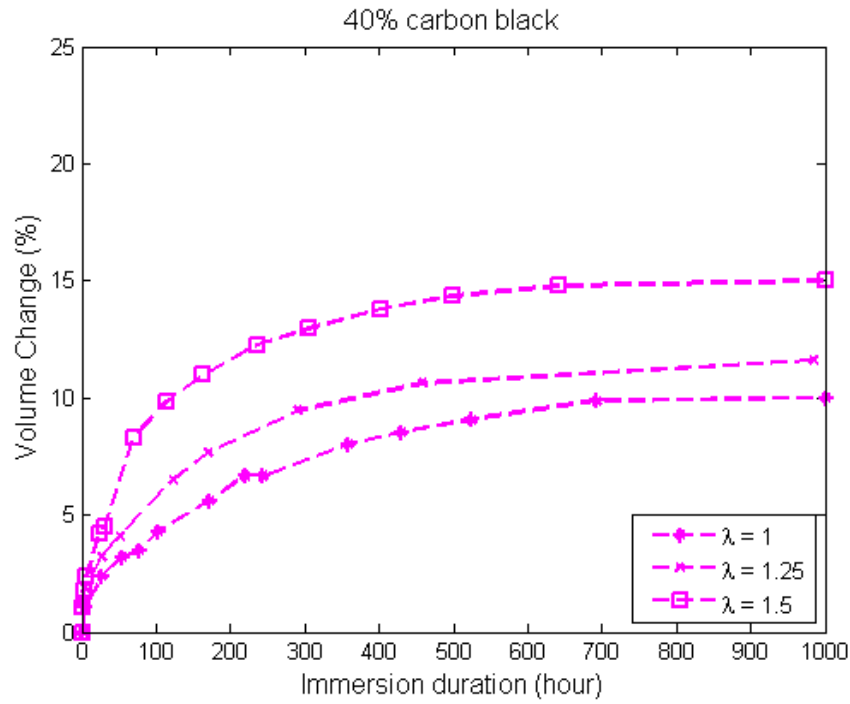


Figure 4.10: Volume change of specimens at different tensile strains for filled elastomer (40 wt% carbon black).

The increasing swelling level with strain could be explained by the hydrostatic part of the Cauchy stress in the elastomer. According to Treloar (1975), negative hydrostatic stress facilitates swelling and the application of tensile strain generates more negative hydrostatic stress. Thus, the resulting swelling increases as more tensile strain is applied to the specimen. The detailed discussion of this theory is provided in Section 4.3.

For filled elastomers, closer investigation on Figures 4.5, 4.6 and 4.7 reveals that the swelling curve of elastomer with 25 wt% carbon black and that with 40 wt% carbon black become closer as higher strain is applied. This observation is related to two opposite roles of filler on the ability of elastomers to absorb solvents. In one hand, as discussed in the previous section, increasing carbon black content yields to a stiffer elastomeric network which acts as barrier for solvent penetration (Mostafa et al., 2009). In another hand, carbon black acts as a strain amplifier when a macroscopic strain is applied to the elastomers (Guth, 1945): the higher the carbon black content, the higher the strain

amplification. The strain amplifying concept considers carbon black as rigid particles which do not participate in the deformation when a strain is applied to the elastomer. The soft rubbery matrix is assumed to behave exactly the same as the pure vulcanizate without the carbon black (Mullins & Tobin, 1965). As a result, the local strain in the elastomer is greater than the macroscopic applied strain due to the strain amplification effect. This, in turn, will generate more negative hydrostatic stress which facilitates solvent penetration. It could be interesting to see whether the two curves will ever be superimposed for higher strain, e.g. $\lambda = 2$. Unfortunately, we did not manage to verify it since the specimens rupture during the swelling test when higher stretch than 1.5 is imposed.

4.1.3 Constrained swelling 2: static multiaxial strain (Design 1)

Figure 4.11 shows the percentage of mass change and volume change of specimens immersed during one week in palm biodiesel under different loading conditions: initially stress-free S0T0, simple tension S20T0, S40T0, S60T0, simple torsion S0T30, S0T60, S0T90, and combined tension-torsion S20T30, S20T60, S20T90, S40T30, S40T60, S40T90, S60T30, S60T60, S60T90. For each condition, three specimens were tested. The effect of mechanical loading, particularly tensile strain, on the amount of swelling is clearly shown in this figure. It is observed that the application of tensile strain to the rubber specimen increases the amount of liquid uptake regardless of the amount of applied twist. In contrast, the effect of the twist to the amount of swelling appears to be not as significant as the effect of tensile strain. Indeed, the application of twist increases only slightly the amount of liquid uptake. The effect of torsion on the amount of swelling is discussed in detail in Section 4.3.

The significant increase of swelling due to the application of tensile strain can be explained by the fact that the initial available surface of the specimen through which diffusion occurs increases (Chai et al., 2011). Moreover, tensile strain generates tensile

stress in the material. In this case, the hydrostatic part of the stress is negative. According to Treloar (1975), negative hydrostatic stress facilitates the liquid uptake.

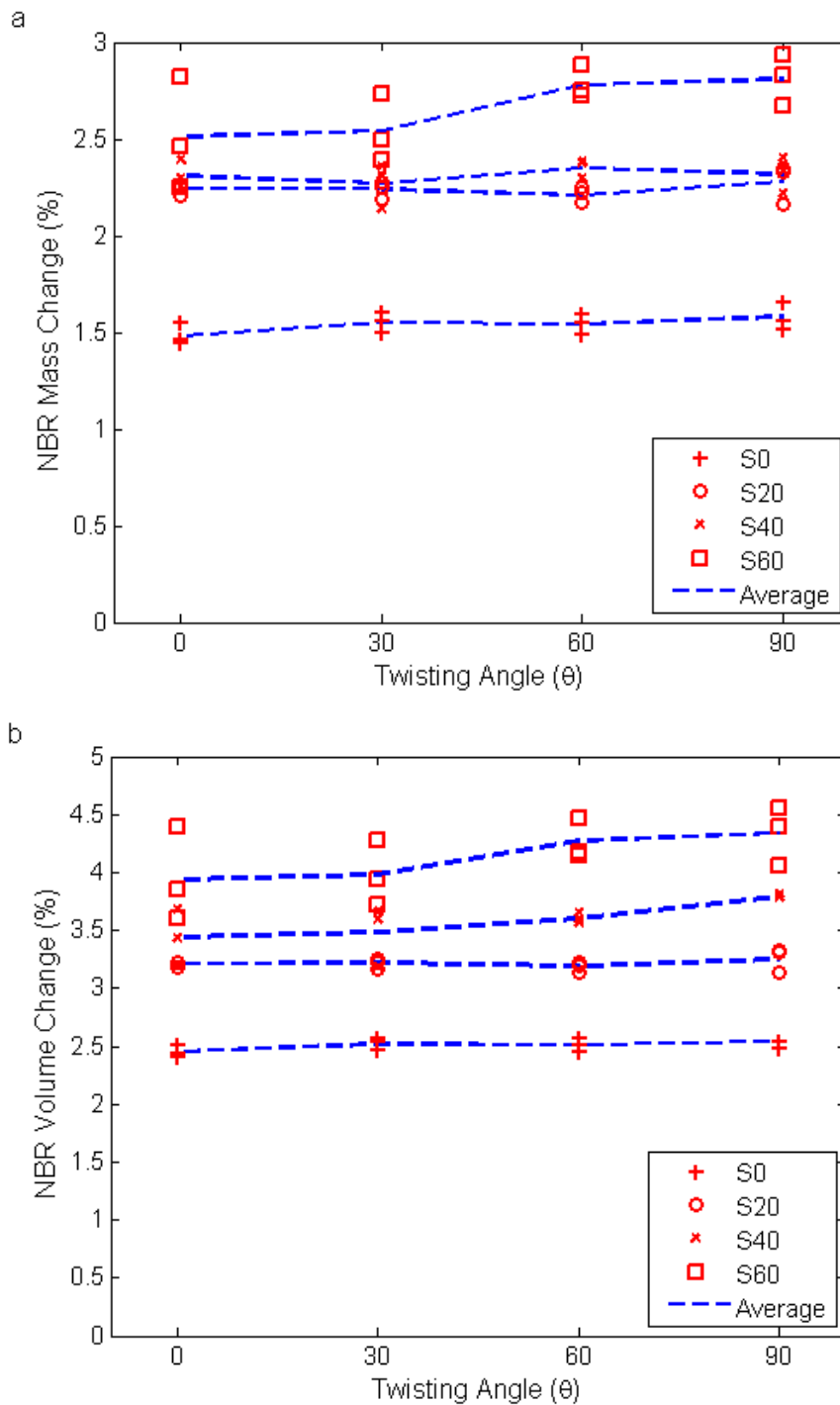


Figure 4.11: (a) Mass change and (b) volume change of NBR after 1 week immersion in palm biodiesel

4.1.4 Constrained swelling 3: static multiaxial strain (Design 2)

The mass and volume change under the presence of a static multiaxial strain for Design 2 are shown in Figure 4.12. Three different twisting angles were imposed: 0° , 10° and 20° . As shown in Figure 4.12, the introduction of torsional strain yields to higher swelling as compared to the initially stress-free specimen. The volume change also increases with increasing duration of immersion. At the end of the immersion period (700 hours), the percentages of volume change are approximately 6.1 %, 6.9 % and 7.9 % for twist angles of 0° (initially stress-free), 10° and 20° , respectively. Similar to our previous observation, the corresponding trend can be explained by considering the hydrostatic part of the Cauchy stress in the material (See Section 4.3).

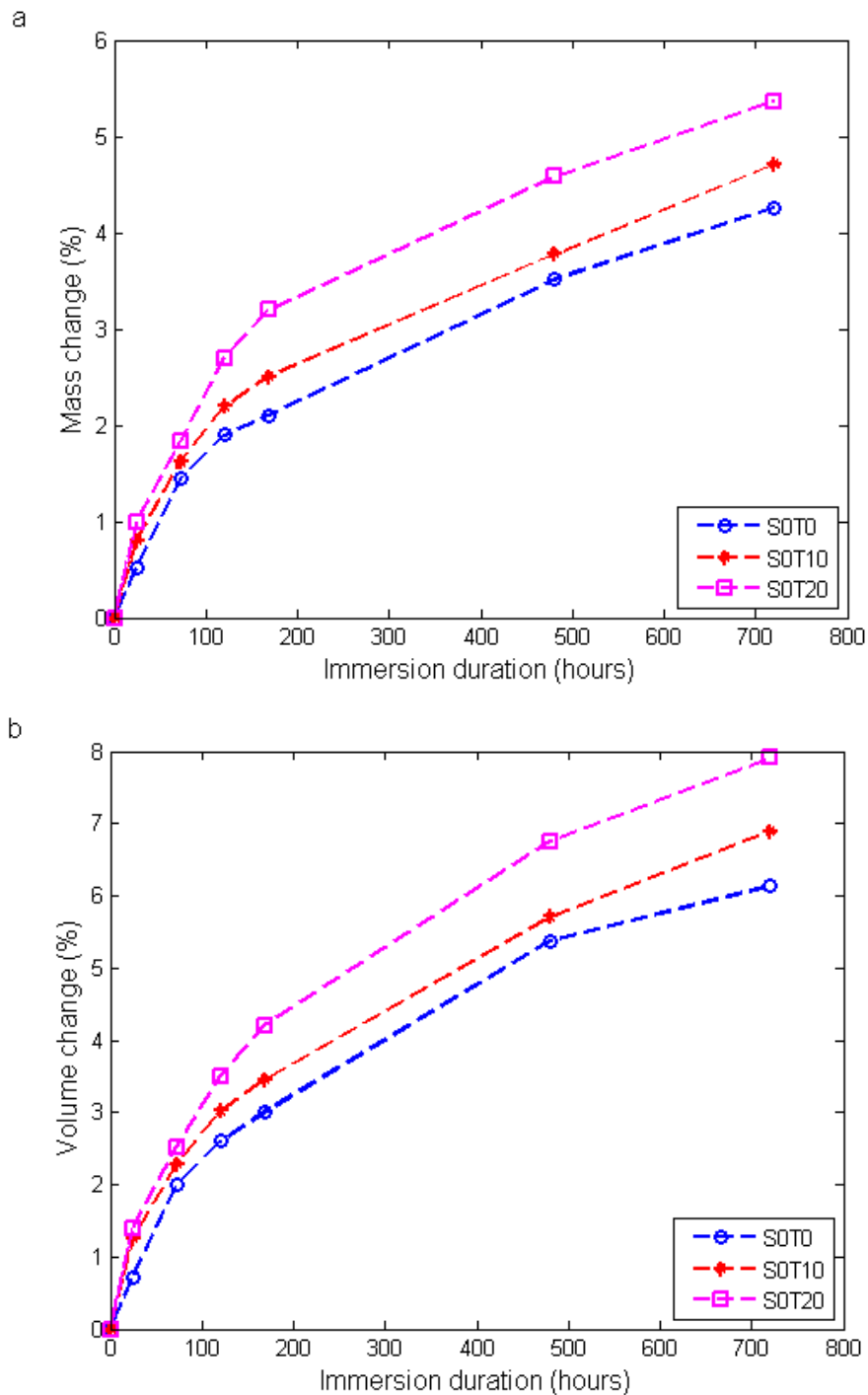


Figure 4.12: (a) Mass change and (b) volume change for different twisting angle.

It is worthy to note that although two different specimens were designed for the purpose of investigating swelling in the presence of a static multiaxial strain, both specimens show different trends. While torsion is shown insignificant to the swelling effect for design 1, swelling is observed to be increasing with the introduction of torsion for design

2. This observation may be caused by the difference in the specimen dimension. The detailed discussion is provided in Section 4.3.

4.2 Mechanical responses

4.2.1 Mechanical responses under monotonic tensile loading

The stress strain curves for dry unfilled and filled elastomers with 25 and 40 % carbon black content under monotonic tensile loading until fracture are depicted in Figure 4.13. The results show an increase of the elastic modulus with an increase of carbon black content in the elastomer. This phenomenon may be caused by the strain amplification due to the filler content in the elastomer (Mullins & Tobin, 1957). Since carbon black is an active filler, also other reinforcement effects take place. When a strain is applied to the soft elastomer matrix containing discrete rigid inclusions, the average local strain in the matrix must exceed the macroscopic applied strain since the rigid inclusions do not take part in the deformation (See Section 2.5).

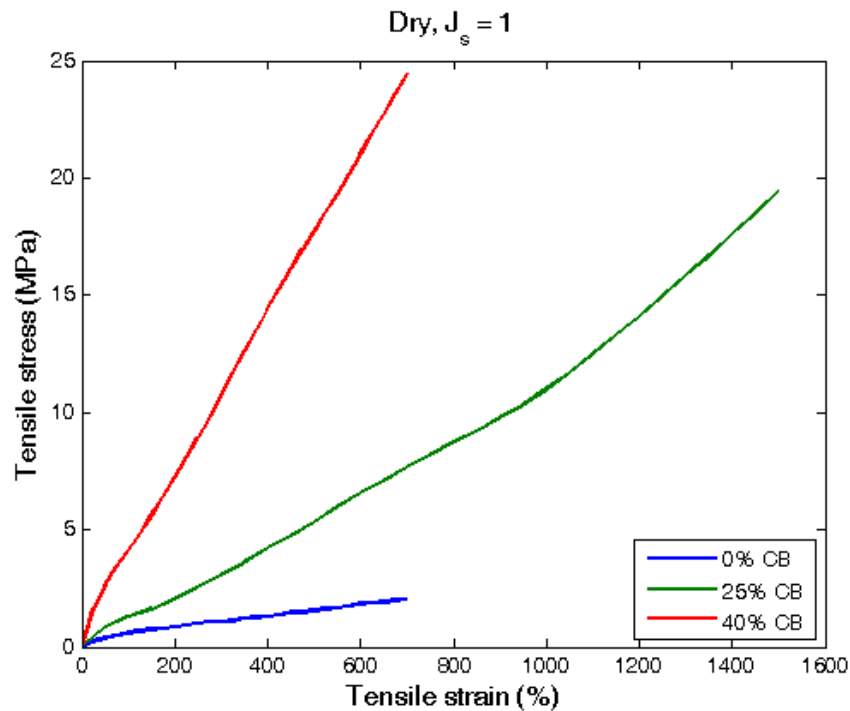


Figure 4.13: Monotonic stress-strain response of dry specimens with different carbon black content.

In addition, it is also observed that elastomers with different carbon black content failure at different tensile strains. For unfilled and filled elastomer with 40 % of carbon black, the specimens failure at 700 % of tensile strain. Meanwhile for the elastomer filled with 25 % carbon black, failure occurs at around 1500 % of tensile strain. Although the addition of carbon black leads to an increase in various properties which include the modulus, hardness, tensile strength, abrasion, tear resistance and resistance to fatigue, it appears that there is an optimum level of filler content which can improve the performance of the elastomer (Ramesan, 2005). Based on this observation, only filled elastomers with 25 % of carbon black content is considered for the multiaxial design.

4.2.2 Mechanical responses under cyclic loading

In this section, the mechanical responses of dry and swollen elastomers under cyclic loadings are presented. In order to avoid buckling, specimens from Design 1 are used. The stress strain response of dry and swollen elastomers for Design 1 under monotonic tensile loadings are recalled and presented as Figure 4.14.

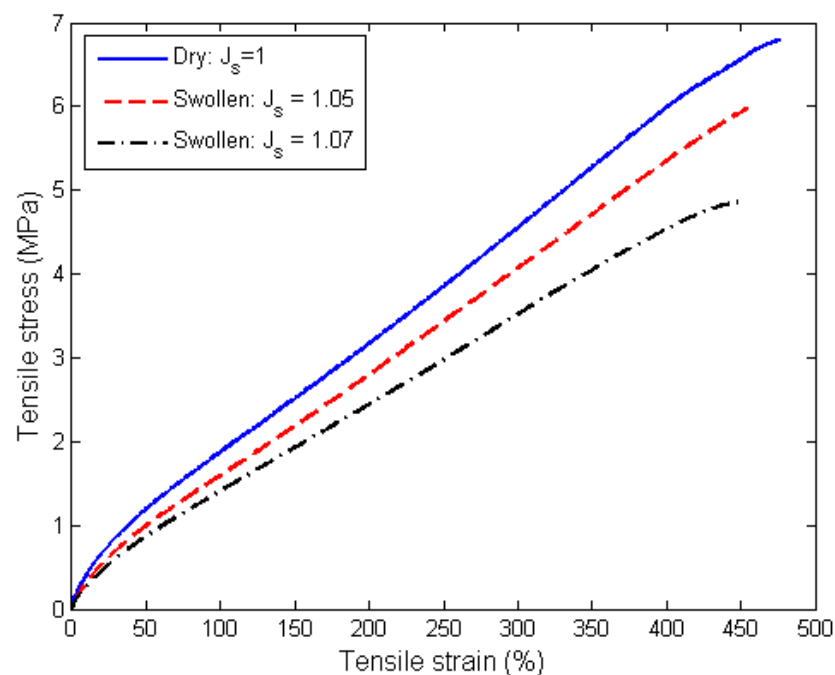


Figure 4.14: Stress-strain curves under monotonic tensile loading.

The stress strain response of dry and swollen elastomers subjected to five cycles of uniaxial tension up to tensile strain of 300 % are presented in Figures 4.15, 4.16 and 4.17. It is clearly seen that both dry and swollen elastomers exhibit inelastic behaviour, i.e. stress softening due to the Mullins effect, hysteresis and permanent set. The Mullins effect is mainly observed between the first and second cycles. Indeed, it is observed that softening which takes place after the second cycle is not significant. Nevertheless, significant hysteresis is still observed even when the material has been softened. Smaller stress-softening and hysteresis are observed in swollen elastomers. The observed results are consistent with the work of Chai, Andriyana, et al. (2013).

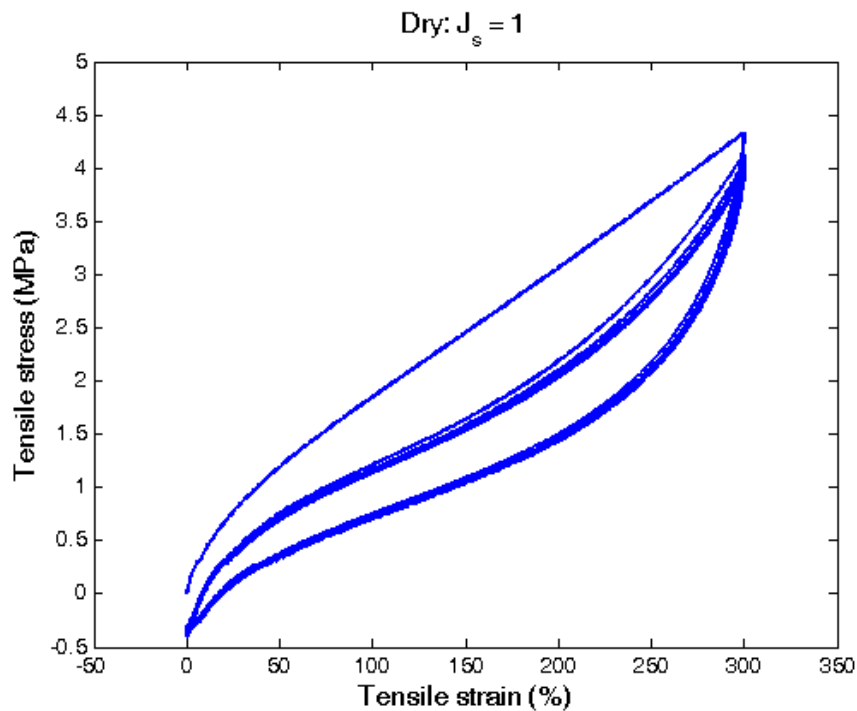


Figure 4.15: Stress-strain curve under 5 cycles of loading for dry specimen ($J_s = 1$).

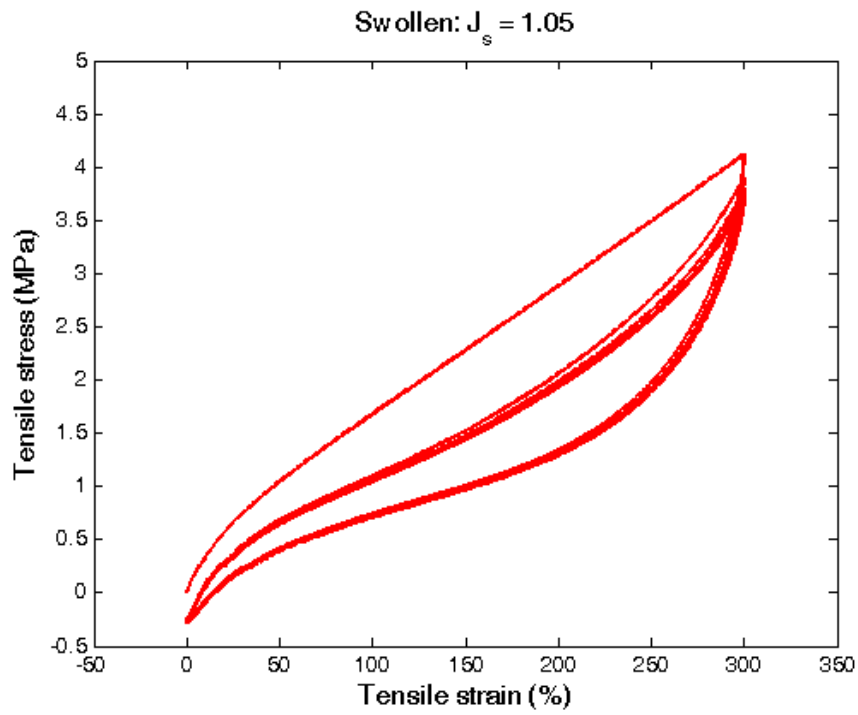


Figure 4.16: Stress-strain curve under 5 cycles of loading for swollen specimen ($J_s = 1.05$).

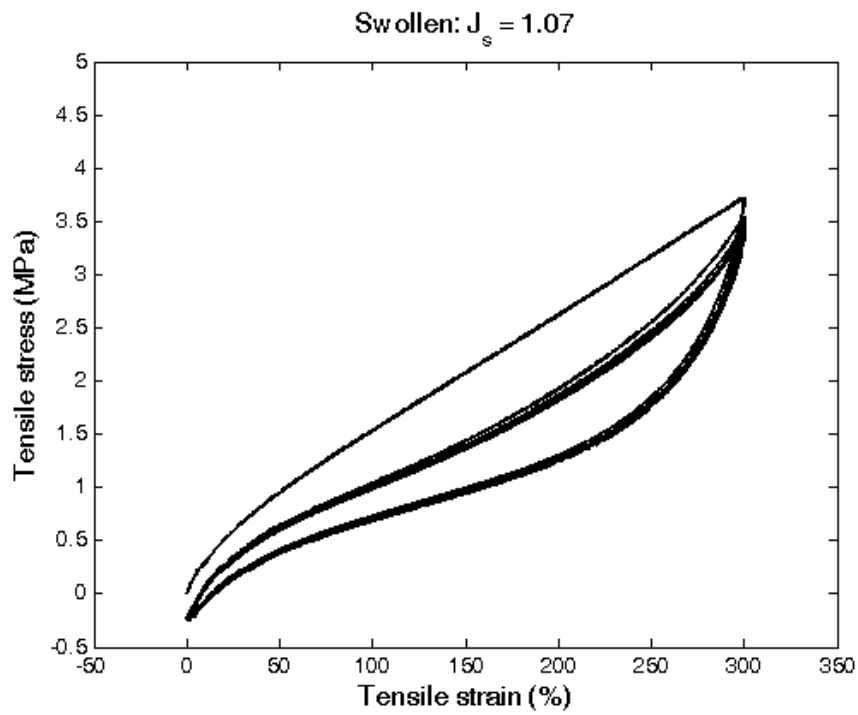


Figure 4.17: Stress-strain curve under 5 cycles of loading for swollen specimen ($J_s = 1.07$).

Before proceeding further, it is important to illustrate the effect of swelling on the stress-softening of the material. For this purpose, stress-softening in both dry and swollen elastomers is calculated based on the relation:

$$\text{Stress softening (dry)} = \frac{P_{d1}^{\text{up}} - P_{d2}^{\text{up}}}{P_{d1}^{\text{up}}} \quad \text{Stress softening (swollen)} = \frac{P_{s1}^{\text{up}} - P_{s2}^{\text{up}}}{P_{s1}^{\text{up}}} \quad (4.1)$$

where P_{d1}^{up} is the stress in the dry elastomer during uploading of the first cycle, P_{d2}^{up} is the stress in the dry elastomer during uploading of the second cycle, P_{s1}^{up} is the stress in the swollen elastomer during uploading of the first cycle and P_{s2}^{up} is the stress in the swollen elastomer during uploading of the second cycle.

The stress-softening exhibited by both dry and swollen elastomers is shown in Figure 4.18. It is observed that for both dry and swollen elastomers, stress-softening decreases as the strain level approaches the maximum strain. Although the discrepancies are not obvious, the presence of solvent appears to decrease stress-softening of the swollen elastomers.

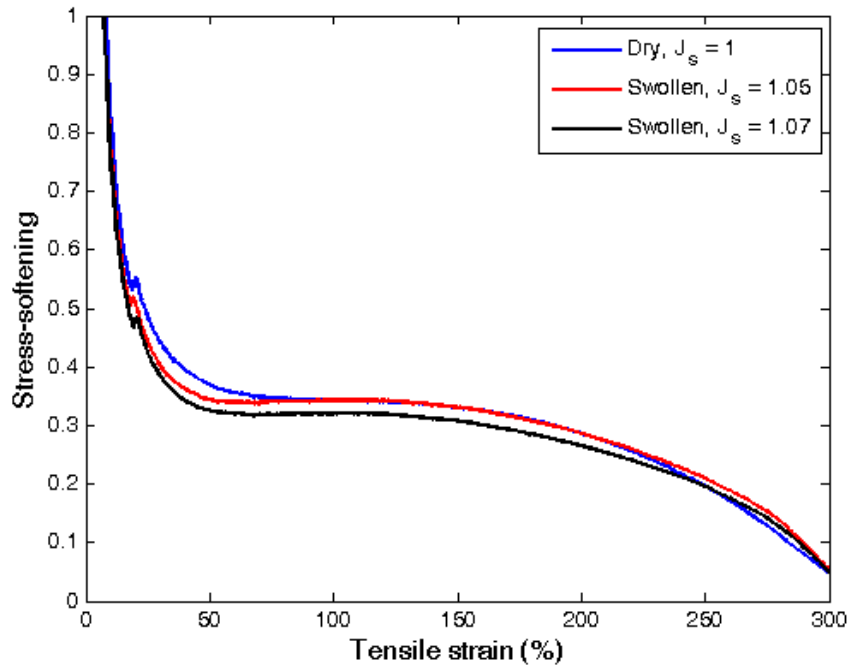


Figure 4.18: Stress-softening in dry and swollen elastomers calculated at second uploading.

The stress strain response of dry and swollen elastomers ($J_s = 1.05, 1.07$) under incremental cyclic tensile loadings is presented in Figures 4.19, 4.20 and 4.21. Generally, the nature of the stress strain curves remains the same for dry and swollen elastomers. However, similarly to the results for monotonic tensile loading, lower stresses are recorded for swollen elastomers for a given strain. The lower stress level in swollen elastomers can be attributed to the elastomer-solvent interaction which leads to the decrease in the strength of the elastomer (George et al., 1999). It is observed that both dry and swollen elastomers exhibit strong inelastic responses: stress-softening (Mullins effect), mechanical hysteresis (viscoelasticity) and permanent set. As indicated in the figures, it appears that the inelastic responses decrease when the degree of swelling is higher.

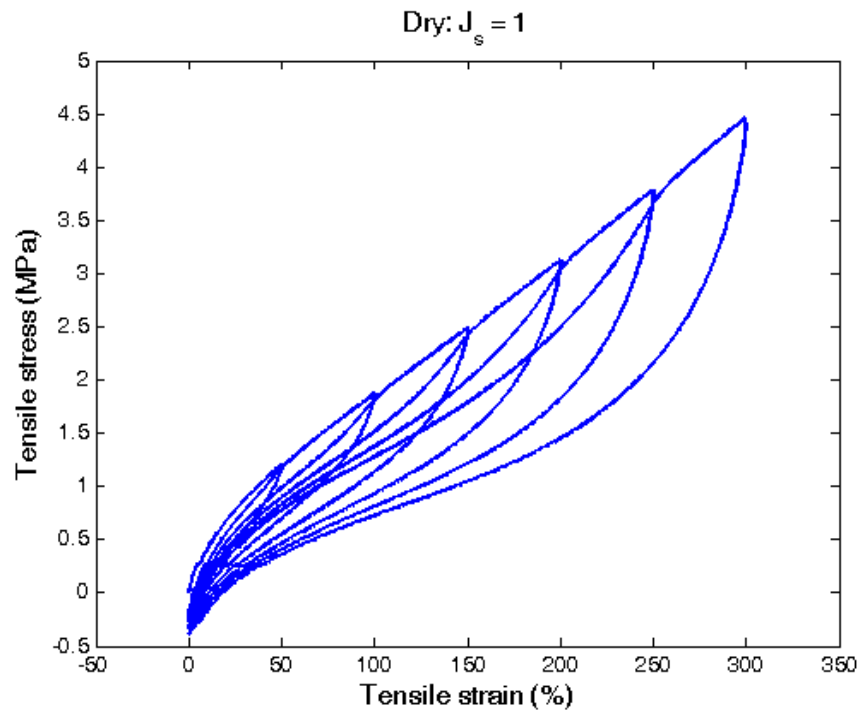


Figure 4.19: Stress-strain curve under cyclic loading with increasing maximum strain for dry specimen ($J_s = 1$).

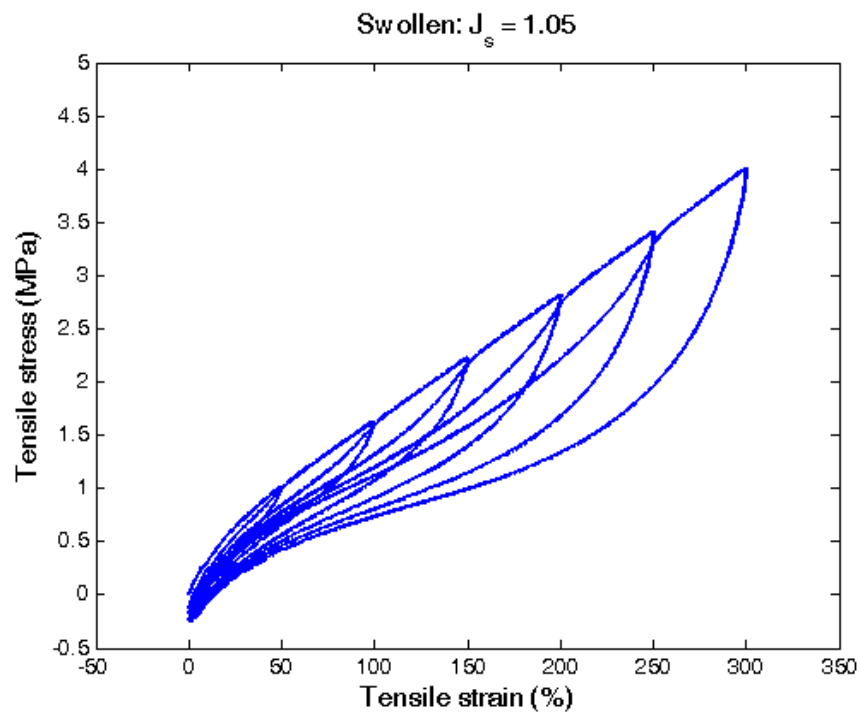


Figure 4.20: Stress-strain curve under cyclic loading with increasing maximum strain for swollen specimen ($J_s = 1.05$).

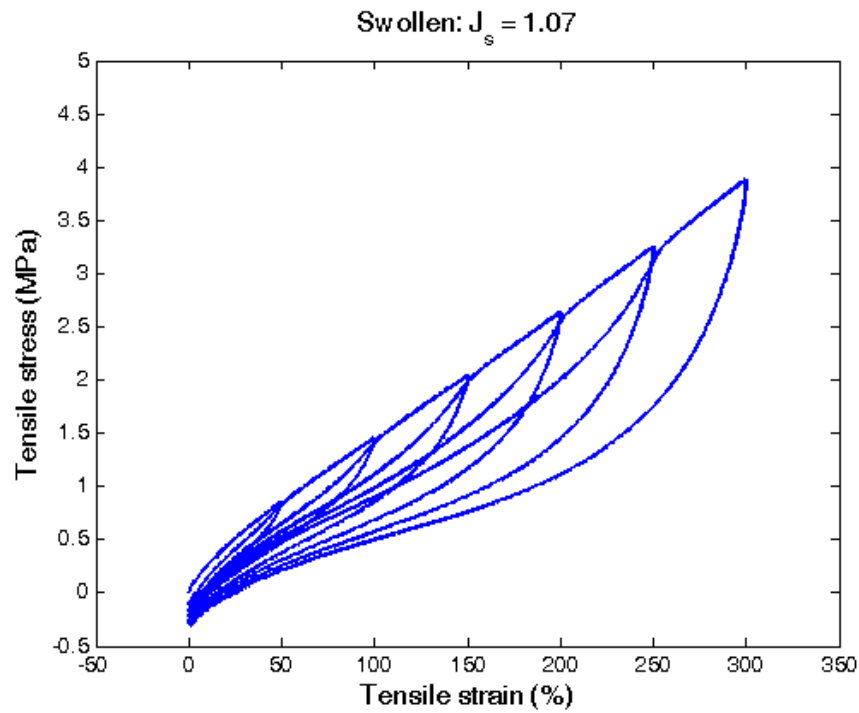


Figure 4.21: Stress-strain curve under cyclic loading with increasing maximum strain for swollen specimen ($J_s = 1.07$).

Figures 4.22, 4.23 and 4.24 show the combination of the stress responses under cyclic loading and monotonic tensile loading. Generally, stress-softening features are preserved for all three conditions under different degrees of swelling. Moreover, it is worth to note that the return of the reloading curve approaches nearly the monotonous curve after being stretched beyond the maximum stretch previously applied. For both dry and swollen rubber, the dependence of the Mullins effect on the maximum deformation previously endured by the materials is clearly shown in these figures. Moreover, they exhibit permanent set which increases as the materials are stretched further. This result is consistent with the observation of Chai, Andriyana, et al. (2013).

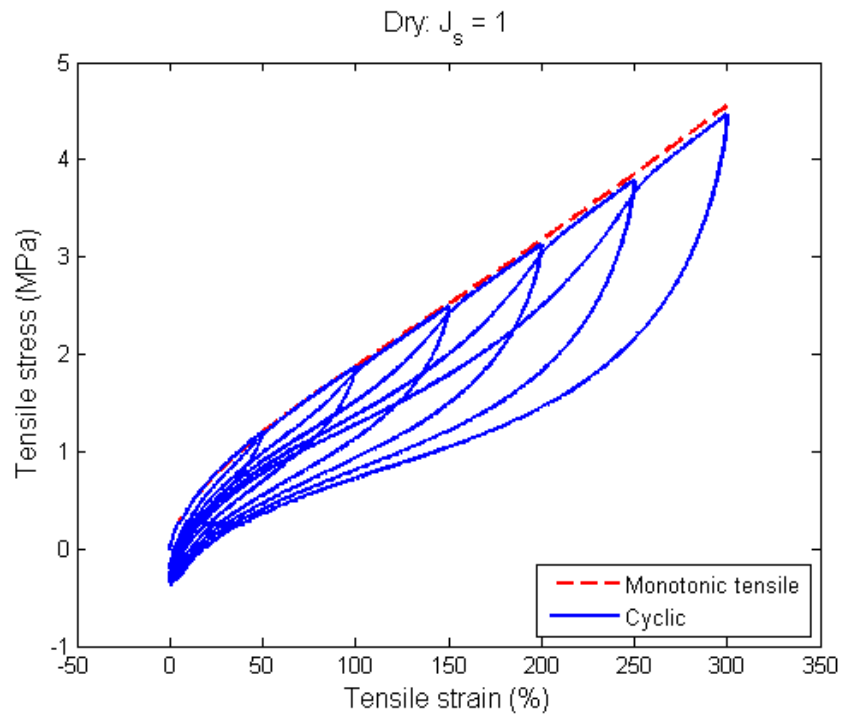


Figure 4.22: Material responses under cyclic loading with increasing maximum stretch for dry specimen ($J_s = 1$).

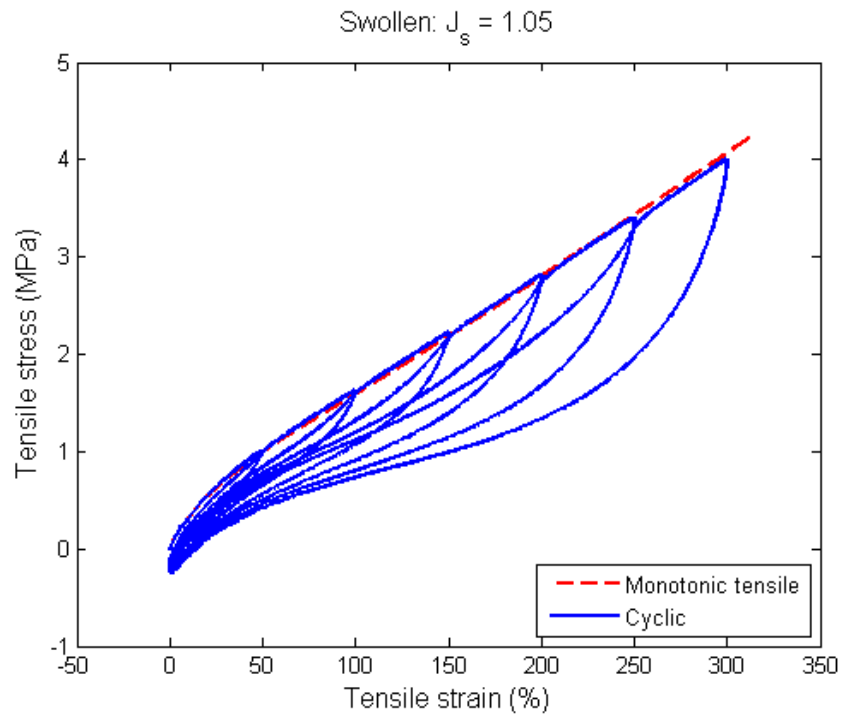


Figure 4.23: Material responses under cyclic loading with increasing maximum stretch for swollen specimen ($J_s = 1.05$).

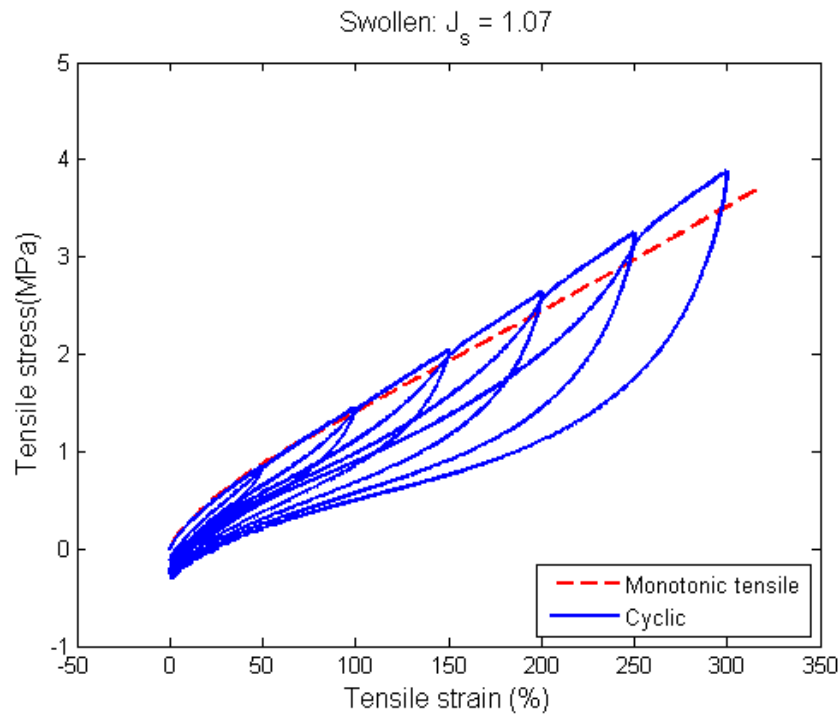


Figure 4.24: Material responses under cyclic loading with increasing maximum stretch for swollen specimen ($J_s = 1.07$).

4.3 Mechanical quantity affecting swelling

As mentioned in the previous section, the reduction or increase in the swelling is mainly governed by the hydrostatic part of the Cauchy stress (Treloar, 1975). A tensile stress (negative hydrostatic stress) favors swelling while a compressive stress (positive hydrostatic stress) restricts swelling. In the present study, complex mechanical loading conditions such as combined tension-torsion are addressed. Hence, the calculation of the hydrostatic part of the Cauchy stress in the specimen requires the analytical solution of the hyperelastic hollow cylinder under corresponding mechanical loading conditions: simple tension, simple torsion and combined torsion-tension.

During the immersion tests, the elastomeric specimens are subjected to static mechanical loadings. Due to viscoelastic behaviour of the materials, the resulting stress decreases with time during the immersion, i.e. the materials experience stress relaxation. The viscoelastic characteristic of our materials is highlighted in Figure 4.19. The de-

crease of stress due to viscoelasticity yields also to the decrease of the hydrostatic part of Cauchy stress. Since the precise kinetics of stress-relaxation during the immersion test is not known, i.e. the stress level in the material at any particular time is not known, we only focus on the initial hydrostatic stress in the dry elastomers before the immersion test.

In Figure 4.19, the engineering stress-engineering strain responses of dry elastomer under cyclic loading conditions are presented. It is observed that the material exhibits strong inelastic responses: stress-softening (Mullins effect), mechanical hysteresis (viscoelasticity) and permanent set. For the sake of simplicity, in the present study, the analytical determination of the hydrostatic stress is only based on the first uploading response of the materials, i.e. the viscoelastic response and stress-softening are neglected. Moreover, the dry elastomer is assumed to be isotropic and incompressible which obeys the Neo-Hookean hyperelastic constitutive equation.

Using a cylindrical coordinate system, the spatial position of a point in a cylinder under combined tensile-torsion is given as (Ogden, 1984):

$$r = \frac{R}{\sqrt{\lambda}} \quad \theta = \Theta + \lambda \gamma Z \quad z = \lambda Z \quad (4.2)$$

λ is the extension ratio and γ is the angle of torsion (in rad) per unit length. The deformation gradient can be written as:

$$\mathbf{F} = \frac{1}{\sqrt{\lambda}} (\mathbf{e}_r \otimes \mathbf{e}_R + \mathbf{e}_\theta \otimes \mathbf{e}_\Theta) + R\sqrt{\lambda} \gamma \mathbf{e}_\theta \otimes \mathbf{e}_Z + \lambda \mathbf{e}_z \otimes \mathbf{e}_Z \quad (4.3)$$

where $(\mathbf{e}_r, \mathbf{e}_\theta, \mathbf{e}_z)$ represent the three unit vectors along radial, circumferential and axial directions respectively in the deformed configuration while $\mathbf{e}_R, \mathbf{e}_\Theta, \mathbf{e}_Z$ are the unit vectors in the undeformed configuration. The left \mathbf{B} and right \mathbf{C} Cauchy-Green tensors are

therefore:

$$\mathbf{B} = \frac{1}{\lambda} \mathbf{e}_r \otimes \mathbf{e}_r + \left(\frac{1}{\lambda} + \lambda^2 \gamma^2 r^2 \right) \mathbf{e}_\theta \otimes \mathbf{e}_\theta + \lambda^2 \gamma r (\mathbf{e}_\theta \otimes \mathbf{e}_z + \mathbf{e}_z \otimes \mathbf{e}_\theta) + \lambda^2 \mathbf{e}_z \otimes \mathbf{e}_z \quad (4.4)$$

$$\mathbf{C} = \frac{1}{\lambda} \mathbf{e}_R \otimes \mathbf{e}_R + \mathbf{e}_\Theta \otimes \mathbf{e}_\Theta + \gamma R (\mathbf{e}_\Theta \otimes \mathbf{e}_Z + \mathbf{e}_Z \otimes \mathbf{e}_\Theta) + (\lambda^2 + \lambda \gamma^2 R^2) \mathbf{e}_z \otimes \mathbf{e}_z \quad (4.5)$$

In the case where the hyperelastic strain energy W depends only on I_1 , the Cauchy stress tensor is given as:

$$\begin{aligned} \boldsymbol{\sigma} = & \left(-q + 2 \frac{\partial W}{\partial I_1} \frac{1}{\lambda} \right) \mathbf{e}_r \otimes \mathbf{e}_r + \left(-q + 2 \frac{\partial W}{\partial I_1} \left(\frac{1}{\lambda} + \lambda^2 \gamma^2 r^2 \right) \right) \mathbf{e}_\theta \otimes \mathbf{e}_\theta \\ & + 2 \frac{\partial W}{\partial I_1} \lambda^2 \gamma r (\mathbf{e}_\theta \otimes \mathbf{e}_z + \mathbf{e}_z \otimes \mathbf{e}_\theta) + \left(-q + 2 \frac{\partial W}{\partial I_1} \lambda^2 \right) \mathbf{e}_z \otimes \mathbf{e}_z \end{aligned} \quad (4.6)$$

For a cylinder, the pressure q can be written as:

$$q(R) = \frac{2}{\lambda} \frac{\partial W}{\partial I_1}(R) + 2\lambda \gamma^2 \int_R^{R_o} s \frac{\partial W}{\partial I_1}(s) ds \quad (4.7)$$

Finally, the expression of each component of $\boldsymbol{\sigma}$ is:

$$\begin{aligned} \sigma_{rr}(R) &= -2\lambda \gamma^2 \int_R^{R_o} s \frac{\partial W}{\partial I_1}(s) ds \\ \sigma_{\theta\theta}(R) &= 2\lambda \gamma^2 \left(R^2 \frac{\partial W}{\partial I_1}(R) - \int_R^{R_o} s \frac{\partial W}{\partial I_1}(s) ds \right) \\ \sigma_{\theta z}(R) &= \sigma_{z\theta}(R) = 2\lambda^{3/2} \gamma R \frac{\partial W}{\partial I_1}(R) \\ \sigma_{zz}(R) &= 2 \frac{\partial W}{\partial I_1}(R) \left(\lambda^2 - \frac{1}{\lambda} \right) - 2\lambda \gamma^2 \int_R^{R_o} s \frac{\partial W}{\partial I_1}(s) ds \end{aligned} \quad (4.8)$$

with $\sigma_{r\theta} = \sigma_{\theta r} = \sigma_{rz} = \sigma_{zr} = 0$. For the special case of a Neo-Hookean hyperelastic material, $\frac{\partial W}{\partial I_1} = C$ and the resulting Cauchy stress tensor at any particular point of the

undeformed configuration is simplified as:

$$\begin{aligned} \sigma(R) = & C\lambda\gamma^2(R^2 - R_o^2)\mathbf{e}_r \otimes \mathbf{e}_r + C\lambda\gamma^2(3R^2 - R_o^2)\mathbf{e}_\theta \otimes \mathbf{e}_\theta \\ & + 2C\lambda^{3/2}\gamma R(\mathbf{e}_\theta \otimes \mathbf{e}_z + \mathbf{e}_z \otimes \mathbf{e}_\theta) + \left[2C\lambda^2 - \frac{1}{\lambda} + C\lambda\gamma^2(R^2 - R_o^2) \right] \mathbf{e}_z \otimes \mathbf{e}_z \end{aligned} \quad (4.9)$$

where R is the radial position of any particular point in the undeformed configuration while R_o is the initial outer radius of the cylinder. The material parameter C identified from the first uploading section of the stress response as mentioned in the previous paragraph. The hydrostatic stress is obtained by taking the trace of the Cauchy stress tensor (Holzapfel, 2000):

$$p = -\frac{1}{3}\text{tr}(\sigma) \quad (4.10)$$

which yields to:

$$p(R) = -\frac{1}{3}[C\lambda\gamma^2(R^2 - R_o^2) + C\lambda\gamma^2(3R^2 - R_o^2) + 2C(\lambda^2 - \frac{1}{\lambda}) + C\lambda\gamma^2(R^2 - R_o^2)] \quad (4.11)$$

For a static uniaxial state of strain, it is obvious that Equation (4.11) can be simplified to $p(R) = -\frac{2C}{3}(\lambda^2 - \frac{1}{\lambda})$ and the value is always negative for any given amount of tensile strain, i.e. when $\lambda > 1$. Thus, it is straight-forward to see that the imposed tensile strain leads to negative hydrostatic stress in the elastomer which leads to higher amount of swelling. The complication of the equation arises for static multiaxial strain since the strain might be non uniform. Thus, the initial hydrostatic stress in the middle part of the specimen at various radial positions for simultaneous tension-torsion (Design 1) is calculated and depicted in Figure 4.25. In this calculation, the values of C for the dry elastomer is 0.554 MPa. Moreover, the inner and outer radii are $R_i = 6.5\text{mm}$ and $R_o = 12.5\text{mm}$, respectively. For a given twist, it is observed that the hydrostatic stress decreases with the increase of radial position. More precisely, under torsion the elastomeric cylinder

experiences compressive stress at the inner surface and tensile stress at the outer surface, i.e. the strain is non-uniform. Thus, the swelling occurs in the presence of non-uniform strain (stress) field.

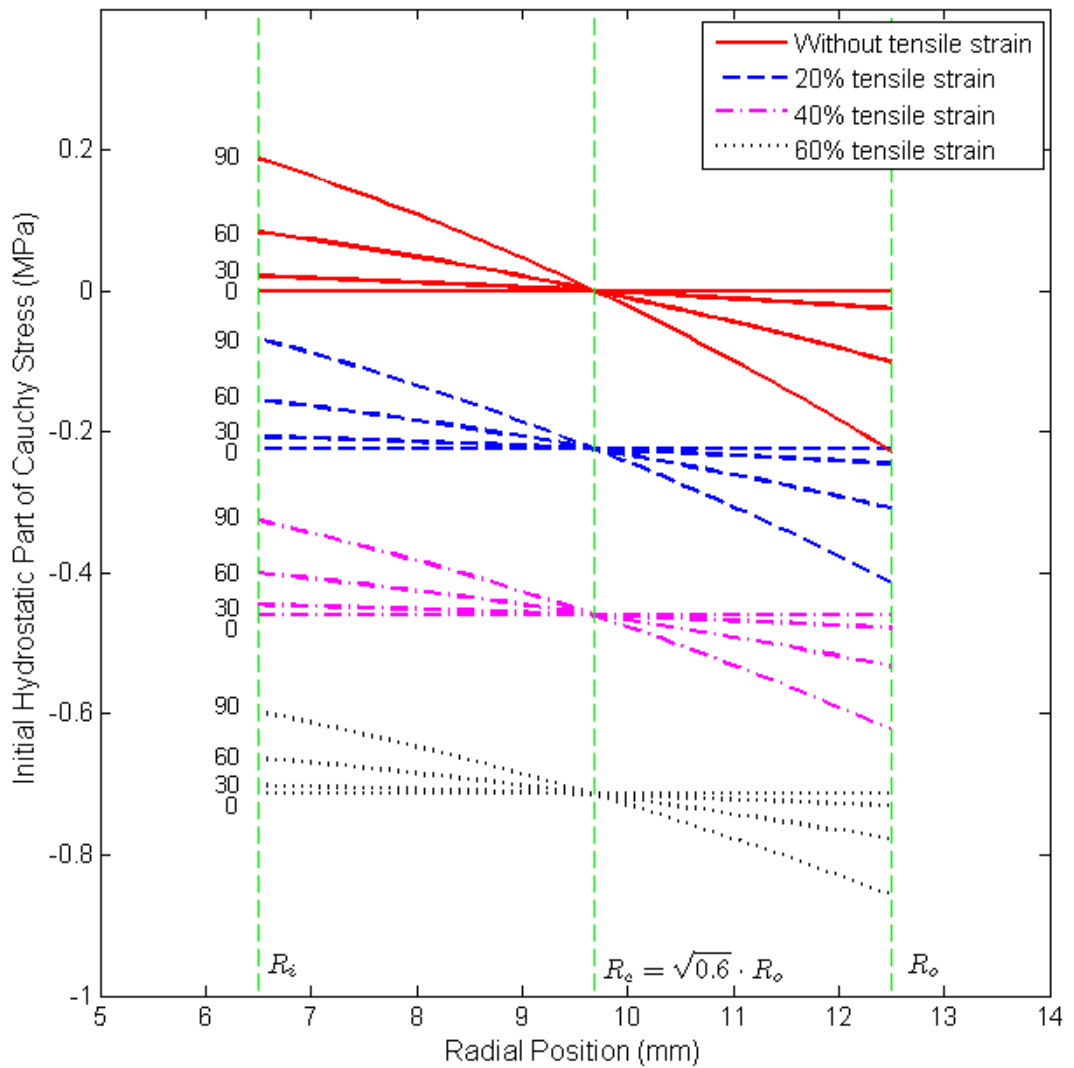


Figure 4.25: Initial hydrostatic part of Cauchy stress at different radial position for Design 1.

As shown in Figure 4.25, there exists a particular plane along which the hydrostatic stress is zero. This particular plane is located at the critical radius $R_c = \sqrt{0.6} \cdot R_o$ which

is independent on the applied twist. Between the inner surface and the particular plane, i.e. $R_i < R < R_c$, the hydrostatic stress is positive (in compression state) while between the particular plane and the outer surface of the cylinder, i.e. $R > R_c$, the hydrostatic stress is negative (in the tension state). The resulting stress state under torsion for Design 1 is illustrated in Figure 4.26. When the twist increases, the hydrostatic stress gradient also increases, i.e. increasing the non-uniformity of strain (stress) field in the materials. Furthermore, it appears that the only effect of tensile loading is to translate vertically downward the curve of hydrostatic stress, i.e. to a more negative value. As indicated in Figure 4.25, the amount of this translation decreases slightly with the radial position. Finally, as the tensile loading increases, its effect becomes more significant which yields to the reduction of the non-uniformity of strain (stress).

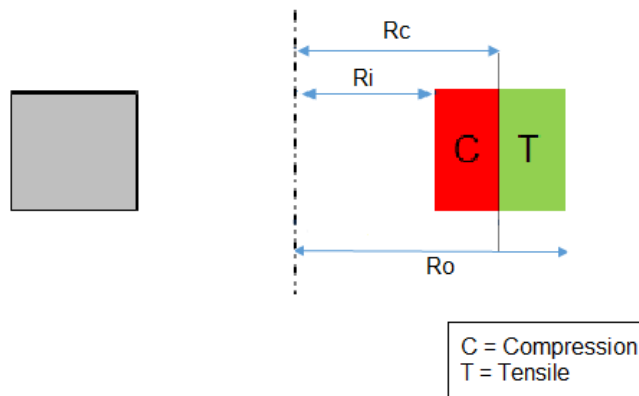


Figure 4.26: Stress state under torsion in the specimen for Design 1.

Since the strain and stress are non-uniform in the rubber specimen, the average value of hydrostatic stress has to be calculated. Figure 4.27 presents the average hydrostatic stress for different loading conditions. In this case, the average hydrostatic stress is calculated from:

$$\bar{p} = \frac{1}{R_o - R_i} \int_{R_i}^{R_o} p dr \quad (4.12)$$

As shown in Figure 4.27, the tensile strain affects significantly the average value of hy-

drostatic stress. In contrast, the average value of hydrostatic stress does not change significantly with the increase of twist. Indeed, for the case of simple torsion, the average hydrostatic stresses are close to zero regardless of the amount of twist. For the sake of clarity, the corresponding average hydrostatic stress is re-plotted in Figure 4.27 (b). These results can be helpful in understanding why the swelling levels in our materials are not greatly affected by the amount of twist.

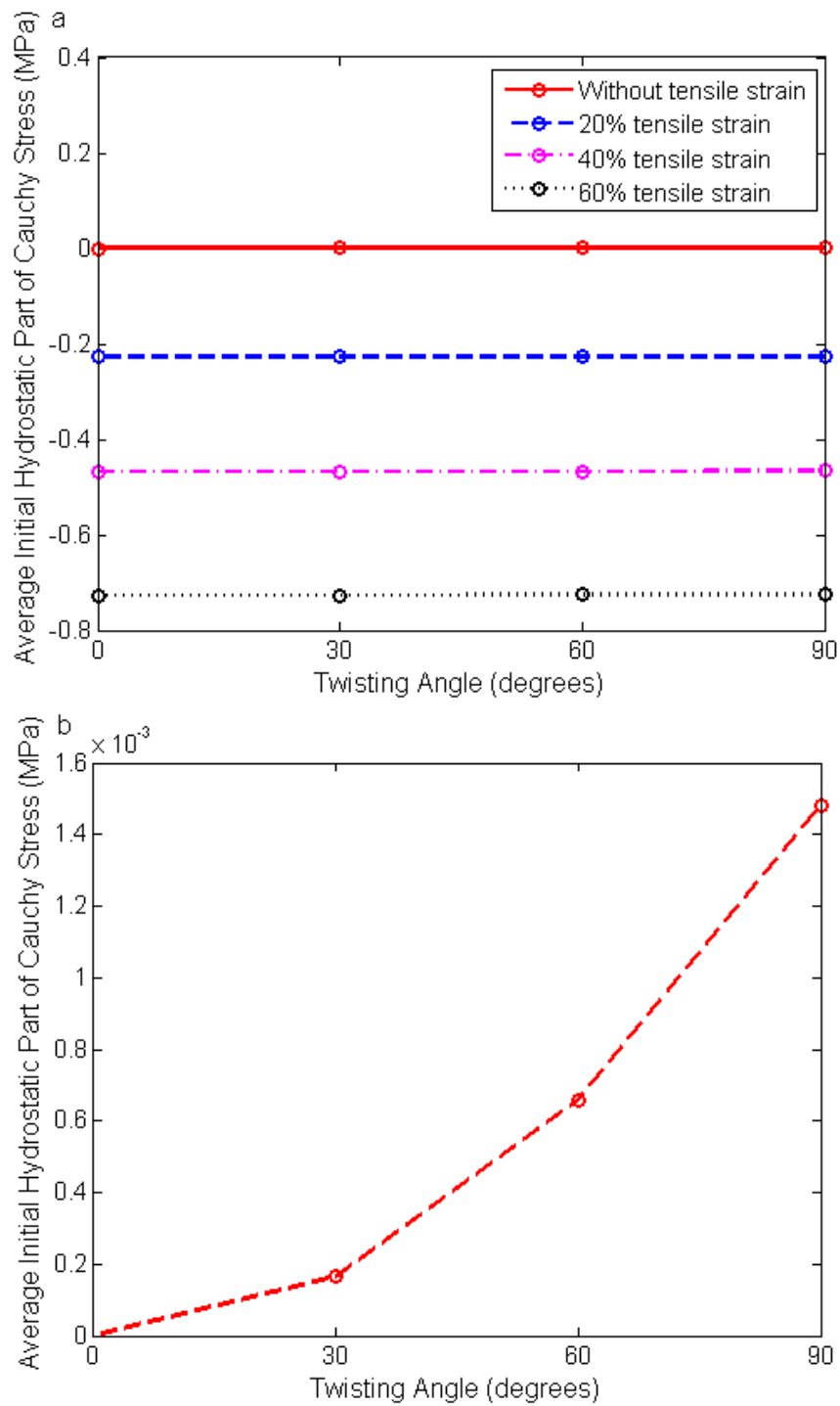


Figure 4.27: Average initial hydrostatic part of Cauchy stress at different twisting angle for (a) NBR and (b) NBR without tensile strain.

To gain an insight view on the effect of simple torsion on the swelling level for our specimen, the percentage of volume change is plotted against the average hydrostatic stress for simple torsion cases in Figure 4.28. When twist is applied, it is found that the

resulting swelling level is systematically higher than the swelling in initially stress-free specimens. The increase of swelling due to the application of twist is in contrast to the prediction of Loke et al. (1972) and Treloar (1972). In the opinion of the author, the corresponding discrepancy could be attributed to the geometry of the specimen. Indeed, while a hollow cylindrical specimen is considered in the present study, Loke et al. (1972) and Treloar (1972) used a solid cylindrical specimen. For a given twist, the zone of the cylinder experiencing compressive hydrostatic stress will be larger in the case of the solid cylinder than that in the case of the hollow cylinder. As discussed and detailed in the previous paragraph, the zone with compressive hydrostatic stress is located in the range $R_i < R < R_c$. Note that in the case of solid cylinder, $R_i=0$. Since the zone experiencing compressive hydrostatic stress is larger in solid cylinder, the resulting average hydrostatic stress becomes higher, i.e. more positive, higher average compressive hydrostatic stress. Thus, under a given twist, the resulting swelling in solid cylinder is lower than that in hollow cylinder.

While the introduction of torsion appears to increase swelling, our results do not clearly indicate the effect of the amount of torsion on the swelling level. The corresponding observation could be attributed to the particular geometry of our specimen. As illustrated in Figure 4.27, the change in the average hydrostatic pressure due to the increase in torsion is not as significant as due to the application of tensile strain.

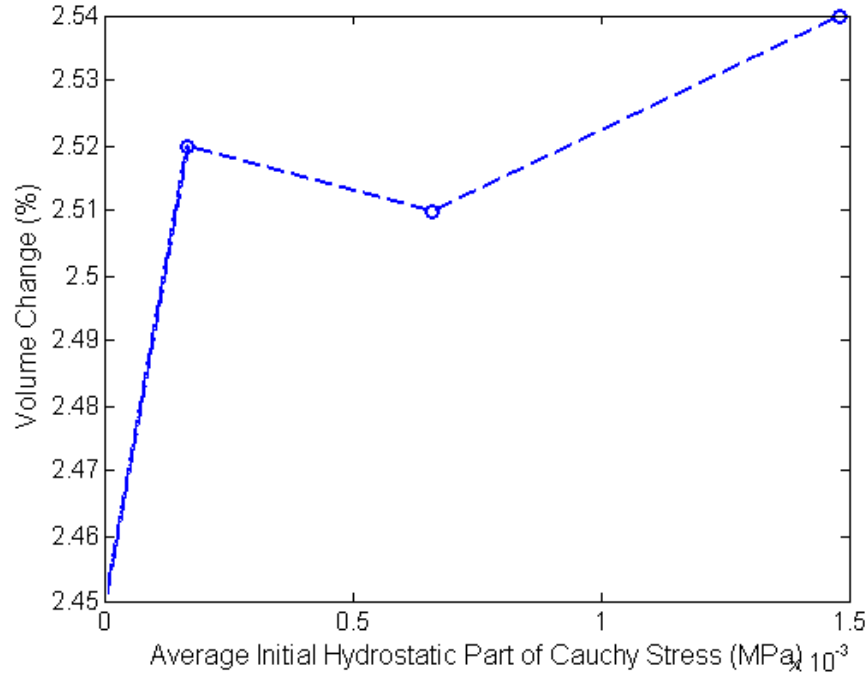


Figure 4.28: Volume change as a function of average hydrostatic component of stress.

Finally, the above observations suggest that the effect of torsion on swelling is dictated by the specimen geometry. In the case of the solid cylinder, the resulting average hydrostatic stress is positive, i.e. swelling is restricted. Thus, lower swelling is expected to occur in comparison with that observed in stress-free cylinders. This case corresponds to the works of Loke et al. (1972) and Treloar (1972). However, when a hollow cylinder having an inner radius larger than the critical radius is used, i.e. with $R_i > R_c$, the resulting average hydrostatic stress is negative and significantly higher swelling is expected to occur than that in the stress-free cylinder. It is straightforward to show that the condition $R_i > R_c$, is equivalent with the ratio $\frac{t}{R_m} < 0.259$, where $t = R_o - R_i$ is the wall thickness and $R_m = \frac{1}{2}(R_o + R_i)$ is the mean radius of the cylinder. For our purpose, a thin-walled cylinder with the above ratio would be preferable than the solid one since a certain level of swelling can be reached within a shorter period of time. Moreover, the resulting stress and strain fields will be more uniform. The middle part of the elastomeric specimens for Design 1 has the thickness-mean radius ratio of $\frac{t}{R_m} = 0.632$. Therefore, no clear influence

of torsion on the swelling level is observed. Based on this observation, a further development of Design 2 for a specimen with the ratio of $\frac{t}{R_m} < 0.259$ is carried out to establish the effect of multiaxial loading on the swelling of elastomers.

Using a similar approach, the initial hydrostatic stress in the middle part of the specimen at various radial positions for multiaxial strain (Design 2) is calculated and depicted in Figure 4.29. The inner and outer radii of the cylinder are $R_i = 38$ mm and $R_o = 43$ mm respectively. Since $R_i > R_c$, all parts of the elastomer will undergo negative hydrostatic stress (in tensile stress) when a torsional load is applied.

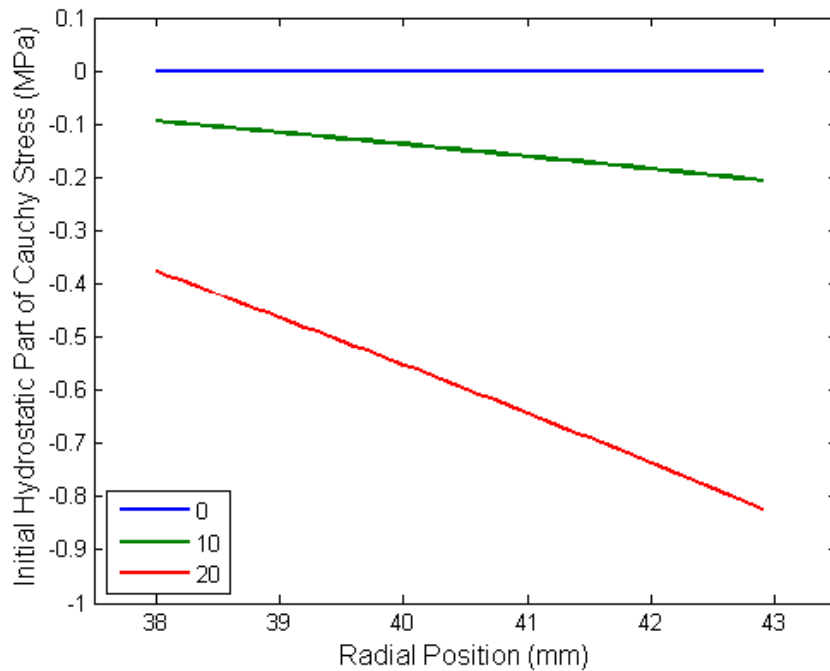


Figure 4.29: Initial hydrostatic part of Cauchy stress at different radial positions for Design 2.

As clearly shown, the hydrostatic stress distribution is non-uniform. Thus, in order to determine the overall swelling in the specimen, the average value of the hydrostatic stress is used and is calculated using Equation (4.12). The resulting average hydrostatic stress for different loading conditions is presented in Figure 4.30. As shown in this figure, a twist angle of 10° creates an average hydrostatic stress of about -0.13 MPa. An additional

10° of twist angle decreases the average hydrostatic stress to about -0.55 MPa. This implies that by doubling the twist angle, we obtain a more than four times lower value for the average hydrostatic stress.

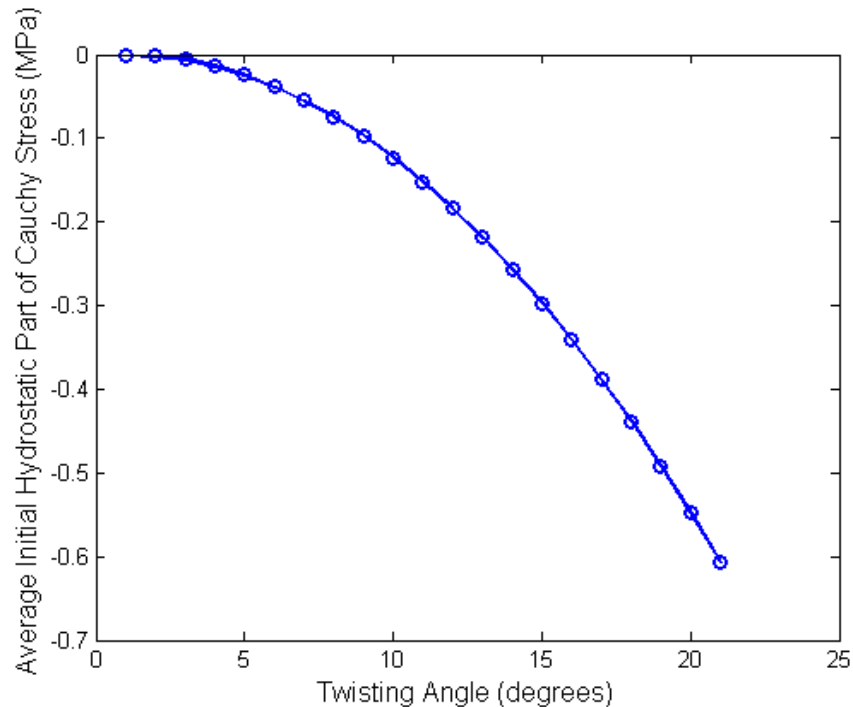


Figure 4.30: Average initial hydrostatic part of Cauchy stress for different twist angles.

In order to understand the effect of hydrostatic stress on swelling, the percentage of volume change for different immersion durations is plotted against the average hydrostatic stress in Figure 4.31. It is shown in this figure that the volume change of the elastomer increases with increasing immersion duration and with the decrease in the average hydrostatic stress. This result is in agreement with the finding of Treloar (1975) but in contrast with the results obtained by Loke et al. (1972) and Treloar (1972) who suggested that swelling decreases with increases in the twist angle. As discussed earlier, the discrepancy between our results and those of Loke et al. (1972) and Treloar (1972) can be explained by the fact that they used a solid cylindrical rubber specimen instead of a hollow one.

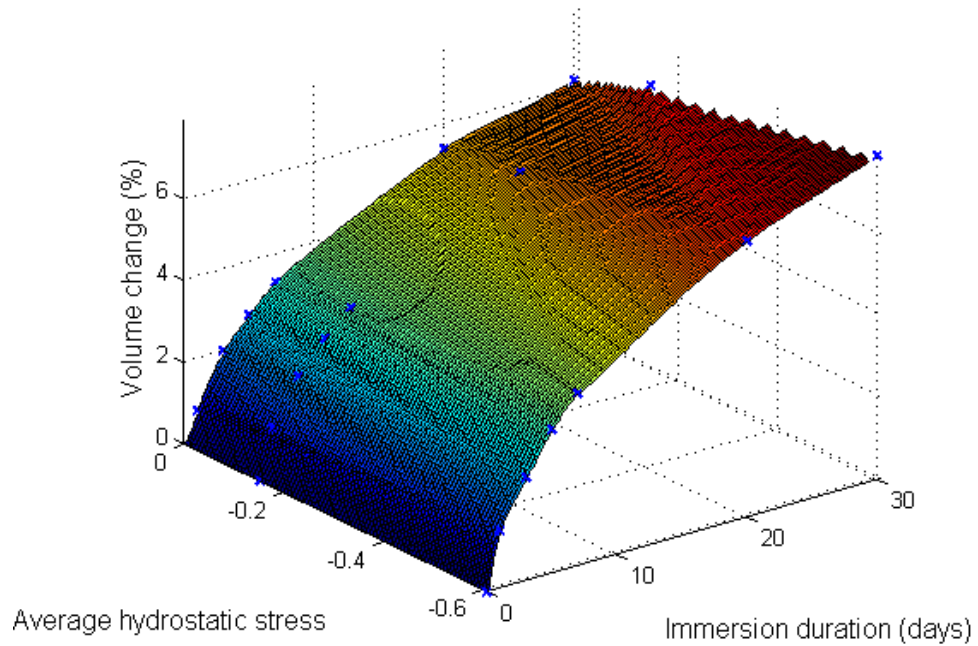


Figure 4.31: Volume change as a function of average hydrostatic stress for different immersion durations.

4.4 Discussion on the experimental specimen and device

In this section, a brief discussion on the advantages and limitations of the specimens and devices used throughout this study is given. This discussion will be helpful especially in understanding the limitations of the existing design for further improvement.

4.4.1 Constrained swelling 1: static uniaxial strain

The advantages of the specimen and device used for conducting static uniaxial strain are summarized below:

1. Static uniaxial strain can be introduced by adjusting the bolts and nuts connecting the metallic plates. This will allow the experimental observation of the coupling between mechanical loading and the diffusion of solvents.
2. The elastomer specimen used is following the ASTM standard. Thus, the specimen is easy to produce.

3. The elastomer specimen used has a thickness of 2 mm which is considerably thin and equilibrium swelling can occur in a short period of time.
4. The metallic device can accommodate up to 3 specimens which enable multiple specimens to be immersed at the same time. Should more than three specimens are required, the device can be easily modified by changing the length of the metallic plates.
5. No adhesive is used in the connection between the metallic device and the elastomeric specimen. Thus, the immersion tests can be conducted using any type of aggressive liquids since debonding between the specimen and the metallic parts is not an issue.
6. The metallic device can be easily attached and dismantled from the specimen and can be reused for further experimental works.

Although the device enables the experimental set up to be carried out successfully, there are some limitations which are listed below:

1. Since the specimen used is flat in shape, buckling is observed when the degree of swelling is sufficiently high which results in complex stress state generated in the specimen. This leads to complexity in understanding the effect of mechanical loading on swelling.
2. The device can not be attached to a tensile testing machine to conduct cyclic mechanical loadings since the specimen will undergo buckling during compressive loading. However, this limitation is related to the geometry of the specimen.

4.4.2 Constrained swelling 2: static multiaxial strain (Design 1)

Apart from the advantages such as no adhesive is used and the device can be attached and dismantled easily, the device and specimen used in Design 1 possess the advantages

such as:

1. Multiaxial strain can be introduced simultaneously to the specimens during the immersion test.
2. Diffusion of liquids practically occurs only along the radial direction, i.e. simple one-dimensional diffusion takes place. Thus, the corresponding experimental results can be used to validate simple mechanical models for investigating the swelling of elastomers in solvents undergoing simultaneously a mechanical loading.
3. Hollow diabolo specimens ensure that the equilibrium swelling can be achieved within a reasonably short period of time while permitting the application of moderate compressive strain without buckling or wrinkling.
4. Different twist angles and axial extensions/contractions can be imposed to the specimen simply by fixing and adjusting bolts and nuts at appropriate positions.
5. The metallic grips are designed so that the device and specimen can be used for several subsequent mechanical testings which follow the immersion tests such as uniaxial tensile, simple torsion, combined torsion-tension or fatigue testing.

Based on the discussion in Section 4.3, there are some limitations that need to be improved in future works:

1. Under simple torsion, the specimen is subjected to a non-uniform strain (or stress) field. Being preliminary work, this additional difficulty dealing with diffusion of liquids in the presence of non-uniform strain (or stress) should be avoided. A relative uniform strain and stress field in the specimen under torsion can be obtained by increasing the inner diameter of the specimen while fixing its wall thickness.

2. Different parts in the specimen undergo different swelling levels due to its geometry. It is preferable to confine the diffusion, i.e. swelling, in the middle part of the specimen since this is the focus of our study. This can be obtained by introducing an appropriate sealing on the specimen such that diffusion takes place only through the inner and outer surfaces of the middle part of the specimen.

4.4.3 Constrained swelling 3: static multiaxial strain (Design 2)

By referring to the limitations of Design 1, an improved version of device and specimen (Design 2) was manufactured and the new design exhibits the following improvements:

1. Under simple torsion, a more uniform strain field is generated throughout the specimen as compared to Design 1.
2. For a given amount of twist, the stress generated in this specimen is higher than that in Design 1. Thus, it increases the rate of diffusion of solvents. Under such circumstances, equilibrium swelling can be achieved within a shorter period of time.
3. Diffusion of solvents only occurs in the middle part of the specimen through the inner and outer surfaces since other parts are properly sealed with the metallic plates.

Although Design 2 manages to overcome some limitations observed in Design 1, the metallic device of Design 2 is not able to carry out mechanical testing. Indeed, when significant stretch is introduced, slip between the elastomeric specimens and the metallic device occurs. Moreover, equilibrium swelling cannot be observed since the specimen breaks prematurely during the immersion test. Further improvements on the setup of the specimen and the device are needed to overcome the above limitations.

CHAPTER 5

MODELING RESULTS AND DISCUSSION

This chapter can be divided into two main sections: modelling the stress-strain response at a given degree of swelling and prediction of equilibrium swelling for different mechanical deformations. The modeling results are then compared with the experimental results presented in Chapter 4.

5.1 Stress-strain relationship at a given degree of swelling

The mechanical responses of both dry and swollen elastomers under cyclic loadings as presented in Section 4.2.2 clearly indicated the complexity of the material responses, i.e. Mullins effect, hysteresis and permanent set take place. To simulate the real engineering components in a swollen state, a complex constitutive model taking into account all the inelastic responses must be developed to simulate the observed mechanical responses. The development of such a complex model is beyond the scope of this research. As a starting attempt, only the Mullins effect is considered in the model. Other inelastic phenomena are not considered in this work.

5.1.1 Data treatment

Since the Mullins effect is the only inelastic response addressed in the present study, the experimental results must be treated in order to highlight the characteristics of it. For this purpose, the data treatment proposed by Chagnon et al. (2004) is adopted and summarized below:

1. Only unloading paths are considered and the reloading paths are assumed to coincide with them.

2. The unloading paths are horizontally shifted such that they start from zero strain (stretch=1).
3. The shifted unloading paths are extended to rejoin the monotonic primary curve.

The resulting treated experimental data are presented in Figures 5.1 to 5.3 and will be used to assess the efficiency of the proposed model.

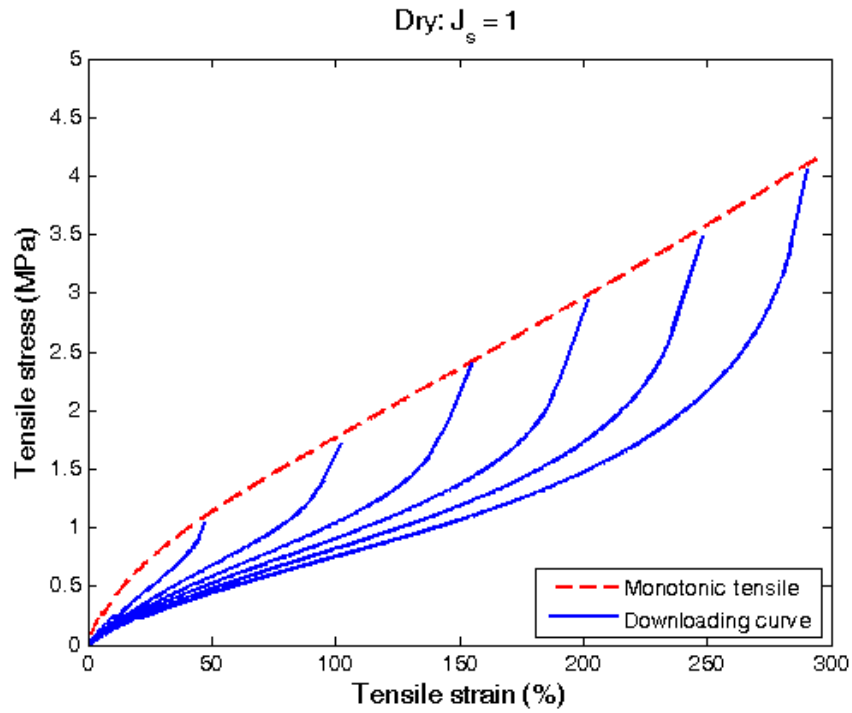


Figure 5.1: Treated experimental data for dry elastomer ($J_s = 1$)

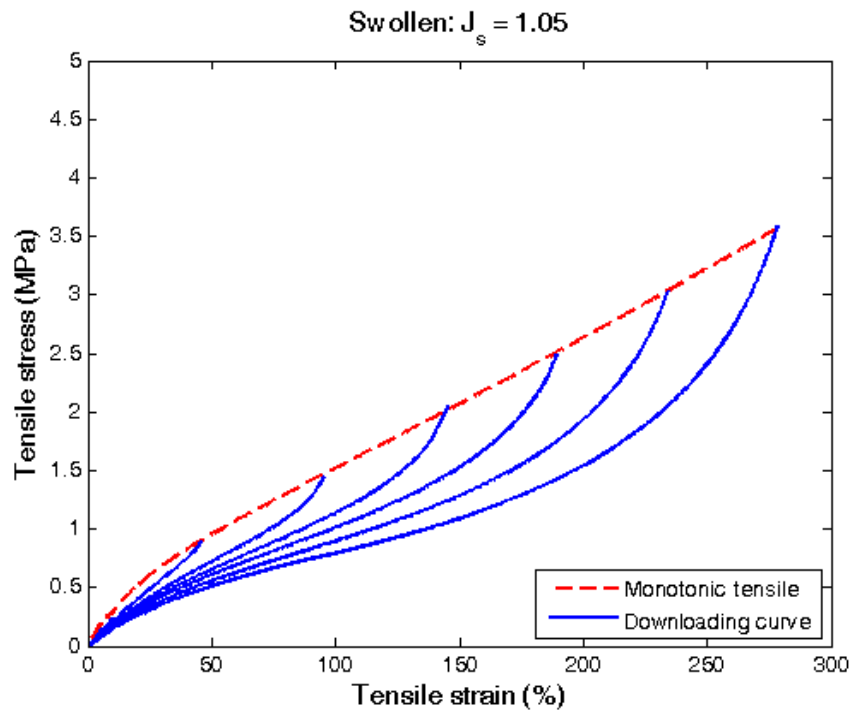


Figure 5.2: Treated experimental data for swollen elastomer ($J_s = 1.05$)

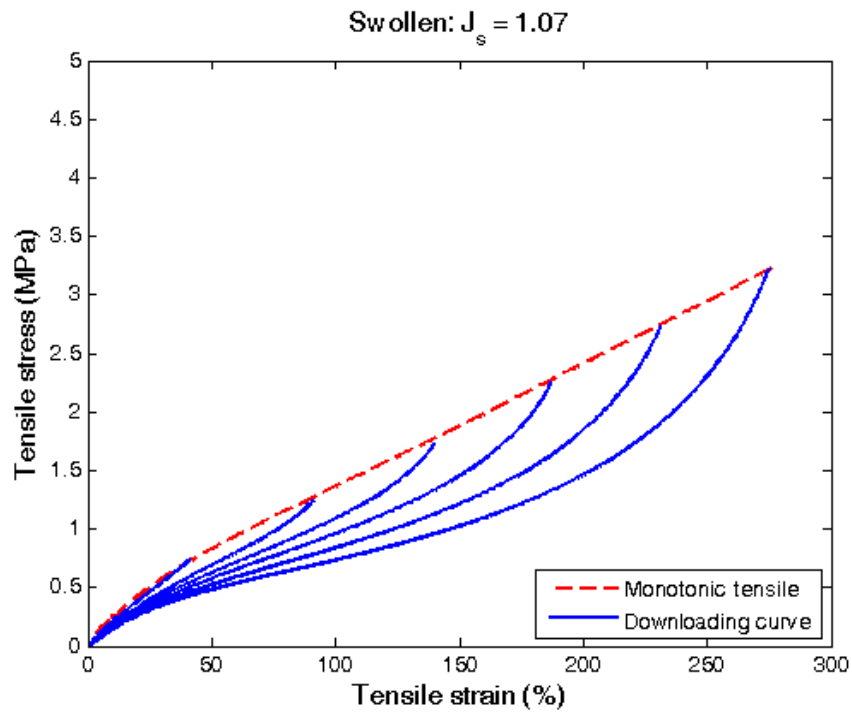


Figure 5.3: Treated experimental data for swollen elastomer ($J_s = 1.07$)

5.1.2 Form of material functions

In order to capture the stress-strain response of rubber under large strains, the eight-chain model of Arruda and Boyce (1993) is retained. The corresponding hyperelastic strain energy density is given by:

$$W_{\text{sp}} = \nu_s \mu_d \left[\sqrt{N} \lambda_{\text{ch,sp}} \beta + N \ln \left(\frac{\beta}{\sinh \beta} \right) \right] \quad (5.1)$$

$$\beta = \mathcal{L}^{-1} \left(\frac{\lambda_{\text{ch,sp}}}{\sqrt{N}} \right)$$

\mathcal{L}^{-1} is the inverse Langevin function, μ_d is the shear modulus of dry elastomer, N is the number of chain segments and $\lambda_{\text{ch,sp}}$ is the amplified mechanical chain stretch. The latter is related to the macroscopic mechanical chain stretch λ_{ch} via (Qi & Boyce, 2004):

$$\lambda_{\text{ch,sp}} = \sqrt{X (\lambda_{\text{ch}}^2 - 1) + 1} \quad (5.2)$$

$$\lambda_{\text{ch}} = \sqrt{\frac{I_{1\text{m}}}{3}}$$

According to Treloar (1975), swelling of elastomers is a physical mixing or inter-diffusion process with no chemical attraction between elastomer and solvent molecules. Furthermore, the only effect of swelling is to reduce the modulus in inverse proportion to the cube root of the swelling degree without changing the form of the stress-strain curves. However, as observed by Chai et al. (2011), deviations from the theory of Treloar were found for NBR swollen by palm biodiesel. Thus, following Durning and Morman (1993), the shear modulus of the swollen elastomer μ_s is assumed to be related to that of dry elastomer μ_d through:

$$\mu_s = J_s^{-n} \mu_d \quad (5.3)$$

where $n > 0$ is a material parameter. It follows that the strain energy function of a mechanical incompressible elastomer (per unit of material volume in unswollen-unstressed

state) which is isotropically swollen is given by (Boyce & Arruda, 2001):

$$W_{\text{sp}} = \nu_s \mu_s N \left[\frac{\Lambda_{\text{ch,sp}}}{\sqrt{N}} \beta_{\text{ch,sp}} + \ln \left(\frac{\beta_{\text{ch,sp}}}{\sinh \beta_{\text{ch,sp}}} \right) - \frac{J_s^{1/3}}{\sqrt{N}} \beta_s - \ln \left(\frac{\beta_s}{\sinh \beta_s} \right) \right] \quad (5.4)$$

where

$$\begin{aligned} \Lambda_{\text{ch,sp}} &= J_s^{1/3} \lambda_{\text{ch,sp}} \\ \beta_{\text{ch,sp}} &= \mathcal{L}^{-1} \left(\frac{\Lambda_{\text{ch,sp}}}{\sqrt{N}} \right) \\ \beta_s &= \mathcal{L}^{-1} \left(\frac{J_s^{1/3}}{\sqrt{N}} \right) \end{aligned} \quad (5.5)$$

The principal values of the Cauchy stress are obtained via Equation (3.45):

$$\sigma_i = -q J_s^{-1} + J_s^{-n-2/3} \frac{\nu_s X \mu_d}{3} \frac{\sqrt{N}}{\lambda_{\text{ch,sp}}} \mathcal{L}^{-1} \left(\frac{\Lambda_{\text{ch,sp}}}{\sqrt{N}} \right) \lambda_i^2 \quad (5.6)$$

The difference between two principal Cauchy stress values is given by:

$$\sigma_1 - \sigma_2 = J_s^{-n-2/3} \frac{\nu_s X \mu_d}{3} \frac{\sqrt{N}}{\lambda_{\text{ch,sp}}} \mathcal{L}^{-1} \left(\frac{\Lambda_{\text{ch,sp}}}{\sqrt{N}} \right) (\lambda_1^2 - \lambda_2^2) \quad (5.7)$$

For the special case of uniaxial tensile strain, where $\lambda_1 = \lambda_m$ and $\lambda_2 = \lambda_3 = 1/\sqrt{\lambda_1}$, the axial Cauchy stress is given by:

$$\begin{aligned} \sigma &= J_s^{-r} \frac{\nu_s X \mu_d}{3} \frac{\sqrt{N}}{\lambda_{\text{ch,sp}}} \mathcal{L}^{-1} \left(\frac{\Lambda_{\text{ch,sp}}}{\sqrt{N}} \right) \left(\lambda_m^2 - \frac{1}{\lambda_m} \right) \\ r &= n + 2/3 \end{aligned} \quad (5.8)$$

The above constitutive equation must be complemented with an evolution equation describing the change in the internal variable ν_s consistent with the second law of thermodynamics (Andriyana, Billon, & Silva, 2010), more precisely the inequality in Equation (3.46). Since $\frac{\partial W_{\text{sp}}}{\partial \nu_s} < 0$, ν_s must be an increasing function of the maximum deformation

which experienced the elastomer during the past history. Adopting a modified form of saturation type for the evolution equation as proposed by Qi and Boyce (2004), the evolution of the soft phase domain v_s is assumed to follow a non-linear evolution equation:

$$\dot{v}_s = A(v_{ss} - v_s) \frac{\sqrt{N} - 1}{\left(\sqrt{N} - \lambda_{\text{ch,sp}}^{\text{max}}\right)^2} \dot{\lambda}_{\text{ch,sp}}^{\text{max}} \quad (5.9a)$$

$$\dot{\lambda}_{\text{ch,sp}}^{\text{max}} = \begin{cases} 0 & \text{if } \lambda_{\text{ch,sp}} < \lambda_{\text{ch,sp}}^{\text{max}} \\ \dot{\lambda}_{\text{ch,sp}}^{\text{max}} & \text{if } \lambda_{\text{ch,sp}} = \lambda_{\text{ch,sp}}^{\text{max}} \end{cases} \quad (5.9b)$$

In the above expression, $\lambda_{\text{ch,sp}}^{\text{max}}$ is the maximum value of amplified mechanical chain stretch $\lambda_{\text{ch,sp}}$ during the loading history. The quantity A is a material parameter and v_{ss} is the theoretical maximum value of v_s . Integrating Equation (5.9), the evolution equation can be recast to:

$$v_s = v_{ss} - (v_{ss} - v_{so}) \exp \left[A \left(1 - \frac{\sqrt{N} - 1}{\sqrt{N} - \lambda_{\text{ch,sp}}^{\text{max}}} \right) \right] \quad (5.10)$$

where v_{so} is the initial volume fraction of the soft phase. To summarize, the material parameters that have to be identified from experimental data are given in Table 5.1.

Table 5.1: Summary of material parameters required in the proposed model.

Material (soft phase) parameters	μ_d	N
Softening parameters	v_{so}	v_{ss} A
Swelling effect parameter	n	

5.1.3 Identification of material parameters

In the following, the identification of the material parameters of the proposed model is described. First, it is necessary to determine the parameters corresponding to the dry elastomer. The properties of the soft domains in dry elastomers can be obtained by con-

sidering the last unloading curve in Figure 5.1, i.e. at $\lambda_{\max} = 4$. Since additional softening is expected to occur if the dry rubber was strained beyond $\lambda = 4$, the volume fraction of the soft domain at this point is estimated to be $v_s(\lambda_{\max} = 5) \approx 0.90$. Using this value, the parameters μ_d and N are estimated to be $\mu_d = 0.21$ MPa and $N = 18$. Next, by fitting simultaneously the primary curve (monotonic tensile) and unloading curves, the following softening parameters are obtained: $v_{so} = 0.37$, $v_{ss} = 0.92$ and $A = 0.4$.

For swollen elastomers, in order to capture the effect of swelling on the softening, the dependence of the parameters v_{so} , v_{ss} and A on the degree of swelling J_s must be examined. For the sake of simplicity, it is assumed here that swelling only affects the initial available soft phase domain v_{so} . The parameters v_{ss} and A are assumed to be independent on the degree of swelling. More precisely, swelling only reduces the initial hard phase domain available to be converted into the soft phase domain during the deformation process while the maximum soft phase domain and the conversion rate at which the hard phase evolves due to a mechanical loading are assumed to be independent on the degree of swelling.

As illustrated in Figures 5.1 to 5.3, stress-softening decreases with the increase in swelling. Consequently, the initial soft phase volume fraction v_{so} is an increasing function of the degree of swelling since the available hard to soft phase conversion during stress softening decreases. For each degree of swelling, by fitting simultaneously the primary and unloading curves in Figures 5.1, 5.2 and 5.3, we obtain: $v_{so}(J_s = 1.05) = 0.42$, $v_{so}(J_s = 1.07) = 0.45$ and $n = 1.67$. In Figure 5.4, the dependence of v_{so} on J_s is depicted.

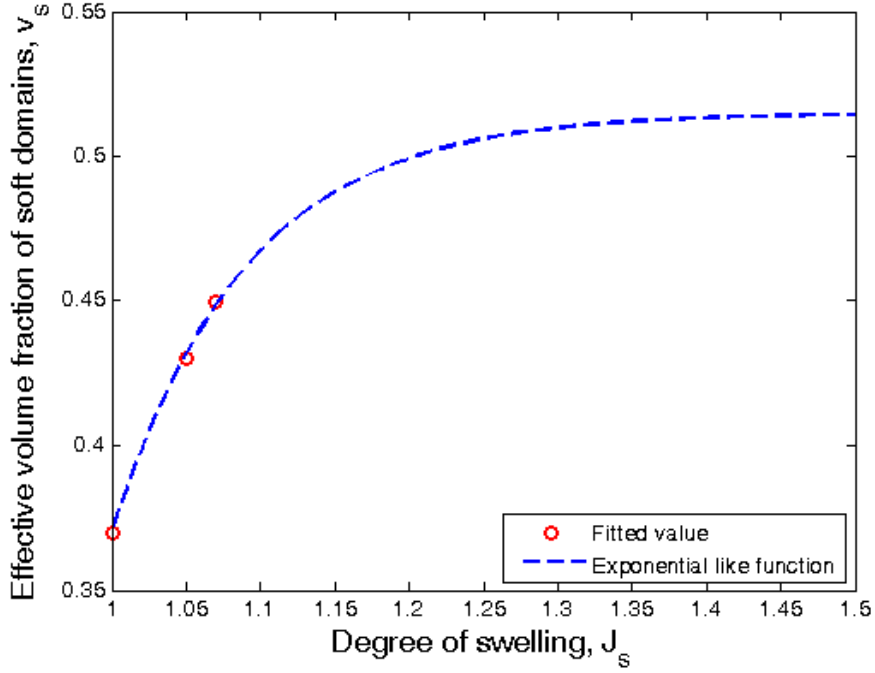


Figure 5.4: Evolution of the initial volume fraction of the soft domain as a function of degree of swelling.

It appears that the corresponding dependence can be described by the following exponential-like function:

$$v_{so}(J_s) = v_{so,d} + C_1 \left[1 - \exp\left(-\frac{J_s - 1}{C_2}\right) \right] \quad (5.11)$$

where $v_{so,d}$ is the initial volume fraction of the soft phase in dry rubber. $C_1 = 0.145$ and $C_2 = 0.090$ are additional parameters obtained by fitting the points in Figure 5.4. Finally, the obtained material parameters are tabulated in Table 5.2.

Remark 3 *The choice of the function selected to represent the evolution of the initial volume fraction of the soft domain as a function of degree of swelling is based on the observation of Chai (2013) where the level of stress-softening appears to be unaffected by the corresponding further increase in swelling. Thus, it is assumed that there should*

Table 5.2: Values of material parameters used in the proposed model.

	Parameter	Value
Material (soft phase) parameters	μ_d	0.21 MPa
	N	18
Softening parameters	$\nu_{so,d}$	0.37
	ν_{ss}	0.92
	A_d	0.4
	C_1	0.145
	C_2	0.090
Swelling parameter	n	1.67

be maximum amount of softening experienced by the material regardless of the increase in the degree of swelling.

Remark 4 The value of $\nu_s(\lambda_{max} = 4)$ is set to 0.9 based on the following considerations:

1. $\lambda_{max} = 4$ is close to the strain at fracture of $\lambda_f = 5$. Even if ν_s has no direct link to fracture, it motivates the consideration that $\nu_s(\lambda_{max} = 4)$ should be close to unity.
2. If $\nu_s(\lambda_{max} = 4)$ is set to another value close to unity such as 0.8 or 0.7, the author found that it does not affect significantly the value of other parameters. However, the model fits best with experimental data when $\nu_s(\lambda_{max} = 4)$ is set to be 0.9.

Remark 5 According to Chai, Andriyana, et al. (2013), elastomeric samples swollen up to 5 % and 7 % are far from thermodynamic equilibrium. Thus, solvent distribution across cross-sections of these specimens is not homogeneous. Being a first attempt to account for the effect of swelling on stress-softening, in the model development we assume that the material is homogeneous. Consequently, the proposed model provides only a rough estimation of the stress states undergone by the material.

5.1.4 Comparison between model and experiment

The comparisons between the simulations based on the proposed model and the treated experimental data are presented in Figures 5.5, 5.6 and 5.7. Note that for swollen

elastomers, the tensile stress is expressed with respect to the swollen-unstressed configuration (initial swollen cross section).

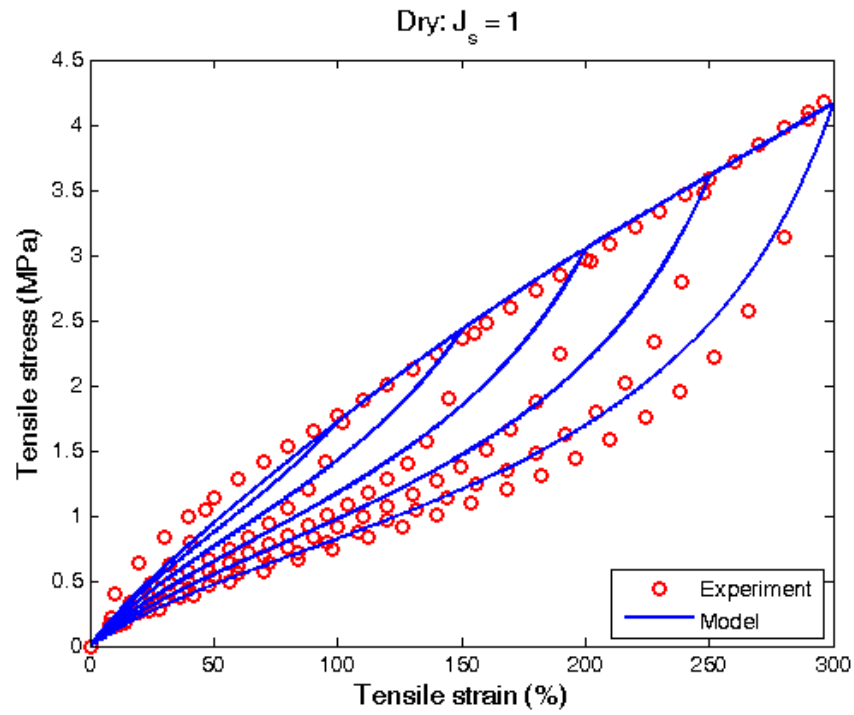


Figure 5.5: Comparison between the proposed model and treated experimental data for dry elastomer ($J_s = 1$).

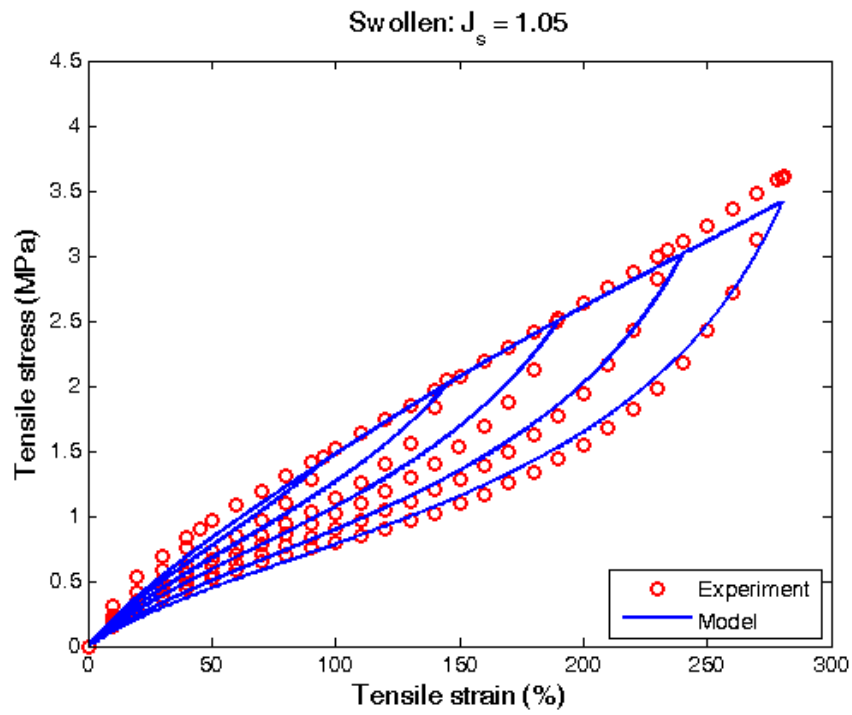


Figure 5.6: Comparison between the proposed model and treated experimental data for swollen elastomer ($J_s = 1.05$).

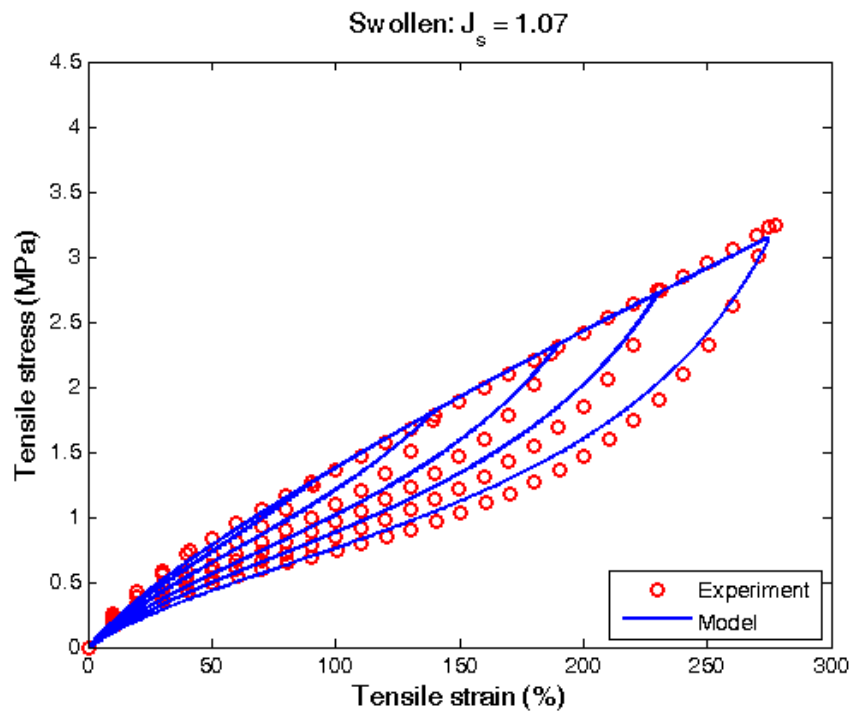


Figure 5.7: Comparison between the proposed model and treated experimental data for swollen elastomer ($J_s = 1.07$).

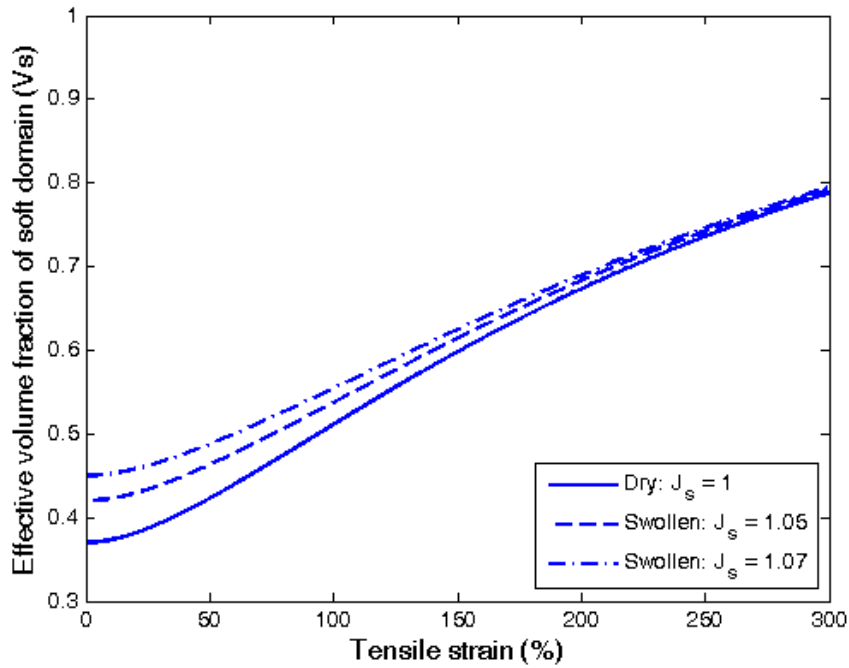


Figure 5.8: Evolution of effective volume fraction of soft phase as a function of maximum tensile strain.

In general, it is observed that the proposed model shows good agreement with experimental data. The primary curves for dry and swollen rubbers are well-captured. Although there are slight discrepancies during the secondary curves at lower stretch levels for the dry specimens, they are acceptable and reduce as the stretch increases. As for the swollen rubbers, both primary and secondary curves are well described by the proposed model. Moreover, the dependence of the stress-softening on the swelling level is well-described: smaller softening is observed for higher degree of swelling.

5.1.5 Simulation for other degrees of swelling

The initial volume fraction of the soft phase at other degrees of swelling is determined by Equation (5.11). Using the same material parameters as obtained above, the model response for other degrees of swelling under uniaxial extension is simulated and presented in Figures 5.9 to 5.11 while the evolution of the effective volume fraction of

the soft phase is plotted in Figure 5.12.

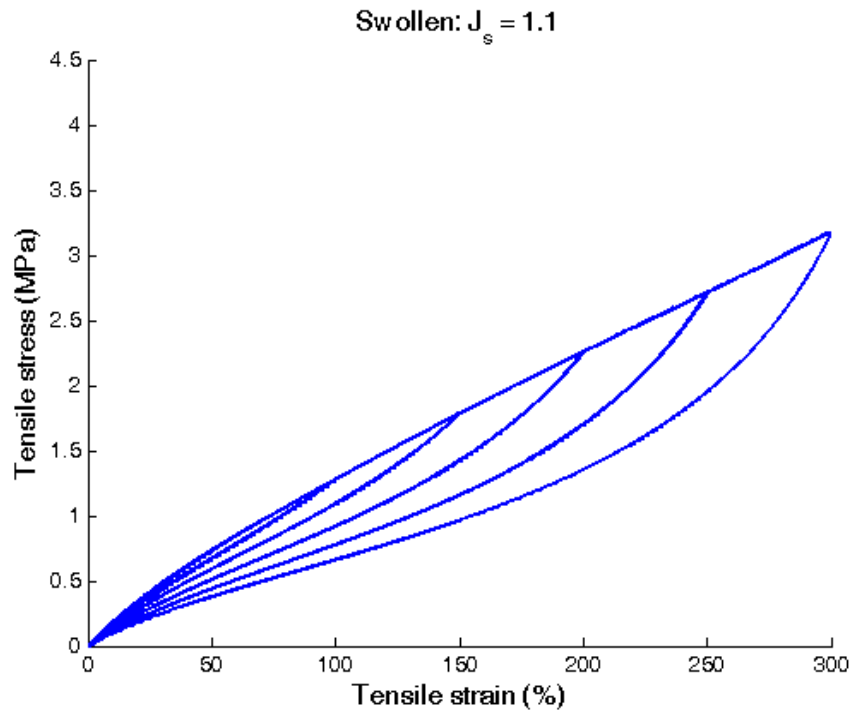


Figure 5.9: Model response under uniaxial extension for swollen elastomer ($J_s = 1.1$).

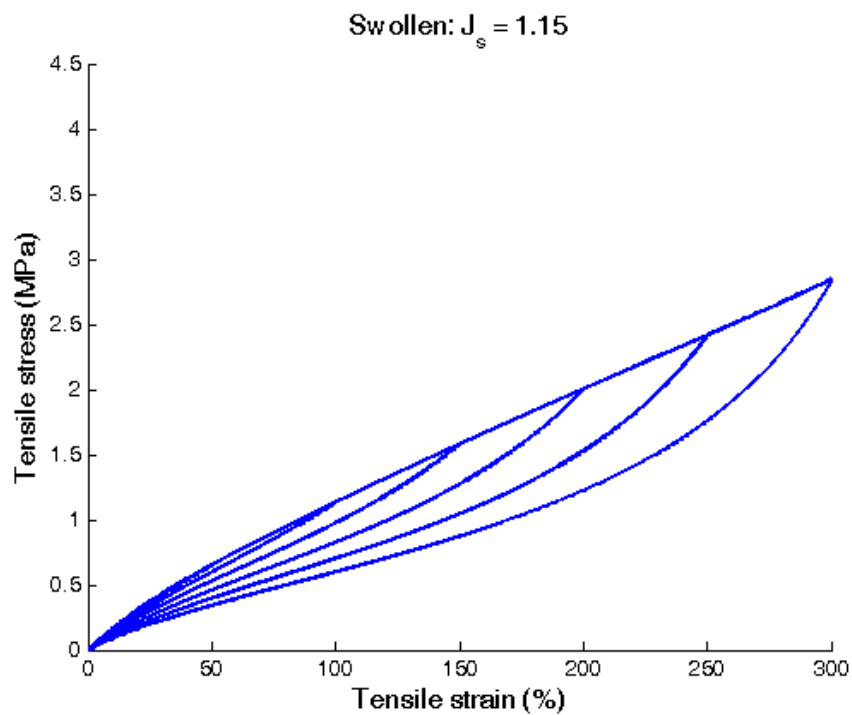


Figure 5.10: Model response under uniaxial extension for swollen elastomer ($J_s = 1.15$).

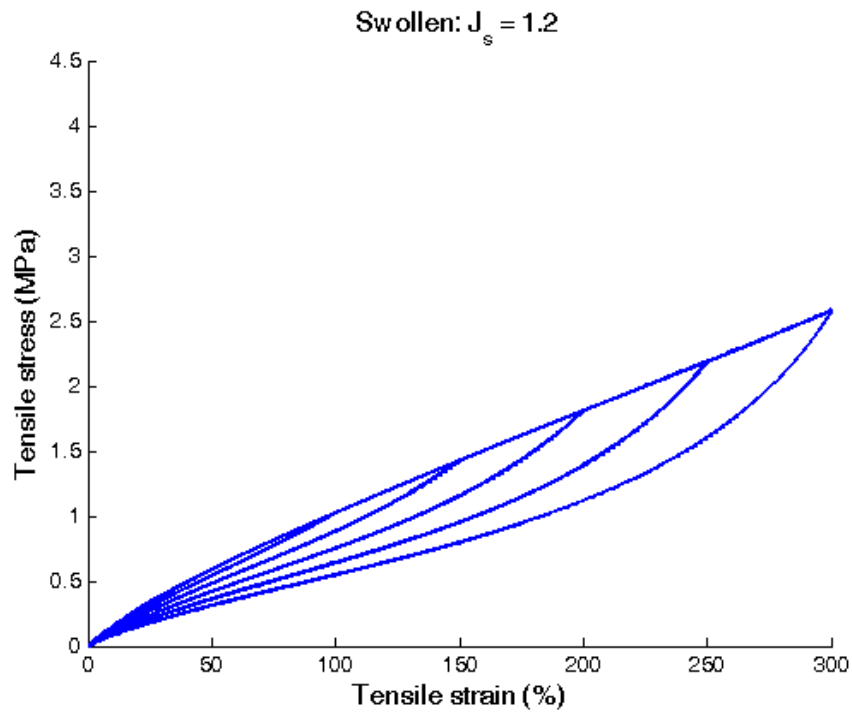


Figure 5.11: Model response under uniaxial extension for swollen elastomer ($J_s = 1.2$).

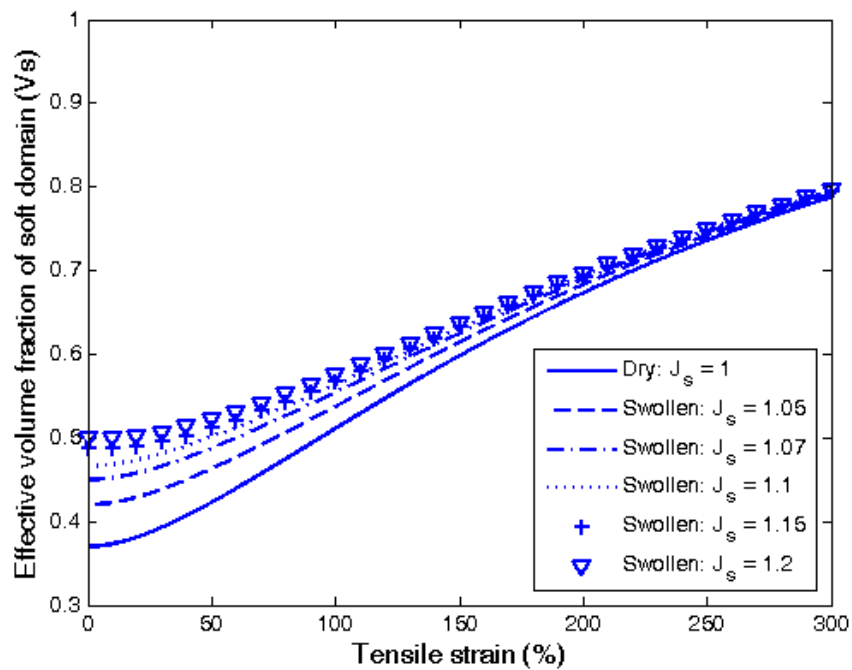


Figure 5.12: Evolution of effective volume fraction of soft phase as a function of maximum tensile strain.

From these figures, it is clearly seen that the proposed model captures the depen-

dence of the stress-softening on the degree of swelling with high quality. Lower stress responses are predicted at a given strain level when the degree of swelling increases. Furthermore, smaller stress-softening is predicted at higher degrees of swelling as shown by Figure 5.12.

5.1.6 Simulation for other deformation modes

In order to simulate the response of the model under multiaxial loading conditions, two deformation modes are considered: equibiaxial extension and planar extension. In these two cases, the governing equations needed are summarized below:

Pure shear

$$\begin{aligned}
\hat{P}_{11} &= J_s^{-r} \frac{\nu_s X \mu_d}{3} \frac{\sqrt{N}}{\lambda_{\text{ch,sp}}} \mathcal{L}^{-1} \left(\frac{J_s^{1/3} \lambda_{\text{ch,sp}}}{\sqrt{N}} \right) \left(\lambda_m - \frac{1}{\lambda_m^3} \right) \\
\lambda_{\text{ch,sp}} &= \sqrt{X (\lambda_{\text{ch}}^2 - 1) + 1} \\
\lambda_{\text{ch}} &= \sqrt{\frac{I_{1m}}{3}} \\
I_{1m} &= \lambda_m^2 + \frac{1}{\lambda_m^2} + 1
\end{aligned} \tag{5.12}$$

Equibiaxial extension

$$\begin{aligned}
\hat{P}_{11} &= J_s^{-r} \frac{\nu_s X \mu_d}{3} \frac{\sqrt{N}}{\lambda_{\text{ch,sp}}} \mathcal{L}^{-1} \left(\frac{J_s^{1/3} \lambda_{\text{ch,sp}}}{\sqrt{N}} \right) \left(\lambda_m - \frac{1}{\lambda_m^5} \right) \\
\lambda_{\text{ch,sp}} &= \sqrt{X (\lambda_{\text{ch}}^2 - 1) + 1} \\
\lambda_{\text{ch}} &= \sqrt{\frac{I_{1m}}{3}} \\
I_{1m} &= 2\lambda_m^2 + \frac{1}{\lambda_m^4}
\end{aligned} \tag{5.13}$$

Similarly to uniaxial extension, the material is simulated to undergo cyclic loading

to six maximum strain levels: $\epsilon = 0.5, 1.0, 1.5, 2.0, 2.5, 3.0$. Using the same material parameters as under uniaxial tension, different degrees of swelling are considered in the simulation: $J_s = 1.0, 1.05, 1.07, 1.1, 1.15, 1.2$. The model responses under planar extension are presented in Figures 5.13 to 5.18 while the evolution of the effective volume fraction of the soft phase is shown in Figure 5.19.

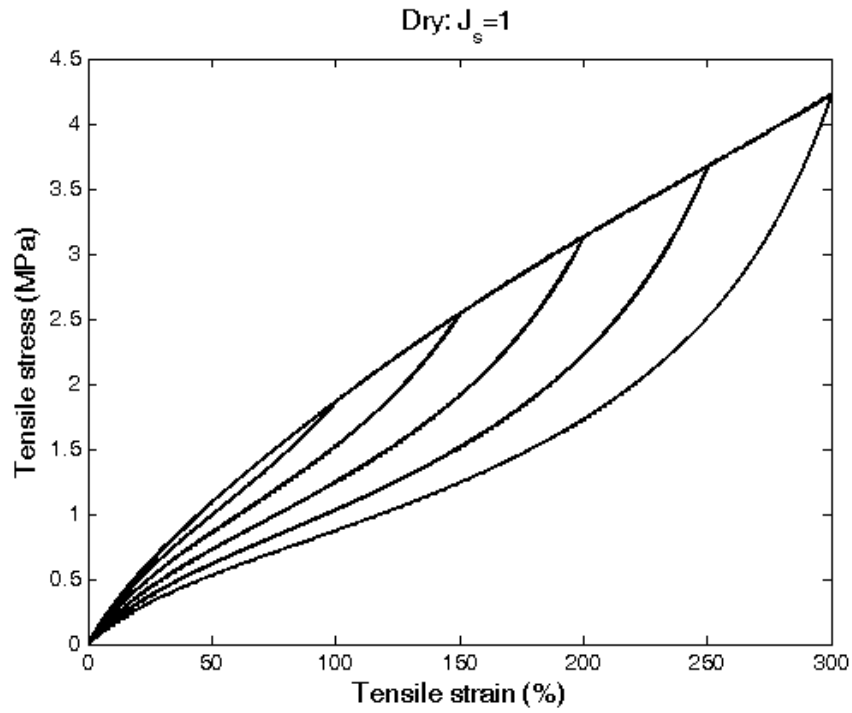


Figure 5.13: Model response under planar extension for dry elastomer ($J_s = 1$).

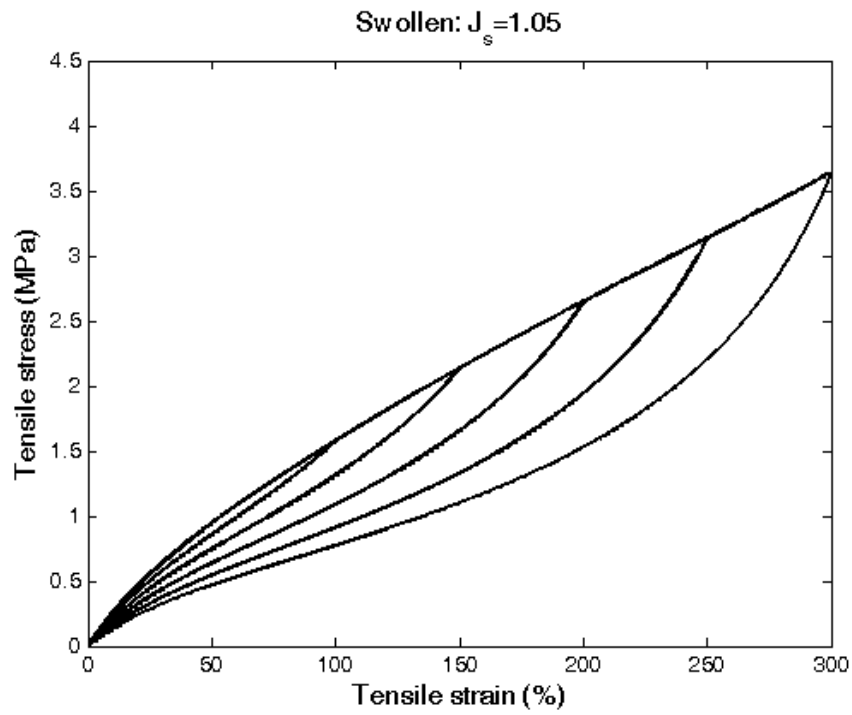


Figure 5.14: Model response under planar extension for swollen elastomer ($J_s = 1.05$).

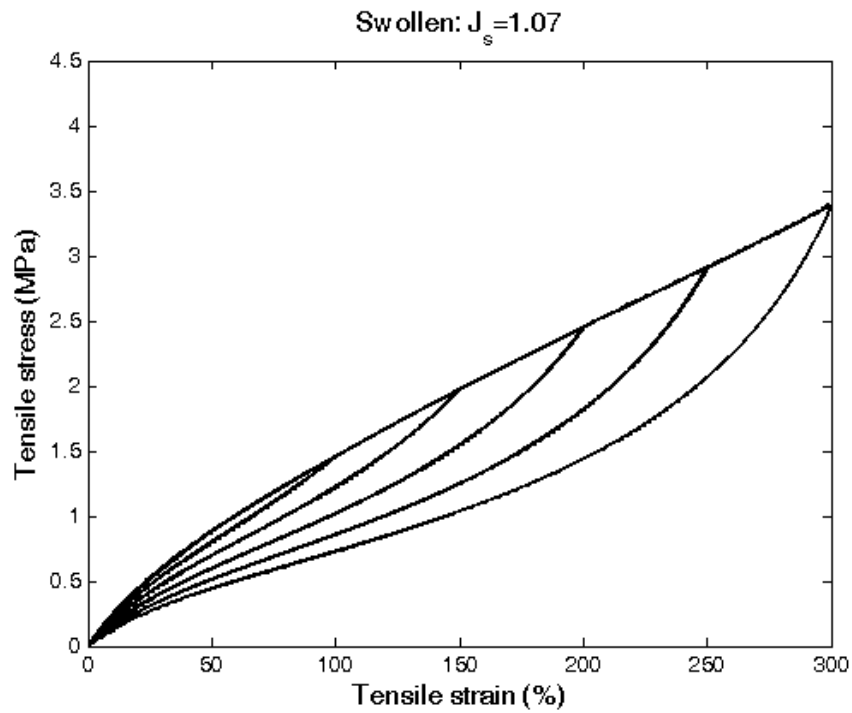


Figure 5.15: Model response under planar extension for swollen elastomer ($J_s = 1.07$).

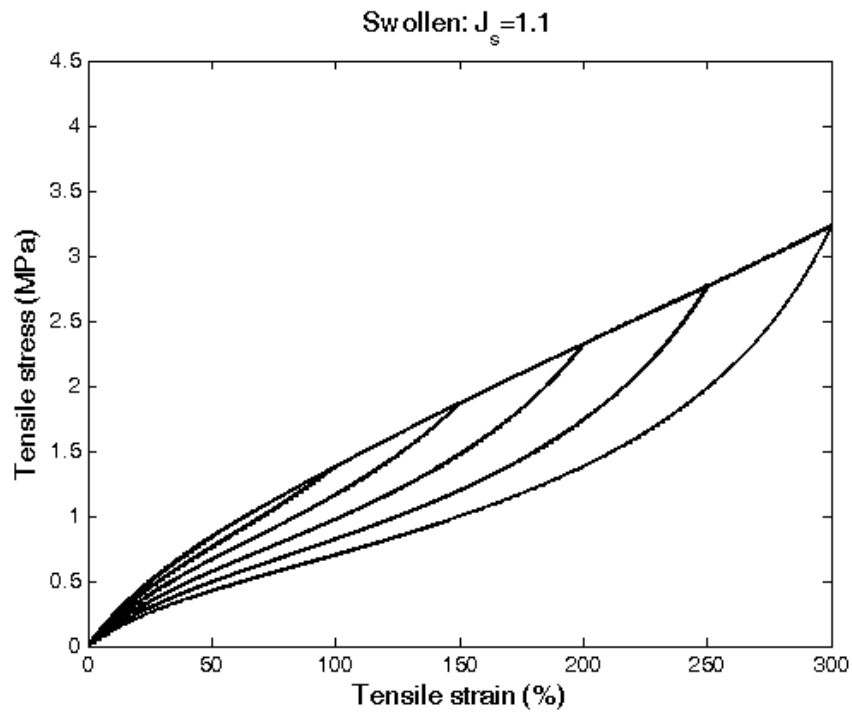


Figure 5.16: Model response under planar extension for swollen elastomer ($J_s = 1.1$).

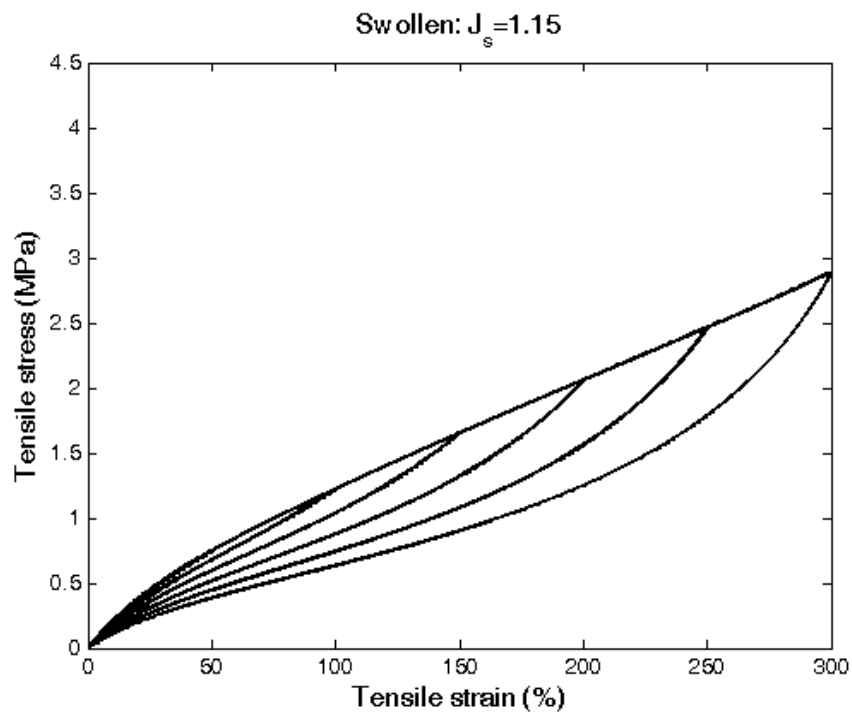


Figure 5.17: Model response under planar extension for swollen elastomer ($J_s = 1.15$).

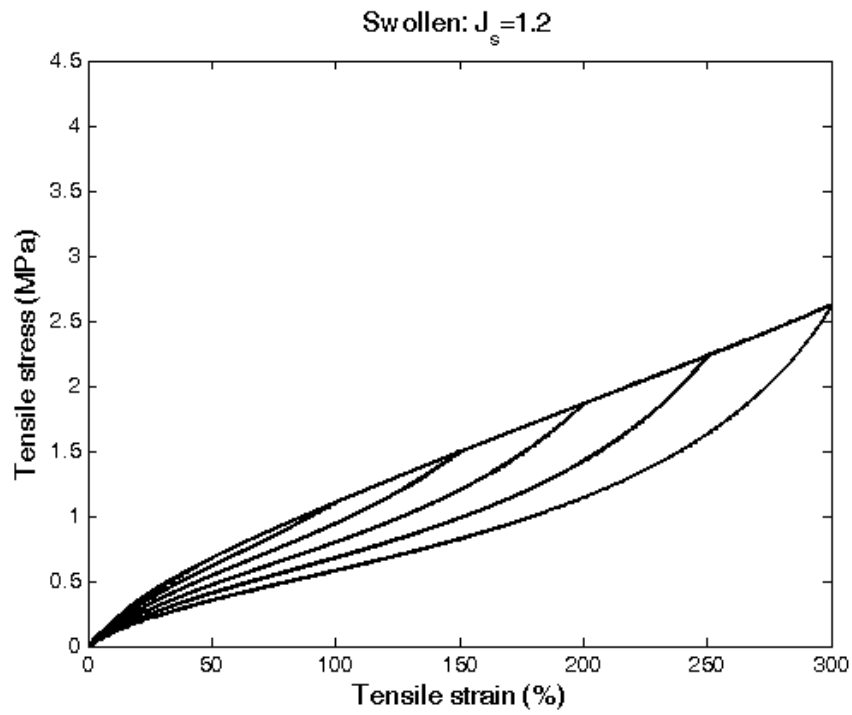


Figure 5.18: Model response under planar extension for swollen elastomer ($J_s = 1.2$).

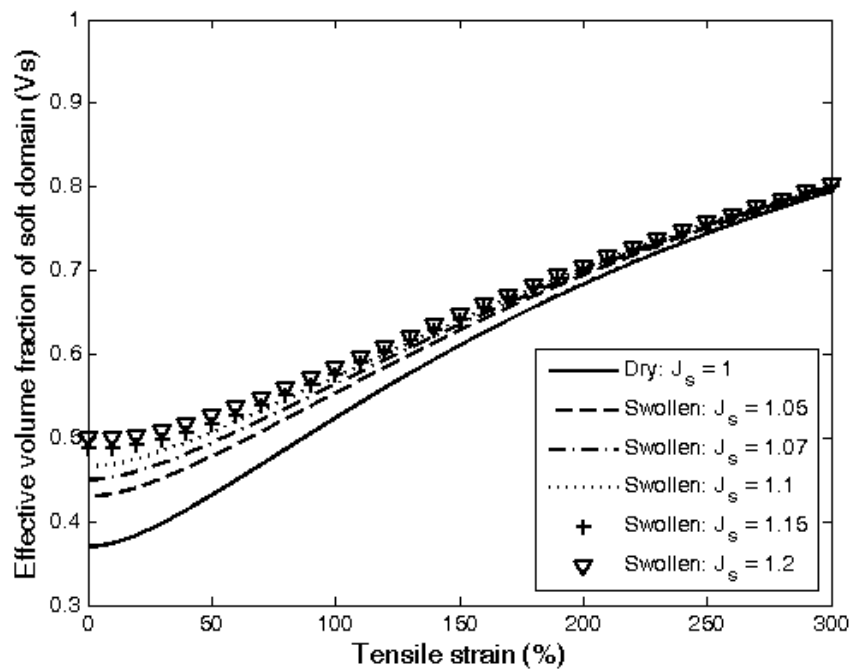


Figure 5.19: Evolution of effective volume fraction of soft phase under planar extension.

Using the same approach, the simulations of the model responses under equibiaxial extension are shown as Figures 5.20 to 5.25 while the evolution of effective volume

fraction of soft phase is shown as Figure 5.26.

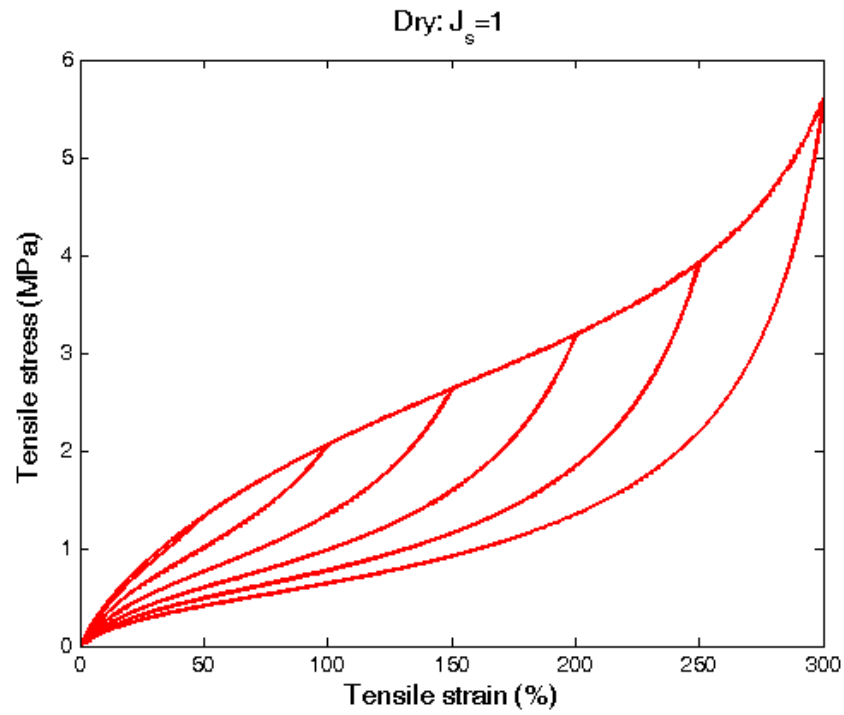


Figure 5.20: Model response under equibiaxial extension for dry elastomer ($J_s = 1$).

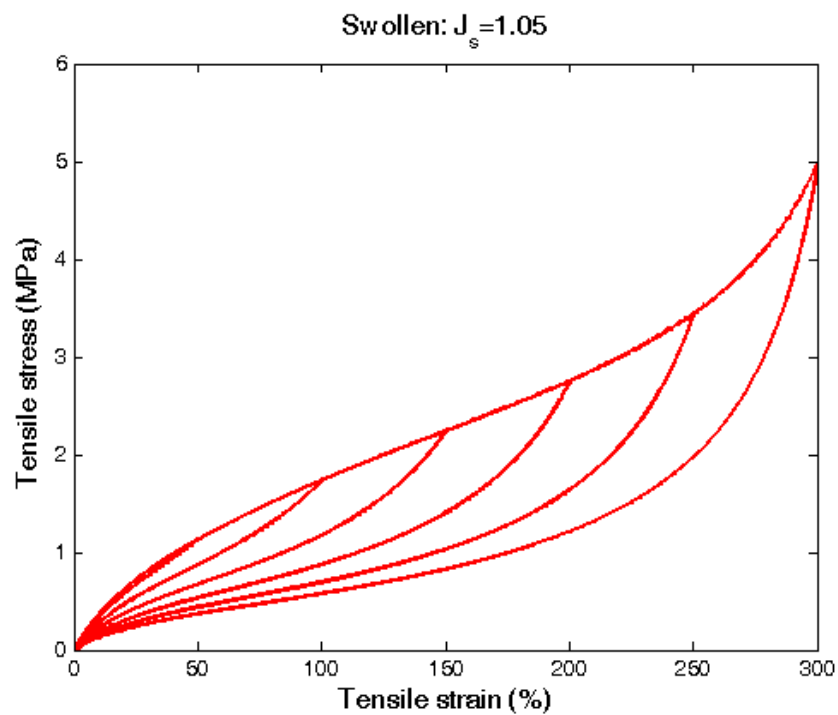


Figure 5.21: Model response under equibiaxial extension for swollen elastomer ($J_s = 1.05$).

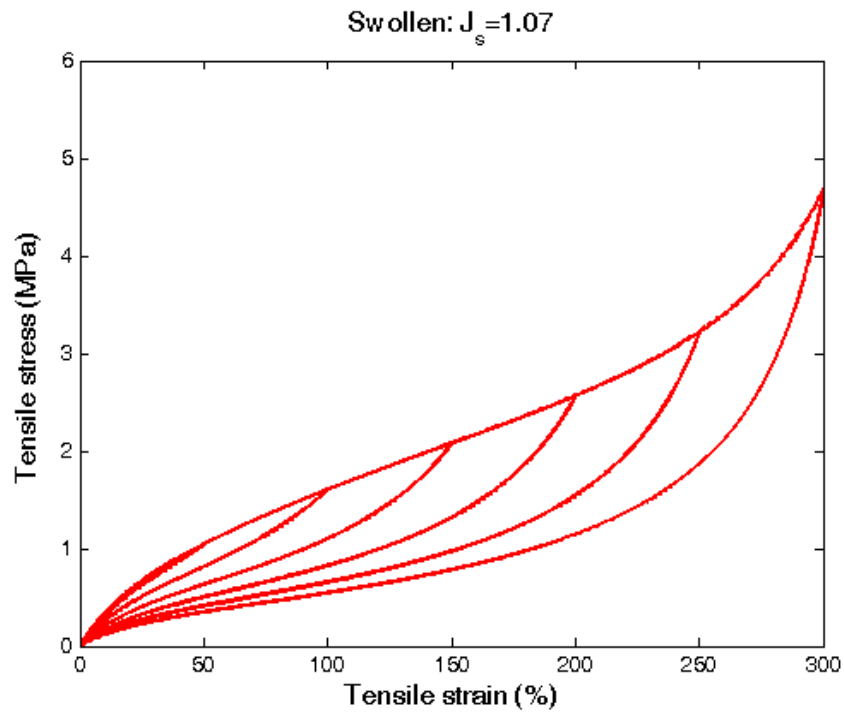


Figure 5.22: Model response under equibiaxial extension for swollen elastomer ($J_s = 1.07$).

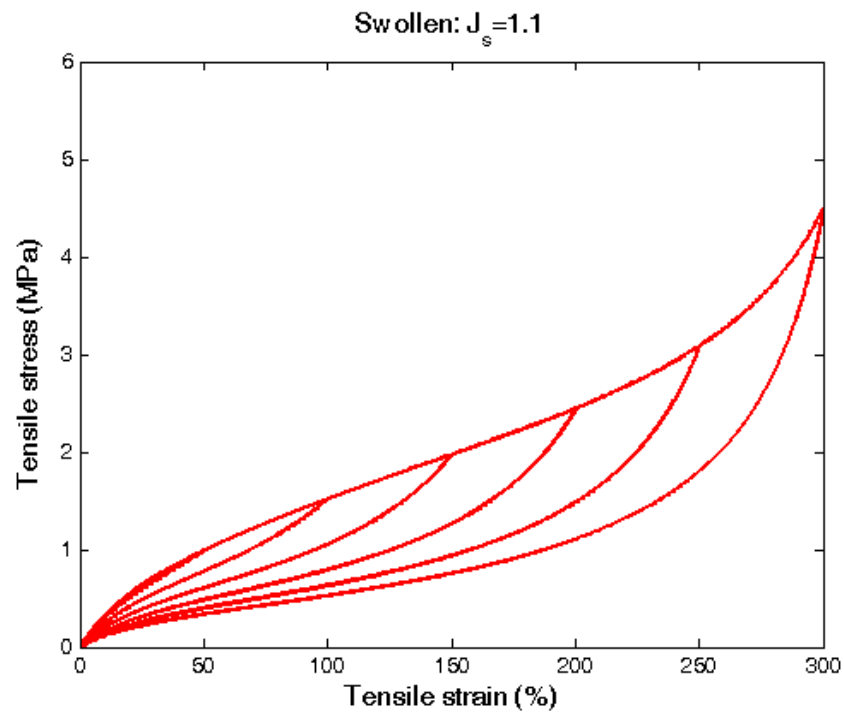


Figure 5.23: Model response under equibiaxial extension for swollen elastomer ($J_s = 1.1$).

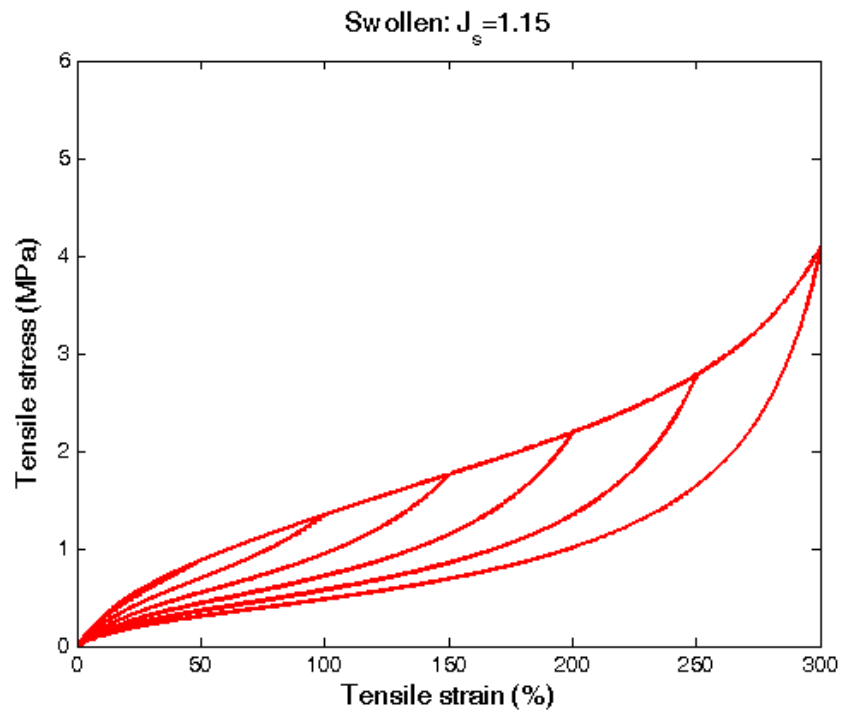


Figure 5.24: Model response under equibiaxial extension for swollen elastomer ($J_s = 1.15$).

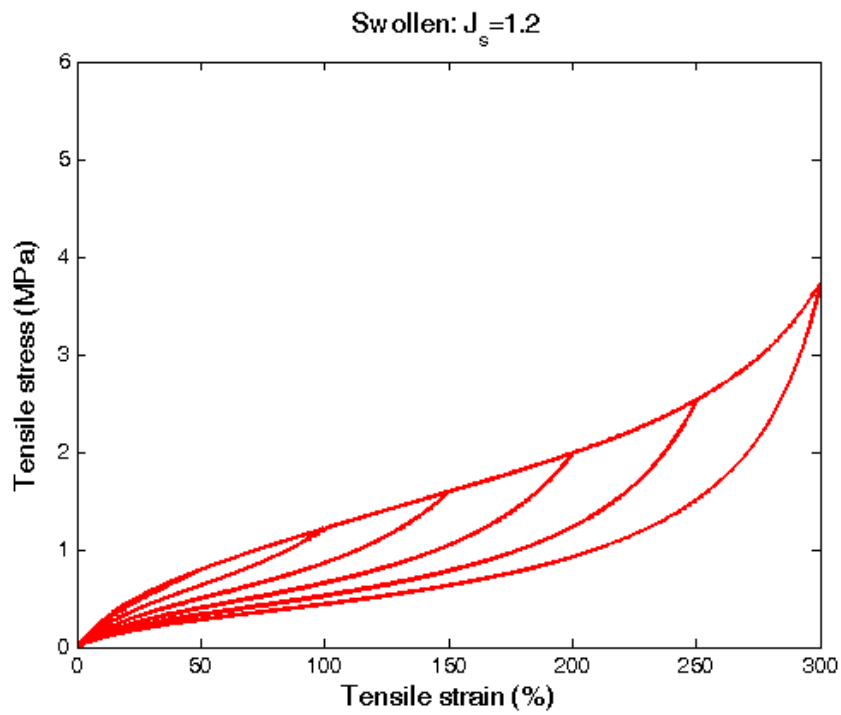


Figure 5.25: Model response under equibiaxial extension for swollen elastomer ($J_s = 1.2$).

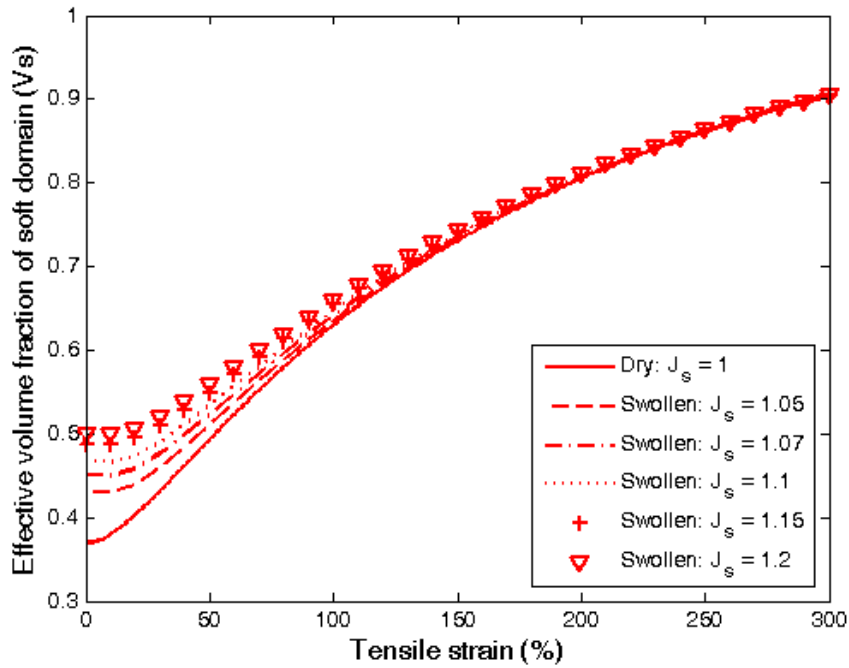


Figure 5.26: Evolution of effective volume fraction of soft phase under equibiaxial extension.

It is observed that for both cases, lower stress levels are recorded for higher degrees of swelling. Moreover, smaller stress-softening is observed when the degree of swelling increases. The evolution of the effective volume fraction of the soft phase appears to be dependent on the deformation mode. Indeed, for a given degree of swelling, the greatest amount of softening is found in the case of equibiaxial extension in comparison with those in planar and uniaxial extension. The corresponding observation can be related to the amount of chain stretch λ_{ch} : for a given strain level, the resulting chain stretch due to equibiaxial extension is the greatest.

5.2 Prediction of equilibrium swelling

As observed in Chapter 4, the amount of solvent uptake in the elastomer is highly dependent on the applied mechanical deformations. It would be beneficial to predict the degree of swelling in elastomers in the presence of a mechanical deformation. In this

work, a model to predict the equilibrium swelling under consideration of the coupling between diffusion and deformation is proposed. Note that the proposed model enables the prediction under equilibrium states since equilibrium swelling is considered as the most severe case while the transient response is not considered in this work.

5.2.1 Constitutive equations

The constitutive equations to predict the degree of swelling in equilibrium states can be derived by choosing the proper strain energy function and free energy due to mixing. Referring to the last term of Equation (3.7), the simplest form of the strain energy function due to stretching of an elastomer is adopted in this study (Flory, 1953):

$$J_s W_m(\mathbf{F}_m, J_s) = \frac{G}{2} [(I_1 - 3) - 2\ln J_s] \quad (5.14)$$

The parameter G is the shear modulus of the dry unfilled elastomer given by $G = NkT$ which can be determined from the stress-strain response. I_1 is the first invariant of the right or left Cauchy Green tensor given as $I_1 = \lambda_1^2 + \lambda_2^2 + \lambda_3^2$. Note that there are many other forms of the strain energy function available in the literature (Marckmann & Verron, 2006; Boyce & Arruda, 2000) and may be used instead of that given in Equation (5.14). Recall from Equation (2.19), for any filled elastomer the amplified strain energy can be written as:

$$J_s W_m(\mathbf{F}_m, J_s) = \frac{G}{2} [(\hat{I}_1 - 3) - 2\ln J_s] = \frac{G}{2} [X(I_1 - 3) - 2\ln J_s] \quad (5.15)$$

where X is the strain amplification factor.

Next, the free energy due to mixing is adopted from the well-known (Flory, 1942)-

(Huggins, 1942a) theory:

$$W_s(c) = kTc \left[\ln \left(\frac{vc}{1+vc} \right) + \chi \left(\frac{1}{1+vc} \right) \right] \quad (5.16)$$

where χ is a dimensionless interaction parameter which is commonly known as chi-parameter which has a specified value for the combination of solvent and elastomer. The chemical potential in Equation (3.34) can be obtained by differentiating the free energy of mixing with respect to c :

$$\frac{dW_s(c)}{dc} = kT \left[\ln \left(\frac{vc}{1+vc} \right) + \frac{1}{1+vc} + \chi \frac{1}{(1+vc)^2} \right] \quad (5.17)$$

or express it in terms of J_s :

$$\frac{dW_s(c)}{dc} = kT \left[\ln \left(1 - \frac{1}{J_s} \right) + \frac{1}{J_s} + \chi \frac{1}{J_s^2} \right] \quad (5.18)$$

Using Equations (5.15) and (3.28), the first Piola-Kirchhoff and Cauchy stress tensors can be written as:

$$\mathbf{P} = -q\mathbf{F}^{-T} + G\mathbf{X}\mathbf{F} \quad \text{and} \quad \boldsymbol{\sigma} = J_s^{-1}(-q\mathbf{I} + G\mathbf{X}\mathbf{B}) \quad (5.19)$$

By inserting the above equations into Equation (3.34), the chemical potential which belongs to equilibrium swelling is given as:

$$\frac{kT}{v} \left[\ln \left(1 - \frac{1}{J_s} \right) + \frac{1}{J_s} + \frac{\chi}{J_s^2} \right] + (q - G)J_s^{-1} = 0 \quad (5.20)$$

In summary, the material parameters that need to be determined in the proposed model are tabulated in Table 5.3. Once all the material parameters are identified, the hydrostatic

Table 5.3: Material parameters used in model.

Free swelling, unfilled elastomer	G
Interaction parameter	χ
Carbon black content	v_f
Fluid molecule volume	v

pressure q can be determined in dependence on the mechanical loading conditions. By substituting all these values into Equation (5.20), we are able to predict the swelling degree at equilibrium state.

5.2.2 Analytical solution for simple problems

5.2.2 (a) Free swelling

First, we consider a simple case of three-dimensional equilibrium swelling under stress-free immersion. By means of stress-free immersion, the dry elastomer is allowed to swell in all directions without constraints and the swelling process is assumed to be homogeneous and isotropic. Since there is no mechanical loading, the only deformation that takes place in the elastomer is contributed from the swelling part of the deformation gradient:

$$\mathbf{F} = \mathbf{F}_s = \begin{bmatrix} \lambda_s & 0 & 0 \\ 0 & \lambda_s & 0 \\ 0 & 0 & \lambda_s \end{bmatrix}, \mathbf{F}_m = \mathbf{I} = \begin{bmatrix} 1 & 0 & 0 \\ 0 & 1 & 0 \\ 0 & 0 & 1 \end{bmatrix} \quad (5.21)$$

Since it is free swelling, there is no stress acting on all directions. Thus, the stress tensors vanish:

$$\boldsymbol{\sigma} = \mathbf{0} \quad \mathbf{P} = \mathbf{0} \quad (5.22)$$

From the combination of Equations (5.19), (5.21) and (5.22), the hydrostatic pressure for stress-free immersion can be calculated as:

$$q = GXJ_s^{2/3} \quad (5.23)$$

and, at equilibrium

$$\frac{kT}{vG} \left[\ln \left(1 - \frac{1}{J_s} \right) + \frac{1}{J_s} + \frac{\chi}{J_s^2} \right] + XJ_s^{-1/3} - J_s^{-1} = 0 \quad (5.24)$$

Using Equation (5.24), the equilibrium swelling degree is plotted as a function of the filler content. In order to compare the effect of different strain amplification factors, the shear modulus of the dry elastomer is arbitrarily chosen as $G = 10000$ Pa. In Figure 5.27, the equilibrium swelling degree is plotted using the strain amplification factor proposed by Guth and Gold (1938) and Nielsen (1966) (Equation (2.17 and 2.18)). Regarding the figure, the Guth-Gold model gives a gradual decrease in the equilibrium swelling degree with the increase in filler content and slowly becomes stable at higher filler content. Contrary to that, the Nielsen model predicts a sharp decrease at low filler contents followed by a more steady decrease from $v_f = 0.2$ to $v_f = 0.7$. At $v_f > 0.7$, the model predicts another sharp decrease which is in contrast with the prediction from Guth-Gold model.

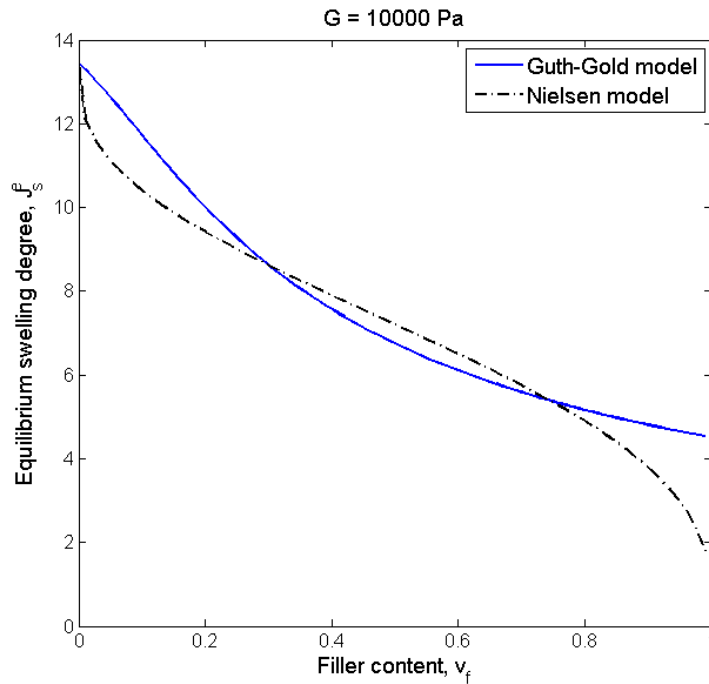


Figure 5.27: Equilibrium swelling degree vs. filler content.

Based on the observation in Figure 5.27, it is clearly seen that the strain amplification factor plays an important role in determining the equilibrium degree of swelling. While the Guth-Gold model gives a gradual decrease in the equilibrium swelling degree, the Nielsen model shows a deviation from the prediction by the previous model. Generally, there are no solid arguments available in the literature on the ability of the existing model on predicting the influence of filler on the mechanical properties of an elastomer. The most direct evaluation on the strain amplification factor is to consider the small strain Young's modulus at different filler content (Bergström & Boyce, 1999). In order to do so, we need a set of reliable experimental data to plot the graph and do the fitting. However, similarly to other authors, we adopt the well-known Guth-Gold model which can take a general polynomial of the form of $X = 1 + av_f + bv_f^2$ depending on the shape and the properties of the fillers and the interactions among particles (Qi & Boyce, 2004). Using the strain amplification factor from the classical Guth-Gold model, we calculate the equilibrium swelling degree for different filler contents as a function of the shear modulus. The results are depicted in Figure 5.28. From the graph, the equilibrium swelling degree is shown to be decreasing with the increase in the filler content and the shear modulus.

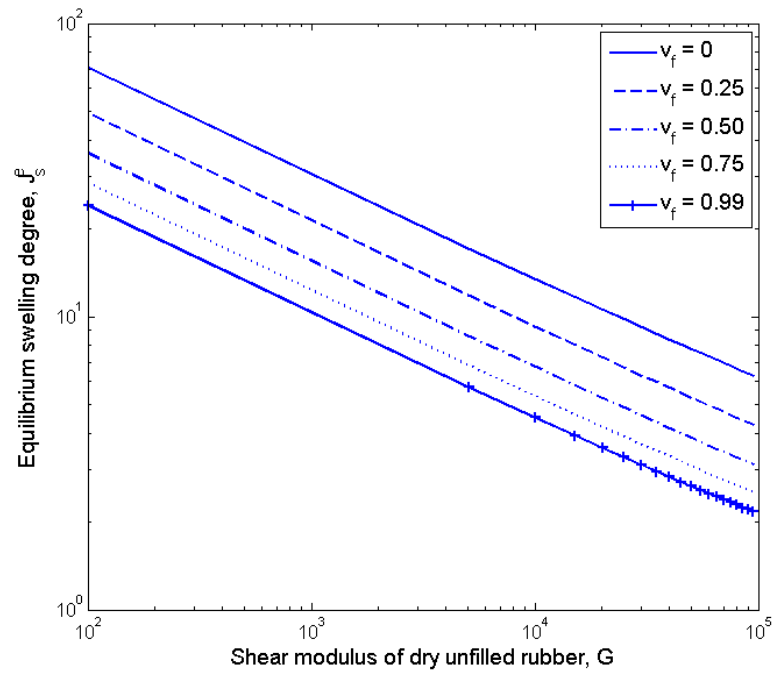


Figure 5.28: Equilibrium swelling degree for different filler content vs. shear modulus of the dry elastomer.

5.2.2 (b) Constrained swelling

For an uniaxial constrained swelling, the dumbbell specimen is subjected to uniaxial tensile deformation in direction x_1^m . Then, with the length fixed in direction x_1^m , the specimen is immersed in a solvent to allow a coupled deformation-diffusion processes. Graphical illustration of the process is sketched in Figure 5.29.

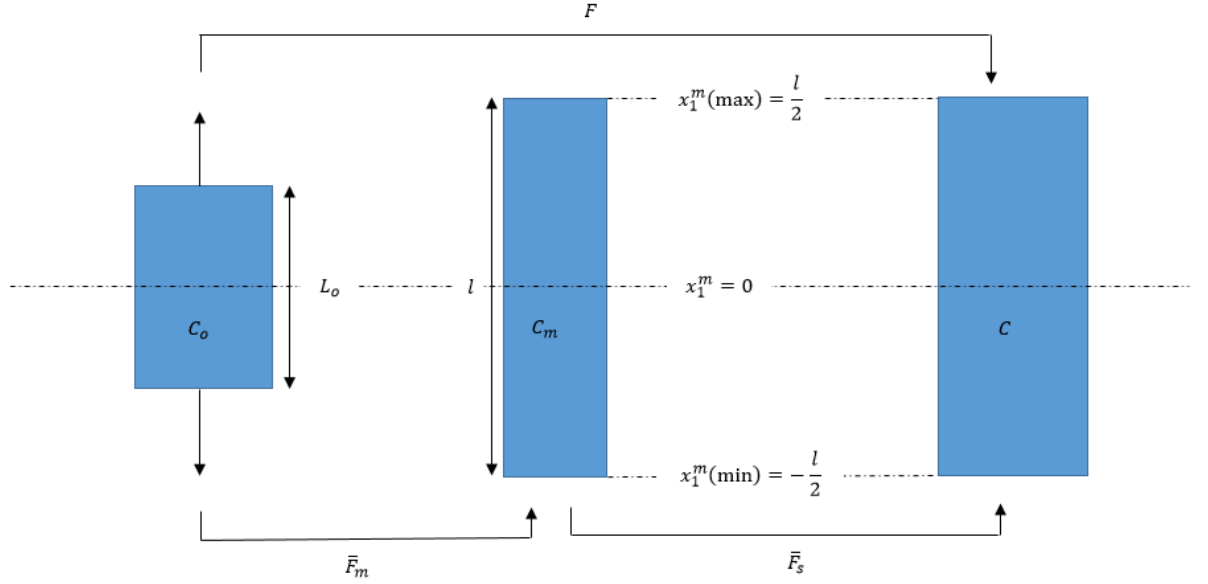


Figure 5.29: Illustration of experimental setup for uniaxial constrained swelling.

The total deformation gradient from the initial configuration C_o to the final configuration C is \mathbf{F} and is given by:

$$\mathbf{F} = \bar{\mathbf{F}}_s \bar{\mathbf{F}}_m \quad (5.25)$$

where $\bar{\mathbf{F}}_m$ is the deformation gradient due to the pure mechanical loading and $\bar{\mathbf{F}}_s$ corresponds to deformation gradient of the coupled deformation-diffusion process. Since the material is assumed to be isotropic during the mechanical deformation, we have:

$$\bar{\mathbf{F}}_m = \begin{pmatrix} \lambda & 0 & 0 \\ 0 & \frac{1}{\sqrt{\lambda}} & 0 \\ 0 & 0 & \frac{1}{\sqrt{\lambda}} \end{pmatrix} \quad (5.26)$$

For the deformation from the intermediate configuration C_m to final configuration C , the dumbbell is assumed to swell freely in directions x_2 and x_3 . Moreover, since the dumbbell is constrained in the stretching direction x_1^m , there will be no swelling along the direction of stretching at $x_1^m = \max$ or \min but swelling is maximum at $x_1^m = 0$. The resulting

deformation gradient from the intermediate configuration C_m to the final configuration C is:

$$\bar{\mathbf{F}}_s = \begin{pmatrix} \lambda_{s1}(x_1^m) & 0 & 0 \\ 0 & \lambda_s & 0 \\ 0 & 0 & \lambda_s \end{pmatrix} \quad (5.27)$$

where λ_{s1} depends on the position along the stretching direction, x_1^m as defined in Figure 5.29. Thus, the total deformation gradient according to Equation (5.25) is:

$$\mathbf{F} = \begin{pmatrix} \lambda \lambda_{s1}(x_1^m) & 0 & 0 \\ 0 & \frac{\lambda_s}{\sqrt{\lambda}} & 0 \\ 0 & 0 & \frac{\lambda_s}{\sqrt{\lambda}} \end{pmatrix} \quad (5.28)$$

In order to adopt the multiplicative split of the deformation gradient mentioned in Section 3.2.1, we can rewrite the imaginary deformation gradient as:

$$\mathbf{F}_m = \lambda_s^{-1} \begin{pmatrix} \lambda \lambda_{s1}(x_1^m) & 0 & 0 \\ 0 & \frac{\lambda_s}{\sqrt{\lambda}} & 0 \\ 0 & 0 & \frac{\lambda_s}{\sqrt{\lambda}} \end{pmatrix} = \begin{pmatrix} \frac{\lambda \lambda_{s1}(x_1^m)}{\lambda_s} & 0 & 0 \\ 0 & \frac{1}{\sqrt{\lambda}} & 0 \\ 0 & 0 & \frac{1}{\sqrt{\lambda}} \end{pmatrix} \quad (5.29)$$

The current degree of swelling is

$$J_s(x_1^m) = \det \mathbf{F} = \lambda_{s1} \lambda_s^2 \quad (5.30)$$

and the stress tensor is

$$\boldsymbol{\sigma}(x_1^m) = J_s^{-1} \left(-q \mathbf{I} + 2 \frac{\partial W}{\partial I_1} \mathbf{B} \right) \quad (5.31)$$

which yields to:

$$\begin{aligned}\sigma_{11} &= J_s^{-1}(-q + G\lambda^2\lambda_{s1}^2) \\ \sigma_{22} = \sigma_{33} &= J_s^{-1}(-q + G\frac{\lambda_s^2}{\lambda})\end{aligned}\tag{5.32}$$

W is the strain energy function adopted from Neo-Hookean model where $\frac{\partial w}{\partial I_1} = \frac{1}{2}G$. For the static mechanical problem, the balance of momentum reads

$$\mathbf{div}\sigma = \mathbf{0}\tag{5.33}$$

which leads to:

$$\frac{\partial \sigma_{11}}{\partial x_1^m} = 0\tag{5.34}$$

Therefore, by substituting J_s from Equation (5.30) into Equation (5.32), we get

$$\frac{\partial}{\partial x_1^m} \left(\frac{q}{\lambda_{s1}} \right) = G\lambda^2 \frac{\partial \lambda_{s1}}{\partial x_1^m}\tag{5.35}$$

which gives us the final form of the pressure q as a function of x_1^m upon integration:

$$q(x_1^m) = G\lambda^2\lambda_{s1}^2 + c\lambda_{s1}\tag{5.36}$$

where c is a constant to be determined based on the boundary conditions. By applying the boundary conditions where $\sigma_{22} = \sigma_{33} = 0$, we get

$$c = G \left(\frac{\lambda_s^2}{\lambda\lambda_{s1}} - \lambda^2\lambda_{s1} \right), \quad q = G\frac{\lambda_s^2}{\lambda}\tag{5.37}$$

Finally, the equilibrium degree of swelling under mechanical loading can be determined

from the chemical potential equation:

$$\frac{\mu}{v} = \frac{\mu_o}{v} + \frac{kT}{v} \left[\ln \left(1 - \frac{1}{J_s} \right) + \frac{1}{J_s} + \chi \frac{1}{J_s^2} \right] + (q - G)J_s^{-1} \quad (5.38)$$

Since the information needed to deduce the dependent of λ_{s1} on the position x_1^m is not available, a form of $\lambda_{s1}(x_1^m)$ must be assumed. Here, instead of assuming a function describing the dependence of λ_{s1} on position, the coupled deformation-diffusion problem will be solved directly by implementing the proposed model into finite element code ABAQUS where we could obtain more information on the degree of swelling at various position.

5.2.3 Identification of material parameters

Volume of the solvent molecule

The volume of the solvent molecules, v can be determined by using the following relation (Cohen, 2007):

$$v = \frac{M_w}{\rho A_v} \quad (5.39)$$

where,

M_w is the molecular weight of the solvent,

ρ is the density of the solvent,

A_v is the Avogadro number, 6.022×10^{23} / mol

Using this equation, the volume of the solvent molecules of biodiesel is calculated as follows:

Table 5.4: Determination of volume of biodiesel molecule.

Molecular weight (g/mol)	290
Density (g/m ³)	880000
Avogadro number	6.022×10^{23}
Volume of solvent molecules (m ³ /molecule)	5.5×10^{-28}

Flory-Huggins interaction parameter

Following Equation (5.24), the Flory-Huggins interaction parameter χ can be determined by using the information at equilibrium swelling. It is calculated for the unfilled elastomer:

Table 5.5: Determination of Flory-Huggins interaction parameter.

Boltzmann constant (J K^{-1})	1.38×10^{-23}
Temperature (K)	293.15
Shear modulus of dry elastomer (Pa)	262900
Degree of swelling at equilibrium	1.23
Volume of solvent molecules ($\text{m}^3/\text{molecule}$)	5.5×10^{-28}
Flory-Huggins interaction parameter	1.30

Strain amplification factor

The strain amplification factor due to the effect of carbon black inclusion in the elastomer is adopted from the general polynomial equation from the Guth-Gold model where:

$$X = 1 + av_f + bv_f^2 \quad (5.40)$$

It can be determined based on the stress-strain response up until fracture for the dry elastomer. From our experimental data, the estimation of the strain amplification factor is such that $a = 7$ and $b = 29$.

5.2.4 Comparison between model and experiment

First, the ability of the proposed model to predict the degree of swelling in the equilibrium state for elastomers with different amounts of carbon black under stress-free immersion is presented in Figure 5.30. In this figure, the model results are obtained by solving Equation (5.24) analytically. Generally, it is observed that the proposed model is in good agreement with the experimental data. The degree of swelling in the equilibrium state decreases as the amount of carbon black in the elastomer increases. Using the pro-

posed model, we are able to predict the degree of swelling as long as we have information on the shear modulus of the dry elastomer, the volume of the solvent molecules and the interaction parameter between the elastomer and the solvent.

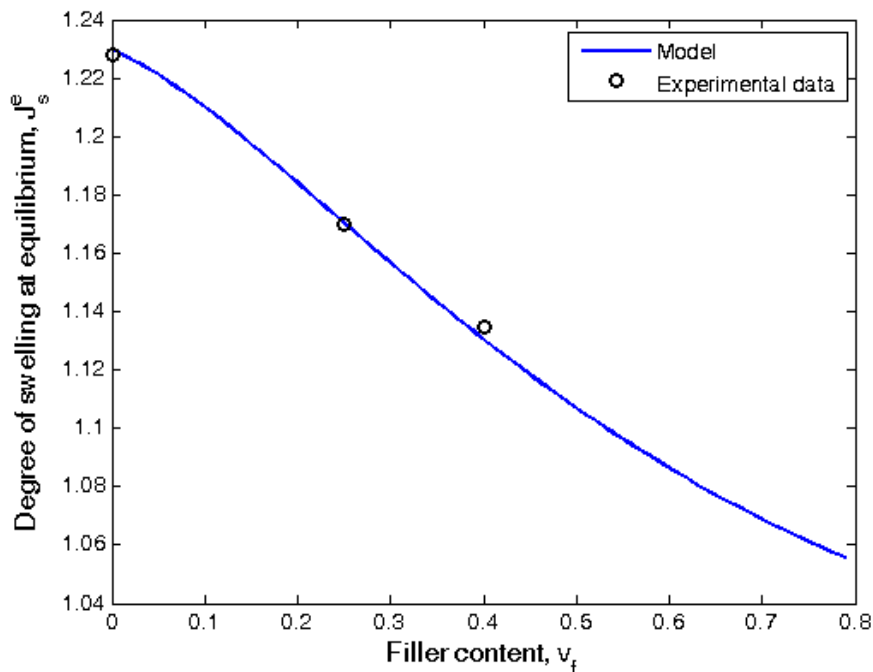


Figure 5.30: Comparison between model and experimental data for stress-free immersion.

5.3 Finite element simulation

5.3.1 Free swelling

Figures 5.31 to 5.33 show the FEA results of the degree of swelling in the equilibrium state for elastomers with different carbon black contents under stress-free immersion. It appears that the degree of swelling is homogeneously distributed over the whole specimen as shown by the uniform colour contour. In the equilibrium state, the degrees of swelling from the FEA results are 1.23, 1.169 and 1.129 for the unfilled, 25 % filled and 40 % filled elastomers respectively. Based on the FEA results, it is obvious that carbon black restricts the diffusion of the solvent which results in a lower degree of swelling when the amount of carbon black is higher in the elastomer.

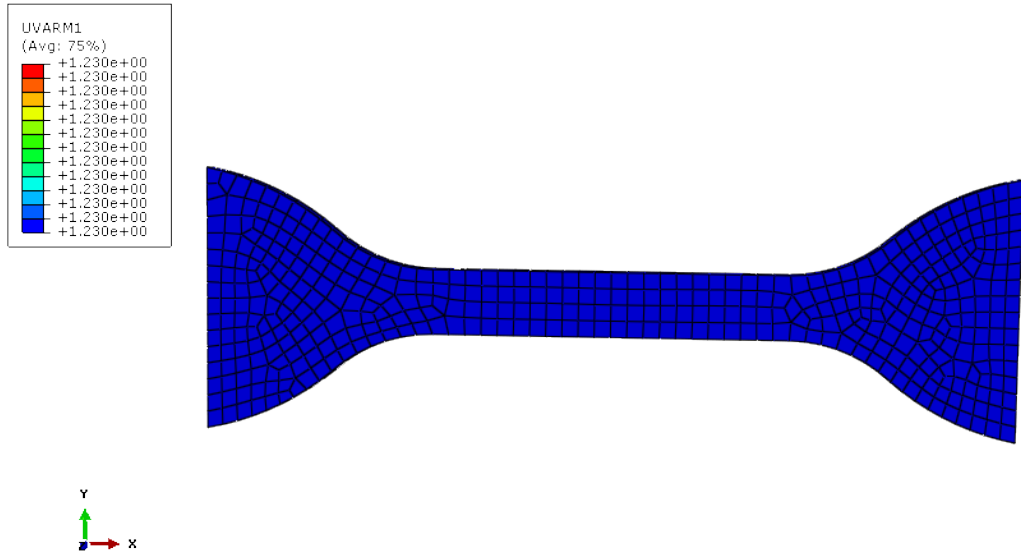


Figure 5.31: Finite element analysis of the degree of swelling in the equilibrium state for stress-free immersion (unfilled elastomer).

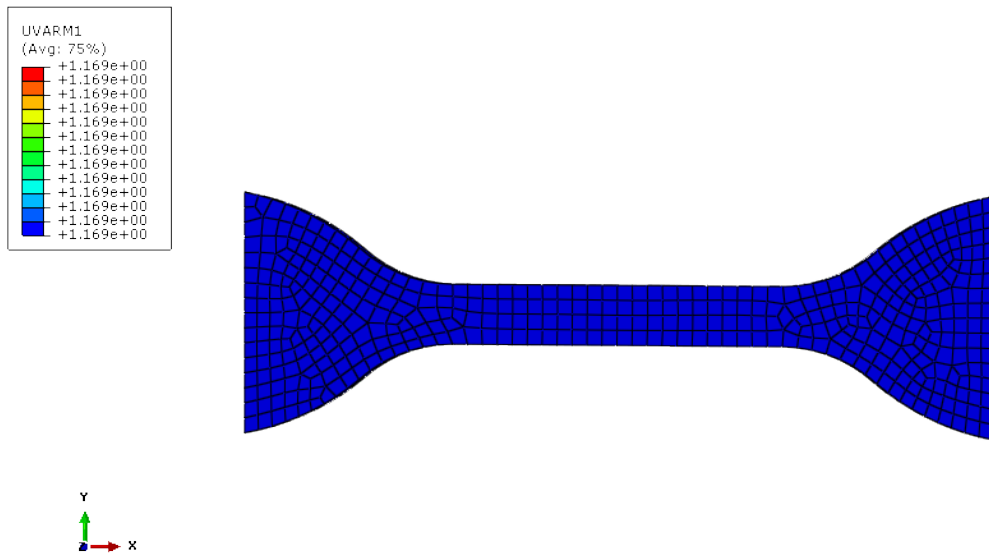


Figure 5.32: Finite element analysis of the degree of swelling in the equilibrium state for stress-free immersion (25 % filled elastomer).

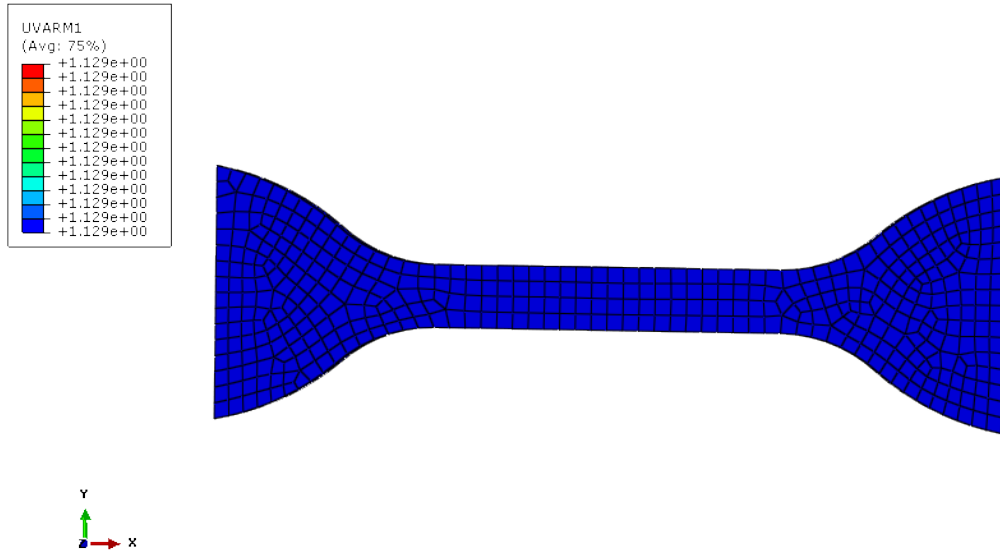


Figure 5.33: Finite element analysis of the degree of swelling in the equilibrium state for stress-free immersion (40 % filled elastomer).

The results obtained from FEA are then being compared with the experimental results and the analytical solution obtained from the proposed model (See Section 5.2.4) and plotted as Figure 5.34. It appears that the results show very good agreement with each other. The degree of swelling in the equilibrium state decreases as the amount of carbon black increases in the elastomer.

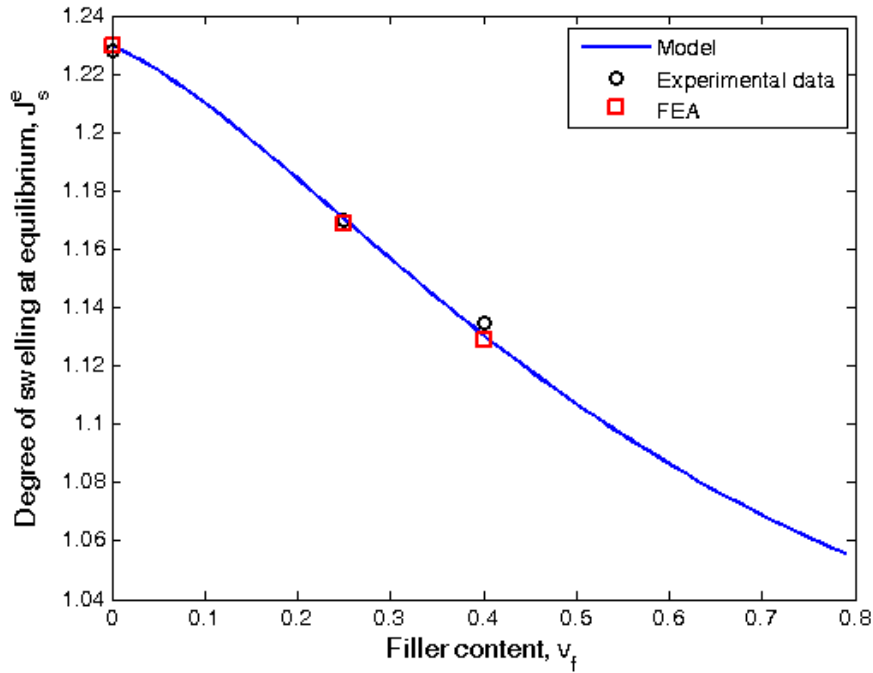


Figure 5.34: Comparison between experimental data, analytical solution and FEA results for stress-free immersion.

5.3.2 Constrained swelling

FEA results for constrained swelling at $\lambda = 1$ are shown in Figures 5.35 to 5.37. Contrary to the uniform degree of swelling over the specimen as observed for the case of stress-free swelling, the FEA results suggest that the degree of swelling is not uniform throughout the whole specimen for constrained swelling. The minimum degree of swelling is observed to occur at the end of the specimen as shown by the colour blue in the figures. However, note that the difference between the maximum and minimum degree of swelling is merely around 0.5 % which is relatively small. Since the degree of swelling is not uniform throughout the specimen, the average equilibrium degrees of swelling need to be obtained and compared with the experimental results.

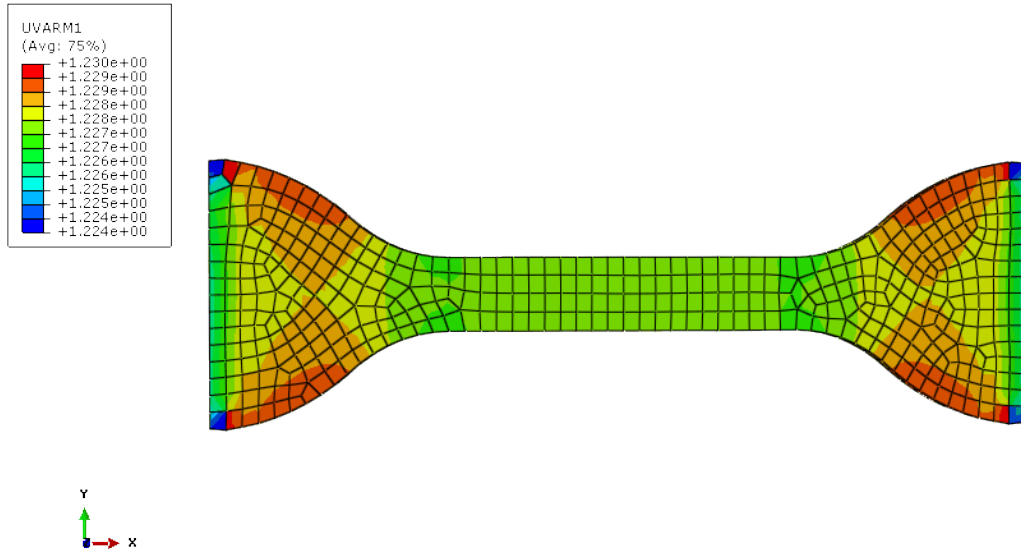


Figure 5.35: Finite element analysis of the degree of swelling in the equilibrium state for constrained immersion ($\lambda = 1$, unfilled elastomer).

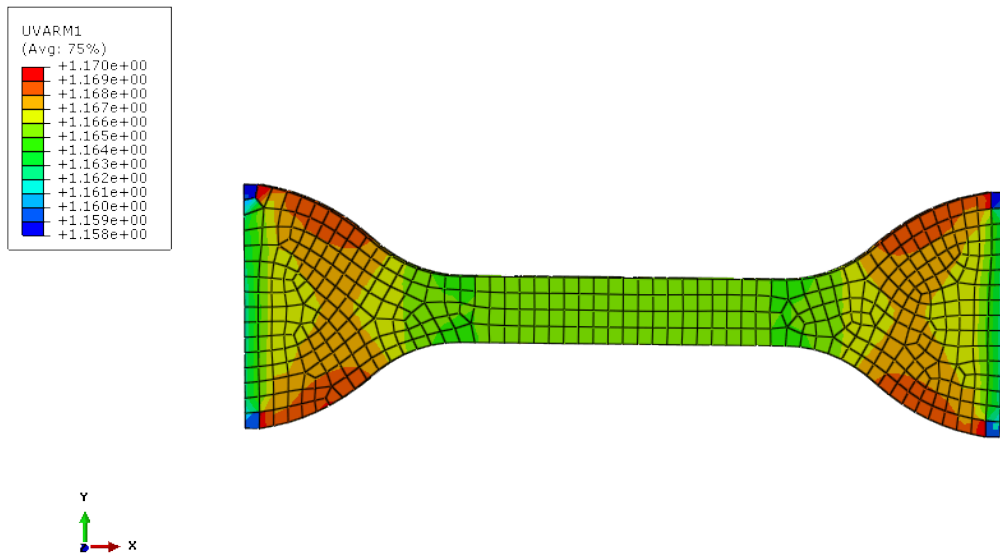


Figure 5.36: Finite element analysis of the degree of swelling in the equilibrium state for constrained immersion ($\lambda = 1$, 25 % filled elastomer).

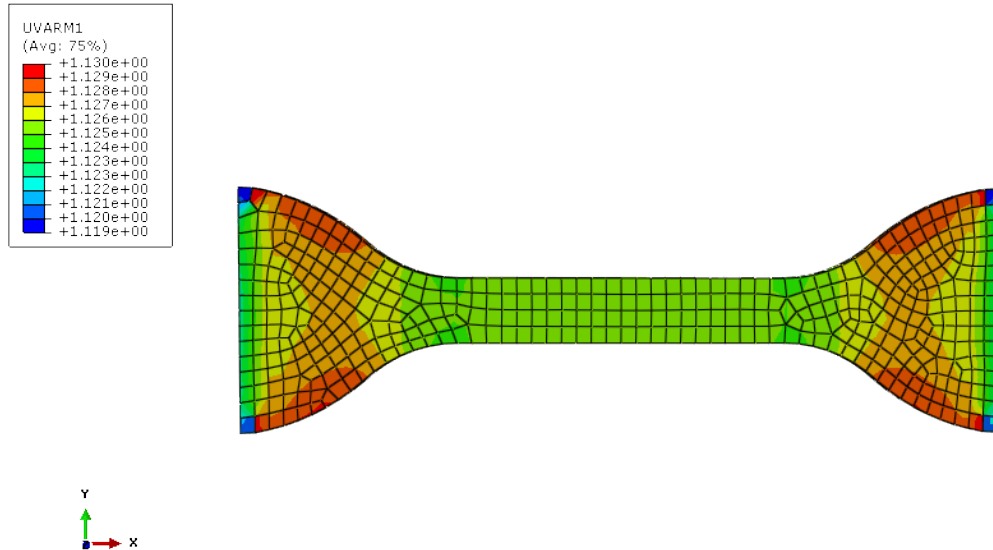


Figure 5.37: Finite element analysis of the degree of swelling in the equilibrium state for constrained immersion ($\lambda = 1$, 40 % filled elastomer).

Using the similar approach, the results obtained from FEA for constrained swelling ($\lambda = 1.25, 1.5$) are depicted in Figures 5.38 to 5.43. It is observed that similarly to the results obtained for $\lambda = 1$, the degree of swelling is not uniform throughout the specimen. For all cases, the differences between the maximum and minimum values are in the range of 0.5%. However, note that the distribution of the degree of swelling shows not the same trend in comparison with the ones obtained for $\lambda = 1$. Minimum swelling is observed at both ends of the specimen which are clamped to the metallic device while maximum swelling is observed in the middle part of the specimen. Following this observation, there is two points on the distribution of swelling under constrained tensile strain worth noting:

- maximum swelling occurs in the central part of the specimen ($x_1^m = 0$ according to Figure 5.29).
- minimum swelling occurs at end parts of the specimen ($x_1^m = l/2$ according to Figure 5.29).

These statements hold true for our observation except for the case of $\lambda = 1$. $\lambda = 1$ is an exceptional case which is initially equal to stress-free immersion.

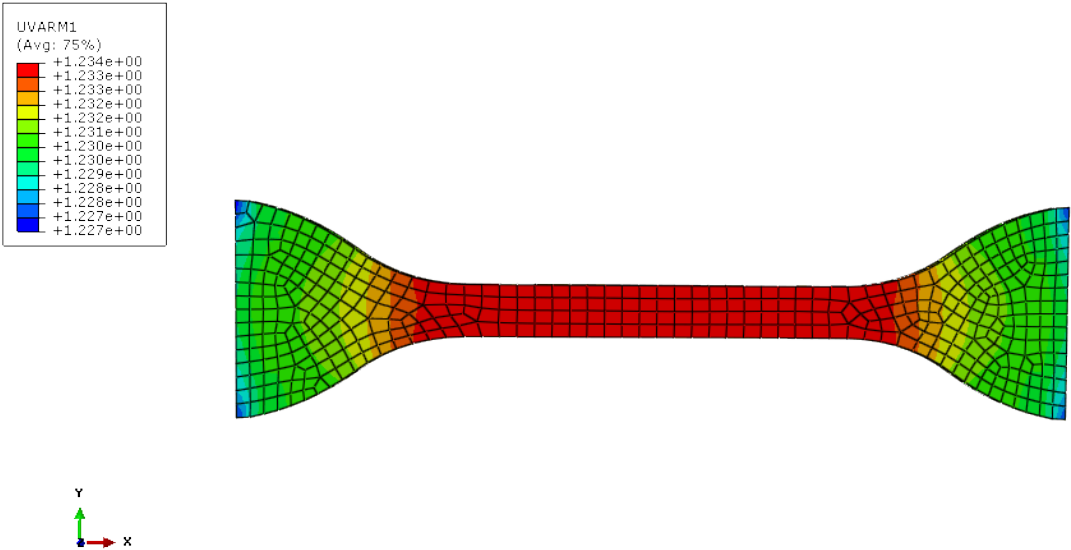


Figure 5.38: Finite element analysis of the degree of swelling in the equilibrium state for constrained immersion ($\lambda = 1.25$, unfilled elastomer).

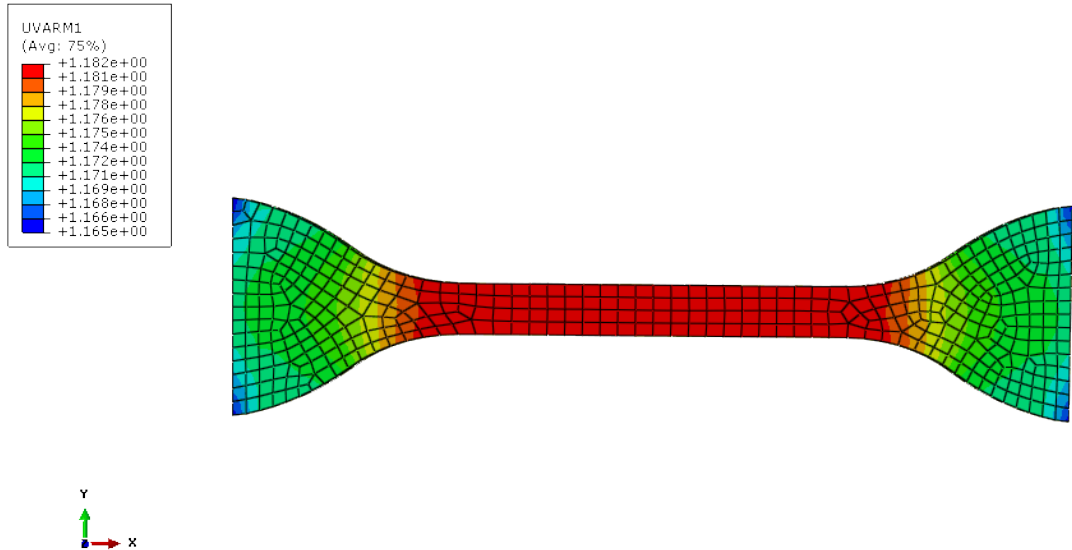


Figure 5.39: Finite element analysis of the degree of swelling in the equilibrium state for constrained immersion ($\lambda = 1.25$, 25 % filled elastomer).

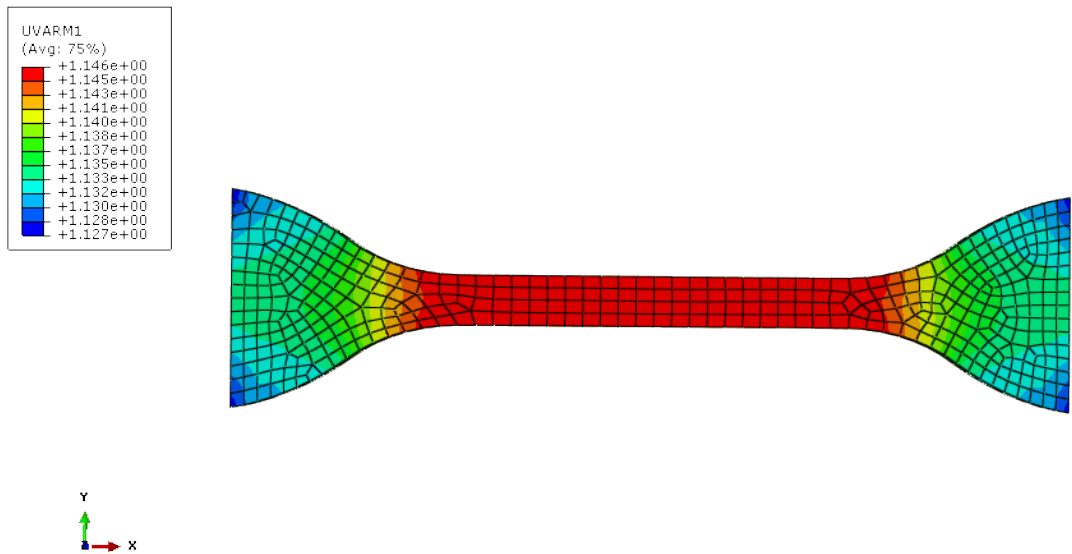


Figure 5.40: Finite element analysis of the degree of swelling in the equilibrium state for constrained immersion ($\lambda = 1.25$, 40 % filled elastomer).

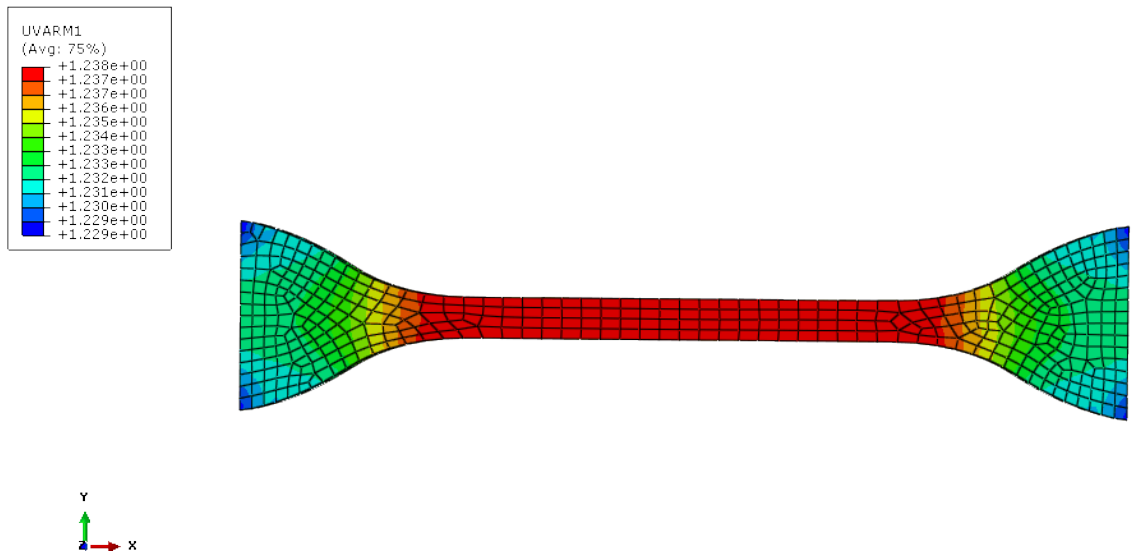


Figure 5.41: Finite element analysis of the degree of swelling in the equilibrium state for constrained immersion ($\lambda = 1.50$, unfilled elastomer).

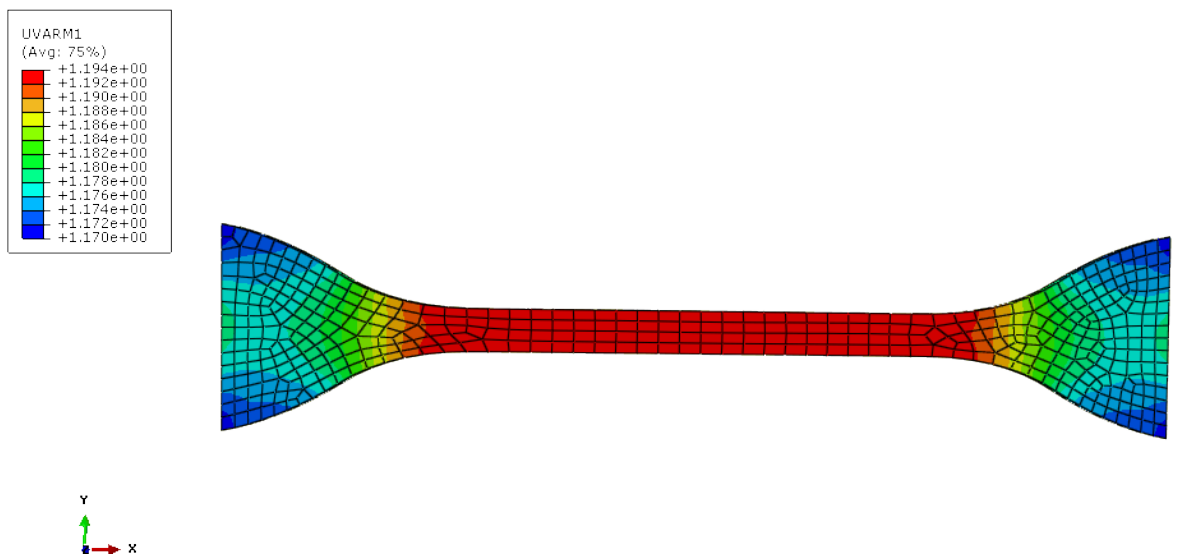


Figure 5.42: Finite element analysis of the degree of swelling in the equilibrium state for constrained immersion ($\lambda = 1.50$, 25 % filled elastomer).

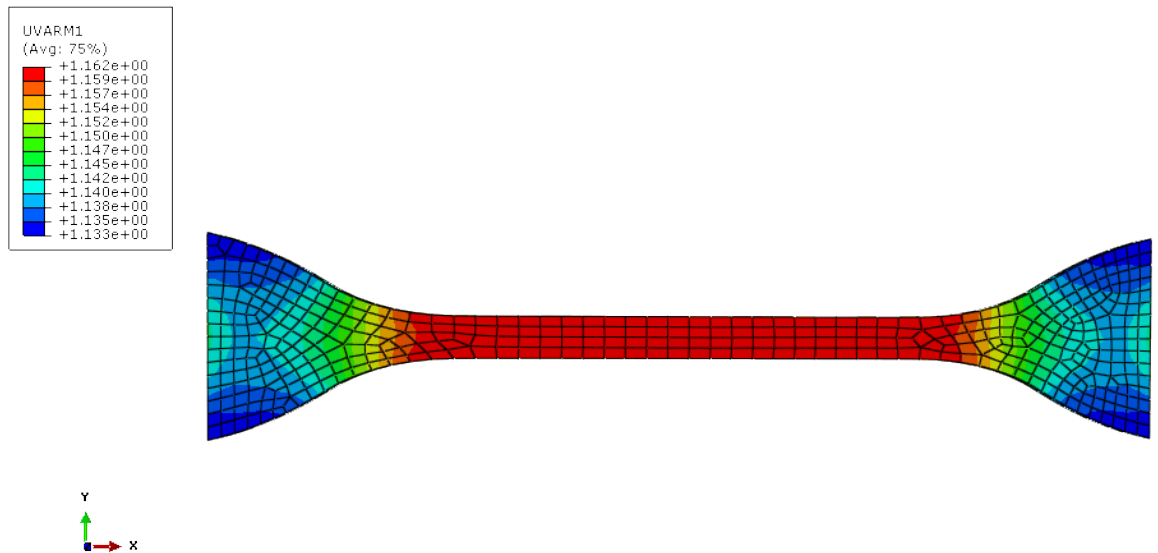


Figure 5.43: Finite element analysis of the degree of swelling in the equilibrium state for constrained immersion ($\lambda = 1.50$, 40 % filled elastomer).

From the FEA results, the dependence of λ_{s1} on the position x_{1m} can be deduced. The values of λ_{s1} at different positions of the unfilled elastomer specimens subjected to different tensile strains are calculated and presented in Figure 5.44. From this figure, it can be seen that for constrained swelling at $\lambda = 1$, the values of λ_{s1} along the material are nearly identical. The variation of λ_{s1} is small since the material undergoes nearly stress-free immersion at the initial stage of immersion. However, for constrained swelling at $\lambda = 1.25, 1.5$, λ_{s1} is maximum in the centre of the specimen and minimum at the end of it. This observation is consistent with the discussion in Section 5.2.2 (b). Furthermore, it is also observed from Figure 5.44 that the maximum value of λ_{s1} increases with the applied tensile strain. Thus, higher tensile strain results in a higher degree of swelling.

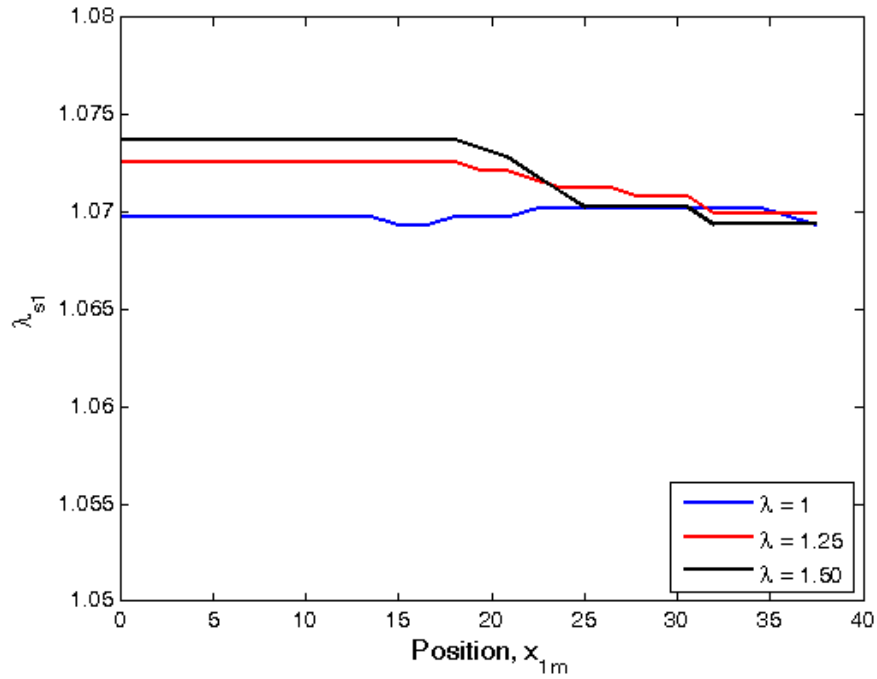


Figure 5.44: λ_{s1} as a function of position x_{1m} .

Finally, in order to verify the efficiency of the proposed model, the resulting degree of swelling in the equilibrium state for constrained swelling is obtained by calculating the average value for the whole specimen. The FEA results are then compared to the experimental results and plotted in Figure 5.45. Figure 5.45 shows that the FEA results are in good agreement with experimental results. Under stress-free immersion, the results obtained from FEA show nearly identical curves as the experimental results. As for constrained swelling, the FEA results are slightly higher than the experimental results. This observation could be caused by the precision during conducting the experimental works. Indeed, it is often difficult to ensure whether the amount of tensile strain applied to the specimen corresponds precisely to the desired value. Moreover, the immersion is conducted in biodiesel where the oily solvent provides a good lubricant between the specimen and the metallic plates. During the immersion, it is difficult to prevent the specimens slip from the metallic plates and thus reduces the accuracy of the experiments. To summarize, the FEA results show the clear trend that swelling increases with the amount

of tensile strain applied and reduces with the amount of carbon black content.

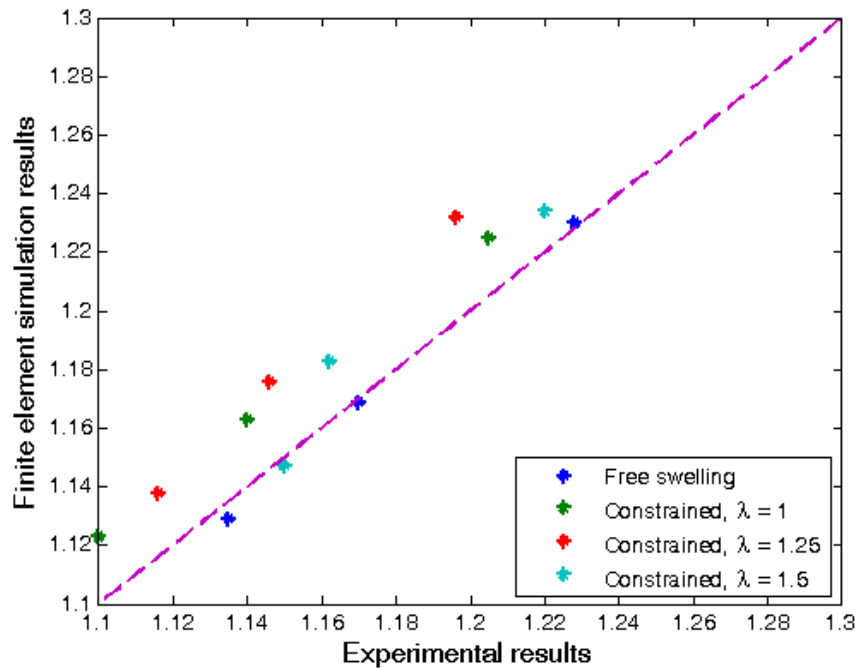


Figure 5.45: Comparison between FEA results and experimental results.

5.3.3 Remark for the case of torsion

The effect of torsion on swelling is an interesting subject to study since there are not many studies conducted on it (Mars, 2001). We attempt to simulate the equilibrium swelling of elastomers in the presence of torsion loading in this study but to no avail. The constraint imposed at the beginning of the load step in order to simulate the torsion effect in step 2 leads to trouble in the stress-free isotropic swelling in step 1. The constraint prevents the nodes on the surface to move such that they are highly distorted. We attempt to simulate the torsion deformation in several ways but to our disappointment, our current attempts did not work out. Works are currently still on going to find a better solution to simulate the equilibrium swelling of elastomers in the presence of a torsion deformation.

CHAPTER 6

CONCLUSION AND FUTURE WORKS

6.1 Conclusion

In order to conclude, the objectives of this research have been achieved.

1. *To develop original devices for investigating swelling of elastomers in biodiesel under the presence of static mechanical deformations.*

Three different original experimental devices have been developed to investigate swelling of elastomers undergoing static mechanical deformation. One of the experimental devices enables the investigation of swelling in the presence of static uniaxial mechanical loading while the other two enable the application of static multiaxial mechanical loading.

2. *To investigate the interaction between diffusion of biodiesel and large deformation in elastomers.*

Static immersion tests of elastomer specimens undergoing uniaxial and multiaxial mechanical loading have been conducted. Generally, it is observed that the degree of swelling increases with the amount of applied tensile strain. On the other hand, our findings suggest that the effect of multiaxial loading on swelling depends strongly on the dimension of the specimen used. The corresponding finding can be related to the hydrostatic part of the Cauchy stress generated in the elastomer.

3. *To develop a simple continuum mechanical model to describe the above interaction.*

The theoretical framework of the model is consistent with the second law of thermodynamics. Two particular cases were considered: (1) modeling the Mullins effect in swollen elastomers and (2) the prediction of the equilibrium swelling of

elastomers in biodiesel in the absence and in the presence of static mechanical deformations. The results show that the proposed model is in good agreement with the experimental observations.

4. *To implement the proposed model in commercial finite element code ABAQUS in order to simulate coupling between diffusion of biodiesel and large deformation in elastomeric materials.*

The proposed model has been implemented into ABAQUS using the user-defined subroutine UHYPER. The FEA results suggest that the degree of swelling in the equilibrium state decreases with the increase in carbon black content. Under tensile strain, the FEA results show that the degree of swelling is higher than under stress-free immersion which is consistent with the experimental observations as well as with the results from our proposed model.

6.2 Suggestions for future works

Based on our discussion in Section 4.4, it is suggested that although three different experimental devices have been developed, each of them possesses different pros and cons and further improvements for future works are needed. Improvements are needed in order to conduct uniaxial tensile tests at higher strain level and to obtain equilibrium swelling for multiaxial mechanical deformations.

As for the continuum mechanical modeling, our proposed model for the Mullins effect in swollen elastomers is based on the existing two phase model of Mullins and Tobin (1957) and Qi and Boyce (2004). Further development to study other inelastic responses such as permanent set and viscoelastic hysteresis is needed to fully understand the mechanical responses of swollen elastomers. In addition, our proposed model is only limited to predict the equilibrium swelling under different mechanical deformations. Further exploration is needed to account for transient effects in achieving the equilibrium state of

swelling.

Finally, the simulation of swelling in the presence of torsion loading will be a priority. Moreover, further improvements are needed in order to predict the equilibrium swelling of elastomers in biodiesel in the presence of general multiaxial mechanical loadings using the finite element code ABAQUS.

Appendices

APPENDIX A

USER SUBROUTINE FOR UHYPER, UVARM

```

                                dumbbell.f
SUBROUTINE UHYPER(BI1,BI2,AJ,U,UI1,UI2,UI3,TEMP,NOEL,
1 CMNAME,INCPFLAG,NUMSTATEV,STATEV,NUMFIELDV,FIELDV,
2 FIELDVINC,NUMPROPS,PROPS)
C=====
C      User defined hyperelastic material subroutine
C      (dumbbell with different carbon black content) free swelling
C      Author: Ch'ng shiau Ying (9 Dec 2013)
C-----
C      Material properties to be passed to the subroutine:
C      PROPS(1) - C0,                shear modulus
C      PROPS(2) - chi,              interaction parameter
C      PROPS(3) - lambda_0,         initial swelling (~1, but not 1)
C      PROPS(4) - vf,              carbon black content
C      State variable:
C      TEMP - (mu-mu0)/kT,          current chemical potential
C      The initial chemical potential, mu0 is determined from
C      initial swelling at t=0, given as:
C      (mu-mu0)/kT |init = Nv*(1/lambda0-1/detF0) + log(1-1/detF0)
C      + 1/detF0 + chi/detF0**2
C      Output:
C      Free-energy function U(I,J) and its derivatives
C      All free-energy density and stress given by the calculation
C      are normalized by kT/v
C=====
      INCLUDE 'ABA_PARAM.INC'
C
      CHARACTER*80 CMNAME
      DIMENSION U(2),UI1(3),UI2(6),UI3(6),STATEV(*),FIELDV(*),
1 FIELDVINC(*),PROPS(*)
      REAL(8) C0, chi, lambda0, detF0, mu_kT, nu, kT, gamma, vf, AF
      C0 = PROPS(1)
      chi = PROPS(2)
      lambda0 = PROPS(3)
      vf = PROPS(4)
      detF0 = lambda0**3
      AF = 1 + 2.5*vf + 14.1*(vf**2)
      nu = 3.3d-27
      kT = 4.0d-21
      gamma = kT/nu/C0
      mu_kT = TEMP ! TEMP is used to represent (mu-mu0)/kT
C
      U(1) = -(mu_kT*(AJ - 1/detF0)
& - (LOG(1 - 1/(AJ*detF0))) + chi/(AJ*detF0))*(AJ - 1/detF0)
& + (2.0*LOG(AJ*detF0) - AF*(AJ**(2.0/3.0)*BI1*lambda0**2 + 3.0))
& / (2.0 *detF0*gamma))
      U(2) = 0
      UI1(1) = (AF*AJ**(2.0/3.0)*lambda0**2.0)/(2.0*detF0*gamma)
      UI1(2) = 0
      UI1(3) = -(mu_kT - LOG(1 - 1/AJ/detF0)
& + (AJ - 1/detF0)*(chi/(AJ**2*detF0)
& + 1/(AJ**2*detF0*(1/(AJ*detF0) - 1)))
& - chi/(AJ*detF0)
& + (2/AJ - (2*AF*BI1*lambda0**2)/(3*AJ**(1.0/3.0)))/(2*detF0*gamma))
      UI2(1) = 0
      UI2(3) = -((2*chi)/(AJ**2*detF0)
& - (AJ - 1/detF0)*((2*chi)/(AJ**3*detF0)
& + 2/(AJ**3*detF0*(1/(AJ*detF0) - 1))
& - 1/(AJ**4*detF0**2*(1/(AJ*detF0) - 1)**2))
& + 2/(AJ**2*detF0*(1/(AJ*detF0) - 1))
& - (2/AJ**2 - (2*AF*BI1*lambda0**2)/(9*AJ**(4.0/3.0)))/(2*detF0*gamma))
      UI2(5) = (AF*lambda0**2)/(3*AJ**(1/3)*detF0*gamma)
      UI3(1) = 0
      UI3(4) = -(AF*lambda0**2.0)/(9.0*AJ**(4.0/3.0)*detF0*gamma)
      UI3(6) = -((AJ - 1/detF0)*((6*chi)/(AJ**4*detF0)

```

```

                                dumbbell.f
& + 6/(AJ**4*detF0*(1/(AJ*detF0) - 1))
& - 6/(AJ**5*detF0**2*(1/(AJ*detF0) - 1)**2)
& + 2/(AJ**6*detF0**3*(1/(AJ*detF0) - 1)**3))
& - (6*chi)/(AJ**3*detF0)
& - 6/(AJ**3*detF0*(1/(AJ*detF0) - 1))
& + 3/(AJ**4*detF0**2*(1/(AJ*detF0) - 1)**2)
& + (4/AJ**3-(8*AF*BI1*lambda0**2)/(27*AJ**(7.0/3.0)))/(2*detF0*gamma))
C
      RETURN
      END
C=====
C
C=====
      SUBROUTINE UVARM(UVAR,DIRECT,T,TIME,DTIME,CMNAME,ORNAME,
1  NUVARM,NOEL,NPT,LAYER,KSPT,KSTEP,KINC,NDI,NSHR,COORD,
2  JMAC,JMATYP,MATLAYO,LACCFLA)
C=====
C      User defined output subroutine which computes
C          1) the swelling degree (Js)
C          2) the polymer volume fraction (phi)
C          3) the volume fraction of liquid (phiL)
C          4) the intradiscal pressure P = 1/3 trace(sigma)
C
C-----
C          Requested variable:
C              LEP      - All principal LOGarithmic strains
C                    (ln(lambda1), ln(lambda2), ln(lambda3))
C              S        - All stress components
C
C      Output:
C          UVAR(1) = UVARM1      - Js
C          UVAR(2) = UVARM2      - phi
C          UVAR(3) = UVARM3      - phiL
C          UVAR(4) = UVARM4      - P
C          - Number of output variables: 4
C=====
      INCLUDE 'ABA_PARAM.INC'
C
      CHARACTER*80 CMNAME,ORNAME
      CHARACTER*3  FLGRAY(15)
      DIMENSION UVAR(NUVARM),DIRECT(3,3),T(3,3),TIME(2)
      DIMENSION ARRAY(15),JARRAY(15),JMAC(*),JMATYP(*),COORD(*)
C
      CALL GETVRM('LEP',ARRAY,JARRAY,FLGRAY,JRCD,
&      JMAC,JMATYP,MATLAYO,LACCFLA)
      UVAR(1) = EXP(ARRAY(1)+ARRAY(2)+ARRAY(3))
      UVAR(2) = 0.05/UVAR(1)
      UVAR(3) = 1.0-UVAR(2)
C
      CALL GETVRM('S',ARRAY,JARRAY,FLGRAY,JRCD,
&      JMAC,JMATYP,MATLAYO,LACCFLA)
      UVAR(4) = 1.0/3.0*(ARRAY(1)+ARRAY(2)+ARRAY(3))
C
      RETURN
      END
C

```

BIBLIOGRAPHY

- Abdul Kader, M., & Bhowmick, A. K. (2003). Acrylic rubber-fluorocarbon rubber miscible blends: Effect of curatives and fillers on cure, mechanical, aging, and swelling properties. *J. Appl. Polym. Sci.*, 89(5), 1442–1452.
- Abdullah, A. Z., Salamatinia, B., Mootabadi, H., & Bhatia, S. (2009). Current status and policies on biodiesel industry in malaysia as the world's leading producer of palm oil. *Energ. Policy*, 37(12), 5440–5448.
- Abu-Abdeen, M., & Elamer, I. (2010). Mechanical and swelling properties of thermoplastic elastomer blends. *Mater. Design*, 31(2), 808–815.
- Agarwal, A. K. (2007). Biofuels (alcohols and biodiesel) applications as fuels for internal combustion engines. *Prog. Energ. Combust.*, 33(3), 233–271.
- Andriyana, A., Billon, N., & Silva, L. (2010). Mechanical response of a short fiber-reinforced thermoplastic: Experimental investigation and continuum mechanical modeling. *Eur. J. Mech. A-Solid*, 29(6), 1065–1077.
- Andriyana, A., Chai, A. B., Verron, E., & Johan, M. R. (2012). Interaction between diffusion of palm biodiesel and large strain in rubber: Effect on stress-softening during cyclic loading. *Mech. Res. Commun.*, 43, 80–86.
- Andriyana, A., Saintier, N., & Verron, E. (2010). Configurational mechanics and critical plane approach: concept and application to fatigue failure analysis of rubberlike materials. *Int. J. Fatigue*, 32(10), 1627–1638.
- Arruda, E. M., & Boyce, M. C. (1993). A three-dimensional constitutive model for the large stretch behavior of rubber elastic materials. *J. Mech. Phys. Solids*, 41(2), 389–412.
- Ayoub, G., Zaïri, F., Naït-Abdelaziz, M., & Gloaguen, J. (2010). Modelling large deformation behaviour under loading–unloading of semicrystalline polymers: application to a high density polyethylene. *Int. J. Plasticity*, 26(3), 329–347.
- Baek, S., & Srinivasa, A. R. (2004). Diffusion of a fluid through an elastic solid undergoing large deformation. *Int. J. Nonlinear Mech.*, 39(2), 201–218.
- Barenblatt, G. I., & Rivlin, R. S. (1997). *[collected papers]; collected papers of rs rivlin*. Springer.
- Bauman, J. T. (2008). *Fatigue, stress, and strain of rubber components: Guide for design engineers*. Carl Hanser Verlag GmbH Co KG.
- Beatty, M., & Krishnaswamy, S. (2000). A theory of stress-softening in incompressible isotropic materials. *J. Mech. Phys. Solids*, 48(9), 1931–1965.
- Becker, A., Dorsch, V., Kaliske, M., & Rothert, H. (1998). A material model for simulating the hysteretic behavior of filled rubber for rolling tires. *Tire Sci. Technol.*, 26(3), 132–148.
- Benjumea, P., Agudelo, J., & Agudelo, A. (2008). Basic properties of palm oil biodiesel–diesel blends. *Fuel*, 87(10), 2069–2075.
- Bergström, J. S., & Boyce, M. (1998). Constitutive modeling of the large strain time-dependent behavior of elastomers. *J. Mech. Phys. Solids*, 46(5), 931–954.
- Bergström, J. S., & Boyce, M. C. (1999). Mechanical behavior of particle filled elastomers. *Rubber Chem. Technol.*, 72(4), 633–656.
- Bessee, G. B., & Fey, J. P. (1997). *Compatibility of elastomers and metals in biodiesel fuel blends* (Tech.

Rep.). SAE Technical Paper.

- Bhattacharya, M., & Bhowmick, A. K. (2008). Polymer-filler interaction in nanocomposites: new interface area function to investigate swelling behavior and young's modulus. *Polymer*, *49*(22), 4808–4818.
- Biot, M. A. (1941). General theory of three-dimensional consolidation. *J. Appl. Phys.*, *12*(2), 155–164.
- Blackman, E. J., & McCall, E. B. (1970). Relationships between the structures of natural rubber vulcanizates and their thermal and oxidative aging. *Rubber Chem. Technol.*, *43*(3), 651–663.
- Bouasse, H., & Carrière, Z. (1903). Sur les courbes de traction du caoutchouc vulcanisé. In *Ann. fac. sci. toulouse* (Vol. 5, pp. 257–283).
- Bowen, R. M. (1976). *Continuum physics*. Acad. Press, New York.
- Boyce, M. C., & Arruda, E. M. (2000). Constitutive models of rubber elasticity: a review. *Rubber Chem. Technol.*, *73*(3), 504–523.
- Boyce, M. C., & Arruda, E. M. (2001). Swelling and mechanical stretching of elastomeric materials. *Math. Mech. Solids*, *6*, 641–659.
- Boyce, M. C., Yeh, O., Socrate, S., Kear, K., & Shaw, K. (2001). Micromechanics of cyclic softening in thermoplastic vulcanizates. *J. Mech. Phys. Solids*, *49*(6), 1343–1360.
- Brieu, M., Diani, J., Mignot, C., & Moriceau, C. (2010). Response of a carbon-black filled sbr under large strain cyclic uniaxial tension. *Int. J. Fatigue*, *32*(12), 1921–1927.
- Bueche, F. (1960). Molecular basis for the mullins effect. *J. Appl. Polym. Sci.*, *4*(10), 107–114.
- Busfield, J. J. C., Deeprasertkul, C., & Thomas, A. G. (2000). The effect of liquids on the dynamic properties of carbon black filled natural rubber as a function of pre-strain. *Polymer*, *41*(26), 9219–9225.
- Callister, W. D. (1997). *Materials science and engineering: An introduction*. John Wiley and Sons, 4th Edition, New York.
- Chagnon, G., Verron, E., Gornet, L., Marckmann, G., & Charrier, P. (2004). On the relevance of continuum damage mechanics as applied to the mullins effect in elastomers. *J. Mech. Phys. Solids*, *52*(7), 1627–1650.
- Chagnon, G., Verron, E., Marckmann, G., & Gornet, L. (2006). Development of new constitutive equations for the mullins effect in rubber using the network alteration theory. *Int. J. Solids Struct.*, *43*(22), 6817–6831.
- Chai, A. B. (2013). *Swelling of elastomer in biodiesel and the resulting mechanical response under cyclic loading*. Unpublished doctoral dissertation, University of Malaya.
- Chai, A. B., Andriyana, A., Verron, E., & Johan, M. R. (2013). Mechanical characteristics of swollen elastomers under cyclic loading. *Mater. Design*, *44*, 566–572.
- Chai, A. B., Andriyana, A., Verron, E., Johan, M. R., & Haseeb, A. S. M. A. (2011). Development of a compression test device for investigating interaction between diffusion of biodiesel and large deformation in rubber. *Polym. Test.*, *30*, 867–875.
- Chai, A. B., Verron, E., Andriyana, A., & Johan, M. R. (2013). Mullins effect in swollen rubber: Experimental investigation and constitutive modelling. *Polym. Test.*, *32*(4), 748–759.
- Chester, S. A., & Anand, L. (2010). A coupled theory of fluid permeation and large deformations for elastomeric materials. *J. Mech. Phys. Solids*, *58*(11), 1879–1906.
- Ch'ng, S. Y., Andriyana, A., Loo, M. S., & Verron, E. (2014). Constitutive modeling of strain-induced

softening in swollen elastomers. *Int. J. Solids Struct.*

- Ch'ng, S. Y., Andriyana, A., Verron, E., Kahbasi, O., & Ahmad, R. (2013). Development of a novel experimental device to investigate swelling of elastomers in biodiesel undergoing multiaxial large deformation. *Exp. Mech.*, 53(8), 1323–1332.
- Cohen, E. R. (2007). *Quantities, units and symbols in physical chemistry*. Royal Society of Chemistry.
- Coleman, B. D., & Gurtin, M. E. (1967). Thermodynamics with internal state variables. *J. Chem. Phys.*, 47(2), 597–613.
- Connell, D. W. (2005). *Basic concepts of environmental chemistry*. CRC Press.
- Dannenberg, E. M. (1966). Molecular slippage mechanism of reinforcement. *Trans. Inst. Rubber, Ind.*, 42.
- Dannenberg, E. M. (1975). The effects of surface chemical interactions on the properties of filler-reinforced rubbers. *Rubber Chem. Technol.*, 48(3), 410–444.
- Diani, J., Brieu, M., & Gilormini, P. (2006). Observation and modeling of the anisotropic visco-hyperelastic behavior of a rubberlike material. *Int. J. Solids Struct.*, 43(10), 3044–3056.
- Diani, J., Fayolle, B., & Gilormini, P. (2009). A review on the mullins effect. *Eur. Polym. J.*, 45(3), 601–612.
- Díaz-Ballote, L., López-Sansores, J. F., Maldonado-López, L., & Garfias-Mesias, L. F. (2009). Corrosion behavior of aluminum exposed to a biodiesel. *Electrochem. Commun.*, 11(1), 41–44.
- Dick, J. S., & Annicelli, R. A. (2001). *Rubber technology: compounding and testing for performance*. Hanser Verlag.
- Dorfmann, A., & Ogden, R. W. (2004). A constitutive model for the mullins effect with permanent set in particle-reinforced rubber. *Int. J. Solids Struct.*, 41(7), 1855–1878.
- Duda, F. P., Souza, A. C., & Fried, E. (2010). A theory for species migration in a finitely strained solid with application to polymer network swelling. *J. Mech. Phys. Solids*, 58(4), 515–529.
- Durning, C. J., & Morman, K. (1993). Nonlinear swelling of polymer gels. *J. Chem. Phys.*, 98(5), 4275–4293.
- Egwaikhide, P. A., Akporhonor, E. E., & Okieimen, F. E. (2007). Effect of coconut fibre filler on the cure characteristics physico-mechanical and swelling properties of natural rubber vulcanisates. *Int. J. Phy. Sci.*, 2(2), 0396046.
- Ehlers, W., Acartürk, A., & Karajan, N. (2010). Advances in modelling saturated soft biological tissues and chemically active gels. *Arch. Appl. Mech.*, 80(5), 467–478.
- Einstein, A. (1906). Eine neue bestimmung der moleküldimensionen. *Ann. Phys. Leipzig*, 324(2), 289–306.
- Fielding, J. H. (1943). Flex life and crystallization of synthetic rubber. *Ind. Eng. Chem.*, 35(12), 1259–1261.
- Flora, S. J. S. (2009). Structural, chemical and biological aspects of antioxidants for strategies against metal and metalloid exposure. *Oxid. Med. Cell. Longev.*, 2(4), 191–206.
- Flory, P. J. (1942). Thermodynamics of high polymer solutions. *J. Chem. Phys.*, 10(1), 51–61.
- Flory, P. J. (1953). *Principles of polymer chemistry*. Cornell University Press.
- Flory, P. J., & Rehner, J. (1943). Statistical mechanics of cross-linked polymer networks ii. swelling. *J. Chem. Phys.*, 11(11), 521–526.

- Flory, P. J., & Rehner, J. (1944). Effect of deformation on the swelling capacity of rubber. *J. Chem. Phys.*, *12*(10), 412–414.
- Frame, E., & McCormick, R. L. (2005). *Elastomer compatibility testing of renewable diesel fuels*. National Renewable Energy Laboratory.
- Franta, I. (2012). *Elastomers and rubber compounding materials* (Vol. 1). Elsevier.
- Freund, M., Lorenz, H., Juhre, D., Ihlemann, J., & Klüppel, M. (2011). Finite element implementation of a microstructure-based model for filled elastomers. *Int. J. Plasticity*, *27*(6), 902–919.
- Fukumori, K., Kurauchi, T., & Kamigaito, O. (1990). Swelling behaviour of rubber vulcanizates: 2. effects of tensile strain on swelling. *Polymer*, *31*(12), 2361–2367.
- Gee, G. (1946). The interaction between rubber and liquids. ix. the elastic behaviour of dry and swollen rubbers. *Trans. Faraday Soc.*, *42*, 585–598.
- Gee, G., & Treloar, L. R. G. (1942). The interaction between rubber and liquids. 1. a thermodynamical study of the system rubber-benzene. *Trans. Faraday Soc.*, *38*, 147–165.
- Gent, A. N. (1992). *Engineering with rubber: how to design rubber components*. Carl Hanser Verlag GmbH Co KG.
- George, S. C., Knörger, M., & Thomas, S. (1999). Effect of nature and extent of crosslinking on swelling and mechanical behavior of styrene–butadiene rubber membranes. *J. Membr. Sci.*, *163*(1), 1–17.
- George, S. C., & Thomas, S. (2001). Transport phenomena through polymeric systems. *Prog. Polym. Sci.*, *26*(6), 985–1017.
- Govindjee, S., & Simo, J. (1991). A micro-mechanically based continuum damage model for carbon black-filled rubbers incorporating mullins' effect. *J. Mech. Phys. Solids*, *39*(1), 87–112.
- Guth, E. (1945). Theory of filler reinforcement. *Rubber Chem. Technol.*, *18*(3), 596–604.
- Guth, E., & Gold, O. (1938). On the hydrodynamical theory of the viscosity of suspensions. *Phys. Rev.*, *53*(322), 2.
- Guth, E., & Simha, R. (1936). Untersuchungen über die viskosität von suspensionen und lösungen. 3. über die viskosität von kugelsuspensionen. *Colloid Polym. Sci.*, *74*(3), 266–275.
- Hanley, J. (2008). *Swelling effects in dynamic equi-biaxial testing of epdm elastomers by the bubble inflation method*. Unpublished doctoral dissertation, Dublin Institute of Technology.
- Harper, C. A. (1996). *Handbook of plastics, elastomers, and composites* (Vol. 2). McGraw-Hill Inc.
- Haseeb, A. S. M. A., Jun, T. S., Fazal, M. A., & Masjuki, H. H. (2011). Degradation of physical properties of different elastomers upon exposure to palm biodiesel. *Energy*.
- Haseeb, A. S. M. A., Masjuki, H. H., Siang, C. T., & Fazal, M. A. (2010). Compatibility of elastomers in palm biodiesel. *Renew. Energ.*, *35*(10), 2356–2361.
- Herzog, A. V., Lipman, T. E., & Kammen, D. M. (2001). Renewable energy sources. *Encyclopedia of Life Support Systems (EOLSS). Forerunner Volume- 'Perspectives and Overview of Life Support Systems and Sustainable Development*.
- Holzappel, G. A. (2000). *Nonlinear solid mechanics: a continuum approach for engineering*. John Wiley & Sons Ltd.
- Hong, W., Liu, Z., & Suo, Z. (2009). Inhomogeneous swelling of a gel in equilibrium with a solvent and mechanical load. *Int. J. Solids Struct.*, *46*(17), 3282–3289.

- Hong, W., Zhao, X., Zhou, J., & Suo, Z. (2008). A theory of coupled diffusion and large deformation in polymeric gels. *J. Mech. Phys. Solids*, 56(5), 1779–1793.
- Huggins, M. L. (1942a). Some properties of solutions of long-chain compounds. *J. Phys. Chem.*, 46(1), 151–158.
- Huggins, M. L. (1942b). Thermodynamic properties of solutions of long-chain compounds. *Ann. NY Acad. Sci.*, 43(1), 1–32.
- Huntley, H. E., Wineman, A. S., & Rajagopal, K. R. (1997). Stress softening, strain localization and permanent set in the circumferential shear of an incompressible elastomeric cylinder. *IMA J. Appl. Math.*, 59(3), 309–338.
- Itskov, M., Haberstroh, E., Ehret, A. E., & Vöhringer, M. C. (2006). Experimental observation of the deformation induced anisotropy of the Mullins effect in rubber. *Kautschuk Gummi Kunststoffe*, 59(3), 93–96.
- Jayed, M. H., Masjuki, H. H., Kalam, M. A., Mahlia, T. M. I., Husnawan, M., & Liaquat, A. M. (2011). Prospects of dedicated biodiesel engine vehicles in Malaysia and Indonesia. *Renew. Sust. Energ. Rev.*, 15(1), 220–235.
- Jha, V. (2008). *Carbon black filler reinforcement of elastomers*. Unpublished doctoral dissertation, Queen Mary, University of London.
- Kalam, M. A., & Masjuki, H. H. (2008). Testing palm biodiesel and NPAA additives to control NO_x and CO while improving efficiency in diesel engines. *Biomass Bioenerg.*, 32(12), 1116–1122.
- Kar, K. K., & Bhowmick, A. K. (1997). High-strain hysteresis of rubber vulcanizates over a range of compositions, rates, and temperatures. *J. Appl. Polym. Sci.*, 65(7), 1429–1439.
- Kaul, S., Saxena, R. C., Kumar, A., Negi, M. S., Bhatnagar, A. K., Goyal, H. B., et al. (2007). Corrosion behavior of biodiesel from seed oils of Indian origin on diesel engine parts. *Fuel Process. Technol.*, 88(3), 303–307.
- Kilian, H. G., Strauss, M., & Hamm, W. (1994). Universal properties in filler-loaded rubbers. *Rubber Chem. Technol.*, 67(1), 1–16.
- Klüppel, M., & Schramm, J. (2000). A generalized tube model of rubber elasticity and stress softening of filler reinforced elastomer systems. *Macromol. Theor. Simul.*, 9(9), 742–754.
- Koleske, J. V. (1995). *Paint and coating testing manual: of the Gardner-Sward handbook* (Vol. 17). ASTM International.
- Kraus, G. (1963). Swelling of filler-reinforced vulcanizates. *J. Appl. Polym. Sci.*, 7(3), 861–871.
- Kraus, G. (1978). Reinforcement of elastomers by carbon black. *Rubber Chem. Technol.*, 51(2), 297–321.
- Lake, G. J., & Lindley, P. B. (1964). Cut growth and fatigue of rubbers. ii. experiments on a noncrystallizing rubber. *J. Appl. Polym. Sci.*, 8(2), 707–721.
- Laraba-Abbes, F., Jenny, P., & Piques, R. (2003). A new ‘tailor-made’ methodology for the mechanical behaviour analysis of rubber-like materials: I. kinematics measurements using a digital speckle extensometry. *Polymer*, 44(3), 807–820.
- Le Cam, J. B., Huneau, B., & Verron, E. (2008). Description of fatigue damage in carbon black filled natural rubber. *Fatigue Fract. Eng. Mater. Struct.*, 31(12), 1031–1038.
- Le Cam, J. B., Huneau, B., & Verron, E. (2013). Fatigue damage in carbon black filled natural rubber under uni- and multiaxial loading conditions. *Int. J. Fatigue*, 52, 82–94.
- Le Cam, J. B., & Toussaint, E. (2010). The mechanism of fatigue crack growth in rubbers under severe

- loading: the effect of stress-induced crystallization. *Macromolecules*, 43(10), 4708–4714.
- Lee, E. H. (1969). Elastic-plastic deformation at finite strains. *J. Appl. Mech.*, 36(1), 1–6.
- Leung, D. Y. C., Wu, X., & Leung, M. K. H. (2010). A review on biodiesel production using catalyzed transesterification. *Appl. Energ.*, 87(4), 1083–1095.
- Lin, W.-C., Fan, W., Marcellan, A., Hourdet, D., & Creton, C. (2010). Large strain and fracture properties of poly (dimethylacrylamide)/silica hybrid hydrogels. *Macromolecules*, 43(5), 2554–2563.
- Lion, A. (1996). A constitutive model for carbon black filled rubber: experimental investigations and mathematical representation. *Continuum Mech. Therm.*, 8(3), 153–169.
- Lion, A. (1997). On the large deformation behaviour of reinforced rubber at different temperatures. *J. Mech. Phys. Solids*, 45(11), 1805–1834.
- Loke, K. M., Dickinson, M., & Treloar, L. R. G. (1972). Swelling of a rubber cylinder in torsion: Part 2. experimental. *Polymer*, 13(5), 203–207.
- Lubarda, V. A. (2004). Constitutive theories based on the multiplicative decomposition of deformation gradient: Thermoelasticity, elastoplasticity, and biomechanics. *Appl. Mech. Rev.*, 57(2), 95–108.
- Machado, G., Chagnon, G., & Favier, D. (2012). Induced anisotropy by the mullins effect in filled silicone rubber. *Mech. Mater.*, 50, 70–80.
- Magryta, J., Dębek, C., & Dębek, D. (2006). Mechanical properties of swelled vulcanizates of polar diene elastomers. *J. Appl. Polym. Sci.*, 99(5), 2010–2015.
- Marckmann, G., & Verron, E. (2006). Comparison of hyperelastic models for rubber-like materials. *Rubber Chem. Technol.*, 79(5), 835–858.
- Marckmann, G., Verron, E., Gornet, L., Chagnon, G., Charrier, P., & Fort, P. (2002). A theory of network alteration for the mullins effect. *J. Mech. Phys. Solids*, 50(9), 2011–2028.
- Marin, J. (1962). *Mechanical behavior of engineering materials*. Prentice-Hall.
- Mars, W. V. (2001). *Multiaxial fatigue of rubber*. Unpublished doctoral dissertation, The University of Toledo.
- Mars, W. V., & Fatemi, A. (2002). A literature survey on fatigue analysis approaches for rubber. *Int. J. Fatigue*, 24(9), 949–961.
- Maru, M. M., Lucchese, M. M., Legnani, C., Quirino, W. G., Balbo, A., Aranha, I. B., et al. (2009). Biodiesel compatibility with carbon steel and hdpe parts. *Fuel Process. Technol.*, 90(9), 1175–1182.
- Miehe, C. (1995). Discontinuous and continuous damage evolution in ogden-type large-strain elastic materials. *Eur. J. Mech. A-Solid*, 14(5), 697–720.
- Mills, N. J., & Walker, N. (1980). Fatigue crack initiation in glassy plastics in high strain fatigue tests. *J. Mater. Sci.*, 15(7), 1832–1840.
- Mostafa, A., Abouel-Kasem, A., Bayoumi, M. R., & El-Sebaie, M. G. (2009). Effect of carbon black loading on the swelling and compression set behavior of sbr and nbr rubber compounds. *Mater. Design*, 30(5), 1561–1568.
- Mullins, L. (1948). Effect of stretching on the properties of rubber. *Rubber Chem. Technol.*, 21(2), 281–300.
- Mullins, L. (1950). Thixotropic behavior of carbon black in rubber. *Rubber Chem. Technol.*, 23(4), 733–743.

- Mullins, L., & Tobin, N. R. (1957). Theoretical model for the elastic behavior of filler-reinforced vulcanized rubbers. *Rubber Chem. Technol.*, 30(2), 555–571.
- Mullins, L., & Tobin, N. R. (1965). Stress softening in rubber vulcanizates. part i. use of a strain amplification factor to describe the elastic behavior of filler-reinforced vulcanized rubber. *J. Appl. Polym. Sci.*, 9(9), 2993–3009.
- Nielsen, L. E. (1966). Simple theory of stress-strain properties of filled polymers. *J. Appl. Polym. Sci.*, 10(1), 97–103.
- Ogden, R. W. (1984). Non-linear elastic deformations. *Eng. Anal.*, 1(2), 119.
- Ogden, R. W., & Roxburgh, D. G. (1999). A pseudo-elastic model for the mullins effect in filled rubber. *P. Roy. Soc. A-Math. Phys.*, 455(1988), 2861–2877.
- Patil, A. O., & Coolbaugh, T. S. (2005). Elastomers: a literature review with emphasis on oil resistance. *Rubber Chem. Technol.*, 78(3), 516–535.
- Paul, D. R., & Ebra-Lima, O. M. (1970). Pressure-induced diffusion of organic liquids through highly swollen polymer membranes. *J. Appl. Polym. Sci.*, 14(9), 2201–2224.
- Phosri, C., Rodriguez, A., Sanders, I. R., & Jeffries, P. (2010). The role of mycorrhizas in more sustainable oil palm cultivation. *Agric. Ecosyst. Environ.*, 135(3), 187–193.
- Qi, H. J., & Boyce, M. C. (2004). Constitutive model for stretch-induced softening of the stress–stretch behavior of elastomeric materials. *J. Mech. Phys. Solids*, 52(10), 2187–2205.
- Rajagopal, K. R. (1995). *Mechanics of mixtures*. World scientific.
- Rajagopal, K. R. (2003). Diffusion through polymeric solids undergoing large deformations. *Mater. Sci. Technol.*, 19(9), 1175–1180.
- Rajagopal, K. R., Wineman, A. S., & Gandhi, M. (1986). On boundary conditions for a certain class of problems in mixture theory. *Int. J. Eng. Sci.*, 24(8), 1453–1463.
- Ramadhass, A. S., Jayaraj, S., & Muraleedharan, C. (2004). Use of vegetable oils as ic engine fuels—a review. *Renew. Energ.*, 29(5), 727–742.
- Ramesan, M. T. (2005). The effects of filler content on cure and mechanical properties of dichlorocarbene modified styrene butadiene rubber/carbon black composites. *J. Polym. Res.*, 11(4), 333–340.
- Rodgers, B., Waddell, W. H., & Klingensmith, W. (2004). *Rubber compounding*. Wiley Online Library.
- Sidoroff, F. (1974). Un modèle viscoélastique non linéaire avec configuration intermédiaire. *J. Mécanique*, 13(4), 679–713.
- Simo, J. C. (1987). On a fully three-dimensional finite-strain viscoelastic damage model: formulation and computational aspects. *Comput. Method. Appl. M.*, 60(2), 153–173.
- Smallwood, H. M. (1944). Limiting law of the reinforcement of rubber. *J. Appl. Phys.*, 15(11), 758–766.
- Soares, J. S. (2009). Diffusion of a fluid through a spherical elastic solid undergoing large deformations. *Int. J. Eng. Sci.*, 47(1), 50–63.
- Trabelsi, S., Albouy, P.-A., & Rault, J. (2003). Crystallization and melting processes in vulcanized stretched natural rubber. *Macromolecules*, 36(20), 7624–7639.
- Trakarnpruk, W., & Porntangjitlikit, S. (2008). Palm oil biodiesel synthesized with potassium loaded calcined hydrotalcite and effect of biodiesel blend on elastomer properties. *Renew. Energ.*, 33(7), 1558–1563.

- Treloar, L. R. G. (1950). The swelling of cross-linked amorphous polymers under strain. *Trans. Faraday Soc.*, 46, 783-789.
- Treloar, L. R. G. (1972). Swelling of a rubber cylinder in torsion: Part 1. theory. *Polymer*, 13(5), 195–202.
- Treloar, L. R. G. (1975). *The physics of rubber elasticity*. Oxford University Press, USA.
- Truesdell, C., & Noll, W. (1992). *The non-linear field theories of mechanics*. Springer.
- Truesdell, C., & Toupin, R. (1960). *The classical field theories*. Springer.
- Tsunoda, K., Busfield, J. J. C., Davies, C. K. L., & Thomas, A. G. (2000). Effect of materials variables on the tear behaviour of a non-crystallising elastomer. *J. Mater. Sci.*, 35(20), 5187–5198.
- Verron, E., & Andriyana, A. (2008). Definition of a new predictor for multiaxial fatigue crack nucleation in rubber. *J. Mech. Phys. Solids*, 56(2), 417–443.
- Voet, A. (1980). Reinforcement of elastomers by fillers: Review of period 1967–1976. *J. Polym. Sci.*, 15(1), 327–373.
- Webber, R. E., Creton, C., Brown, H. R., & Gong, J. P. (2007). Large strain hysteresis and mullins effect of tough double-network hydrogels. *Macromolecules*, 40(8), 2919–2927.
- Wineman, A. S., & Huntley, H. E. (1994). Numerical simulation of the effect of damaged induced softening on the inflation of a circular rubber membrane. *Int. J. Solids Struct.*, 31(23), 3295–3313.
- Yamaguchi, K., Busfield, J. J. C., & Thomas, A. G. (2003). Electrical and mechanical behavior of filled elastomers. i. the effect of strain. *J. Polym. Sci. Pol. Phys.*, 41(17), 2079–2089.
- Zairi, F., Naït-Abdelaziz, M., Gloaguen, J.-M., & Lefebvre, J.-M. (2008). Modelling of the elasto-viscoplastic damage behaviour of glassy polymers. *Int. J. Plasticity*, 24(6), 945–965.
- Zairi, F., Naït-Abdelaziz, M., Woznica, K., & Gloaguen, J.-M. (2005). Constitutive equations for the viscoplastic-damage behaviour of a rubber-modified polymer. *Eur. J. Mech. A-Solid*, 24(1), 169–182.
- Zuyev, Y. S., Pravednikova, S., Zhrebkova, L., & Zaitseva, V. (1964). The tear-resistance of rubbers in the presence of physically aggressive media. *Polym. Sci. USSR*, 5(2), 269–276.

LIST OF PUBLICATIONS

Academic Journals

1. **Ch'ng, S.Y.**, Andriyana, A., Tee, Y.L., & Verron, E. (2014). Effects of carbon black and the presence of static mechanical strain on the swelling of elastomers in solvent. *The Scientific World Journal*. Submitted.
2. Andriyana, A., Loo, M.S., Chagnon, G., Verron, E., & **Ch'ng, S.Y.** (2014). Modeling the Mullins effect in elastomers exposed to palm biodiesel. *Meccanica*. Submitted.
3. **Ch'ng, S.Y.**, Andriyana, A., Loo, M.S., & Verron, E. (2014). Constitutive modeling of strain-induced softening in swollen elastomers. *Int. J. Solids Struct.*, Article in press.
4. **Ch'ng, S.Y.**, Andriyana, A., Tee, Y.L., & Verron, E. (2014). Effect of carbon black content on the swelling of elastomers in solvent in the presence of static mechanical loading. *Mat. Res. Innov.*, Article in press.
5. Chai, A.B., Andriyana, A., **Ch'ng, S.Y.**, Verron, E., Johan, M.R. (2014). An extended two-phase model for Mullins effect in swollen rubber. *Mat. Res. Innov.*, Article in press.
6. **Ch'ng, S.Y.**, Andriyana, A., Verron, E., Kahbasi, O., & Ahmad, R. (2013). Development of a Novel Experimental Device to Investigate Swelling of Elastomers in Biodiesel Undergoing Multiaxial Large Deformation. *Exp. Mech.*, 53(8): 1323-1332.
7. **Ch'ng, S.Y.**, Andriyana, A., Verron, E., & Ahmad, R. (2013). Diffusion of Palm Biodiesel in Elastomers Undergoing Multiaxial Large Deformations. *Defect Diffus. Forum*, 334: 77-82.

Conference Proceedings

1. **Ch'ng, S.Y.**, Andriyana, A., Tee, Y.L., & Verron, E. (2013). Effect of carbon black content on the swelling of elastomers in solvent in the presence of static mechanical loading. Proceedings of *International Conference on the Science and Engineering of Materials (ICoSEM)*. 13-14 November 2013. Kuala Lumpur, Malaysia.
2. Chai, A.B., Andriyana, A., **Ch'ng, S.Y.**, Verron, E., Johan, M.R. (2014). An extended two-phase model for Mullins effect in swollen rubber. Proceedings of *International Conference on the Science and Engineering of Materials (ICoSEM)*. 13-14 November 2013. Kuala Lumpur, Malaysia.
3. **Ch'ng, S.Y.**, Andriyana, A., Verron, E., & Ahmad, R. (2013). Effect of multiaxial mechanical loading on the swelling of rubber in biodiesel. In: *Constitutive Models for Rubber VIII*. Gil-Negrete & Alonso (eds). Page 79-84. Taylor & Francis Group Publisher. ISBN 978 1 138 00072 8.
4. Chai, A.B., Andriyana, A., **Ch'ng, S.Y.**, Verron, E., & Johan, M.R. (2013). Modeling the Mullins effect in swollen rubber. *Constitutive Models for Rubber VIII*, 443. In: *Constitutive Models for Rubber VIII*. Gil-Negrete & Alonso (eds). Page 443-448. Taylor & Francis Group Publisher. ISBN 978 1 138 00072 8.
5. **Ch'ng, S.Y.**, Andriyana, A., Verron, E., & Ahmad, R. (2012). Diffusion of Palm Biodiesel in Elastomers Undergoing Multiaxial Large Deformations. Proceedings of *8th International Conference on Diffusion in Solids and Liquids (DSL)*. 25-29 June 2012. Turkey, Istanbul.
6. **Ch'ng, S.Y.**, Andriyana, A., Verron, E., & Ahmad, R. (2012). Degradation of NBR and CR due to simultaneous diffusion of palm biodiesel and large deformations. Proceedings of *The Asian International Conference on Materials, Minerals, and Polymer 2012 (MAMIP)*. 23-24 March 2012. Penang, Malaysia.